GEOLOGICAL SURVEY EXPLANATORY REPORT

SHEET 49 (8514N)

ST MARYS

TASMANIA DEPARTMENT OF MINES

GEOLOGICAL SURVEY 1:50 000 EXPLANATORY REPORT SHEET 49 (8514N) ST MARYS 1987 ISBN 0 7246 1947 X

TASMANIA DEPARTMENT OF MINES

1987

GEOLOGICAL SURVEY EXPLANATORY REPORT

GEOLOGICAL ATLAS 1:50 000 SERIES
SHEET 49 (8514N)

ST MARYS

by N. J. Turner, B.Sc.(Hons)
C. R. Calver, B.Sc.(Hons)

with appendices on petrology by J. L. Everard, B.Sc.(Hons)
and on economic geology by C. A. Bacon, B.Sc.(Hons)
and V. M. Threader, M.Sc., B.Sc.(Hons)

DEPARTMENT OF MINES, GPO BOX 56, ROSNY PARK, TASMANIA 7018 ISBN 0 7246 1947 X

CONTENTS

LIST OF PLATES

LIST OF FIGURES

LIST OF TABLES

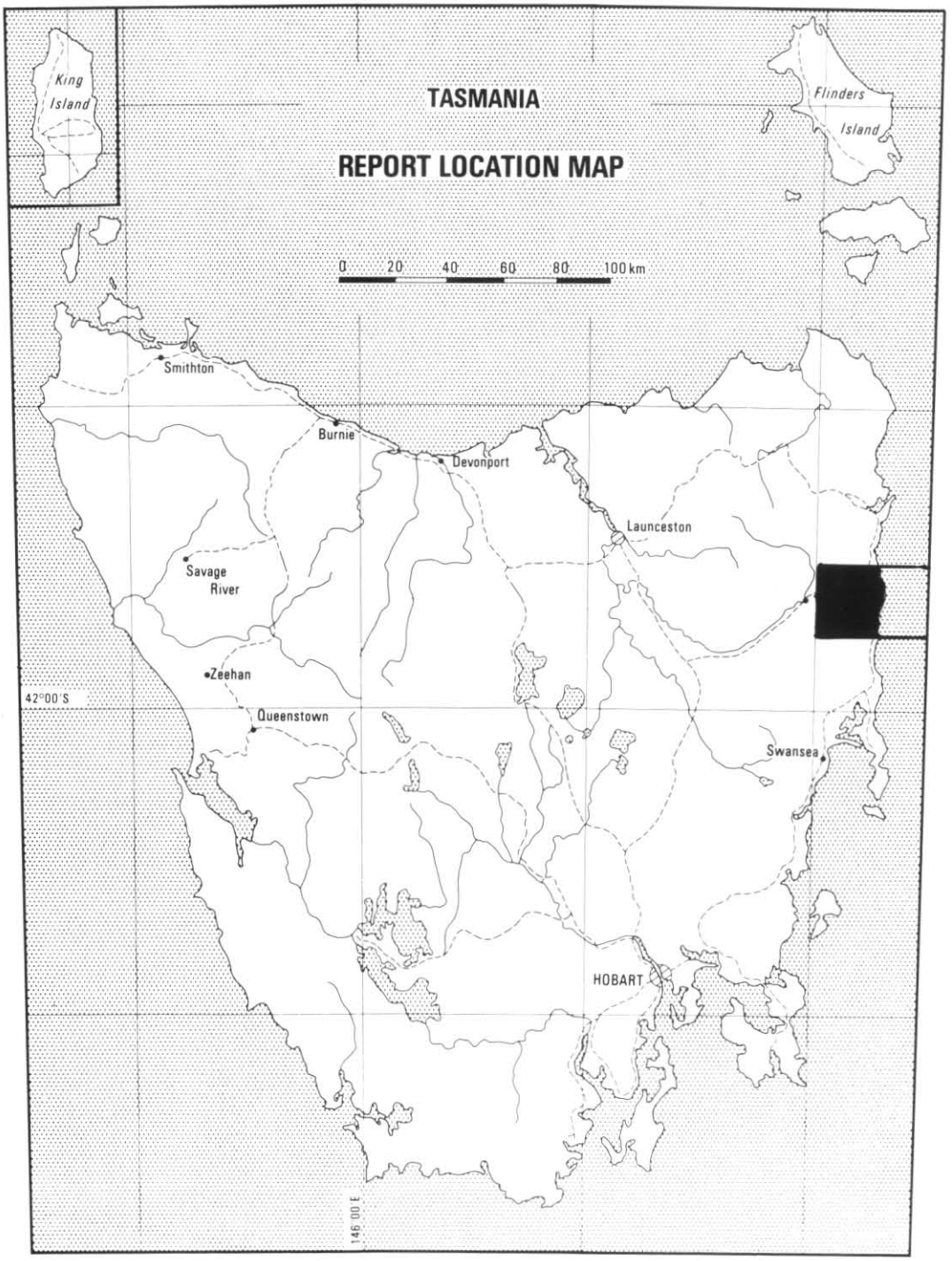

Figure 1. *Location map*

5 cm

INTRODUCTION

The St Marys Quadrangle is situated on Tasmania's east coast, between latitudes 41°30′ and 41°45′S and longitudes 148° and 148°30′E (fig. 1). The Tasman Sea covers nearly half the area of the quadrangle. The largest settlement, St Marys (population 677 at the 1976 census), is connected by the Esk Highway and a 1·067m gauge railway, via Fingal, to Hobart and Launceston. The Tasman Highway, following the east coast, detours inland to pass through St Marys.

Precipitation occurs throughout the year but with a winter maximum. St Marys receives an average annual rainfall of 1019 mm. Rainfall increases markedly with altitude. Agriculture is limited to relatively flat land along the floor of the Fingal Valley and a narrow coastal plain. The remainder of the quadrangle is covered in open, dry sclerophyll forest, with some wet sclerophyll and small remnants of temperate rainforest at high altitudes.

Forestry, farming and coal mining provide most of the local employment. Pastoral activities are centred upon extensive sheep farming, with some dairying and beef production.

Logging operations by Tasmanian Pulp and Forest Holdings are current on Fingal Tier and the Nicholas Range. Timber is extracted mostly for woodchips. Radiata pine has been planted on much of the country north and east of Mt Nicholas.

The St Marys Quadrangle contains the bulk of Tasmania's reserves of black coal. Several seams, all within the Upper Parmeener Super-Group (Triassic), have been exploited, all yielding a dull, medium rank bituminous steaming coal with high ash and low sulphur content.

Since the late 19th century, when mining commenced, the Duncan, Mt Nicholas and Cornwall collieries, and several smaller operations, have been responsible for almost all of the State's coal output. Two collieries, the Duncan on the northern slopes of Fingal Tier, and the Blackwood on the southern slopes of Mt Nicholas, are currently in operation, annually producing approximately 300 000 t and 150 000 t respectively.

In the course of coal exploration, more than 150 holes have been drilled, mostly by the Shell Co. of Australia-IMI consortium and by the Department of Mines. Locations and summarised details of those boreholes publicly available at mid-1984 are indicated on the geological map.

A network of secondary roads and four-wheel drive tracks constructed for logging and drilling operations provides easy access to most parts of the quadrangle. Mapping the Permian and younger rocks has been hampered by widespread dolerite talus cover. However, the borehole data provide a great deal of supplementary stratigraphic and structural information.

The quadrangle was mapped between 1977 and 1983 by R. H. Castleden, C. R. Calver, N. J. Turner and P. W. Baillie. The 1:50 000 geological map was published in 1984.

C. R. Calver and N. J. Turner compiled the following report, and J. L. Everard and C. A. Bacon contributed appendices on igneous petrology and economic geology, respectively. The geologist mainly responsible for each section is named with the section-heading; other geologists responsible for any given information are referred to by their initials within parentheses.

PHYSIOGRAPHY

C. R. Calver

The distribution of dolerite is the most significant physiographic determinant, as this rock type caps every major topographic high within the quadrangle. The southern half of the land area of the quadrangle is dominated by the high (600–800 m a.s.l.), undulating dolerite plateau of Fingal Tier. The plateau has a network of shallow, marshy depressions drained mostly by south-flowing streams, and becomes deeply dissected along the southern margin of the map sheet. North of Fingal Tier, the dolerite and underlying Parmeener Super-Group have been largely removed by erosion, leaving as prominent outliers the Nicholas Range, St Patricks Head and Mt Elephant. The dolerite caps on these mountains are predominantly of linear, ridge-like form, even though most are considered to be part of a once-continuous sheet rather than separate dyke-like intrusions. Steep to precipitous gradients often delineate the eroded edges of the dolerite sheet, a result of the characteristic vertical columnar jointing of this rock type.

These dolerite-capped highlands overlook the eastern end of the Fingal Valley, a broad, flat-floored depression about 250 m a.s.l., drained by the Break O'Day River that flows west to join the South Esk at Fingal. There is no evident structural control for the Fingal Valley, which on St Marys Quadrangle is cut into flat-bedded rocks of the Parmeener Super-Group.

Particular units within the Parmeener Super-Group that are relatively resistant to erosion tend to form minor topographic knick-points, cliffs, benches and flat-topped hills. The most consistent of such units are the lower sandstones of Ps; limestones in Pc; the pebbly glauconitic sandstone (Pag) upon which benches are developed around Mt Elephant; basalt (Rb) that tends to form the lips of waterfalls in streams flowing north off the Nicholas Range; and quartz sandstone (Rq), which underlies several low, flat-topped hills on the floor of the Fingal Valley. Dissected lobes of dolerite talus also cap minor

highs in the Fingal Valley. The pre-Permian erosion surface (St Clair Surface of Davies, 1959) has been uncovered around Beauty Flat, around St Patricks Head and east of Mt Elephant.

The Permian and younger rocks dip gently south, so that basement of granitic rock types and folded quartzwackes is exposed along the northern foot of the Nicholas Range and in a broad coastal zone that narrows southwards. These rock types have largely been deeply incised by numerous steep, youthful streams that flow east into the sea or north into the Scamander River.

A narrow (1–3 km) coastal plain is interrupted by a stretch of steep, rocky coastline between Falmouth and Chain of Lagoons. Along the coastal plain, small lagoons (Templestowe and Henderson Lagoons) are trapped behind recent dune sands.

PREVIOUS WORK

Early work in the area was concerned mainly with coal resources (Milligan, 1849; Gould, 1861; Twelvetrees, 1902). Hills *et al.* (1922), as part of a state-wide coal resources survey presented a general geological account of the coalfields and a synthesis of exploration activity up to that time and provided a geological sketch map (by H. G. W. Keid) covering much of the St Marys Quadrangle.

Voisey (1938) described the Permian stratigraphy at Elephant Pass.

Permian limestone on the southern slopes of Mt Elephant, and in the Piccaninny Creek area, was investigated by Everard, *in* Hughes (1957) and Hughes (1957). Sketch maps showing limestone distribution, and some analyses, were presented.

Walker (1957) mapped and described the geology of an extensive area north-east of St Marys.

The stratigraphy of the Parmeener Super-Group (Permian and Triassic rocks) within the map sheet is briefly described by Banks (1962) and Hale (1962) in the context of a Tasmania-wide synthesis.

McDougall and Leggo (1965) provided data on the isotopic ages of the St Marys Porphyrite and the Piccaninny Creek adamellite.

McNeil (1965) mapped and described the geology of the Mt Elephant–Piccaninny Point area, subdividing the Permian into four formations.

A report by Threader (1968) on the coal resources of the Fingal–St Marys region includes a general geological synthesis and a map covering most of the area of the St Marys Quadrangle.

Rock distributions provided by the last two studies were incorporated into the 1:250 000 Launceston geological map sheet (McClenaghan and Baillie, 1974; explanatory notes McClenaghan and Baillie, 1975).

Williams and Groves (1967), Gee and Groves (1971) and Gee and Groves (1974) all considered aspects of the granodiorite contact zone at Piccaninny Point.

Calver (1980) and Calver and Castleden (1981) demonstrated a Triassic age for the extensive basalt north-west of St Marys, at present the only *in situ* igneous rocks known from the Parmeener Super-Group.

Within the last decade, coal exploration has been greatly accelerated, with a regional gravity survey and a wide coverage of diamond drill-holes now completed over prospective areas in the Quadrangle. The gravity survey (Leaman and Richardson, 1981) extended over the whole central-eastern Tasmanian region, with a high-resolution 'core area' over the Fingal Tier on St Marys Quadrangle. Concealed dolerite feeder structures were elucidated. Other geophysical methods were also applied to a lesser extent (Leaman and Richardson, 1980; Leaman, 1980; Richardson and Leaman, 1981). Threader and Bacon (1983) summarise the results of diamond drilling by the Department of Mines in the south-west portion of the map sheet. Elsewhere, the Shell Co. of Australia-I.M.I. consortium has undertaken most drilling activity.

Turner *et al.* (1976) outline the general relationships of the older (pre-Permian) rocks in the quadrangle, in particular, of the St Marys Porphyrite. They also provide data on the major, trace and rare earth element chemistry of the igneous rocks and new data on the Rb-Sr and K-Ar ages of those rocks. Higgins *et al.* (in press) provide data on the mineral chemistry of the igneous rocks and discuss the genesis of the magma from which the St Marys Porphyrite was derived.

STRATIGRAPHY

Mathinna Beds (?Ordovician–?Silurian–Early Devonian) (Sds)

N. J. Turner

Walker (1957) gave the name Scamander Quartzite and Slate to the older rocks that extend northwards from the area between Mt Nicholas and St Marys Pass in the St Marys Quadrangle to near St Helens. Banks (*in* Spry and Banks, 1962) grouped the Scamander Quartzite and Slate with other pre-Permian sedimentary rocks in north-eastern Tasmania under the regional name of Mathinna Beds. Subsequently McNeil (1965) included the older rocks in the southern part of the St Marys Quadrangle in the Mathinna Beds. A graptolite of probable Pragian (Late Siegenian) age has been described from the Mathinna Beds (Scamander Quartzite and Slate) near Scamander (Rickard and Banks, 1979). However, the only fossils found in the St Marys

Quadrangle are fragmentary, carbonised, vascular plants. These are widespread and it therefore seems unlikely that any part of the Mathinna Beds in the St Marys Quadrangle is much older than Early Devonian.

In the St Marys Quadrangle the Mathinna Beds comprise an interbedded sequence of poorly-sorted sandstone, siltstone and mudstone in which sandstone is volumetrically predominant. Very low grade, regional dynamic metamorphism has caused induration of sandstone and imparted a slaty fabric to some pelitic rocks, particularly in the southern part of the quadrangle. The metamorphism has caused recrystallisation of the argillaceous component in the original sediments to form fine-grained white mica but there appears to have been little recrystallisation of quartz.

Sandstones in the eastern half of the quadrangle are siliceous. They are mostly of fine to medium grain size but occasionally coarse sand grains and granules occur near the bases of beds. Angular, undulose, monocrystalline quartz is the most common clast constituent. Muscovite and fine-grained, chert-like, polycrystalline quartz are minor constituents as is metapelite consisting of fine-grained, carbonaceous muscovite. Pelite also occasionally forms quite large angular clasts up to 100 mm across which are apparently derived by cannibalism of earlier formed Mathinna Beds. The feldspar content of the sandstones is variable and low, being less than about 5%. The feldspar grains are relatively unaltered and include polysynthetically twinned plagioclase and untwinned or simply twinned material which may include orthoclase. Volcanic fragments were found to form a small proportion of the clasts in one sample of more feldspathic sandstone. They consist of felted feldspar microlites with minor, indeterminate, interstitial material and may be andesitic to trachytic in composition.

Sedimentary structures indicate that deposition of the sandstone beds was by turbidity currents (see also Williams, 1959). The beds may display Bouma subdivisions A to D or they may consist of a few subdivisions. Their thickness ranges from a few centimetres to about 1·5 m and there may either be no interturbidite mudstone (Bouma E) between them or there may be a thickness of mudstone ranging up to about one metre. Sole marks are commonly present on the bottoms of Bouma A subdivisions. These include flute casts which may have associated flame structures due to loading. Longitudinal furrow and ridge structures (Dżulynski and Walton, 1965) are also present. They consist of shallow, rounded, linear grooves separated by cusps spaced at about 30 mm intervals. They form a strong lineation from which the palaeocurrent trend was measured. Palaeocurrent direction was obtained from flute clasts. All current data are presented in Figure 2 and show a strong NNW-SSE trend of flow and a direction of flow towards the NNW.

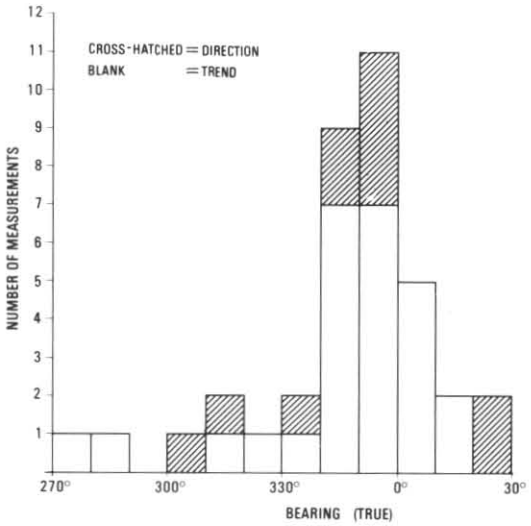

Figure 2. *Histogram of palaeocurrent lineation data derived from the Mathinna Beds in St Marys Quadrangle. Most data are from the area near the northern edge of the sheet, east of* Dapl. *The remainder are from Elephant Pass and adjacent areas. Each measurement has been rotated to the horizontal using the dip and strike of the outcrop in which the measurement was made and the statistical fold axis for the structural sub-area in which the outcrop occurs.*

Breccia zone below the St Marys Porphyrite (Early Devonian) (Dsb, Ds)

N. J. Turner

DISTRIBUTION AND TYPES OF DEPOSITS

At various localities around its northern, basal contact the St Marys Porphyrite overlies breccia, Mathinna Beds which contain breccia-filled fractures, and coherent Mathinna Beds. At one locality [FQ003042] the porphyrite body overlies a succession of graded sandstone, indurated mudstone and breccia (Ds). The succession is about 3 m thick and unconformably overlies Mathinna Beds. The various deposits below the St Marys Porphyrite together comprise a thin zone (Dsb) which is regionally concordant with the base of the porphyrite body. At a local scale bedding in Ds is also approximately concordant with the base of the porphyrite which suggests that Ds and the porphyrite have a super-positional rather than an intrusive relationship. Such a relationship is consistent with the absence of thermal metamorphism in Ds and Dsb and with textural evidence in the porphyrite which suggests that it is extrusive.

Where the St Marys Porphyrite overlies breccia or fractured Mathinna Beds there appears to be no corresponding disruption of the basal contact and no porphyrite is incorporated in the breccia.

Therefore the fractures and breccia in Dsb are considered to have formed before emplacement of the porphyrite body. The favoured interpretation of the fractures is that they correspond to relatively shallow-seated structures in an areally extensive landslip or slump system which developed prior to extrusion of the porphyrite. Breccia which immediately underlies the porphyrite body and which is not clearly associated with fracturing may partly represent the surface product of slumps or slips. The instability reflected by the fractures and breccia may have resulted from disturbances associated with the igneous activity which preceded volcanism. If brecciated Mathinna Beds at EQ998042 are part of Dsb and if the base of Dsb dips parallel to the base of the porphyrite body (22°) then the zone has a maximum thickness of about 160 m. However, almost all fracturing and brecciation is within 20 m stratigraphically of the base of the St Marys Porphyrite.

Ds is thought to have formed at much the same time as fractures and breccia elsewhere in Dsb. Its restricted lateral extent may indicate that it was deposited in a channel or that it is a remnant of a more extensive deposit that was largely disrupted by slumping.

OUTCROP AND PETROGRAPHIC FEATURES

Fracture-related breccia is well exposed in the creek near EQ998040. It forms a thin (400 mm), gently curving seam which dips gently south and transects uniformly-dipping Mathinna Beds (plate 1). The breccia consists of angular to subrounded fragments of Mathinna Beds sandstone up to about 60 mm across which are supported by a matrix of sandy pelite. Other well-exposed examples of fracture-related breccia occur near EQ998080, EQ994037, and FQ018037. In the last two localities the fractures dip both shallowly and steeply. In the first locality breccia

Plate 1. *Shallowly-dipping seam of breccia in coherent Mathinna Beds in* Dsb *below the northern basal contact of the St Marys Porphyrite at EQ998040. The length of the hammer is 330 mm.*

Plate 2. *Matrix-supported breccia in Dsb which directly underlies the St Marys Porphyrite at FQ000042. Rare, well-rounded cobbles of Mathinna-type sandstone occur in the same vicinity. The diameter of the lens cap is 49 mm.*

occurs within coherent Mathinna Beds as irregular patches ranging in size from about 300 mm to a few metres across. In some smaller patches the progressive disruption of coherent beds contiguous with the patches can be observed. There is no quartz veining associated with the fractures or patches and there is no shearing in adjacent Mathinna Beds. In thin section the fragments in the breccia comprise relatively massive Mathinna Beds and the matrix consists of what appears to be disaggregated Mathinna Beds. The matrix is well cleaved, the cleavage being microscopically defined by fine, anastomosing stringers of very fine-grained, opaque (?carbonaceous) material.

Between EQ999042 and FQ004044 there are some striking exposures of cleaved breccia, directly overlain by St Marys Porphyrite. The breccia is very poorly sorted and much like the material that occurs in fractures except that the fragments are larger, commonly ranging up to about 250 mm (plate 2). In the breccia exposed at FQ003042 there is a 4 m block of Mathinna Beds which contains breccia-filled fractures. Most fragments in the breccia consist of sandstone but there is a small proportion of pelitic fragments. The matrix is cleaved (plate 3) and ranges in composition from sandy pelite to pelitic quartz sand. Almost all fragments in the breccia are angular to poorly rounded but a few well-rounded cobbles of indurated sandstone occur near FQ000042. Similar cobbles also occur near FQ018041. These cobbles provide the clearest evidence outside of the Ds succession of the involvement of aqueous transportation processes in the formation of breccia in Dsb.

The thin Ds succession has a basal breccia 600 mm thick which rests on a sharp, clean contact which truncates the underlying Mathinna Beds. The breccia consists of angular to moderately rounded fragments of siltstone in a silty matrix.

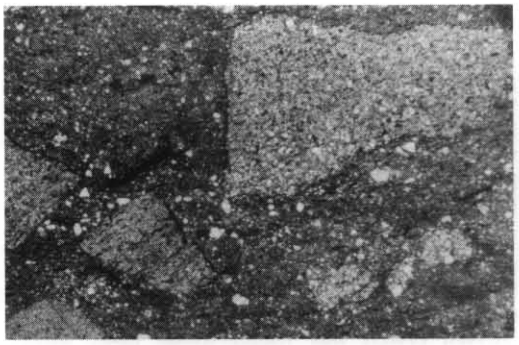

Plate 3. *Photomicrograph (plane-polarised light) of a sample of breccia from* Dsb *at EQ998042. Cleavage in the matrix is defined by thin stringers of ?carbonaceous material. The same material adheres to the margins of many rock fragments. Width of the field of view is 4·2 mm.*

High in the succession there is matrix-dominated breccia which contains rounded fragments of sandstone as well as siltstone and pelite. The matrix also contains sandy material. It displays the same type of anastomosing cleavage that occurs elsewhere in Dsb.

Sandstone comprises less than half the Ds succession and is mostly in the lower part. It is much coarser grained than sandstone in the Mathinna Beds (plate 4) and is of different composition, being feldspathic and lithic (plates 5, 6) rather than siliceous. The beds are graded and comprise Bouma A units. The bed which overlies the basal breccia has flute clasts on its sole which indicate a N-S current trend. Mineral grains in the sandstone include monocrystalline, undulose quartz, feldspar, clastic green biotite, clastic muscovite and accessory amounts of green

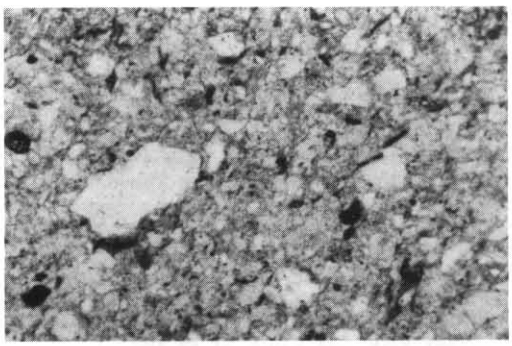

Plate 4. *Photomicrograph (plane-polarised light) of a sample of Mathinna Beds sandstone from the base of a 350 mm bed just below the unconformity at the base of* Dpr. *Relatively large grains of quartz are surrounded by smaller grains of quartz and flakes of transparent muscovite and opaque carbonaceous mudstone. Width of the field of view is 1.55 mm.*

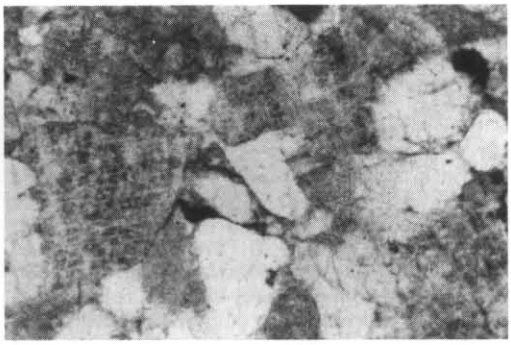

Plate 5. *Photomicrograph (plane-polarised light) of sandstone in* Ds. *Width of the field of view is 1.55 mm. Clear grains of quartz with turbid grains of feldspar and mottled grains of chert.*

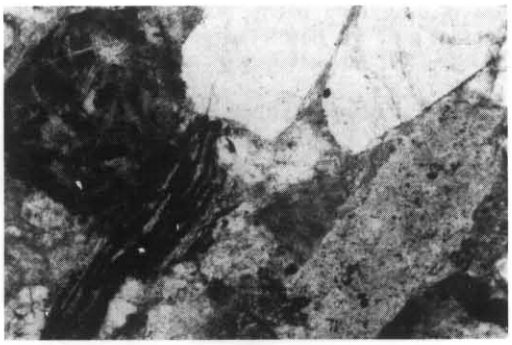

Plate 6. *Photomicrograph (plane-polarised light) of sandstone in* Ds. *Width of the field of view is 1.55 mm. Clear grains of quartz with mottled grains of chert accompany a flake of carbonaceous shale and a grain of basic or intermediate volcanic material.*

to brown tourmaline and zircon. Rock fragments include sericitic chert, metachert, psammite and pelite of low metamorphic grade, carbonaceous pelite and mafic or intermediate volcanic fragments. The psammite and pelite display disoriented foliation. They closely resemble lithologies in the Mathinna Beds but the other rock types and the green biotite are derived from elsewhere, possibly from the same provenance as the Mathinna Beds. However, the green biotite is unlike anything seen in the Mathinna Beds.

St Marys Porphyrite (Early Devonian) (Dpr, Dpm)

N. J. Turner

Previous workers (e.g. McNeil, 1965) have regarded the St Marys Porphyrite as an intrusive body. However, evidence is presented in this report and elsewhere (Turner *et al.*, 1986) that the northern and eastern part of the body (Dpr)

is extrusive whilst the south-western part is intrusive (Dpm). This evidence is dealt with in detail in the section of the report concerned with igneous rocks.

In brief, the northern and eastern part of the body is regarded as extrusive because its relationship with the underlying rocks appears to be superpositional and does not involve significant thermal metamorphism. In addition there is locally preserved vitroclastic texture in tuff-like rocks above the basal, northern contact. The widespread, shallowly-dipping foliation in Dpr appears to be due to compaction and small, igneous inclusions give rise to a eutaxitic style of texture in part of the basal zone. Layers rich in metasedimentary lithic fragments are probably equivalent to parts of ash-flow units and changes in matrix texture with height above the basal contact are consistent with progressive recrystallisation of glass. The composition of Dpr is essentially dacitic with minor rhyolitic material near the base. The estimated minimum thickness of the sequence is about 1400 m.

Lower Parmeener Super-Group

C. R. Calver

INTRODUCTION

The Lower Parmeener Super-Group (Forsyth *et. al.*, 1974) within the St Marys Quadrangle is an essentially flat-lying sequence unconformably overlying a basement of cleaved and folded Siluro-Devonian Mathinna Beds and Devonian granitic rocks. The sequence is thinner than in most other parts of Tasmania, as the north-east region (including the St Marys Quadrangle) formed a broad basement high (Banks, 1962), and consequently the Lower Marine Sequence (Forsyth *et. al.*, 1974) is usually missing. Also, the Upper Marine Sequence is condensed, and is truncated by a phase of erosion that preceded deposition of the overlying Upper Parmeener Super-Group. The Lower Parmeener Super-Group within the St Marys Quadrangle is wholly Permian in age.

Within the map sheet, the thickness of the Lower Parmeener Super-Group varies markedly in response to basement relief and to the later erosive phase. The known thickness ranges from 7 m to 172 m.

The sequence is well exposed in some creeks that run steeply off the north slopes of the Nicholas Range [EQ930000], the east and south slopes of Mt Elephant [FP038915], and the lower eastern slopes of the Fingal Tier. Over most of the area of the Quadrangle, the Lower Parmeener Super-Group exists in the subsurface. Two fully cored drill holes fully intersect the sequence, hole 9 [EQ886011] and hole 85 [EP912905]. The Killymoon and Harefield boreholes (at EP915960 and EP983925 respectively) also intersected the whole sequence but the cores were discarded. South of the southern edge of the map sheet, Seymour no. 4 borehole [FP067767] and Department of Mines no. 10 borehole (FP045733, at Douglas River) penetrated the whole sequence. The latter intersected a section unusually thick by virtue of the presence of a substantial Lower Marine Sequence correlate. The lithostratigraphy and biostratigraphy of this cored section are described by Calver *et al.* (1984).

Voisey (1938), Walker (1957) and McNeil (1965) all subdivided the Lower Parmeener Super-Group, from work in different parts of the Quadrangle. A subdivision similar to that of McNeil (1965) was found to be most widely applicable. His 'Gray Siltstone and Sandstone' could not be recognised and was not differentiated; and the glauconitic sandstone was mapped as a separate formation. The Lower Parmeener Super-Group is thus divided on the geological map, into four conformable formations: the lowest, Ps, of dominantly quartzarenite and shale, with intermittent basal conglomerate, passing up into poorly sorted sandstone and mudstone; Pc, of bioclastic limestone, calcareous mudstone and sandstone, usually richly fossiliferous; Pag, of pebbly glauconitic sandstone; and Pam, of unfossiliferous, poorly bedded, poorly sorted mudstone. Ps, except perhaps for its topmost part, belongs to the Lower Freshwater Sequence; the rest are part of the Upper Marine Sequence.

BASEMENT TOPOGRAPHY

Basement topography may be inferred by using Pag as a datum. This unit, usually 2–3 m thick, is a convenient marker horizon over most of the map sheet. It was not affected by the later erosive phase, and overlaps all known basement highs. It is not appreciably diachronous. An isopach map of the sequence below Pag therefore probably closely reflects basement topography (fig. 3).

The most pronounced high is centred on Yorkys Creek [FQ991018], with only 3–5 m of sub-Pag sediments overlying basement. The sequence thickens rapidly to the west, with a maximum combined thickness of Ps and Pc of about 140 m around Huntsmans Creek [EQ945025] before becoming thinner again between Durham Creek and the western margin of the quadrangle, in response to a broader and less pronounced basement high. South of the Yorkys Creek high, the sub-Pag sequence thickens rapidly to about 100 m, and remains relatively constant as far south as Piccaninny Creek [FP047835]. A small basement high just south of St Patricks Head [EQ968030] is tentatively inferred from high-level granite now stripped of its Permian cover. Just south of the map sheet, the sequence again thickens rapidly in response to the localised basin intersected by the Douglas River borehole, which contains the oldest known Lower Parmeener Super-Group rocks in the region (Calver *et. al.*, 1984).

Palaeocurrents in the lower part of Ps in the Huntsmans Creek area have a strong preferred southerly direction (see later section), suggesting that the basement low there extends southward as a deepening trough, probably merging with the small basin at the Douglas River.

DOMINANTLY QUARTZARENITE AND SHALE (Ps)

Ps is essentially a fining-upwards sequence, with impersistent basal conglomerate, predominant quartzarenite and siltstone, shale becoming prevalent towards the top, and culminating in probably marine pebbly bioturbated sandstone and mudstone.

Over most of the quadrangle, the top of Ps is taken at the base of the first poorly-sorted bed, usually a mudstone with marine fossils, assigned to the overlying formation (Pc). In the far western part of the quadrangle, however, between the Break O'Day River [EP845948] and Beauty Flats [EQ860020], Ps has been more

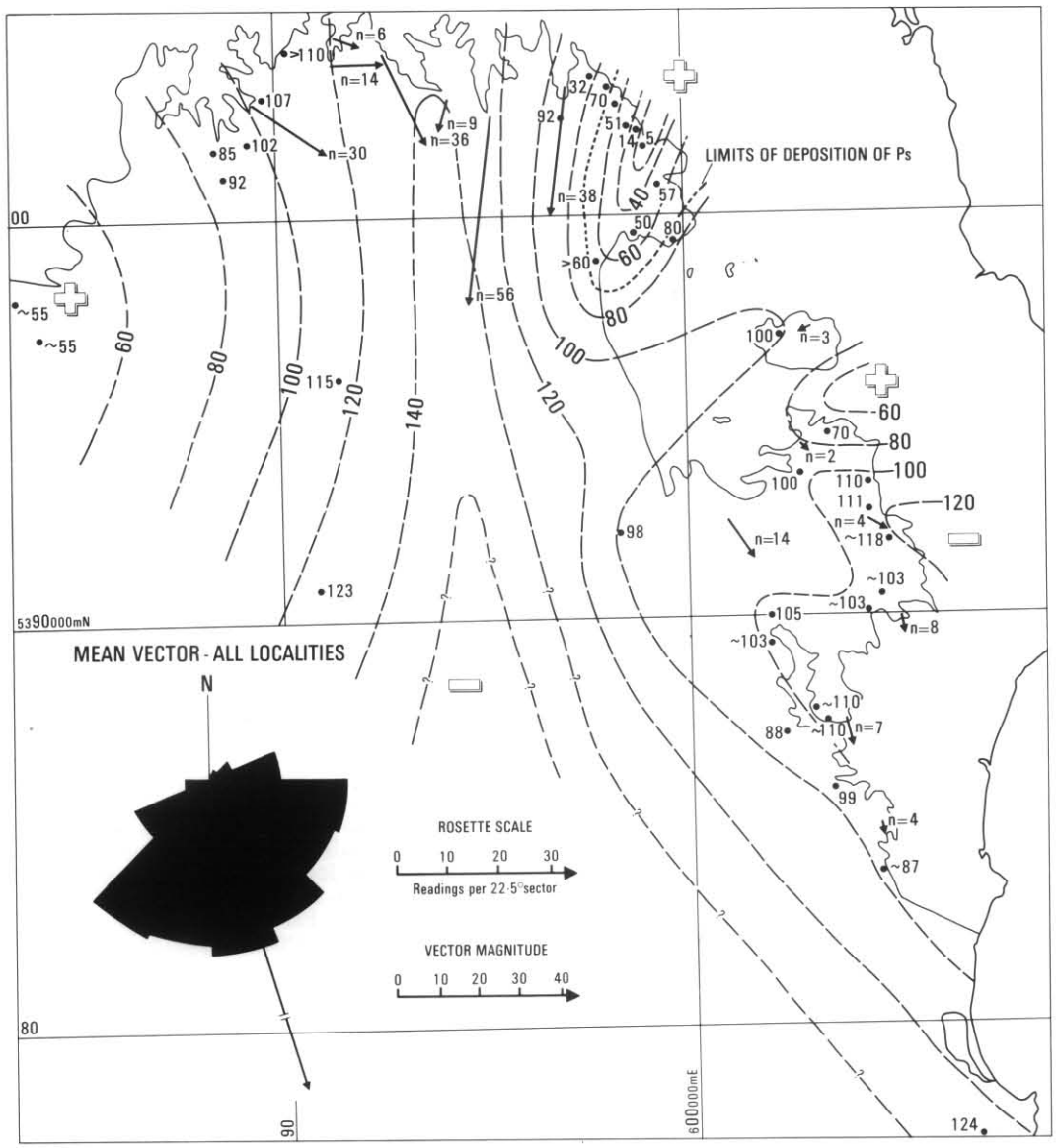

Figure 3. *Inferred Permian basement topography and palaeocurrent vectors in the lower part of* Ps *(Lower Freshwater Sequence equivalent).*

broadly defined to include some poorly-sorted mudstone and sandstone, probably partly equivalent to the lowest beds of Pc elsewhere, and the top of Ps is taken at the base of the first calcareous bed (P.W.B.).

The thickness varies in response to basement topography, averaging 20–40m over most of the map sheet, with a known maximum of about 70 m in Huntsmans Creek [EQ945025]. The formation is incomplete or absent over basement highs. On the Yorkys Creek basement high, Ps is overlapped by Pc (fig. 3).

LITHOSTRATIGRAPHY

Ps is divided below into a number of facies that are complexly interbedded but tend to be arrayed in the sequence described below. The sequence is incomplete over basement highs. The best exposed sections, illustrating this lateral variability, are shown in Figure 4.

Basal rudite-dominated facies

On Mathinna Beds the unconformity usually shows, on outcrop scale, irregular relief controlled by pre-existing joints. Neptunean dykes penetrate opened joints in the basement, in places surrounding angular blocks to form an *in situ* breccia (plate 7).

A unit of breccia and conglomerate usually follows, but is only rarely developed on granitic basement. It is usually less than 10 m thick, and attains a maximum thickness of 17 m in borehole 85 [EP913904].

The basal breccia consists of joint-bounded blocks of Mathinna Beds lithologies, up to 0.4 m in diameter, in open-framework, with a moderately sorted arkosic sandstone matrix. No fabric or imbrication is evident. Crude stratification may be defined by variations in clast-matrix proportion. Within a few metres, the rock becomes texturally more mature, typically an open-framework conglomerate containing well-rounded pebbles of quartzite (mostly psammitic Mathinna Beds) and vein quartz, with beds of coarse arkosic quartzarenite.

The Huntsmans Creek section has an unusual development of carbonaceous rocks in this part of the sequence. The basal breccia becomes rich in carbonaceous material, before passing upwards into about 0·5 m of coal, overlain by a few metres of carbonaceous laminated fine-grained sandstone (fig. 4). The conglomerate in borehole 85 contains sparse flecks and wisps of reworked coal.

Over granitic basement, the usual basal lithology is an immature coarse arkose, in places difficult to distinguish from weathered granite. Well-sorted coarse arkose with lenses of pebble conglomerate, typically follows. Pebbles of granitic lithologies are rare.

Quartzarenites

Five to ten metres of cross-bedded sandstones ranging from very coarse arkoses to medium-grained quartzarenites overlie the basal conglomerate, or directly overlie basement. Cross-bedded sandstones are absent from moderately attenuated sections, but are well-developed between Durham Creek [EQ891022] and Catos Creek [EQ970028], and at most localities around and south of Mt Elephant. They often form cliffs. Bedding tends to be undulose and lenticular; trough and planar cross-bedding are developed with sets up to one metre, usually 0·2–0·5 m, thick. Interbeds of fissile, micaceous and carbonaceous sandstone are present. Pebbly horizons may be developed.

At FP037967 on the east slopes of St Patricks Head, and at EQ978034 in Bolpeys Creek, a distinctive massive bimodal quartzarenite crops out within a few metres of the unconformity. It consists of quartz granules and coarse sand in an abundant quartz siltstone matrix. Many of the larger grains resemble phenocrysts from the St Marys Porphyry (N. J. Turner, pers. comm.), in thin section displaying rounded, embayed and pitted outlines.

There is an upward transition from cross-bedded quartzarenite into flat-bedded, flaggy, medium to very fine-grained quartzarenite. This tends to be medium to thin-bedded, with coarse flakes of mica and comminuted plant debris on interbed partings. Ripple cross-lamination is abundant. The flaggy, ripple cross-laminated sandstone is best developed in Huntsmans Creek, where it is about 20 m thick. It may be interbedded with the laminated siltstone and shale described below.

Laminated siltstone and shale

Typically present near the top of Ps is an interval up to 20 m thick, in which dark grey carbonaceous shale and light-coloured fine quartzarenite or siltstone are thinly interbedded or interlaminated. Either lithology may be predominant. Flaser bedding is usual, with the siltstone laminae displaying blebby, lenticular forms and low-angle festoon cross-lamination (plate 8). Plane lamination is less commonly developed. Small-scale slumping, convolute lamination, and load structures are all rarely seen. This facies is best exposed in Durham Creek, Elephant Farm Creek (fig. 4) and Piccaninny Creek [FP048836].

In Piccaninny Creek, the sand flasers are unusually coarse: of coarse sand to granule grain size.

Rare lonestones are found in this facies, most notably a granite boulder, one metre in diameter, at FP041855. In borehole 9, Durham Creek, Catos Creek, (fig. 4), and Gleadow Creek [EQ873017] coal seams are present near the transition between the laminated shale and siltstone and the overlying bioturbated sandstone

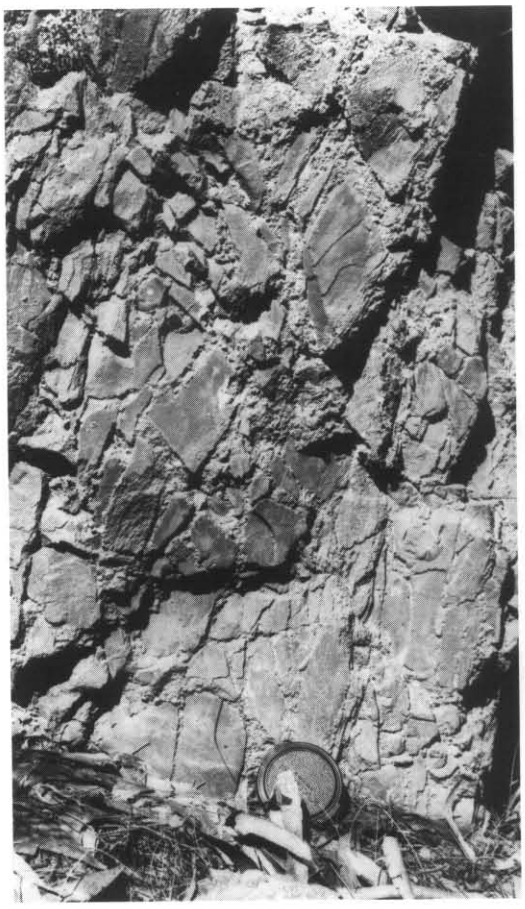

Plate 7. *Network of sandstone-filled neptunean dykes penetrating Mathinna Beds basement immediately below the unconformity at FP044856. Lens cap is 50 mm in diameter.*

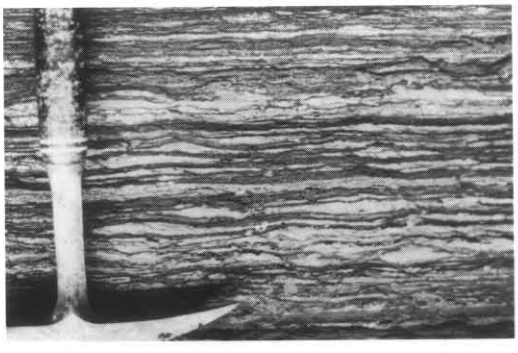

Plate 8. *Flaser bedding at Durham Creek [EQ893019]. Lenses and pods of fine-grained quartz sandstone interlaminated with carbonaceous shale. There is slight bioturbation.*

facies. They are very thin (a few centimetres) except for two seams, 0·2 m and 0·6 m thick, in Catos Creek. The coals are pyritic, and in drill core are associated with melanterite, a hydrous iron sulphate (J. L. Everard, pers. comm.). Plant fossils including *Glossopteris* are preserved in carbonaceous shale at EQ922045.

Bioturbation appears in the top part of the laminated siltstone and shale interval. It is evident as random, or sometimes predominantly horizontal, burrow-fillings of sand in mud, or mud-lined sand fillings in sandstone, about 5 mm in diameter (plate 9). Larger (50 x 10 mm) vertical escape structures may also be present.

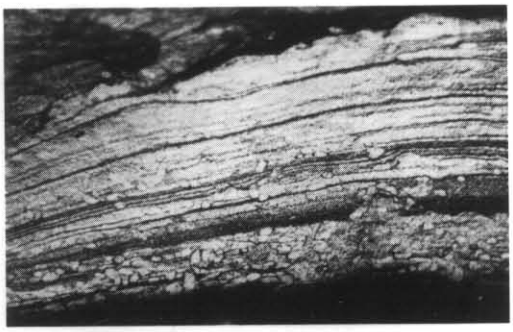

Plate 9. *Sand-filled burrows, each about 5 mm in diameter, in laminated siltstone and shale.*

Bioturbated sandstones

Usually developed at or near the top of Ps is 2–4 m of thoroughly bioturbated thickly-bedded to massive fine-grained quartz sandstone. This unit is erosionally resistant and may crop out prominently. Burrow mottling is usually pervasive and conspicuous, and in places the rock is homogenised to an almost uniform, grey, slightly muddy sandstone. Pebbles are present as lonestones and as conglomerate horizons. Fragments of coal are common and at EQ886018, two transported silicified logs were seen. In borehole 9 (fig. 4), a few disoriented and disarticulated large spiriferids and fragments of probably *Eurydesma* occur within this interval.

Carbonate concretions, and calcite-cemented quartzarenites displaying lustre mottling, were observed in a few places. The calcite cement partially replaces the grains, but in thin section (M82), feldspar grains and rock fragments are relatively well-preserved. Muscovite, microcline, orthoclase and plagioclase are present, and rock fragments of chert, mudstone and fine-grained quartzite.

Highly attenuated sections

The thinnest developments of Ps are exemplified by sections near EP999994 ('Rays Hill' locality of earlier workers) on the eastern flank of the Yorkys Creek basement high, and at EQ982032 (Binns Creek) on the western flank.

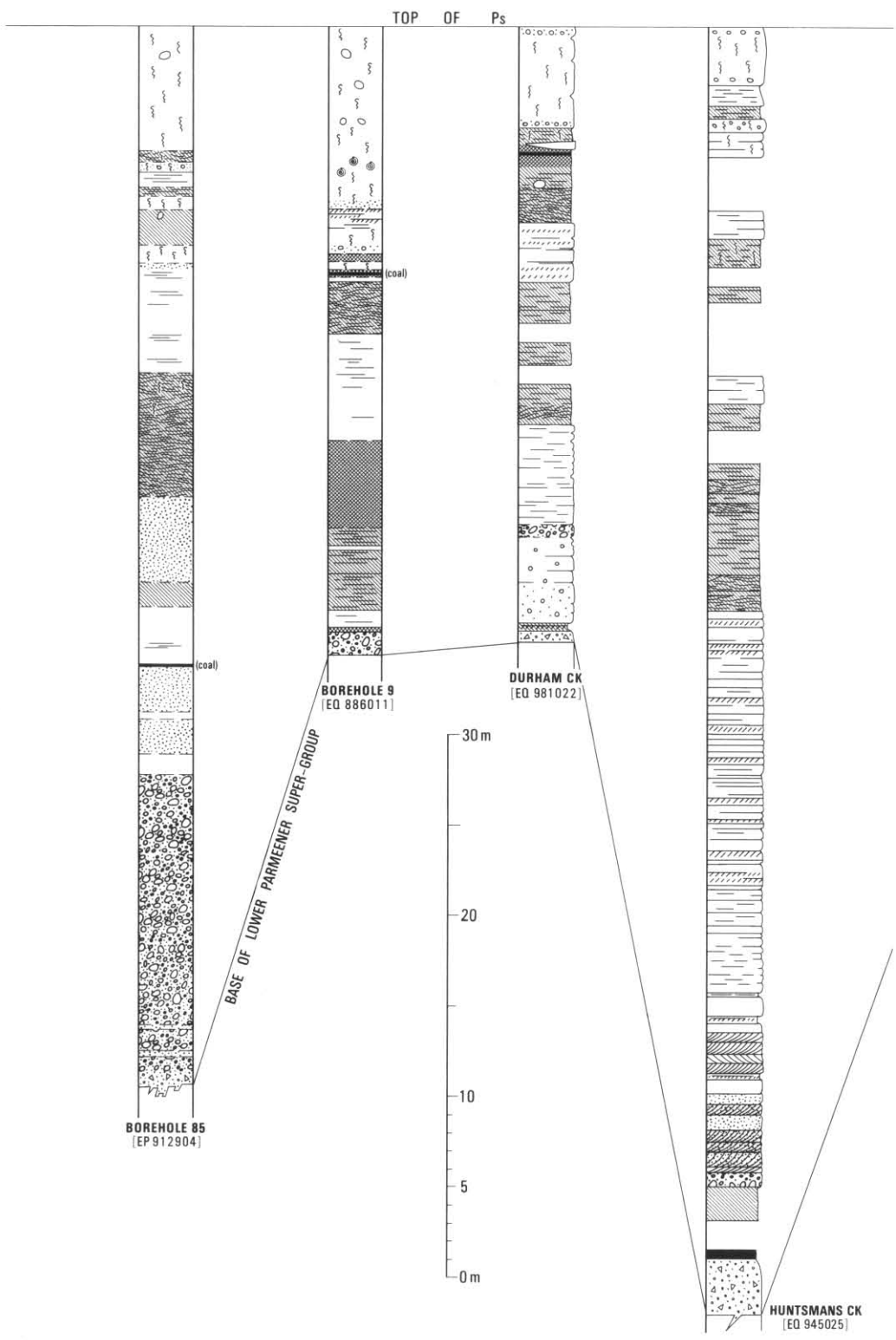

Figure 4. *Selected measured sections through* Ps.

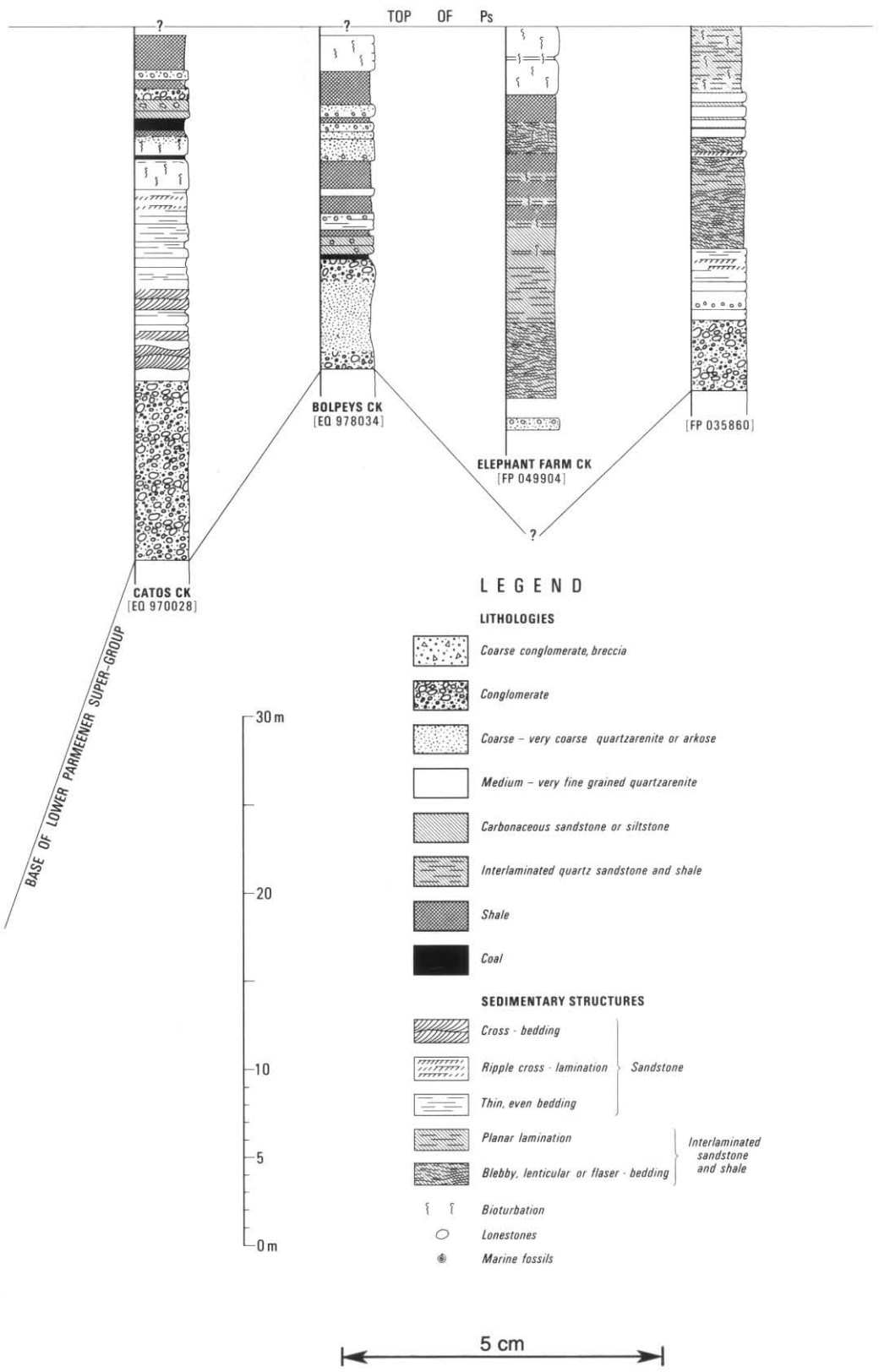
TOP OF Ps
?
?
?
BOLPEYS CK
[EQ 978034]
ELEPHANT FARM CK
[FP 049904]
[FP 035860]
CATOS CK
[EQ 970028]
BASE OF LOWER PARMEENER SUPER-GROUP
30 m
20
10
5
0 m
LEGEND
LITHOLOGIES
Coarse conglomerate, breccia
Conglomerate
Coarse – very coarse quartzarenite or arkose
Medium – very fine grained quartzarenite
Carbonaceous sandstone or siltstone
Interlaminated quartz sandstone and shale
Shale
Coal
SEDIMENTARY STRUCTURES
Cross - bedding
Ripple cross - lamination
Thin, even bedding
Sandstone
Planar lamination
Blebby, lenticular or flaser - bedding
Interlaminated sandstone and shale
Bioturbation
Lonestones
Marine fossils
5 cm

At the former locality the unconformity is exposed. Coarse arkose at the base passes up into several metres of fine-grained quartzarenite, with a thin coal seam 3 m above the unconformity. Nearby, at EP996992, within 3 m of basement there crops out a gritty fine quartzarenite with sparse flecks of coal; pebbles and cobbles are sparsely concentrated along a few horizons. Near the top of this 3 m thick interval there are abundant flattened, strap-shaped coalified woody fragments and poorly-preserved *Glossopteris* impressions. The overlying 2 m of pebbly, bioturbated fine-grained quartzarenite contains an abundant shelly fauna, dominantly gastropods. The top of Ps probably closely succeeds this bed but is not exposed.

At Binns Creek, on the western flank of the high, Ps probably does not exceed 10 m in thickness. The basal 4 m are exposed, consisting of interbedded boulder conglomerate, pebble conglomerate and laminated shale. The lowest beds contain a two metre-long granite boulder.

Relatively incomplete at Durham Creek (fig. 4), Ps becomes thinner to the west in response to a broad basement high. In the area between the Break O'Day River [EP845948] and Beauty Flats [FP860020] Ps is much attenuated, but on the geological map the unit has been more broadly defined to include overlying poorly-sorted non-calcareous mudstone and sandstone. Here, the sequence begins with about 10 m of thick-bedded, sparsely pebbly, fine-grained quartzarenite. Rare marine fossils (brachiopods, bryozoans and molluscs) occur near the top of this interval. Then follows about 20 m of sparsely fossiliferous, poorly-sorted sandstone, pebbly siltstone and mudstone. This latter part of the sequence is assigned to Ps, but is equivalent to the lowest Pc as used elsewhere on the map-sheet. The first occurrence of calcareous beds marks the base of Pc in this western area (P.W.B.).

The combined thickness of Ps and Pc in this area, between 50 and 60 m, is thinner than Pc alone in more fully-developed sections, suggesting that Ps (even as narrowly defined) is locally diachronous, and younger over this western basement high, than elsewhere on the map sheet.

PALAEOCURRENTS

In the cross-bedded sandstone near the base of Ps, foreset dip directions were measured in selected areas of good outcrop. Palaeocurrent directions from any one locality are unimodal but vary systematically from place to place (fig. 3).

Basement relief appears to be the controlling influence, as vector means are roughly tangential to known basement highs. The prevailing direction is from the north or north-west. As mentioned previously and indicated on Figure 3, the drainage pattern suggests that the basement low at Huntsmans Creek continues and deepens to the south.

PALAEONTOLOGY

Well-preserved plant fossils are rare and only *Glossopteris* has been tentatively identified at two localities mentioned above.

Macro-invertebrates are also rare, being known only from the top of the formation in borehole 9 (heavy-walled spiriferids and *Eurydesma*), rare bryozoans, brachiopods and bivalves in the Beauty Flats–Break O'Day area and the more abundant fauna at 'Rays Hill'. Here, leached fine-grained quartzarenite contains abundant moulds of *Keeneia, Peruvispira, Sulciplica, Trigonotreta, Ambikella, Etheripecten, Deltopecten, Eurydesma* and *Vacunella* (M. J. Clarke, pers. comm.). Poor preservation precludes identification to species level.

DEPOSITIONAL ENVIRONMENTS

The basal rudite consists entirely of material derived from local basement, and contain no suggestions of marine influence (such as marine fossils or exotic lonestones). They probably reflect subaerial weathering followed by localised fluvial reworking. The succeeding cross-bedded quartzarenites were laid down by south-flowing streams that were diverted around local basement highs. The competence of the streams waned as base level rose, and ripple-laminated sandstones and some laminated siltstones and shales were deposited.

Rare lonestones of up to boulder size suggest that the laminated facies is, at least in part, paralic or marginal marine. The common flaser and lenticular bedding suggest littoral deposition. The carbonaceous shales and thin sulphurous coals probably reflect a restricted paralic environment.

The bioturbated sandstone facies contains more abundant evidence of marine influence. Lonestones are common. Marine macrofossils are occasionally present. Similar rocks in the Douglas River borehole, south of the St Marys quadrangle, contain abundant acritarchs (Truswell, *in* Calver *et al.*, 1984). The sparsity of shelly benthos, in conjunction with the abundant infauna, suggest that brackish or schizohaline conditions prevailed.

The thinnest developments of Ps, on basement highs at 'Rays Hill' and in the Break O'Day–Beauty Flats area, are evidently shallow-marine as suggested by the presence of marine fauna.

The thickest development of Ps, in Huntsmans Creek, comprises an anomalously thick development of the Lower Freshwater Sequence. The coal seam near the base of this section, if paralic — as are those higher in the sequence, may represent marginal conditions at the conclusion of Lower Marine Sequence sedimentation.

AGE AND CORRELATION

The lithologic correlate of Ps in the Douglas River borehole has been entirely referred to the Lower Freshwater Sequence (Calver *et al.*, 1984). If the term 'Lower Freshwater Sequence' is used, *sensu* Forsyth *et. al.*, 1974, as a lithostratigraphic term, then the upper parts as well as the lower parts of Ps are assignable to this Sequence. Where fully developed, such as at Huntsmans Creek, Ps is considerably thicker than other developments of the Lower Freshwater Sequence in Tasmania. It is probably comparable to the Douglas River section where palynological data indicate that the Lower Freshwater Sequence extends over a greater timespan than elsewhere (Truswell, *in* Calver *et al.*, 1984). Here, the lower part of the sequence contains a Substage 3a microflora (Late Tamarian), older than known non-marine sequences elsewhere in Tasmania. A Stage 4 microflora at the very top suggests that the top may also be younger.

LIMESTONE, CALCAREOUS MUDSTONE AND SANDSTONE (Pc)

Pc is composed of interbedded massive fossiliferous mudstone, siltstone and sandstone, all generally poorly-sorted and calcareous; and bioclastic limestone. The formation is variable laterally and vertically, but generally the terrigenous lithologies predominate in the lower half of the unit, and limestone predominates in the upper half.

The formation is about 65 m thick everywhere on the map sheet except over basement highs in the Break O'Day–Beauty Flats and Yorkys Creek areas. On the latter, it thins to a minimum of only 3–5 m. Resistant limestones in the upper part of the formation often crop out prominently, but exposure is otherwise poor. The most complete sections are exposed at Durham Creek [EQ893013], and in creeks draining the southern slopes of Mt Elephant [FP024904, FP049908]. These and others are shown in Figure 5.

LITHOSTRATIGRAPHY

The usual succession of lithologies is as follows. The lowest 5 m or so consist of poorly-bedded, poorly-sorted dark grey mudstone and bioturbated siltstone, with minor sandstone and fine-grained silty limestone. Simple foraminifera (described later) are present but other shelly fossils may be initially rare. Higher up, ramose bryozoans and fenestellids become particularly abundant and brachiopods and molluscs are common. Fenestellids are oriented subparallel to bedding and are often sufficiently abundant to impart a fissility to leached mudstone in outcrop. Fossiliferous mudstone predominates up to about 30 m above the base of the formation, with subordinate medium to thick beds of tough limy sandstone and sandy calcarenite.

Sections at Elephant Farm Creek (FP049908, fig. 5) and to the south around FP035859, differ in that they contain developments of uninterrupted thick-bedded sandy calcarenite 6 m or more in thickness, near the base of the formation. A thin section of this limestone from Elephant Farm Creek contains mostly ramose bryozoan fragments, some molluscan and brachiopod debris and a few per cent fine quartz sand. The bioclasts display considerable compactive crushing, there is no calcite cement and pore space is filled with authigenic clays.

Limestone predominates through the rest of the formation. Subordinate interbeds and beds of terrigenous lithologies, typically bryozoal mudstone, are present in the lowest and topmost parts of this interval, leaving the middle third of the interval (*i.e.* approximately between 10 and 20 m below the top of the formation) as relatively pure carbonate. This part of the section often crops out as cliffs. The limestone is pale grey to off-white, thick-bedded to massive bioclastic calcarenite, of fine to very coarse grain size, with a minor admixture of quartz sand and gravel. Most fossils are fragmented but large spiriferids and fallen fenestellid fronds remain intact in some beds. Minor lenticular patches of the rock have been replaced by chalcedony. Stylolites parallel to the bedding are rarely observed. In some sections there is a coarsening-upward trend culminating in a bed of very coarse calcarenite to calcirudite (1–10 mm grain size), a few metres thick, 10-15 m below the top of the formation. Such coarse limestones may occur, however, lower in the section (e.g. Elephant Farm Creek, fig. 5).

Bedding in the limestones may be strongly lenticular. At Elephant Pass [FP034896], two thick pods of very coarse biocalcarenite, about 1–2 m thick and 2–5 m long, occur in one horizon. The pods have rounded extremities and their lower surfaces are more strongly convex than their upper surfaces. Bedding in the surrounding limy mudstone is distorted by differential compaction. They probably originated as isolated dunes of coarse bioclastic debris on a muddy sea floor. Early submarine cementation of the pods, followed by differential compaction, probably contributed to their remarkably thick form.

In thin section, the coarser limestones are seen to consist entirely of bioclasts, cement, and a few per cent quartz sand. They are well-washed and mud-free. Bioclasts are predominantly bryozoan fragments with lesser proportions of mollusc, brachiopod, and crinoid debris. Ultrastructure is well-preserved. Clear, coarse calcite occludes porosity; a single crystal may fill an entire complex pore space. Crinoid ossicles display syntaxial overgrowths. The open, uncompacted fabric of the clastic constituents (e.g. E324, plate 10), suggests that cementation was very early.

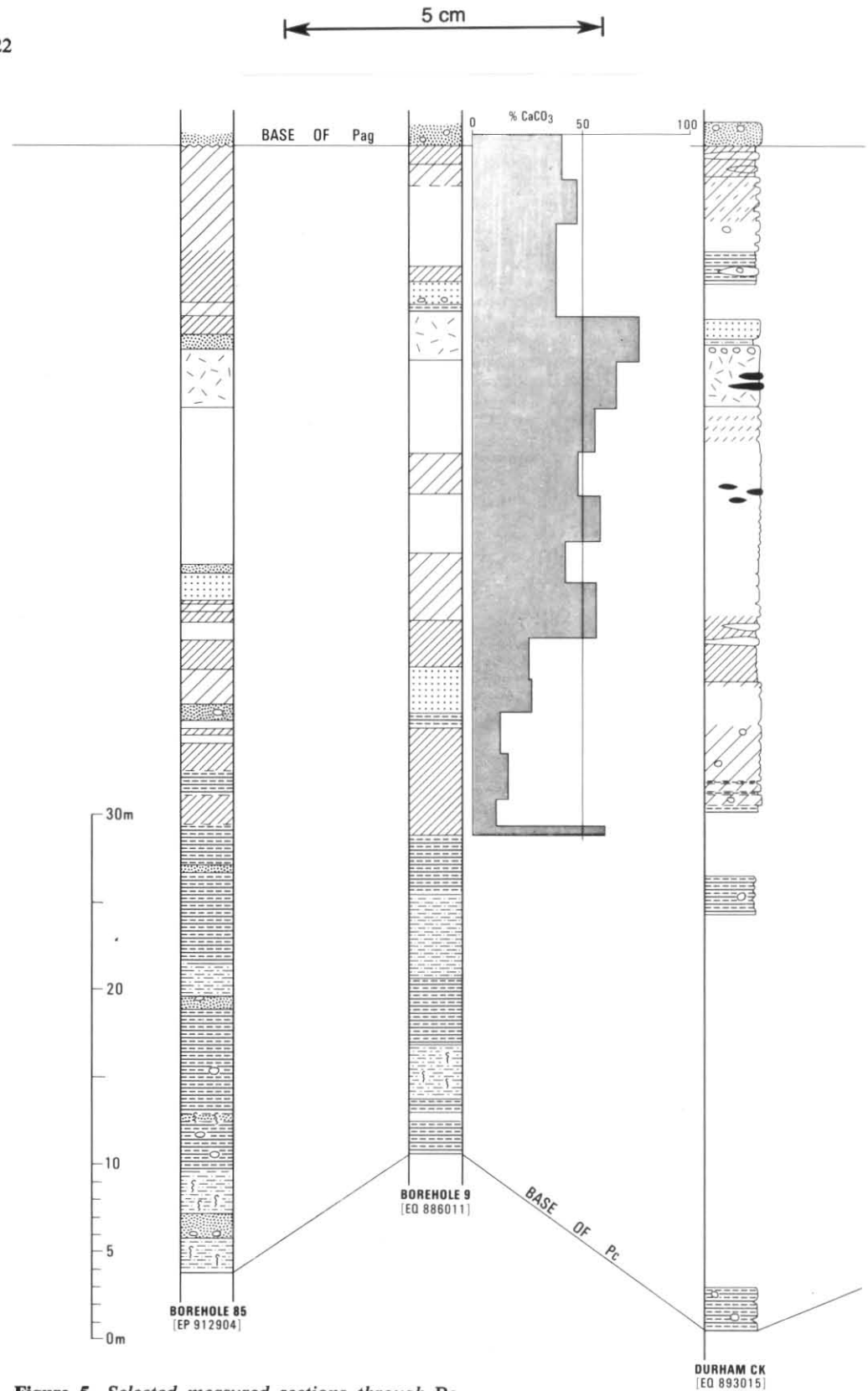

Figure 5. *Selected measured sections through* Pc.

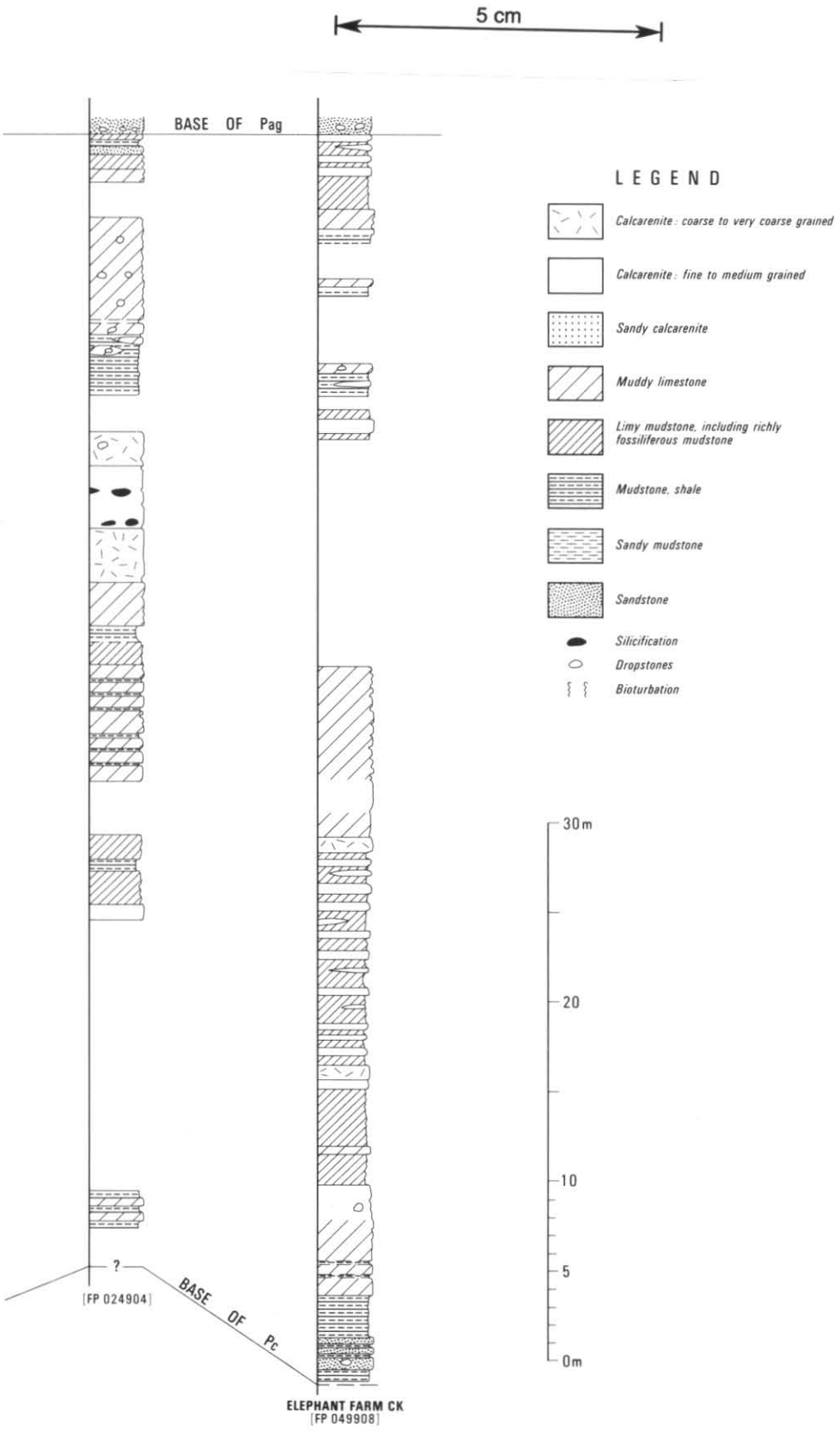
5 cm
BASE OF Pag
LEGEND
Calcarenite : coarse to very coarse grained
Calcarenite : fine to medium grained
Sandy calcarenite
Muddy limestone
Limy mudstone, including richly fossiliferous mudstone
Mudstone, shale
Sandy mudstone
Sandstone
Silicification
Dropstones
Bioturbation
30m
20
10
5
0m
?
BASE OF Pc
[FP 024904]
ELEPHANT FARM CK
[FP 049908]

Plate 10. *Thin section of coarse-grained calcarenite (x 12, plane-polarised light). Open, uncompacted fabric supported by coarse sparry calcite cement. Fossil fragments are predominantly bryozoans, with some punctate brachiopods and crinoids (lower left). Sample E324 [FP049908].*

Fine calcarenites are similarly composed except bioclasts are more finely comminuted and crinoid ossicles are rare. Micrite and/or microspar fills pore space.

Figure 5 shows $CaCO_3$ and $MgCO_3$ contents of continuous split-core samples from the calcareous portion of Pc in borehole 9 [EQ886011]. $CaCO_3$ content increases upwards, attaining a maximum of 75·2% in the coarsest calcarenites 10–12 m below the top of the formation. In aggregate, this section contains only 42·9% $CaCO_3$ and 1·1% $MgCO_3$, with 51·4% acid insoluble including 45·4% SiO_2, 1·3% Fe_2O_3, 3·8% Al_2O_3, and 0·25% P_2O_5 (Analyst K. Austin, arranged by V. M. Threader).

Lonestones are common in Pc, except for the interval approximately between 15 and 35 m below the top of the formation, in which none were observed in the measured sections. Rarely, they are concentrated along particular horizons. Commonest lithologies are quartzite, vein quartz and granitic rocks. A 0·5 m boulder of quartz-feldspar porphyry resembling the St Marys Porphyry was observed, and a one metre boulder of quartz-mica schist.

There are no major facies changes associated with the Yorkys Creek basement high. This feature was emergent during deposition of most of Pc, but was evidently too small to have been a substantial source of terrigenous material.

Incomplete sequences on the basement high are well exposed on Scamander Road [EQ987027] and nearby creeks, and in creek sections at EQ995009 and EP988996. In the latter section, the basal few metres is a winnowed calcirudite consisting mostly of abraded fragments of *Eurydesma*, with lesser amounts of brachiopod and crinoid debris, and terrigenous gravel. The lower parts of incomplete sections in the Yorkys Creek area typically consist of thick-bedded sparsely fossiliferous ostracodal calcareous siltstone (well exposed on Scamander Road). The upper parts are comparable to equivalent horizons elsewhere on the map sheet.

To the west, in the Break O'Day–Beauty Flats area [EP845945–EP850010], as mentioned previously Pc is somewhat attenuated over a less pronounced basement high. As depicted on the geological map, Pc in this area has been more narrowly defined to include only the upper calcareous part of the generalised sequence described above. This sequence is 20–25 m thick, beginning with a distinctive calcareous siltstone rich in *Anidanthus*, succeeded by calcareous bryozoal mudstone and siltstone, with a relatively thin (4–5 m) development of limestone near the top (P.W.B.).

PALAEONTOLOGY

Most of the formation is richly fossiliferous. Leached mudstone or siltstone provides the most readily identifiable material. Fourteen fossiliferous outcrops selected by C. R. Calver and R. H. Castleden were examined in the field by M. J. Clarke, who identified the forms listed in Table 1. The table shows the distribution of the taxa between localities and indicates the approximate relative stratigraphic positions of the localities. Faunal elements not listed include crinoid debris, ostracods and the enormously abundant fenestellids and other bryozoans.

The lowest assemblage (locality 1) includes *Cancrinella, Ambikella ovata*, and *A. profunda* indicating a Bernacchian age (Clarke and Farmer, 1976). *Taeniothaerus subquadratus* and *Terrakea pollex*, usual indicators of a Late Bernacchian age (Faunizone 5 of Clarke and Banks, 1975) were not recorded at the localities tabulated but the former appears near the base of Pc at Elephant Pass, and the latter enters only a few meters above the base of the correlate of Pc in the Douglas River borehole (Clarke *in* Calver *et. al.*, 1984), suggesting that the base may be in Faunizone 5. Within 15 m of the base of Pc (localities 2, 3, 4) other taxa indicating an age not older than Faunizone 5 are found (*Trigonotreta wairakiensis, Ambikella plana, Etheripecten fittoni).*

Table 1

DISTRIBUTION OF TAXA AMONGST SELECTED LOCALITIES, SHOWING APPROXIMATE STRATIGRAPHIC DISTRIBUTION RELATIVE TO BASE AND TOP OF Pc

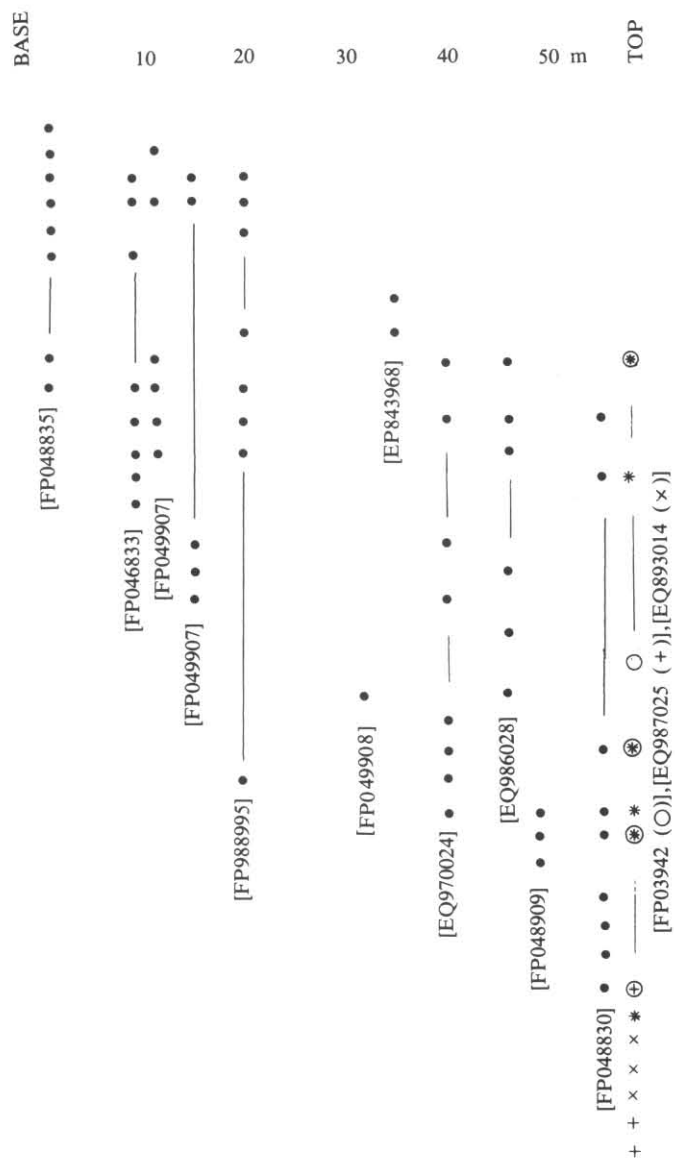

Forty metres above the base (locality 5) *Terrakea concava* is present, and is followed at higher levels by more forms indicative of a Lymingtonian age (Faunizone 6 and above) such as *Sulciplica transvera, Trigonotreta lethamensis*, and *Terrakea brachythaera.*

Elements of Faunizone 9 are present immediately below the top of the formation (*Fusipirifer avicula, Glendonia duodecimcostata*).

Pc thus ranges in age from probably Late Bernacchian (Faunizone 5) to late Middle Lymingtonian (Faunizone 9). South of St Marys Quadrangle, Pc correlates with similar calcareous sequences at Douglas River, the Friendly Beaches and Coles Bay. The formation is equivalent to the Counsel Creek Formation and the lower part of the Marra Formation (Clarke, *in* Clarke and Baillie, 1984) of Maria Island.

To the west, equivalents of Pc on the Ben Lomond Quadrangle have much reduced thicknesses of limestone, and mudstone is greatly predominant.

DEPOSITIONAL ENVIRONMENT

Shallow marine conditions with normal salinity were established with the onset of sedimentation of Pc. Winnowed (mud-free) calcarenites probably were deposited at or above wavebase, representing the accumulated debris of prolific shelly benthic organisms. Quieter conditions, probably below wavebase, prevailed as the muddy terrigenous sediments were laid down. Conditions varied spatially and temporally, but there was probably an overall upward-shallowing of environments through the sequence. There is no regular cyclic limestone-shale alternation as seen in the Berriedale Limestone (Brill, 1956; Rao, 1981).

The sediments progressively onlapped the Yorkys Creek basement high until its eventual burial near the end of deposition of Pc. Emergent during deposition of most of the formation, this feature was evidently too small to have been a substantial source of terrigenous material. The basal *Eurydesma* calcirudite at EP988996 may be a gravelly beach deposit representing the initial phase of transgression up the flanks of the high. Runnegar (1979) showed that *Eurydesma* is most abundant in rocks deposited on or near rocky shorelines.

Marine sedimentary rocks throughout the Lower Parmeener Super-Group contain a diversity of evidence for very low temperatures during sedimentation. Faunal evidence is reviewed by Clarke and Banks (1975); sedimentological evidence by Rao (1981). Palaeolatitude was high (80°S; Embleton, 1973). Glacial dropstones (lonestones) are common throughout the Upper Marine Sequence in St Marys Quadrangle. The apparent absence of dropstones from part of Pc may reflect a temporary climatic amelioration or more probably, merely an increased rate of carbonate deposition with concomitant dilution of the terrigenous input.

PEBBLY, POORLY-SORTED SANDSTONE, USUALLY GLAUCONITIC (Pag)

Pag is composed of essentially unfossiliferous thickly to very thickly-bedded poorly-sorted sandstone, with subordinate conglomerate and poorly-sorted mudstone. The glauconite content, rarely exceeding 15%, diminishes to the north and west, and is absent from outcrops in and north of the Fingal Valley and west of Huntsmans Creek [EQ951021]. The formation is only 2–4 m thick over most of the map sheet.

Pag is erosionally resistant and may form a distinct bench on hillside sections, often cropping out prominently or traceable as a line of boulder-sized rubble. It is an excellent marker horizon.

The formation is distinctly more pebbly than either Pc or Pam. Most beds contain 1–2% of scattered lonestones, but pebbles and cobbles are often concentrated into a horizon at or near the base of Pag, and may form a thin layer of clast-supported conglomerate with a glauconitic sandstone matrix. Two such layers are developed at Templestowe Beach [FP068811] and further north at FP037849. The clasts are rounded; lithologies include quartzite, vein quartz, cleaved quartzwacke and slate characteristic of the Mathinna Beds, phyllite, schist, chert, granitic rocks, and siliceous conglomerate.

The predominant lithology in Pag is tough, grey or yellow-brown,slightly glauconitic sublithic quartzwacke or sandstone, rarely mud-free. The sand fraction is 80–90% angular quartz; the rest is lithic fragments derived from the lithologies listed above, with K-feldspar, rare plagioclase, biotite and muscovite also present. Glauconite comprises 10–15% of the rock near the base of the formation but the proportion diminishes upwards in most sections. Rare patches of 50–80% glauconite were observed. The mineral occurs as structureless, cryptocrystalline, spheroidal to colloform peloids 0·125-0·5 mm in diameter but with a narrower size range in any one hand specimen. The glauconite has not been appreciably transported.

Pag abruptly overlies Pc. In some outcrops [FP068811, FP031861] and in borehole 85, the sharp, irregular bottom contact suggests a hardground or disconformity. At the above two outcrops and at FP025905, the top of the underlying mudstone bed contains what appear to be borings filled with glauconitic sandstone from the overlying bed.

An unusually thick (about 10 m) development of Pag occurs north of Mt Elephant at FP034942. Here, most of the section consists of thick-bedded to massive, very slightly glauconitic sandy mudstone that is sparsely fossiliferous. *Paraconularia* occurs near the top of this interval. Spiriferids at EP037896 are the only other fauna recorded from Pag.

Pag grades upward into the overlying mudstone (Pam), fining upwards through 1–2 m of fine-grained, tough, grey to purplish-grey, very

slightly glauconitic, sandy or silty mudstone. The top of Pag is taken as the top of the last resistant glauconitic or sandy bed.

CORRELATION

Pag passes west into a somewhat thicker (*c.* 10m) poorly-sorted non-glauconitic pebbly sandstone on the Ben Lomond Quadrangle. Pag is probably a lithological correlate of the Garcia Sandstone (McKellar, 1957) of the Poatina-Golden Valley area. To the south, slightly thicker developments of glauconitic sandstone are correlates of Pag at the Douglas River and Friendly Beaches. Pag correlates with the upper, glauconitic part of the Marra Formation (Early-late Middle Lymingtonian, Clarke *in* Clarke and Baillie, 1984) of Maria Island.

DEPOSITIONAL ENVIRONMENT

Glauconite accumulates in open-marine shelf environments with reduced sediment influx, and its formation is also favoured by cooler climates and upwelling (Odin and Matter, 1981). The well-oxygenated turbulent waters of shallow

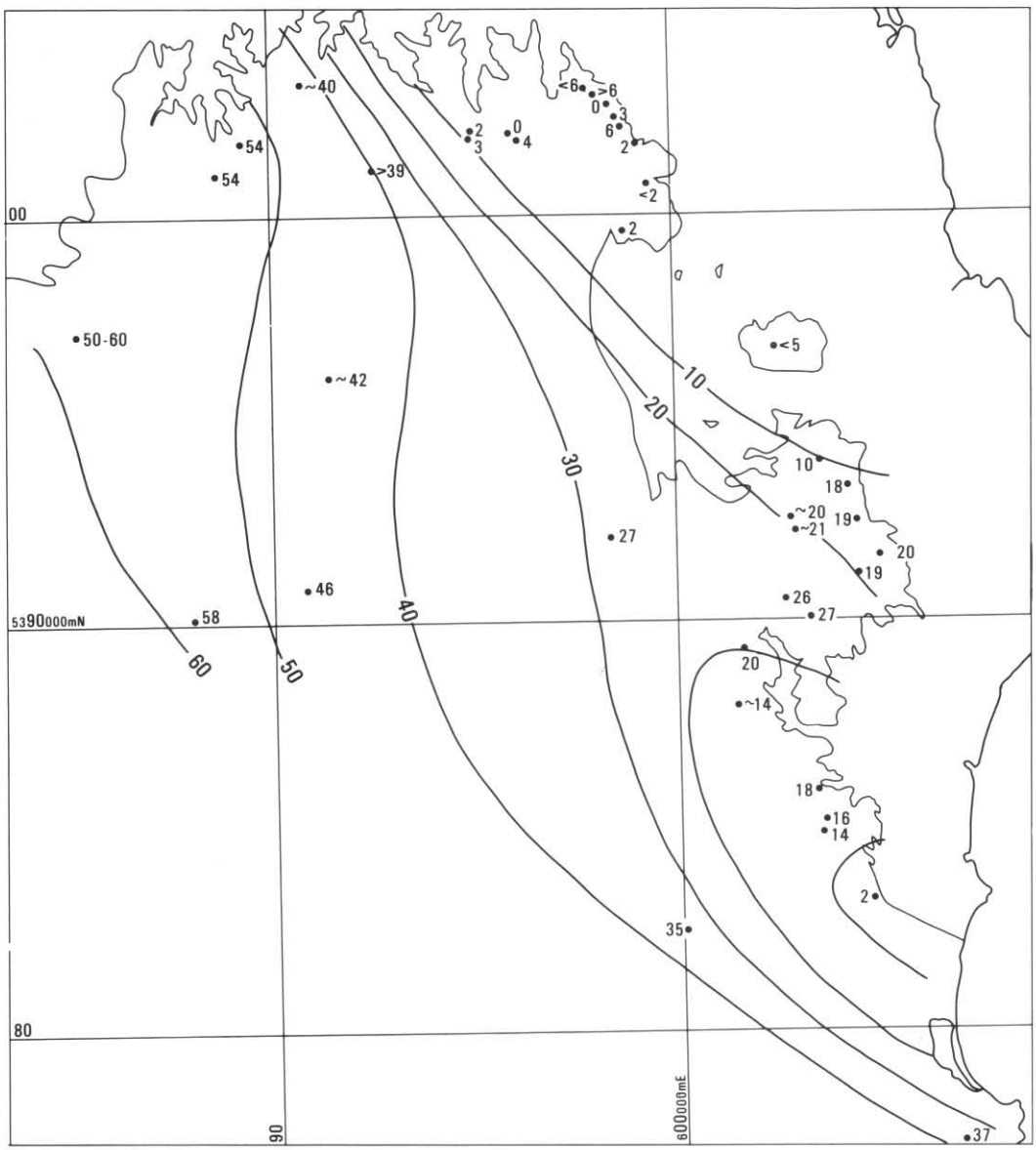

Figure 6. *Isopachs of poorly-sorted mudstone* (Pam), *thicknesses in metres.*

depths are unfavourable to glauconitisation *(ibid)*. For the deposition of Pag, a deepening relative to the coarse calcarenites of the upper parts of Pc is therefore indicated. The lateral transition to non-glauconitic sandstones in the north-western part of the quadrangle may reflect shallowing, increased sediment influx or a subtler chemical control.

Van Houten and Purucker (1984) in a review of ancient glauconite-bearing successions, show that the typical glauconitic formation overlies a sequence which coarsens and shoals upward. A hardground frequently occurs immediately beneath the unit and the abundance of glauconite decreases upwards into the overlying transgressive mudstones.

The sequence on St Marys closely follows this succession, except that the coarsest (shallowest?) limestones occur some 10–15 m below Pag. The abundance of pebbles and larger clasts suggests that ice rafting became a significant source of detritus, although this may be merely a result of reduced input from other sources. Locally, winnowing of fines led to the accumulation of conglomerate layers.

POORLY-SORTED MUDSTONE (Pam)

Pam is a rather uniform, poorly-bedded, slightly sandy grey mudstone. It is absent in the Binns Creek section, in the north-east [EQ983028], and thickens in a non-uniform manner, to the south-west (fig. 6) attaining a maximum known thickness of 58 m in borehole 4 [EP880900]. It is locally thin at 'E' Road [FP047831]. This thickness variation, as discussed below, is the result of an erosive phase that preceded deposition of the Upper Parmeener Super-Group.

The formation is erosionally recessive and outcrop is generally poor. Good exposure occurs in Durham Creek [EQ893014] and around FP016876. Borehole 4, as well as 9 and 85, intersects the whole formation. Most coal exploration holes on the Fingal Tier bottom in Pam, and boreholes 30, 32, 55 and 75 intersect substantial thicknesses of the formation.

In outcrop the mudstone is a medium grey colour, is closely-jointed and displays a distinctive weathering pattern in which the rock readily breaks up into 10–20 mm cuboidal fragments. Bedding is usually manifested as an alternation of uniform mudstone layers with poorly-defined, slightly shaly layers. Sparse, rounded lonestones are present throughout, of the same suite of lithologies represented in Pag and Pc.

Beds of tough grey siltstone, some carbonate-cemented, were occasionally observed, usually near the base of the formation. Rare calcite concretions, up to 0·3 m in diameter, are present.

The formation is unfossiliferous except for sparse foraminifera, described below.

In drill-core, the unweathered rock presents a rather different aspect. It is massive and very dark grey in colour; foraminifera and the arenaceous component are more readily visible. Sand and pebbles are both dispersed and concentrated into sharp-based, graded layers 10–50 mm thick. The lower surface is usually wavy or load-casted. Occasional small pockets or clumps of poorly-sorted pebbly sandstone occur. Some, being graded and vertically elongate (plate 11), are probably isolated load casts, others may have originated as till clasts. Foraminifera, too, are both dispersed and concentrated into clumps or thin layers, that are usually distinct from the sandy-pebbly layers. Rare coal fragments were observed in the Douglas River borehole.

Much of the formation is seen in drill-core to be silty mudstone that is faintly mottled, probably thoroughly bioturbated. Thorough bioturbation would explain the poor bedding and uniformity of the formation generally.

Cored sections through Pam can be readily divided into two units. The lower unit, 20–24 m thick is marked by a very low arenaceous content ($<<1\%$). The upper, embracing the rest of the formation, has a distinctly higher content of sand and grit; core surfaces are speckled with perhaps 1–3%. The two units intergrade over a few metres.

A distinctive thin (1–2 m) unit of pebbly quartz sandstone occurs about 45 m above the base in boreholes 9, 4 and cropping out at EQ878014 on the Mt Nicholas Road, and in nearby Durham Creek [893012]. It is generally a mud-free coarse quartzarenite, with 1–2% dispersed pebbles and a concentration of pebbles at the base. In borehole 4 the bed appears to be bioturbated; it has a sharp basal contact and sand-filled borings 5 mm wide penetrate 100 mm into the underlying mudstone. This sandstone layer appears to be widely distributed, as a similar bed occurs at about the same stratigraphic level on the Ben Lomond Quadrangle.

Invariably the rock is bleached to a very pale grey to grey-green colour within two metres of the base of the Upper Parmeener Super-Group, probably a result of weathering preceding deposition of the overlying sequence. The contact with the overlying coarse quartzarenite is abrupt.

PALAEONTOLOGY

Other than pervasive bioturbation, the only fauna in evidence in Pam are white, thin-walled cylindrical tubes up to 1 mm wide and 10 mm long, thought to be foraminifera. They are usually considerably flattened as if by compaction. In thin section, the walls, *ca.* 0·1 mm thick, are composed of coarse secondary (post-compaction) strongly pseudopleochroic calcite poikilitically enclosing tiny inclusions, silt and occasionally spicule fragments (plate 12). Rarely, the tubes have a siliceous cherty

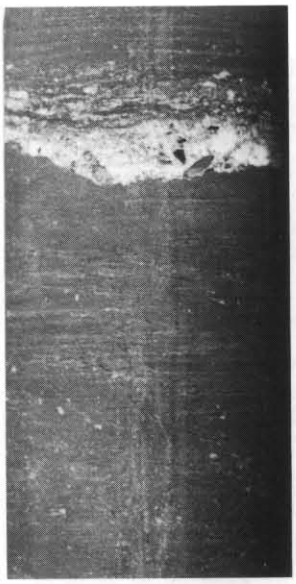

Plate 11. *Above: Graded layer of poorly sorted pebbly sandstone in mudstone. Drill core, borehole 85, 360·4 m.*

Below: Vertically elongate graded sandstone body, borehole 85, 349·8 m. Core diameter 44 mm.

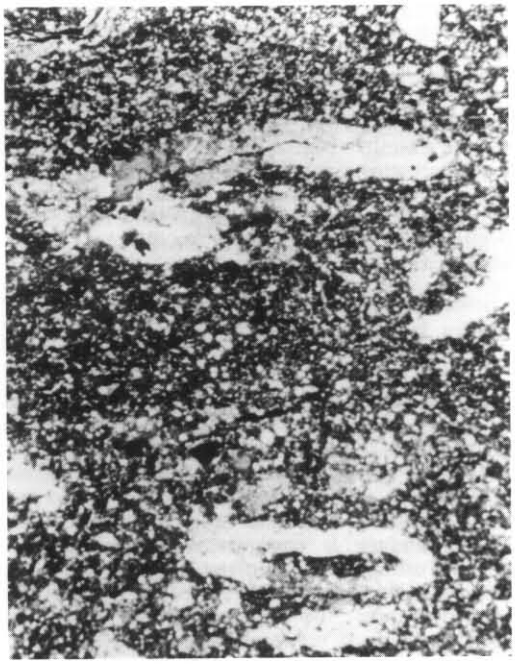

Plate 12. *Foraminifera in mudstone. Thin section, × 11, crossed nicols. Foraminifera are composed of secondary calcite; one (top) includes spicule fragments. Sample N12, from 96.4 m in borehole 9 [EQ886012].*

composition. They are probably the tests of simple agglutinating foraminifera. As noted above, they also occur in mudstone low in Pc. Similar fossils have been noted in the Oatlands Quadrangle (Forsyth, 1984, p. 22).

CORRELATION

Outside the St Marys map sheet, equivalents of Pam continue to thicken to the west and south. Pam can be lithologically correlated with the Bogan Gap Group (*c.* 200 m) of the Poatina area, via a mudstone of intermediate thickness on Ben Lomond Quadrangle. The Toarra Formation (120–165 m) of Maria Island correlates with Pam. A fossiliferous bed about 60 m above the base of the Toarra Formation contains a Late Lymingtonian fauna (Clarke, *in* Clarke and Baillie, 1984). A late Middle to Late Lymingtonian age for Pam may therefore be inferred.

DEPOSITIONAL ENVIRONMENT

Banks (1962) considered Pam a lithological correlate of the Ferntree Mudstone, for which he suggested an estuarine environment of deposition. The lack of body fossils, the probably abundant infauna, occasional woody debris and generally low-energy conditions in Pam are in accord with this interpretation. Agglutinated foraminifera are typical of brackish-water conditions (Heckel, 1972).

Ice-rafted debris is relatively insignificant volumetrically. The graded sandy layers seen in drill core may be material dumped from overturning or tilting icebergs, an important mode of sedimentation in modern glaciomarine environments (Ovenshine, 1970). Cascading onto a soft muddy bottom, this sediment would readily develop pronounced load structures. The laterally persistent sandstone bed 45 m above the base of Pam, however, suggests a temporary shallowing of the environment to above wavebase.

Lower Parmeener–Upper Parmeener Super-Group boundary

C. R. Calver

The base of the Upper Parmeener Super-Group is exposed at many localities on St Marys Quadrangle (e.g. Durham Creek [EQ893012], Webber Falls [EQ962019], Scamander Road [EQ986024], and 'E' Road [FP047831]) and has been intersected by many fully-cored drill holes. The boundary is everywhere disconformable: abrupt, usually flat but often wavy or irregular, and with Pam-derived clasts often included in the lowermost few centimetres of overlying conglomerate or coarse sandstone.

Within Pam, the sandstone bed 45 m above the base, and the upward transition at 20–24 m into sandier mudstone, may be regarded as marker horizons. These maintain a constant stratigraphic height above the base of the formation, being absent from thinner sections. This indicates that the base of the Upper Parmeener Super-Group regionally transgresses bedding in Pam, and that the thickness variations in Pam must therefore be due to post-Pam erosion.

Palynological and radiometric evidence discussed in a later section indicates a Middle Triassic age for the base of the Upper Parmeener Super-Group. The disconformity therefore represents a substantial hiatus, embracing much of the Late Permian and all of the Early Triassic. Slight tilting of the Lower Parmeener Super-Group relative to the Upper Parmeener Super-Group can be inferred by changes in the separation of marker horizons between widely-spaced sections. Pag in the Lower, and the 'G' seam (the lowest widely correlative coal seam) in the Upper Parmeener Super-Group, diverge in a W-SW direction in the Fingal Tier area while maintaining relative parallelism with bedding in their respective super-groups. A W-SW dip of about 0·3° of the Lower Parmeener Super-Group, relative to the upper, is indicated.

Borehole data from the Fingal Tier indicate that, relative to bedding (laterally extensive coal seams, see fig. 9) in the Upper Parmeener Super-Group the disconformity also has an overall dip to the west or south-west but is irregular, suggesting that the erosional surface had gently undulose relief. This basement topography was filled by quartzarenite (Rq), the lowest mapped unit of the Upper Parmeener Super-Group.

Upper Parmeener Super-Group

C. R. Calver

INTRODUCTION

In the St Marys Quadrangle, an erosional disconformity separates the Upper Parmeener Super-Group from the Lower, as described in the preceding section. The sequence is truncated by a massive sheet of Jurassic dolerite; the thickness at any point is thus controlled by the level of the base of the intrusion. The sequence is 200–300 m thick over most of the map sheet, reaching a known maximum of 385 m in borehole GY9 [EP958831].

Within the mapped area there are no thick developments of quartzarenite characteristic of the lower parts of the Upper Parmeener Super-Group elsewhere in the State (Cygnet Coal Measures, Ross Sandstone, etc.). The sequence consists essentially of a variable succession of lithic arenite, mudstone and coal (Rl), with a relatively thin (2–30 m) basal quartzarenite formation (Rq), and two basalt formations (Rbm, Rbw), each up to 30 m thick, near the base in the north of the map sheet. The sequence is Middle to Late Triassic in age, and is wholly non-marine. Exposure is severely limited by dolerite-derived slope deposits. However, detailed stratigraphic information is available from a large number of widely-distributed boreholes drilled for coal exploration.

The three major mappable subdivisions (Rq, Rb, Rl) are described below, followed by a discussion on the age and correlation of the Upper Parmeener Super-Group as a whole.

QUARTZARENITE PREDOMINANT (Rq)

Rq is composed dominantly of coarse- to medium-grained, cross-bedded quartzarenite with subordinate interbedded grey and green mudstone and minor, thin coaly intervals. On the northern slopes of the Nicholas Range and around Mt Elephant as far south as Piccaninny Creek [FP036847], it is a thin (2–3 m), sheet-like deposit of very coarse sandstone resting on the eroded top of the Lower Parmeener Super-Group. It thickens rapidly to the south and west, attaining a maximum exposed thickness of about 30 m in Cardiff Creek [EP877912] and over 12 m at 'E' Road [FP047831]. It is about 30 m thick in the subsurface under the western part of the Fingal Tier.

A pebbly layer, seldom more than one or two clasts thick, may be present at the base. The pebbles are lithologically and morphologically similar to dropstones in the underlying sequence, and probably represent an erosional lag deposit. The basal few metres are of granule to very coarse sand grade, are moderately to well-sorted, usually feldspathic (subarkose) and may contain abundant platy intraclasts of grey mudstone. In places, compacted mudstone intraclasts may be difficult to distinguish from matrix.

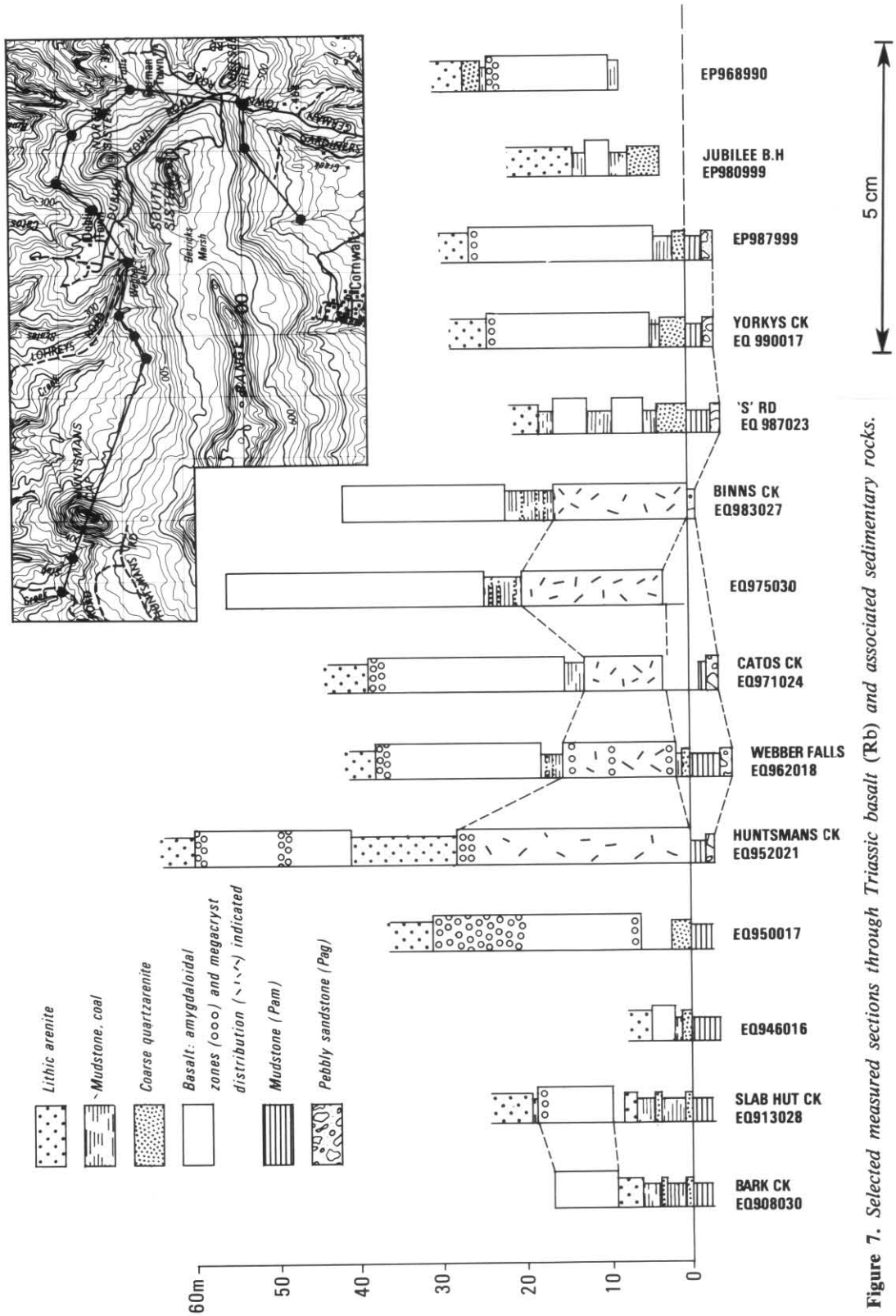

Figure 7. *Selected measured sections through Triassic basalt* (Rb) *and associated sedimentary rocks.*

5 cm

Where Rq exceeds 2–3 m in thickness, the coarse sandstones pass up into clean, well-sorted, medium to fine-grained, trough cross-bedded quartzarenite. In Cardiff Creek, the sets are mostly 0·5–1 m thick and 3–4 m wide; an exceptional 3 m thick set is exposed at EP877911. Intraclasts of mudstone and coal are common.

Interbeds of micaceous siltstone, carbonaceous shale and mudstone are present. About 10 m above the base of the 'E' Road section, grey mudstone and shale beds contain a moderately well-preserved coalified flora that includes (S. M. Forsyth, pers. comm.) *Dicroidium odontopteroides* var. cf *obtusifolium, D.*? *prolongatum, D. dubium* var. *dubium, Johnstonia stelzneriana* var. *stelzneriana, Taeniopteris,* ?*Gingkophytopsis* cf *Dicroidiopsis*, and a rare large leaf comparable to *Chiropteris zeilleri*. Two metres higher in the same section are two horizons with well-preserved polygonal desiccation cracks in sandy grey mudstone, filled with coarse sandstone.

Rq normally grades up into Rl over several metres; and the top of the formation is taken to be the highest sandstone perceptibly richer in quartz than the lithic arenites that remain virtually uniform in composition throughout the rest of the Upper Parmeener Super-Group. Rq thus includes, towards its top, quartz-rich lithic arenites.

The distribution of Rq and Rl around the Triassic basalts (Rb) north of St Marys is shown in Figure 7.

In the interval, less than 10 m thick, between the base of the Upper Parmeener Super-Group and the basalt, coarse feldspathic quartzarenites predominate, passing up into poorly sorted carbonaceous sandstone or silty mudstone immediately beneath the basalt.

Rocks sandwiched between the two basalt units between Webber Falls [EQ962018] and Binns Creek [EQ983027] have been assigned to Rq. This interval, 2–6 m thick, is predominantly micaceous grey shale and carbonaceous mudstone, with some beds of coarse subarkose and poorly sorted carbonaceous sandstone. Ragged clasts of weathered basalt in a carbonaceous mudstone matrix occur immediately above the lower basalt unit at Webber Falls. Lithic sandstone (Rl) occupies the interval between the basalts at Huntsmans Creek [EQ954020]. At 'S' Road [EQ986023] 3 m of rock of questionable assignment occurs between two thin basalt units. This is unstratified, friable, grey-brown, poorly-sorted mudstone with coalified plant debris including *Dicroidium* and a few weathered, rounded basalt clasts. Coarse quartz sandstone crops out immediately above the upper basalt unit at Catos Creek [EQ971023]; and above the (upper?) unit at EP968992 coarse quartz sandstone is interbedded with carbonaceous mudstone and lithic sandstone.

Except for the coarse basal facies and the poorly-sorted rocks associated with the basalts, Rq exhibits a similar range of sedimentary structures and textures as Rl, and probably shared a similar fluvial environment of deposition.

The eroded top of the Lower Parmeener Super-Group formed a gently undulose, gently SW-dipping basement upon which Rq was deposited (see previous section). The basement was probably progressively onlapped by Rq, resulting in a NE-thinning wedge-shaped lithosome.

Orientations of foresets from a single locality, Cardiff Creek, suggest a prevailing palaeocurrent direction from the NNE (fig. 8).

Figure 8. *Palaeocurrent directions from cross-bedding in quartz sandstone* (Rq) *at Cardiff Creek.*

BASALT (Rb)

Basalts in the St Marys area were assumed to be Tertiary (McNeil, 1965; Threader, 1968) until Calver (1980), Baillie (1980*a,b*) and Calver and Castleden (1981) found field evidence demonstrating conformity and contemporaniety with the Upper Parmeener Super-Group. A radiometric (K-Ar whole-rock) minimum age of 233 ± 5 Ma was obtained from the lower basalt (Rbm) (Calver and Castleden, 1981).

Field relationships of the basalts are described below, while petrography, mineral chemistry, geochemistry, petrogenesis and geochronology are discussed in detail in Appendix A.

The basalts occupy a stratigraphic position near the base of the Upper Parmeener Super-Group north of a line joining Bark Creek [EQ908030] to Sunny Banks [EP973953] to St Patricks Head

[FP030968]. Selected measured sections are shown in Figure 7. Two basalt units, each attaining a maximum individual thickness of about 30 m, and separated by a few metres of sedimentary rock, are present in a central area between Huntsmans Creek [EQ954020] and 'S' Road [EQ986023]. The lower unit (Rbm) has sparse (1%) plagioclase megacrysts; the upper unit (Rbw) is without megacrysts. There are also minor, but distinct, petrographic and chemical differences between the units. The megacryst presence-absence criterion suggests that the upper unit overlaps the lower to the east and west. However, the westernmost basalt at Slab Hut Creek [EQ913030], while devoid of megacrysts, is chemically closer to the lower unit; and at 'S' Road both units lack megacrysts. As the lateral relationships between the sections in Figure 7 are uncertain due to lack of outcrop, the presence of more than two discrete units is possible.

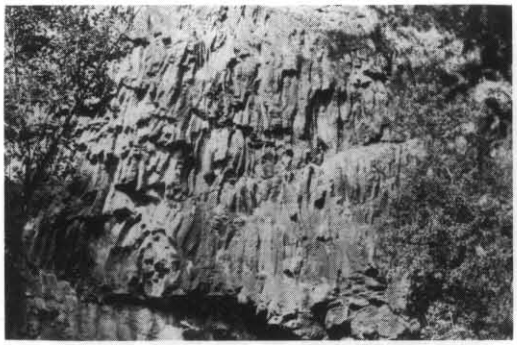

Plate 13. *Columnar jointing in Triassic basalt at a waterfall in Huntsmans Creek [EQ953021]. The columnar-jointed interval is about 15 m thick.*

Unaltered rock from the middle parts of thick sections is typical uniform black basalt. Plagioclase megacrysts are clear, rounded and up to 30 mm in diameter. Polygonal columnar jointing is well-displayed in the lower unit in a waterfall in Huntsmans Creek [EQ952021] (plate 13). Adjacent to contacts there is a zone, 2–10 m thick, through which the basalt, approaching the contact, becomes progressively more altered, finer-grained and amygdaloidal. The rock becomes light grey, greenish, and eventually pale yellow-brown. Where the basalt thins to less than 5 metres, for example at 'S' Road and in the Jubilee borehole [EQ980000] it may thus become wholly altered to a very fine-grained pale green or yellow-brown amygdaloidal rock. A white kaolinite-montmorillonite mixture (XRD determination by R. N. Woolley) fills amygdules in these most altered rocks; elsewhere, coarsely crystalline calcite is the most common filling material. Some also contain botryoidal goethite (older than the calcite) and clear, euhedral quartz (younger). Most are small (10 mm), spherical to ellipsoidal, commonly in parallel flow-alignment. Rare large (0·5m) irregular amygdules were observed. Wispy xenoliths of hornfels and veins of calcite-cemented hornfels-breccia are common in the altered contact zones.

Except where the basalt rests directly on the eroded top of the Lower Parmeener Super-Group, lower contacts tend to be undulose, or lobate with flame structures of baked sediment projecting up into the base of the flow (plate 14). This feature is best developed at Webber Falls, where the upper unit's lower contact displays elongate, branching tongues of baked sediment that penetrate 0·5 m or more into the basalt. In the Jubilee borehole, the base of the basalt displays extensive *in situ* brecciation, with a matrix of dark baked siltstone and hornfels, impregnated with hydrothermal calcite, partly in the form of cone-in-cone structures.

Plate 14. *Triassic basalt overlying carbonaceous mudstone, Scamander Road [EQ986023].*

Upper contacts suggest both intrusive and extrusive relationships. At EQ983028 and EQ975030, the top of the lower unit is strongly undulose, with conformably undulose laminae in the adjacent 100–150 mm of baked mudstone. Baking is also observed above the highly irregular upper contact of the lower unit at 'S' Road. Angular chips of altered basalt are present within the baked zone.

At Slab Hut Creek, irregular apophyses of amygdaloidal basalt, up to one metre long, intrude the overlying baked carbonaceous, brecciated, calcite-cemented sandy mudstone bed.

Complex intrusive upper contacts are exposed near EP968992, and are described in detail by Baillie (1980*a*). At one contact, the uppermost part of the basalt is cut by 2–10 mm wide sub-vertical sedimentary dykes, apparently cooling cracks filled with sediment from the overlying bed. The sediment within the dykes has been pyrometamorphosed, and displays involute folds that indicate that it moved downwards into the cracks. The overlying bed is relatively unmetamorphosed but heavily impregnated with hydrothermal calcite veinlets. Downstream at EP968989, the overlying rocks are brecciated and unusually strongly hornfelsed.

At EQ989017, in a tributary of Yorkys Creek, a contact overlain by baked mudstone and lithic sandstone is largely conformable, but becomes partly transgressive as the contact abruptly truncates the 3–4 m of overlying strata at a steep angle.

In a few places, notably the last two localities discussed, anomalously steep dips (20–40°) and gentle folding are observed in the few metres of sediment overlying the basalt. This deformation may originate from the time of intrusion.

No baking was observed above upper contacts at Webber Falls (the lower unit), at 'S' Road (the upper unit) and in Yorkys Creek. At 'S' Road, a lens of carbonaceous mudstone fills a gentle depression in the top of the flow. At Yorkys Creek, the upper contact has a lobate, 'ropy' configuration, and is overlain by scoriaceous agglomerate of limited lateral extent.

Contact metamorphic effects extend only 10–14 mm below the lower contact and 100–150 mm above upper contacts. Except in the hornfels dykes and inclusions, no recrystallisation is evident; the rocks are merely indurated, and oxidised in the case of carbonaceous sediments. In some places, faint spotting is evident immediately above the basalt. in the hornfels dykes described by Baillie (1980*b*), small porphyroblasts of retrograde ?cordierite occur immediately adjacent to the basalt.

The marginal features of the basalts thus indicate both extrusion, and intrusion at very shallow depths into wet, unconsolidated sediment. Very little associated air-fall material has been found.

LITHIC ARENITE PREDOMINANT (Rl)

INTRODUCTION

Rl is predominantly lithic arenite, interbedded with mudstone, minor coal, rare conglomerate and rare tuff. Arenites volumetrically exceed lutites by about 7:3. The sequence is up to 350 m or so in thickness, depending on the level of dolerite intrusion. Stratigraphic subdivision of Rl is precluded by rapid lateral and vertical facies changes, inadequate exposure and the uniformity of major lithologies through the sequence.

Areas of dominantly lithic sandstone (Rls) and dominantly mudstone (Rlm) have been differentiated on parts of the Nicholas Range, but no stratigraphic significance can be attached to these categories.

Borehole data indicate that many coal seams, and a conglomerate bed high in the sequence, are laterally persistent across much of the map sheet. Rare tuff layers and pebbly horizons also offer potential as stratigraphic indicators.

The lithic arenites crop out preferentially, often forming cliffs on the slopes of Mt Nicholas, Fingal Tier and Mt Elephant, particularly the latter where dolerite talus is less extensive. The sequence is well exposed in a few creeks, most notably in the unnamed creek above EP968994 (Baillie, 1980*a*). Here a marked fining-upward fluvial cyclicity is evident, with cross-bedded lithic sandstone overlain by massive mudstone, sometimes laminated towards the top, followed by coal (Baillie, 1980*a*).

Lithological descriptions below are of outcrop, unless otherwise stated.

LITHIC ARENITES

The arenites are well-sorted, of coarse to fine, usually medium grain size (0·1–1 mm, usually 0·25–0·5 mm), light grey-green in colour with a speckled 'salt-and-pepper' appearance due to the presence of numerous green and dark-coloured lithic grains and white weathered feldspar grains.

They are thickly to very thickly bedded, and may occur in uninterrupted units up to 15 m thick. Bedding tends to be undulose and lenticular. A coarse parting may be developed, induced by comminuted carbonaceous debris, coarse muscovite flakes, and the compactive flattening of lithic grains. Unlike Rq, most beds appear internally uniform in outcrop, often exhibiting spheroidal weathering or superficial pachydermal jointing. However, under certain weathering conditions — such as beneath overhangs — trough cross-bedding is seen to be present in virtually every sandstone bed. Sets are up to 40 m long, several metres wide and 1·5 m thick, more usually 0·5–1 m thick.

Calcite cementation of the lithic arenites was observed at several localities. At EP974928, ellipsoidal, interconnected concretions about one metre in diameter are entrained in parallel E-W rows within a single thick sandstone bed. The sandstone becomes mostly replaced by calcite in the cores of the concretions.

Frequently seen in outcrop are gently undulose erosional interfaces between coarse sandstone above and finer sandstone or lutite below, reflecting a predominant fining-upwards cyclicity. The coarsest arenites commonly contain platy mudstone fragments and flattened wisps of coal. these intraclasts are up to 0·3 m long, and are orientated subparallel to bedding. In abundance, they develop coarse intraclastic open-framework breccias; which, however, seldom persist more than 0·5 m above basal scours.

In thin section, quartz grains are seen to constitute only an estimated 10–25% of the lithic arenites. A few quartz grains are well-rounded, but most are angular. There is a few per cent feldspar in all slides; in some, K-feldspar (mostly orthoclase, some microcline, rare perthite) predominates (*e.g.* J25); in some, plagioclase (oligoclase—?andesine: optical determination) predominates (e.g. E253). Feldspars are usually weathered to varying degrees; but some

plagioclase is water-clear. Many grains retain angular cleavage fragment shapes.

Lithic fragments constitute the bulk of the rock in all slides. Porosity is largely occluded by authigenic clay and compactive deformation of lithic grains. Most are of indeterminate origin, being too fine-grained or weathered for accurate identification. However, grains of indubitable volcanic origin are present in all samples sectioned, and are conceivably the most abundant component. Those most easily recognised are probably of intermediate composition, typically with a fine-grained mesh of feldspar laths in a turbid cryptocrystalline groundmass or mesostasis (plate 15). Such grains exhibit great variation in grain size and fabric (often trachytic; commonly intersertal to hyalopilitic, ranging from granular to sparsely microporphyritic). The groundmass may be of granular opaques and chlorite or more usually a probably originally glassy, green-grey cloudy material. Some volcanic rock fragments contain chloritised equant microphenocrysts. Dark brown, turbid, cryptocrystalline grains are common; a few have spherulitic textures and microlites that suggest a volcanic origin. Acid and intermediate volcanic grains, and abundant biotite, were identified in a poorly sorted reworked tuffaceous sandstone (PM18) from just above the basalt at EP968992 (Baillie, 1980*b*).

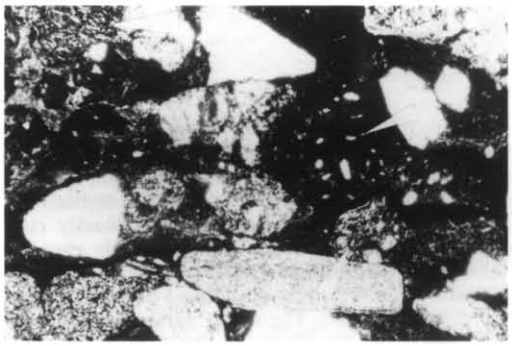

Plate 15. *Coarse-grained lithic arenite. Thin section, × 16, plane-polarised light. Several trachytic-hyalopilitic volcanic rock fragments indicated by arrows. Sample E85, from FP032920.*

Other identifiable lithic fragments that do not together constitute more than several per cent of the rock, include mudstone, metasedimentary rock types (slate, quartzite, phyllite and schist), chert and granitic detritus (micrographically intergrown quartz and orthoclase).

Many grains are composed of a clay mineral, usually poorly crystalline but occasionally occurring as aggregates of vermiform crystals with a basal cleavage. It is, at least in part, of a secondary origin as the mineral partly replaces volcanic grains in E146. However, an unusual sandstone at EP9967907 is composed almost entirely of similar, much larger (0·5 x 2 mm) vermiform, pale brown crystals in a carbonaceous mudstone matrix. This mineral was identified as kaolinite by X-ray diffraction (R. N. Woolley). Such abundance suggests a primary volcanic origin.

Muscovite and biotite are present and epidote and garnet are rare. Bacon (1979) recorded accessory rutile, zircon and tourmaline.

Calcite cement, where present, partially replaces the sandstone, and is very coarse grained, each calcite crystal poikilitically enclosing several grains (e.g. E146). Secondary fibrous chlorite fringes grains in E167.

PEBBLY HORIZONS AND CONGLOMERATE OF EXTRABASINAL ORIGIN

Well-rounded extrabasinal pebbles and cobbles up to 250 mm in diameter are occasionally found dispersed along the basal surface of coarse arenite beds. Flute structures are scoured into the top of the underlying bed on the lee side of some clasts. The following lithologies are represented: quartz-feldspar porphyry, quartzite, chert, vein quartz, granitic rocks, metamorphosed siliceous conglomerate, and Permian siltstone containing ramose bryozoans and fenestellids. Large mudstone intraclasts and rare transported silicified tree trunks are associated with these horizons. Being erosionally resistant, the pebbles are common as surface float in many areas.

Of fifteen such pebbly horizons observed, none were seen in the lowest 150 m of the lithic sandstone-dominated sequence (Rl). A stratigraphic control is strongly implied.

Quartz-feldspar porphyry is the commonest clast type at many horizons, and comprises a suite of acid to intermediate volcanic rock types including tuffs, ignimbrites and probably rhyolites. In thin section, examples of probable rhyolite consist of euhedral phenocrysts of K-feldspar, including sanidine and orthoclase, and bipyramidal quartz, in an abundant felsic devitrified glassy groundmass. Some, e.g. E66, have flow-banding defined by zones of slightly coarser groundmass recrystallisation (plate 16). Sample 8055·9 includes a few per cent biotite as phenocrysts with a well-developed preferred orientation. Samples M181 and M182 are ignimbrites from the Dalmayne Conglomerate (see below). They contain sparse fragmental phenocrysts of sodic plagioclase and quartz, and pumiceous rock fragments, in a eutaxitic groundmass of densely welded glass shards (plate 17). In M182 the groundmass texture is partly obscured by secondary spherulitic recrystallisation.

E166 is a coarse (5 mm) lithic crystal tuff, composed of euhedra of orthoclase, plagioclase

and quartz, fragments of glassy trachyte, and sedimentary rock fragments in a fine-grained altered felsic groundmass.

Samples 8055/4 and 8055/5, of the Dalmayne Conglomerate (see below), include pebbles of a sparsely sanidine-phyric shard-rich tuff and very fine-grained vitric ash tuffs.

Only at a single horizon high in the sequence are the extrabasinal clasts sufficiently abundant to develop a closed-framework conglomerate layer. Known informally as the Dalmayne Conglomerate, it is a useful marker bed in the subsurface (discussed below) but crops out at only two localities, in Micks Creek [EP931901] and at FP006891, near Gray. Quartz-feldspar porphyry is the dominant clast lithology; other compositions mentioned above are also present.

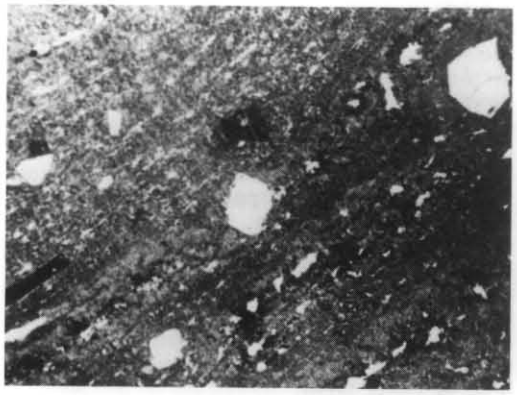

Plate 16. *Rhyolite pebble. Thin section, × 6·8, plane-polarised light. Phenocryst of bipyramidal quartz and altered tabular sanidine in a flow-banded, devitrified, glassy groundmass. Sample E66 from the Dalmayne Conglomerate at EP931901.*

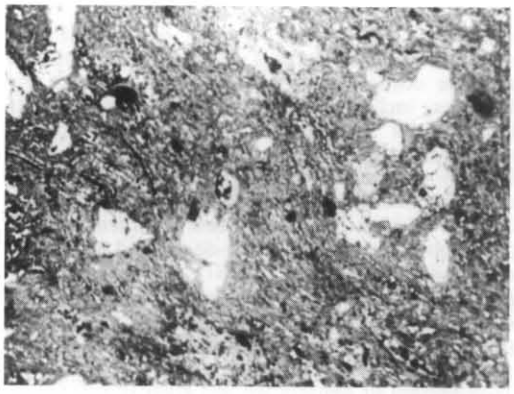

Plate 17. *Ignimbrite pebble. Thin section, × 6·8, plane polarised light. Fragmentary feldspar, volcanic rock fragments and minor quartz in a groundmass of densely welded shards. Sample M181, from the Dalmayne conglomerate at EP931901.*

LUTITES

Mudstones and claystones are pale grey to olive-grey in colour with a transition to black with increasing organic content. They are usually internally uniform, with a hackly, cuboidal fracture; fragmentary carbonaceous remains and muscovite may impart a shaly fissility. Laminated mudstones are subordinate, and in drill core, sometimes exhibit slumping (Bacon, 1983*a*). Fragmental coalified plant remains are common, and *in situ* root traces are occasionally seen. Desiccation cracks have been observed in drill core (Bacon, 1983*a*).

COALS

General features

Coals are dull, with a small proportion of lustrous 'bright' bands. They are interbedded and transitional with carbonaceous mudstone, and occasionally contain thin beds of white clay (composed of montmorillonite and kaolinite: Bacon, 1979). Highly fissile 'paper coals', largely composed of compacted *Johnstonia* leaves, were observed in a few places. Clastic material within some coal seams occasionally shows laminar or lenticular bedding, indicating that at least some coals are allochthonous rather than *in situ* (Baillie, 1980*a*). No *in situ* roots were observed beneath seams. However, *in situ* fossil trees are known from the Duncan Mine (Townrow *in* Hale, 1962).

Petrography

C. A. Bacon

Coal from the Duncan and Blue seams has been examined petrographically (Smyth 1980; Bacon, 1984*a*, 1984*b*; see below for seam nomenclature). The coal is extremely dull, being typically rich in inertinite. The vitrinite content rarely exceeds 25% and the dominant exinite maceral is cutinite. The inertinite is largely composed of semifusinite and inertodetrinite. The mean maximum vitrinite reflectance of the Duncan seam is 0·56. The coals have an inherent ash content of around 15–25% with clay minerals filling cellular plant cavities, indicating a steady influx of clastics during peat formation.

TUFFS

Fine-grained acid tuffs were first described from the Upper Parmeener Super-Group by Bacon (1979) and Bacon and Everard (1981*a*,*b*). Many occurrences have now been noted in drill-core, principally from the Fingal Tier area (Bacon, 1983*a*). Near *in situ* blocks of tuff occur at FP012890, near Gray. This is a tough, white, aphanitic rock; in thin-section (E60,15) composed almost entirely of fragmented, devitrified very pale brown glass shards of a highly silicic composition, compacted so that porosity is negligible; with a sprinkling of angular quartz silt, biotite, zircon, rare sodic plagioclase and

carbonaceous debris. It is a possibly slightly reworked airfall tuff.

MACROFLORA

Coalified plant remains of fair preservation are common. According to Townrow (*in* Hale, 1962) Tasmanian Triassic coal measures (Rl and equivalents) are dominated by the fern *Cladophlebis*, the pteridosperms *Dicroidium, Xylopteris*, and *Halleophyllum*, and the possibly gingkoalean *Phoenicopsis elongata*. Cycad leaves are common and gingkoaleans (e.g. *Gingkoites, Sphenobaiera*) are locally abundant.

At EP997904, well-preserved plant fossils were collected from a slightly baked pale grey mudstone. Taxa include (S. M. Forsyth, pers. comm.) a common leaf very similar to *Linguifolium tenison-woodsi, Xylopteris elongata, Sphenobaiera* cf *tenuifolia, Gingkophytopsis* cf *lacerta* and *Dicroidium odontopteroides* var. cf *crassum*. Nearby, at EP996906, another baked mudstone contains *Dicroidium* cf *lancifolium*.

LITHOSTRATIGRAPHY

C. R. Calver
C. A. Bacon

Uniformity of major lithologies and lack of outcrop have precluded stratigraphic differentiation of Rl in the field. The apparent absence, mentioned above, of extrabasinal pebbles from the lowest 150 m of the sequence is an observation of possible stratigraphic utility, however. For example, the lack of pebbles from the extensive outcrops along Doctors Creek between FP040774 and FP063785 suggest, in the absence of corroborative field evidence, that these rocks are low in the sequence.

The widespread coverage of coal exploration drill holes has provided a wealth of stratigraphic and structural information on the Upper Parmeener Super-Group. The following briefly summarises the stratigraphy of the Fingal Tier and Nicholas Range areas, focussing mainly on the economically interesting and stratigraphically useful major coal seams.

Fingal Tier Area

A grid of Department of Mines drill holes intersects the Upper Parmeener Super-Group under the western half of the Fingal Tier on St Marys Quadrangle, whilst a grid of Shell-IMI drill holes covers the eastern half of the Tier. Threader and Bacon (1983) have erected a coal seam stratigraphic framework for the Department of Mines' grid. Although the coal seams tend to vary greatly in quality and thickness, even between adjacent holes, eight major coal seams or coaly intervals appear to be persistent over much of the area. These are (from the uppermost) the A, B, C, D, E, F (the Duncan seam), G (the East Fingal Seam; often split into two: Gu and Gl), and H (usually embracing a cluster of minor seams). Correlations are based on stratigraphic heights above the base of the Upper Parmeener Super-Group, interseam separations, and in some cases, internal coal seam stratigraphy.

Similarly, Taylor and Brunton (1978) have independently erected a stratigraphy of major persistent coal seams for the eastern part of the Fingal Tier. These seams have been named the Dalmayne A (DA), Dalmayne B (DB), etc. seams. Comparison of adjacent holes of these two areas, specifically Department of Mines holes 79 and 82 with GY11 and GY9, suggest the following correlations.

Department of Mines	*Shell-IMI*
A	mudstone layer (unnamed)
B	DB
C	DC
D	DC1
E	DDU
absent	DDL
F	absent
Gu	DE
Gl	DE2

The DA seam of Shell-IMI is stratigraphically too high to be represented in most Department of Mines holes. These correlations are preferred to those tentatively suggested by Bacon (1983*a*), which imply a dubious rapid eastward thickening of the sequence.

Representative borehole sections, along a W-E transect across the Fingal Tier, incorporating the revised correlations, are shown in Figure 9.

The Dalmayne Conglomerate, described above, is 0·5–5 m thick in the subsurface (often of doubtful exact thickness as this interval is prone to core loss during drilling) and occurs 50–60 m above the A seam. It is used as a marker bed in the eastern half of the Fingal Tier (Taylor and Brunton, 1979) and it persists westward into the Department of Mines' grid, but in most holes is not preserved as the dolerite sheet intrudes below this horizon. The Dalmayne Conglomerate also persists south into parts of the Bicheno Quadrangle (Sansom, 1980).

The correlations suggested above have been used in the construction of an isostrat diagram of the base of the dolerite sheet on Fingal Tier (fig. 43).

Infrequent layers of fine-grained acid tuff have been intersected in the upper part of the

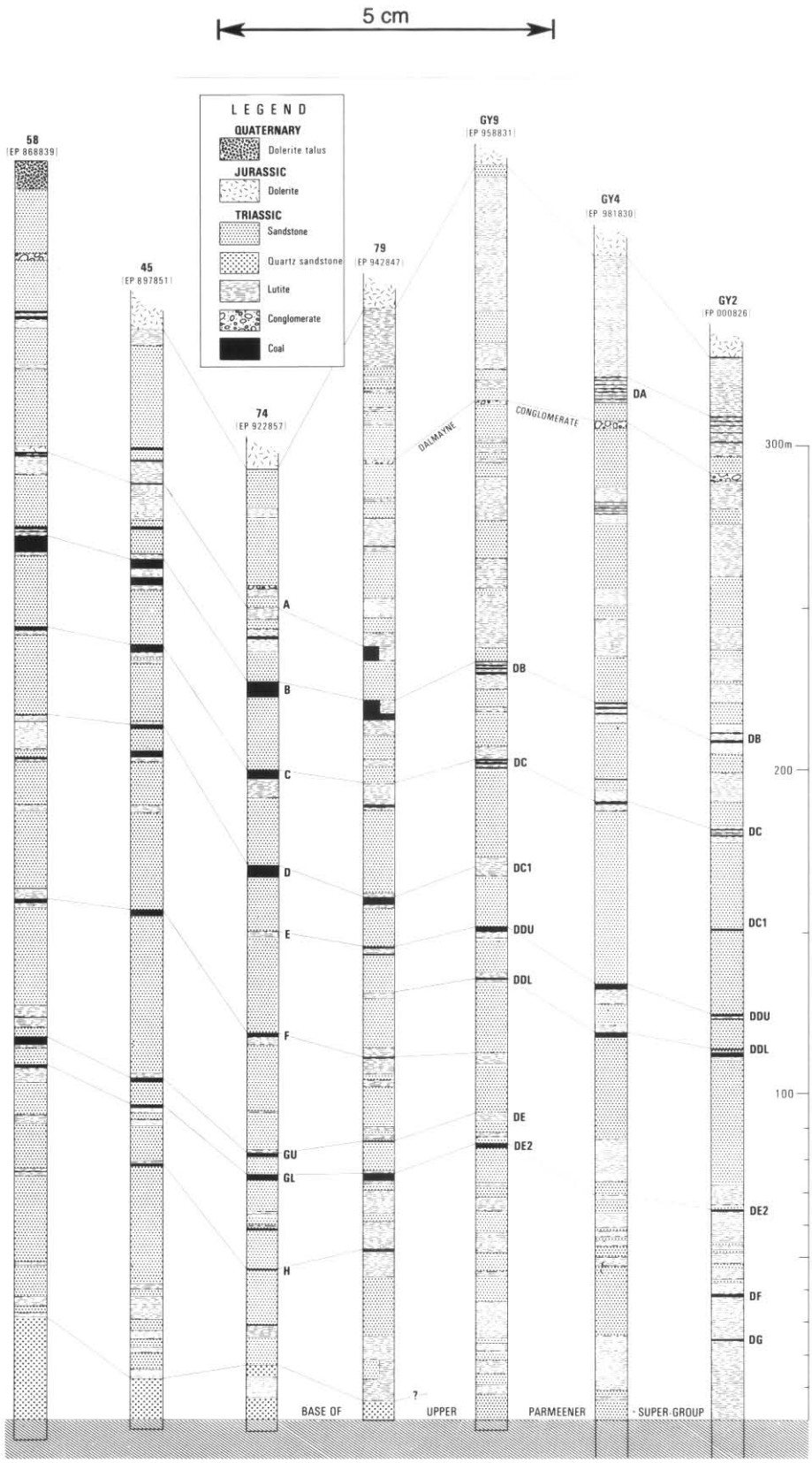

Figure 9. *Selected fully-cored drill hole sections through the Upper Parmeener Super-Group, Fingal Tier. Sections arranged from west (left) to east.*

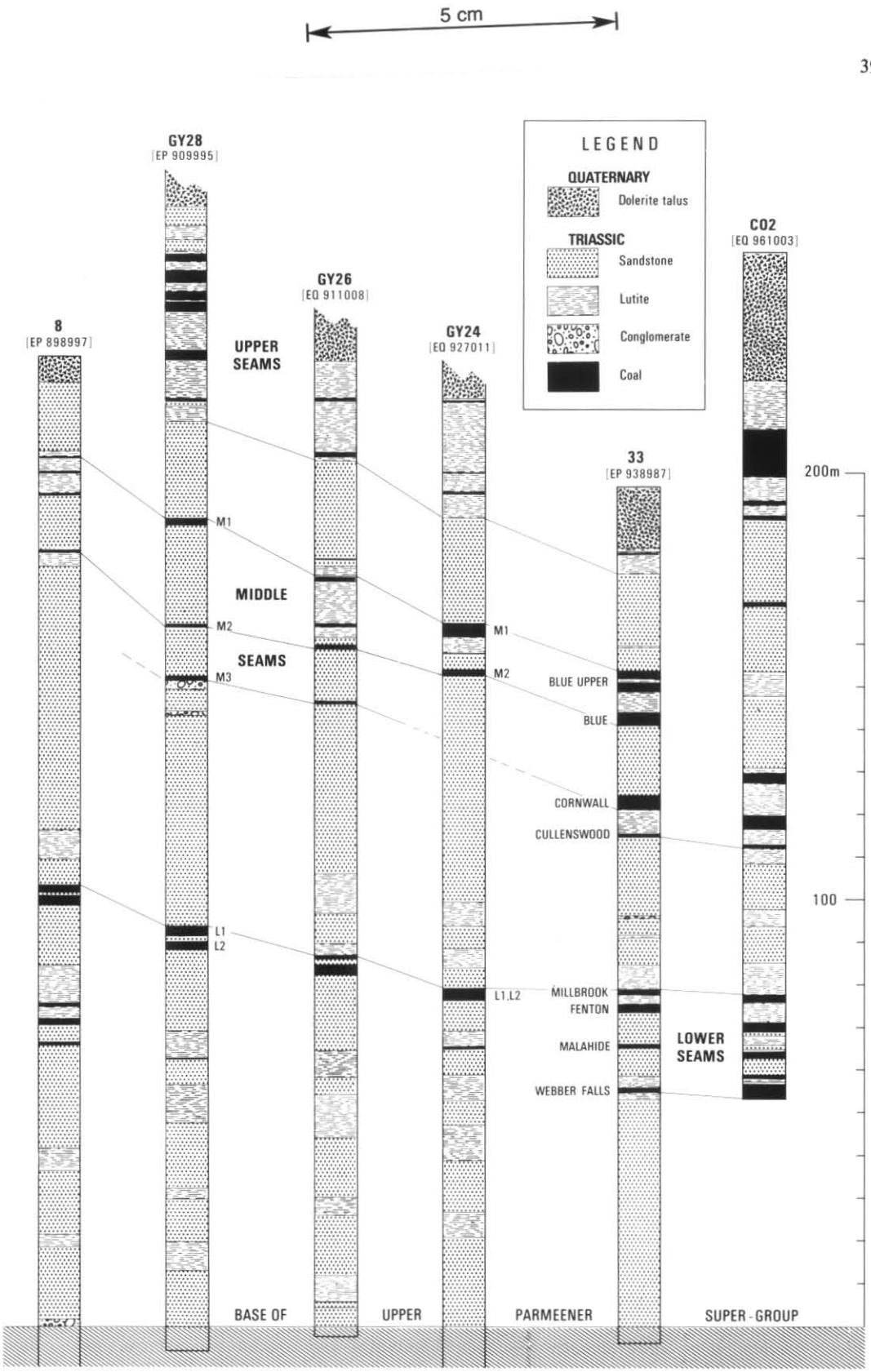

Figure 10. *Selected fully-cored drill hole sections through the Upper Parmeener Super-Group, Mt Nicholas Range*

sequence. The tuffs, up to about one metre thick, are individually impersistent, and of no utility as marker beds (Bacon, 1983*a*). They do, however, appear to be stratigraphically restricted to that part of the sequence above the B seam.

Nicholas Range

In the Nicholas Range area, the Upper Parmeener Super-Group attains a maximum known thickness of 264 m in GY28 [EP909995] (Sansom, 1980). Under a separate system of nomenclature, coal seams are grouped into the upper, middle and lower groups of seams. Equivalent historical mining nomenclature and correlations within the coalfield are given by Bacon (1983*b*). Representative sections from boreholes along a west-east transect are depicted in Figure 10.

A single tuff layer has been recorded from just above the upper seams in GY119 [EQ907011]. Pebbly horizons are recorded from just below, and above, the middle seams in GY28 and GY24 [EQ927011].

No firm correlation of individual seams between the Nicholas Range and the Fingal Tier can be made, but the positions of the tuff and pebbly horizons, and a side-by-side comparison of sections, suggest that the upper group of seams may be loosely equivalent to the A-B interval, the middle group of seams to the D–F interval and the main lower seams (the L1 and L2) to the G seam. These correlations are preferred to those of Bacon (1983*b*), which, if valid would necessitate a substantial northward thickening of the sequence, for which there is no evidence.

The sequence as a whole becomes thinner eastward on the Nicholas Range (fig. 10). On Fingal Tier, a similar, but less marked, trend is observed from south-west to north-east. The nearest edge of the depositional basin, therefore, was probably to the east or north-east.

PROVENANCE (Rl)

Volcaniclastic grains in Tasmanian Triassic sandstones have long been suspected of originating from a coeval phase of acid to intermediate volcanic activity (Lewis and Voisey, 1938; Spry, 1962). This seems highly probable in the case of Rl considering the abundance of the grains and the known occurrence of acid tuffs high in the sequence (Bacon and Everard, 1981*a,b*, and this work). Furthermore, this activity was in part simultaneous with known basic volcanism within the basin (Rb).

The quartz-feldspar porphyries found as pebble- and cobble-sized clasts, like the sand-sized grains, are of acid to intermediate composition. They are undeformed and not readily comparable to known Tasmanian basement lithologies (N. J. Turner, K. D. Corbett, pers. comm.). A Triassic age for similar clasts near Bicheno has been suggested by Bacon and Everard (1981*a,b*), and similar clasts occur in the correlate of Rl in the Oatlands Quadrangle (Forsyth, 1984).

Other pebbles are of mixed provenance, apparently largely western Tasmanian; but the presence of Permian clasts suggests that many may be recycled dropstones.

The source area therefore included a calcalkaline volcanic terrain that was probably active throughout deposition of the lithic arenites. Uplifted Permian sedimentary rocks, and possibly metasedimentary and plutonic sources also contributed detrital constituents to the basin.

Coeval vulcanism is proven by the presence of thin tuffs, interpreted as distal ash-fall deposits. The preservation potential of the unconsolidated ash was low in the fluvial environment, as suggested by partial reworking of the deposits, and their impersistence. The stratigraphic distribution of tuffs and pebbly horizons suggests that vulcanism and instability increased during deposition of Rl.

No prevailing direction of sediment transport could be determined from preliminary palaeocurrent determinations (n = 49) from cross-bedding in the lithic arenites of the St Marys Quadrangle. Correlates of Rl in the Oatlands Quadrangle have a predominant palaeocurrent direction from the south-east (Forsyth, 1984).

DEPOSITIONAL ENVIRONMENT (Rl)

C. A. Bacon
C. R. Calver

Alluvial fining-upward cycles were noted in drill core by Threader (1968). Bacon (1979) recognised fluvial cycles on the basis of Markov chain analysis of borehole data from Fingal Tier, and proposed a meandering fluvial system of moderate to high sinuosity, the arenites representing channel deposits, the lutites and coal overbank deposits on extensive floodplains. Intraclastic breccias and pebbly horizons represent channel lags.

The sequence as a whole differs from the classical high-sinuosity meandering depositional models of Allen (1965) and Walker and Cant (1979) in the high proportion (about 7:3) of arenite to lutite. Fine-grained overbank deposits predominate in the models. Also, abandoned channel-fill 'clay plugs', which should have good preservation potential in high-sinuosity regimes, do not appear to be common in the sequence.

The high proportion of arenites in the sequence may be partly attributed to repeated erosion of upper (overbank) parts of cycles during channel migration, producing the relatively thick (>20 m) sections composed only of channel sandstones in which incomplete fining-upward cyclicity may still be discerned. Lateral and vertical changes in the gross arenite-lutite proportion suggest temporal and spatial variation in the fluvial regime (Bacon, 1979), lutites being more significant in the lowest and highest parts of the sequence (fig. 9, 10).

The major coal seams evidently developed as accumulations of peat on wide flood plains. Frequent intercalations of mudstone within the seams attest to periodic inundation of the peat beds with sediment-bearing floodwaters. The coals are dull, with high inertinite and low sulphur contents, indicating that the peat beds were well-oxidised, presumably with a lowered water table for at least some of the time. This is supported by the presence of *in situ* trees rooted in the top of the Duncan seam, which would require a well-drained substrate (Townrow *in* Hale, 1962).

According to Smith (1962), coals with such a high (80–90%) inertinite content probably never had a permanent water cover.

The maceral composition of the coals can be more precisely related to the environment of deposition and early coalification using the approach of Diessel (1982, 1983). Two indices, TGI (tissue gelification index) and TPI (tissue preservation index) are derived from relating macerals with a high diagnostic value to each other.

The TGI is a measure of the amount of moisture available in the environment of peat deposition. Wet conditions of peat formation allow gelification of the peat, while under conditions of slow subsidence a drier environment is more likely and the plant tissue products can become fusinitised (oxidised). The Duncan seam plies all exhibit a low TGI (Bacon, in prep.), showing that the coal was deposited in the dry terrestrial moor environment of Diessel (1983).

The TPI contrasts the tissue bearing macerals with the macerals which have been derived from the destruction of cell tissue and may be regarded as a wood ratio. A low TPI indicates the absence of woody tissue in coal, due to either absence of wood in the original peat or near complete destruction of woody tissue by the oxidation of the peat swamp (Diessel 1983). The Duncan seam coal has a low wood ratio (Bacon, in prep.).

Coal from the Blue seam exhibits higher TPI and TGI ratios than the plies of the Duncan seam, but nonetheless a similar environment of deposition is indicated.

The coals therefore accumulated partly *in situ*, and partly transported, on flood plains as extensive beds of peat that were subject to periodic flooding and drying out.

The local vegetation was dominated by ferns, seed ferns, gingkoaleans and cycads (Townrow, *in* Hale, 1962), an association that fits the broadleaf forest (*Dicroidietum odontopteroidum*) association of Retallack (1977).

Tasmania had a high (>70°) latitude during the late Triassic (Schmidt and Embleton, 1980). In the light of this, Smyth (1980) suggested that the coal-forming peats accumulated in Arctic-like palsamires (characterised by continuous permafrost) and that the sub-freezing conditions prevented complete oxidation of the peat beds despite their relatively dry environment of formation.

However, no corroborative evidence for such cold conditions, such as ice-wedge pseudomorphs, has been found.

Townrow (1964) has suggested that certain aspects of the flora of the Tasmanian Triassic coal measures (Rl and equivalents) indicate a cool, temperate climate. Morrison and Bacon (in prep.) state that plant growth patterns from fossil wood indicate marked seasonality and an absence of climatic extremes. They suggest a generally humid, temperate climate amenable to plant growth.

AGE AND CORRELATION

The age of the Upper Parmeener Super-Group of the St Marys Quadrangle is defined by both radiometric and palynological data.

Samples from immediately below and above the lower basalt unit at Webber Falls [EQ962019] (horizons mapped as Rq) have yielded a microflora than can be correlated with the *Aratrisporites parvispinosus* Assemblage Zone and the *Duplexisporites problematicus* microflora of de Jersey (1975) (Forsyth, 1984), considered to be Anisian or Ladinian (Middle Triassic).

A whole-rock K-Ar minimum radiometric age of 233 ± 5Ma was obtained from the lower basalt unit. This age is very close to the Anisian-Ladinian boundary of 235 ± 5Ma given in Webb's (1981) revised Triassic timescale.

Playford (*in* Threader, 1968) examined miospore assemblages from several coal seams within Rl. The Duncan Mine and Valley Mine (both F seam) on Fingal Tier were sampled, and various seams belonging to the middle and lower groups of seams on Mt Nicholas. All assemblages were qualitatively similar, and showed close affiliation with the Brady Formation. All belong to the *Craterisporites rotundus* zone (Forsyth, 1984) which in the Bowen Basin is considered to represent the Karnian (early Late Triassic) (de Jersey, 1975).

Biotite extracted from a Triassic tuff exposed in the Denison Rivulet, south of the St Marys map sheet, has been radiometrically dated at 214 ± 1 Ma (Bacon and Green, 1984), approximating the 215 ± 5 Ma Karnian–Norian boundary age proposed by Webb (1981). This tuff crops out in the upper part of the lithic arenite (Rl-equivalent) sequence. On Fingal Tier, similar acid tuffs are restricted to that part of the sequence above the 'B' seam. A spore assemblage from about 50 m stratigraphically below the dated tuff belongs again to the *Craterisporites rotundus* Zone (Forsyth *in* Bacon and Green, 1984).

The Upper Parmeener Super-Group on St Marys Quadrangle is therefore mostly Karnian, and Anisian or Ladinian at the base.

Outside the St Marys Quadrangle, correlates of the quartzarenite-dominant unit (Rq) continue to thicken rapidly to the south and west. At nearby Tower Hill on Ben Lomond Quadrangle, for example, the unit is approximately 70 m thick. In central and southern Tasmania the base of the Upper Parmeener Super-Group is much older (Late Permian) and considerable thicknesses of quartzarenite predominate in the lower part of the section. In the Midlands, a unit of interbedded quartzarenite, lutite and carbonaceous beds (Rsq′) occurs near the top of this interval (Forsyth, 1984) and is similar in age and lithology to Rq of St Marys Quadrangle.

The lithic arenite-dominated unit (Rl) is a lithological correlate of the volcanic lithic arenite (Rg) of the Midlands (Forsyth, 1984), the upper part of the Brady Formation (McKellar, 1957) the New Town Coal Measures, and similar lithic arenite-coal measure sequences widespread in eastern and central Tasmania.

The Triassic basalts (Rb) of the St Marys Quadrangle are the only *in situ* igneous rocks yet known from the Parmeener Super-Group.

Tertiary

Surficial deposits of probable Tertiary age occur in the far north-west of the St Marys Quadrangle. They are gravels consisting of well-rounded Mathinna Beds-derived quartz and quartzite pebbles, and do not appear to be related to the present river system. They are juxtaposed with an area of basalt that is also probably of Tertiary age, being chemically very similar to known Tasmanian Tertiary basalts (see later section). (P.W.B., R.H.C.).

Quaternary

C. R. Calver
N. J. Turner

INTRODUCTION

Deposits of Quaternary age include beach deposits and coastal dunes (Qhb), alluvium (Qha, Qad), talus (Qpt), lag gravel (Qpl) and undifferentiated aqueous deposits and aeolian sand (Qpc). Of these various categories Qhb is clearly related to the present coastline and Qha to present stream valleys. Qad may be in part an older deposit. It is derived from dolerite talus, typically extending from the foot of talus-covered slopes onto the adjacent plains. Qpc and Qpl are older deposits related to the coastline although the position of the shoreline was apparently different during their formation. In particular Qpl appears to record a high-level shoreline. Qpl and Qpt are the oldest Quaternary deposits in the quadrangle. Qpt is dissected by the present drainage system in places and appears to be overlain by Qpc, Qhb and Qad. It may also be overlain by Qpl.

TALUS (Qpt)

C. R. Calver

Talus deposits have been differentiated according to their composition. Well-jointed Jurassic dolerite which caps the major hills and ranges in the quadrangle has produced by far the thickest and most areally extensive talus. Localised deposits derived from Parmeener Super-Group lithologies and Mathinna Beds have also been mapped, but they generally either remain within areas in which the parent rock types are sub-outcropping or only move short distances laterally (e.g. FP055919).

Dolerite talus covers the flanks of the Fingal Tier and the Nicholas Range, and less extensive deposits surround St Patricks Head and Mt Elephant. A separate, nearly continuous strip of talus extends along the axis of the Fingal Valley. In many instances, downslope transport distances of several kilometres can be inferred, for example at EP846975 and elsewhere in the Fingal Valley, and at FP060835. Isolated areas of talus occur in many areas (e.g. around Mt Elephant), typically on interfluves and capping small hills, indicating substantial dissection by the present drainage system. The talus is deeply incised by present day streams.

The thickest known developments of talus on the map sheet occur on the northern slopes of the Fingal Tier, and around Mt Nicholas. On Fingal Tier, borehole 49 [EP910900] intersected 165 m of talus (see cross-section on 1:50 000 geological map). South of Mt Nicholas, GY132 [EP914998] penetrated 120 m of talus, while to the north, GY26 [EQ911008] and GY24 [EQ927011] intersected 109 and 106 m, respectively. These holes are sited over the thick, proximal parts of wedge-shaped talus deposits that overlie a relatively gently inclined bedrock surface of Upper Parmeener Super-Group (see cross section). Distally, the bedrock surface steepens and the mantle of talus becomes thinner, sheet-like and subject to penetration by stream erosion.

Dolerite talus is composed of angular boulders mostly up to 6 m across, in a matrix of smaller platy fragments, sand and clayey weathering products. Larger boulders (*c.* 10 m) are commonly seen, and boulders of 20–30 m in maximum dimension were seen in a few places. Distal parts of dolerite talus deposits commonly contain subordinate fragments of resistant lithologies derived from the Parmeener Super-Group, notably hornfelses and pebbles recycled from conglomerates.

Large talus boulders were usually distinguished from discontinuous dolerite outcrop by the absence of consistent vertical jointing, textural

variations between boulders and by a lack of topographic prominence. Surface magnetometer traverses were used in several places to distinguish talus from dolerite outcrop using the method outlined by Leaman and Richardson (1983). Dolerite capping two hills at EP847975 and EP847965 was thus confirmed as talus (P.W.B.), outcrop was confirmed at EP858919, and boundaries between dolerite outcrop and talus with probably Triassic subcrop were located at EP856901, EP857902, EP859903, EP862899, EP862896.

In many places there is a transition zone between outcrop and talus, consisting of large (*c.* 20 m) blocks of near *in situ* dolerite that are tilted, *en masse*, in a downhill direction. Jointing, vertical in outcrop, indicates that tilting progressively increased downhill to perhaps 90° at which point the fabric becomes haphazard and the blocks probably no longer rest directly on bedrock. These zones may be a few hundred metres wide, and the most extensive examples occur on the south facing escarpment between EP863785 and EP904807 (R.H.C.) and on the eastern side of the ridge extending north of Bedggood Hill [FP042782].

Almost everywhere, dolerite clasts are quite fresh with only the thinnest of weathered rinds. Several exposures were recorded, however, that have been subjected to prolonged *in situ* chemical weathering, suggesting an older phase of talus development. These deposits consist mostly of clay, with wholly or partially weathered cobbles of dolerite. Most occurrences were recorded in the Mt Nicholas area, at EQ908035, EQ915029, EQ924035, EQ895001, EQ902021, EQ893009 (all R.H.C.); EP901994 (P.W.B.); and EQ914032 (C.R.C.). In most of these exposures the weathered talus is seen to be abruptly overlain by fresh, more clast-rich, younger talus. An exposure at FP035933 contains a completely weathered boulder one metre in diameter.

Recent soil development and dissection by the present drainage system indicate that the talus deposits are for the most part presently stable. Minor landslips on steeper slopes provide evidence for some contemporary movement. Previous work (Nicholls, 1958; Davies, 1967) suggests that extensive dolerite talus mantles originated predominantly by mass wasting under periglacial conditions during the Pleistocene, when solifluction and frost creep were more effective than at present. Caine (1983) gives a detailed discussion of the dolerite solifluction mantles of north-east Tasmanian mountains.

LAG GRAVEL (Qpl)

N. J. Turner

Lag gravel classed as Qpl occurs at elevations of 20–60 m above sea level west of Falmouth [FQ060040] and Piccaninny Point [FP077834]. At higher elevations the gravel consists of well-rounded cobbles and pebbles of vein quartz, Mathinna Beds quartzite and resistant Parmeener Super-Group lithologies and sometimes contains rounded quartz granules and quartz sand. At lower elevations in the Falmouth district the lag includes cobbles of St Marys Porphyrite.

On the seaward facing slopes west of Piccaninny Point the highest lag is distributed discontinuously over a distance of about 3 km at a constant elevation of 50–60 m. This elevation corresponds to a change from gently inclined, lower slopes to steeply-inclined, upper slopes. Lag gravel in the Falmouth district attains a similar maximum elevation and there is a corresponding but less pronounced change in slope. This change in slope at about 50 m above sea level is evident along the entire coast between Falmouth and Piccaninny Point and is thought to represent an old shoreline. The lag gravel at 50–60 m is interpreted as the remnant of associated beach deposits and gravel at lower elevation is thought to have formed either offshore or during transgression or regression.

In creeks in the Falmouth district (e.g. at FQ041031, FQ041021, FQ030030) there are *in situ* cobble beds which may be representative of the parent deposits of the lag gravel. They consist predominantly of deeply weathered clasts of St Marys Porphyrite in a weathered feldspathic matrix. There is a small component of clasts of resistant rock types which could be concentrated on removal of the weathered felsic material to give a lag resembling the Qpl of higher elevations.

UNDIFFERENTIATED AQUEOUS DEPOSITS AND AEOLIAN SAND (Qpc)

N. J. Turner

Deposits of this class are confined to relatively flat, soil covered areas below 20 m a.s.l. The two main areas are in the Falmouth district and between Chain of Lagoons (FQ064860) and Seymour (FP061776). There is no similar physiographic feature of equivalent elevation along the coast between Falmouth and Lagoons Beach.

In the Falmouth district (e.g. at FQ046028) the Qpc deposits overlie deeply weathered cobble beds of unknown thickness which consist mainly of St Marys Porphyrite. The Qpc deposits consist of 3–4 m of bedded sandy clay, granuly sand with sparse pebbles and festoon cross-bedded, coarse-to medium-grained sand. Charcoal fragments are common throughout and two soil horizons are present in places. Iron enrichment is associated with the lower soil horizon near FQ046027. Near Henderson Lagoon [FQ055047] there is peaty, sandy clay which contains common shells.

Exposure of the deposits in the Chain of Lagoons to Seymour area is poorer than near Falmouth. At Chain of Lagoons there is a 3 m section in Wardlaw Creek of horizontally bedded sand

containing carbonaceous material. Nearby [FP068865] similar sand has a ferruginous cement. In a one metre section at FP072862 well-sorted, medium-grained sand is overlain by 0·3 m of peat thence by windblown sand. South of Piccaninny Point there are water-lain and aeolian sands on which a soil horizon is developed and there is cobbly sand containing shells at FP066815.

The deposits classed as Qpc in the St Marys Quadrangle resemble deposits in the Boobyalla Quadrangle (Baillie *et al.*, 1980) which are also classed as Qpc and are assigned a Pleistocene age. They occupy a similar geomorphological setting and comprise similar types of deposit.

DOLERITE ALLUVIUM (Qad)

C. R. Calver

Qad consists of immature dolerite-derived stream gravels and fine talus, and forms sheet-like deposits covering a large part of the floor of the Fingal Valley and the coastal plain north of Seymour. The gravels are dominantly composed of platy dolerite fragments, 50–200 mm long, in closed framework with a brown clayey sand matrix. Rare clasts of other resistant lithologies may be present. The clasts have a sub-horizontal preferred orientation and are often crudely imbricate. Stratification is usually evident as variations in clast size, and lenticular beds of clayey sand are often present. Present day streams, such as Lightwood Rivulet [EP970934] have cut through the deposit, exposing sections through the gravels and reaching bedrock in places. In the Fingal Valley, Qad attains a maximum thickness of over 6 m near the foot of the Tier, and becomes thinner northwards. An old alluvial terrace composed of Qad occurs above the level of the alluvial plain on the south side of Piccaninny Creek at FP053840.

Qad is nearly everywhere overlain by recent soil developments. At FP056823 it overlies dolerite talus (Qptd). The dolerite clasts in Qad are nearly everywhere quite fresh, except for a deeply weathered, and therefore possibly substantially older, exposure at FP072784 at the southern end of Templestowe Lagoon.

STREAM SEDIMENT AND SWAMP DEPOSITS (Qha)

N. J. Turner
C. R. Calver

Alluvium of well-sorted sands and gravels occupies low-lying areas adjacent to the Break-O'Day River. It is mostly overlain by recent soil horizons and is being reworked by present day streams. The alluvium is 8–12 m thick in the Killymoon borehole [EP915959].

Streams draining eastwards to the sea and northwards to Scamander River are very youthful. They have generally steep gradients and are actively erosional, undercutting their banks and transporting fragments of up to boulder size. Depositional tracts are small level areas which occur mainly at low elevations near the sea. Their boundaries are taken at the surrounding break of slope.

Wardlaw Creek has a depositional tract at Chain of Lagoons which contains a cobble deposit near its upstream end. The deposit is about 1·5 m thick, clast supported, imbricated and consists mainly of Mathinna Beds fragments. It fines upwards and is overlain by a soil horizon. Coarse material decreases downstream and the deposit passes laterally into Qpc. Lenses of gravel, sandy clay and coarse sand are exposed where other streams have undercut their alluvial plains.

Qha occupying numerous small basins on the Fingal Tier plateau probably includes swamp deposits as well as alluvium.

DUNE SAND AND BEACH DEPOSITS (Qhb)

N. J. Turner

Long sandy beaches backed by low, partly vegetated dunes are a feature of the southern part of the coastline in the St Marys quadrangle. The dunes have obstructed streams seeking to enter the sea thus causing either the stream to deviate (e.g. Lower Marsh Creek - FP072872) or the damming of the stream forming a shallow lagoon (e.g. Templestowe Lagoon, FP065795). Dunes at Piccaninny and Long Points have been subjected to blowout.

The remainder of the coastline in the quadrangle is mainly rocky with scattered boulder and gravel deposits. Aboriginal middens and implements are common along the coast.

IGNEOUS ROCKS

Devonian felsic extrusive/intrusive rocks (St Marys Porphyrite) (Dpr/Dpm)

N. J. Turner

STATUS OF OTHER PUBLISHED WORK

Walker (1957) named the St Marys Porphyrite and on the basis of features evident in the northern part of the body he suggested that it was either extrusive or a high-level intrusion. Walker (1957), McNeil (1965) and McDougall and Leggo (1965) all recognised similarities between the St Marys Porphyrite and volcanics of broadly similar age in Victoria. However, McNeil (1965) showed the south-western contact of the porphyrite body to be intrusive and the body has subsequently been regarded as a high-level intrusion.

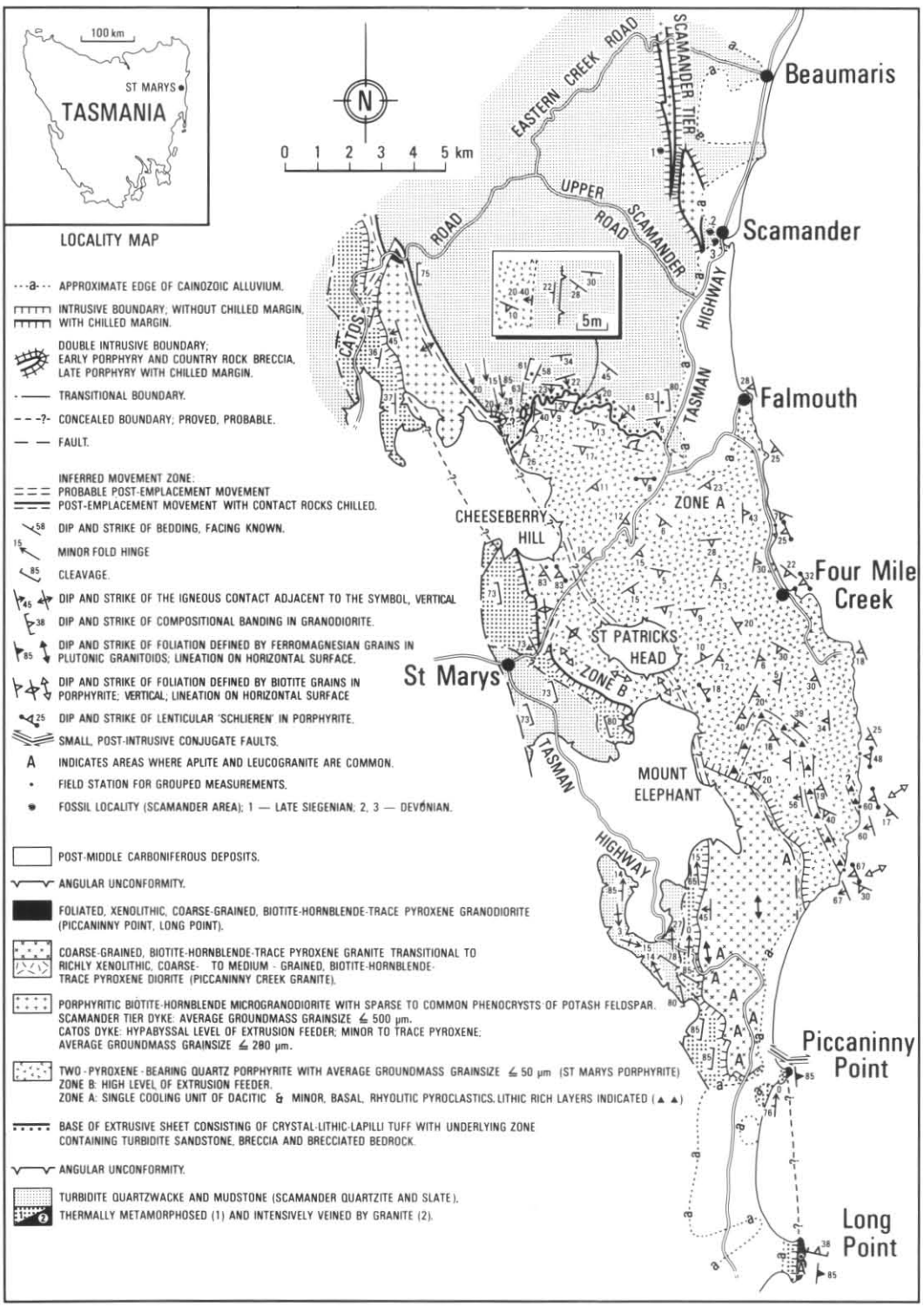

Figure 11. *Simplified map of the pre-Permian rocks in the St Marys Quadrangle and in the adjacent part of the St Helens Quadrangle.*

5 cm

Although the mapping and associated work described in this report confirm McNeil's (1965) finding that the south-western contact of the St Marys Porphyrite is intrusive, it disputes the view that the body is a single entity. Rather, the work indicates that the body consists of extensively recrystallised, ash-flow tuff in the north and east (Dpr = Zone A in fig. 11) and intrusive rocks in the south-west (Dpm = Zone B in fig. 11).

The form of the St Marys Porphyrite and the Rb-Sr geochronology and comparative geochemistry of all the major felsic, igneous bodies in the St Marys district are discussed in Turner *et al.*, 1986. K-Ar isotopic data are given in the same paper and in McDougall and Leggo (1965). The mineral chemistry, crystallisation history and petrogenesis of the St Marys Porphyrite and associated rocks are discussed in Higgins *et al.*, 1986.

TERMINOLOGY

On the basis of field and petrographic evidence the northern to eastern part of the St Marys Porphyrite is regarded as ash-flow tuff in which the matrix has been generally extensively recrystallised. On the same basis rocks in the south-western part of the porphyrite body are regarded as intrusive but they appear to have also undergone vesiculation and recrystallisation. Chemically both the extrusive and intrusive parts of the body are predominantly dacitic (fig. 12) with volumetrically minor rhyolitic material near the northern, basal contact. Combining the chemical, petrographic and field evidence the porphyrite body may be designated as a volcanic complex consisting of recrystallised, dacitic and minor rhyolitic, ash-flow tuff and recrystallised, vesiculated, intrusive dacite. Although based on sound evidence the use of this essentially genetic terminology on a lithostratigraphic map would be potentially confusing because most rocks in both parts of the body are very similar in hand-specimen and thin-section. For this reason use of the non-genetic term porphyrite is retained.

In their original usage the nouns porphyry and porphyrite had connotations of texture and of the type and volumetric importance of feldspar phenocrysts (Joplin, 1964). The adjective porphyritic was descriptive of texture only. Modal analyses (table 2; McNeil, 1965, p. 37) show that in the consistently porphyritic St Marys Porphyrite plagioclase is the principal phenocryst phase. Potash feldspar phenocrysts are very minor in dacitic rocks and they are subordinate to plagioclase phenocrysts in rhyolitic rocks. The term porphyrite is thus a reasonably precise and simple name for the dacitic rocks which make up the great bulk of the body.

McNeil (1965) favoured the term adamellite porphyry instead of porphyrite in order to recognise both the texture and the presence of considerable potash feldspar in the matrix. However, accurate determination of the proportions of each type of feldspar in the

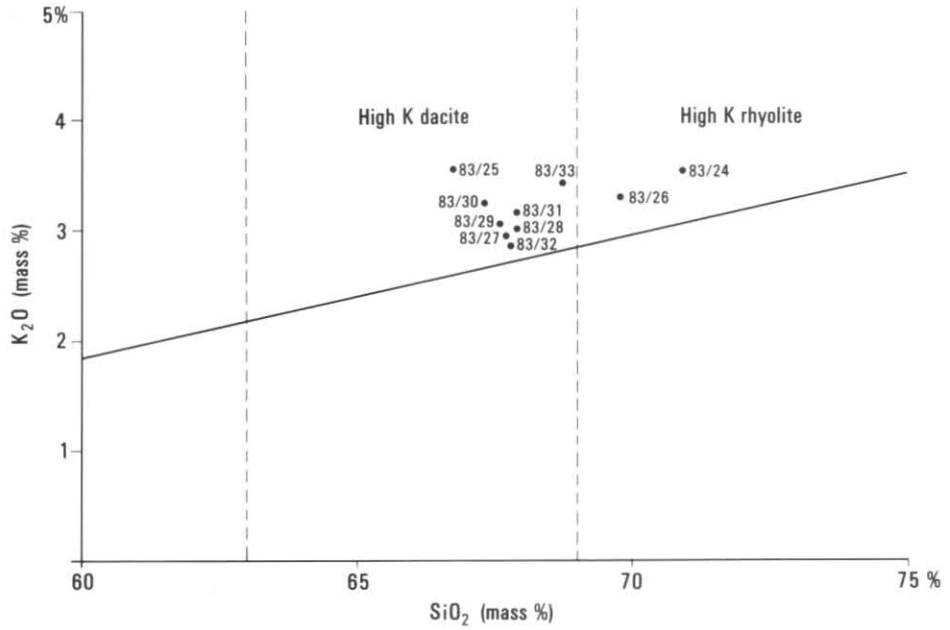

Figure 12. *K_2O/SiO_2 data for the St Marys Porphyrite relative to the dacite and rhyolite classification fields of Ewart (1979). See Table 2 for full chemical analyses and for the grid co-ordinates of sample sites. The rhyolitic samples (83/26, 83/24) and the least siliceous dacitic sample (83/25) were all collected near the base of the body west of the Tasman Highway.*

Table 2

MODAL ANALYSES OF SAMPLES FROM ST MARYS PORPHYRITE

Grid. ref.	FQ024031	FQ030032	FQ034020	FP027998	FP030983	FP02978	FQ004957	FP054884	FP077833
Q	19·7	6·5	18·6	21	16 (19·6)	14·4 (20·3)	13·9 (13·0)	34	30·8
P	21·2	26·1	30·0	27·2	24·7 (6·1)	24·5 (9·3)	24·8 (2·4)	31·9	33·2
P(A).....	0·5	tr	0·1	0·1	1·2	0·7	1·7	1	4·2
K	4·6	0·5	1·9	1·5	0·6 (16·1)	2·3 (15·5)	2·6 23·3	19·6	16·4
B	3·5	5·7	8·7	7·5	8·5	10·0	7·9 (5·0)	9·8	6·9
Px	tr	5·4	6·3	3·8	0·3	0·1	0·2		
H	0·7(F)	tr	1·4	0·3	4·1	1·5	1·5	2·8	5·7
C	0·7	0·1	0·4	0·7	0·3	tr	0·6	0·8	2·1
O	tr	0·9	tr	tr	tr	tr	tr	tr	tr
NaG.....	0·5	0·3	-	-	2·4	-	3·1	-	-
ML.....	1·8	0·6	-	-	-	-	-	-	-
Acc.....	tr	tr	tr	tr	tr	tr	tr	tr	tr
TG	46·8	53·8	32	37·5	42·4	45·1	43·7	-	-
Counts.....	2032	2115	694	909	1977	925	1766	925	909
P:K	-	-	-	-	66:34	66:34	53:47	63:37	70:30
Chem.....	rhyolite	dacite	dacite	dacite	dacite	dacite	dacite	-	-

matrix is generally difficult because of fine grain size also Table 2 shows that the total composition when the matrix is taken into account may be either granodioritic (83/30) or adamellitic (83/33). In addition, SiO_2 contents (fig. 12) indicate that the compositions of other rocks in the St Marys Porphyrite cluster around the boundary between granodiorite and adamellite (*c.* 69% SiO_2). Thus the use of either term in the name of the body is undesirable from the point of view of accuracy. Their use is also undesirable because they have a plutonic connotation.

Some modern authorities (e.g. Gary *et al.*, 1977) regard the term porphyrite as obsolete and consider it to be synonymous with porphyry. The terms are considered to have a textural connotation only. By this usage St Marys Porphyry would replace St Marys Porphyrite. However, Walker's (1957) term porphyrite has precedence and is precise. Therefore there seems little point in changing to another name.

FEATURES OF THE NORTHERN, BASAL ZONE

GENERAL APPEARANCE

The rocks are short-jointed but otherwise massive and dense. They are porphyritic, containing abundant mineral grains ranging in size from less than one millimetre across to about 8 mm across. In rocks nearest the contact the upper size limit of grains is smaller at about 5 mm. The mineral grains rest in a groundmass or matrix which is dark grey and aphanitic throughout the basal zone. Small, angular, elongate metasedimentary rock fragments up to about 30 mm across occur widely. Igneous rock fragments are also present but appear to be confined to the area east of Styx Creek. The fragments are discoidal in shape and appear to have been flattened. Possibly they were pumice. No compositional banding was recognised in the basal zone in the field either at the scale of the map or in outcrop. However, a gently dipping foliation is generally discernible in outcrop. It is defined by aligned biotite flakes, elongate metasedimentary lithic fragments and pumice? fragments.

CHEMICAL COMPOSITION

Sampling of the basal part of the St Marys Porphyrite for chemical analysis was restricted to three localities (fig. 11) which are in the area between Styx Creek and Ferntree Glen Creek. The analyses (table 3, 4; fig. 12) demonstrate the presence of both rhyolitic and dacitic rocks. The rhyolitic rock-type is distinctive in thin-section but it was not distinguished from dacitic material in the field. In both localities from which rhyolitic material was collected there are pumice? fragments but none was observed in the dacitic locality. Further work may establish a correlation between rhyolitic material and pumice? which could be useful in determining the precise field relationships of the rhyolitic material.

The three samples analysed indicate that the basal zone of the porphyrite body is compositionally layered and possibly interlayered. One sample of rhyolitic material (83/26) was collected 75 m laterally from the basal contact (near FQ032031). Dacitic material (83/25) of particularly low silica content was collected in the same vicinity at a distance of about 10 m from the contact. Since the contact dips gently beneath the sample sites it appears that there is a sequence of basal silica-poor dacite overlain by rhyolite which is in turn overlain by normal dacite that occurs further from the contact. The second rhyolitic sample (83/24) was collected 800 m west at a distance of about one metre from the contact. It may

Table 3

MAJOR ELEMENT GEOCHEMISTRY, ST MARYS PORPHYRITE

Sample	83/25	83/26	83/28	83/32	83/37	83/38	83/35	83/33	83/24	83/27	83/29	83/31	83/30	83/34	83/36
Grid	FQ	FQ	FQ	FP	FP	FP	FP	FP	FQ	FQ	FP	FP	FP	FP	FP
ref.	032032	032031	028010	005960	077833	082774	054884	004957	024031	034020	027998	008970	030983	055887	055877
SiO_2	66·74	69·78	67·89	67·82	67·11	65·91	69·04	68·75	70·94	67·67	67·59	67·92	67·32	70·60	68·00
Al_2O_3	15·25	14·32	14·52	14·62	13·94	14·17	14·18	14·34	13·78	14·51	14·54	14·38	14·50	14·16	14·34
Fe_2O_3	1·13	1·01	1·11	1·30	0·71	1·00	0·85	1·03	1·11	1·04	1·18	1·11	0·96	-	-
FeO	3·15	2·70	3·38	3·08	3·23	3·30	2·70	2·77	2·16	3·46	3·23	3·23	3·30	-	-
Total Fe	-	-	-	-	-	-	-	-	-	-	-	-	-	3·40	3·87
TiO_2	0·66	0·49	0·62	0·62	0·51	0·57	0·48	0·53	0·39	0·61	0·62	0·60	0·60	0·47	0·53
MnO	0·08	0·07	0·09	0·09	0·08	0·08	0·06	0·07	0·07	0·09	0·08	0·08	0·08	0·06	0·07
CaO	3·67	3·34	3·92	3·72	3·98	4·29	3·41	3·23	2·81	3·97	3·92	3·79	3·77	3·31	3·78
MgO	1·61	1·42	1·78	1·85	3·00	3·26	1·52	1·51	1·14	1·77	1·75	1·71	1·71	1·37	1·55
K_2O	3·55	3·30	3·00	2·89	3·47	3·27	3·51	3·41	3·53	2·94	3·03	3·19	3·25	3·91	3·50
Na_2O	2·83	2·75	2·74	2·82	2·38	2·35	2·72	2·81	2·49	2·80	2·81	2·70	2·88	2·31	2·55
P_2O_5	0·16	0·14	0·18	0·16	0·14	0·17	0·12	0·14	0·12	0·17	0·16	0·18	0·13	0·11	0·11
CO_2	0·13	0·16	0·12	0·12	0·08	0·11	0·14	0·12	0·17	0·15	0·14	0·10	0·10	-	-
L.O.I.														0·75	0·89
H_2O^+	0·95	0·83	1·01	1·38	1·37	1·63	1·19	1·36	1·05	0·94	1·04	0·92	1·20	-	-
H_2O^-	0·05	0·00	0·02	0·03	0·00	0·00	0·01	0·00	0·01	0·00	0·00	0·09	0·01	-	-

Table 4

TRACE ELEMENT GEOCHEMISTRY, ST MARYS PORPHYRITE

Sample	83/25	83/26	83/28	83/32	83/37	83/38	83/35	83/33	83/24	83/27	83/29	83/31	83/30	83/34	83/36
Grid	FQ	FQ	FQ	FP	FP	FP	FP	FP	FQ	FQ	FP	FP	FP	FP	FP
ref.	032032	032031	028010	005960	077833	082774	054884	004957	024031	034020	027998	008970	030983	055887	055877
Ag	4	4	4	4	4	4	4	4	4	4	4	4	4	n.d.	n.d.
Sb	5	5	5	5	5	5	5	5	5	5	5	5	5	n.d.	n.d.
Sn	175	48	22	12	37	38	18	7	8	13	6	5	7	n.d.	n.d.
Th	18	14	13	11	19	17	14	17	15	13	18	14	14	n.d.	n.d.
Sr	250	230	250	270	220	240	220	270	220	260	250	250	240	224	250
U	6	7	5	5	6	7	8	5	9	7	5	7	7	n.d.	n.d.
Rb	160	155	135	135	155	150	160	155	160	130	135	140	140	173	176
Y	35	32	32	32	33	26	38	34	33	33	31	33	33	29	40
Zr	220	165	210	190	130	150	160	190	155	200	200	195	195	144	158
Nb	11	7	6	6	7	9	8	8	7	8	7	7	8	9	9
Mo	2	2	2	2	2	2	2	2	2	2	2	2	2	n.d.	n.d.
Pb	33	27	23	20	21	20	19	16	28	20	18	21	22	n.d.	n.d.
As	35	31	26	20	18	17	25	53	24	27	27	19	19	n.d.	n.d.
Bi	5	5	5	5	5	5	5	5	5	5	5	5	5	n.d.	n.d.
Ga	17	15	16	15	15	15	16	16	15	16	16	16	15	n.d.	n.d.
Zn	67	54	61	60	48	52	45	47	50	61	59	60	60	n.d.	n.d.
Cu	10	7	6	6	6	9	6	6	6	6	8	6	7	n.d.	n.d.
Ni	6	5	5	6	32	35	3	5	5	7	5	6	6	n.d.	n.d.
Sc	14	16	16	17	15	16	13	13	13	14	15	15	14	13	15
V	68	52	67	66	72	83	60	60	43	65	71	68	69	n.d.	n.d.
Cr	28	23	29	26	125	140	30	22	20	27	25	25	27	n.d.	n.d.
Co	5	5	7	7	11	12	5	7	5	6	7	5	5	n.d.	n.d.
Ba	670	540	600	710	370	520	660	590	560	580	600	620	590	711	604

represent an earlier rhyolite interval or it may have come from a transgressive part of the same interval that contains 83/26. Either way the variation in chemical composition indicates that more than one magma pulse is represented in the basal part of the St Marys Porphyrite. The presence of more felsic material near the base and cyclicity of early eruptions are typical of many volcanic suites (see Higgins *et al.*, 1986).

MINERALOGY

In order of decreasing abundance the principal minerals comprising the dacitic sample 83/25 are plagioclase, quartz, biotite and pyroxene (table 2). There are minor amounts of opaque minerals, potash feldspar, rock fragments and chlorite. In the rhyolitic sample 83/24, the order of abundance is similar but the relative importance of pyroxene and potash feldspar is reversed and rock fragments are more abundant. There is also minor fibrous hornblende or actinolite, probably after pyroxene.

Pyroxene minerals in the St Marys Porphyrite include both hypersthene and augite. Plagioclase grains show oscillatory zoned rims and may have corroded calcic cores. Resorbtion is a common feature of quartz grains. Alkali feldspar grains may either be homogenous with small $2V$ or microperthitic. Staining reveals that potash feldspar is also a major matrix mineral. Other felsic minerals in the matrix are too fine grained for identification in the basal rocks but are probably quartz and plagioclase since these minerals are major constituents of the more coarsely crystallised matrix in dacite higher above the base of the body. Tiny biotite flakes are abundant in the matrix of some material in the basal zone.

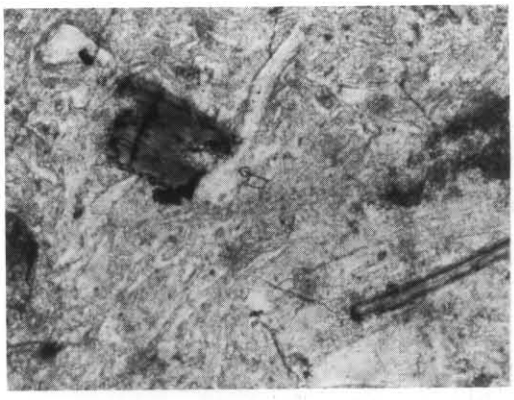

Plate 18. *Photomicrograph (plane-polarised light) of shard pseudomorphs (vitroclastic texture) preserved in the matrix of probably dacitic material collected from one metre laterally from the basal contact at EQ999042. The width of the field of view is 0.35mm.*

From a consideration of compositional zonation, inclusions and reactions displayed by minerals throughout the St Marys Porphyrite the following crystallisation sequence has been deduced (Higgins *et al.*, 1986). assemblage number 6 is prominent in both the intrusive rocks and and higher extrusive rocks whose slow cooling allowed subsolidus reactions to occur. Small fragments 2–4 m across of fine-grained (0·5–1 mm) norite and hypersthene gabbro are present throughout the porphyrite body (table 2) and may represent either early crystal cumulate or chilled phases of the parent magma. Their assemblages are opx (mg73) - plag (An_{80}); opx (mg73–68) - cpx (mg78) - plag (An_{80}).

Phenocryst assemblage	1 cpx (mg73) – opx (mg63) – plag? (An_{67-55})
	2 cpx (mg55) – opx (mg45) – plag (An_{55-50}) – biot – qtz
	3 cpx (mg50) – opx (mg42) – plag (An_{50-40}) – kfels – biot – qtz
	4 plag (An_{45-50}) – kfels – biot – qtz
Groundmass	5 kfels – plag (An_{15}) – qtz
Subsolidus	6 Reaction cpx, opx, = hnbld + qtz + kfels

Note: mg = 100 Mg / Mg + Fe

MICROTEXTURES

Quartz and feldspar phenocrysts in the basal rocks commonly have several crystal faces and one or more faces produced by fracturing. Alternatively quartz phenocrysts may be rounded and embayed due to resorption. Both quartz and plagioclase grains are generally strained and display undulose extinction. Biotite flakes also show strain and may be bent or kinked.

Groundmass textures vary according to the degree of recrystallisation. Vitroclastic texture is very poorly preserved, being present only locally within a few metres of the basal contact. In dacitic and probably dacitic rocks there are shard pseudomorphs which average about 50 μm in length. High magnification is necessary to discern them (plate 18) and they may only be preserved in parts of thin sections. The pseudomorphs are mostly straight to gently curved but some curve tightly through 180° and there are rare tricuspate forms. Texture within the pseudomorphs appears to be very finely granular although wavy extinction suggests a relict fibrous character. Where vitroclastic texture is absent the groundmass is very finely recrystallised and snowflake texture (Anderson, 1969) is often present (plate 19). Tiny biotite flakes in the groundmass may show alignment with shard pseudomorphs in a fabric that is deflected around coarse grains. In float of probable dacitic composition collected near EP880270 this flattening fabric is very strongly developed (plate 20) and 'beards' are developed adjacent to feldspar and quartz grains. In general

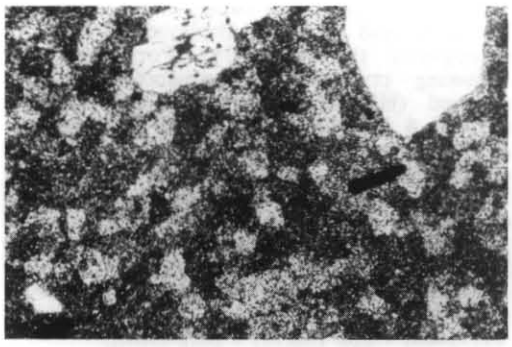

Plate 19. *Photomicrograph (crossed nicols) of snowflake texture (which reflects an early stage of recrystallisation) in the matrix of an igneous inclusion (?pumice fragment) in rhyolitic material collected near the basal contact of the St Marys Porphyrite at FQ032031. Width of the field of view is 1.55 mm.*

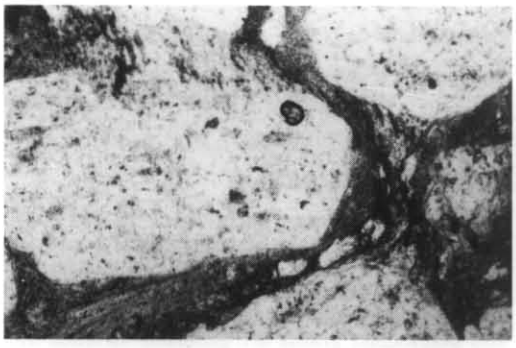

Plate 20. *Photomicrograph (crossed nicols) of well-developed beards adjacent to feldspar and quartz grains in strongly flattened St Marys Porphyrite. The sample was collected from float within a few metres of the basal contact at EQ989028. Width of the field of view is about one millimetre.*

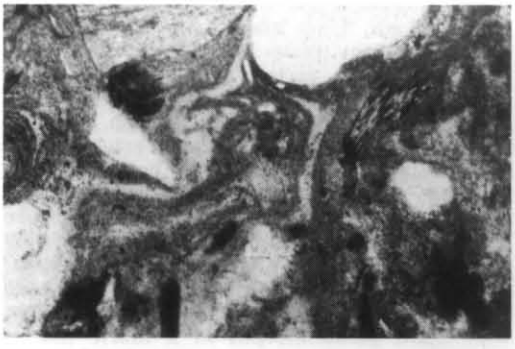

Plate 21. *Photomicrograph (plane-polarised light) of possible vitroclastic texture in the matrix of rhyolitic material collected about one metre laterally from the basal contact at FQ024031. The width of the field of view is 1.55 mm.*

the matrix fabric is parallel to aligned, relatively coarse biotite flakes and elongate rock fragments which impart a weak to distinct macroscopic foliation to outcrops in the basal zone.

In rhyolitic material the groundmass texture is evident at lower magnification. It consists of shard-like structures (plate 21) up to 350 um across and discontinuous microbands of uneven thickness and spacing that involve segregation of potash feldspar from other matrix constituents. These microbands are deflected around projections on large grains and appear to have been 'squeezed' into embayments in quartz crystals. There is a distinct variation in grain size with potash-rich areas having extremely fine grain size and other areas being markedly coarser grained (15 μm). The microbands may represent highly flattened shards but this was not demonstrated. Possibly they are due to chemical segregation during either compaction and recrystallisation or perhaps during a period of flow. Snowflake texture is a feature of recrystallisation in rhyolitic rocks.

PROBABLE PUMICE FRAGMENTS

The fragments of igneous rock that are common in the basal zone east of Styx Creek are porphyritic. They have the same phenocryst assemblage as the surrounding host material and they may contain common norite and gabbro fragments. The phenocrysts show less evidence of fragmentation and some are substantially larger than the largest in the host. Matrix comprises a much greater proportion (about 70% by volume) of the fragments than it does of the host. The matrix displays well-developed snowflake texture.

In the field the fragments are only clearly visibly on surfaces that have experienced the right degree of weathering. On these surfaces the matrix of the fragments is a dead white colour which contrasts with the brownish oxidised character of the surrounding surface. On fresh surfaces the fragments are identifiable with difficulty as almost black patches in very dark grey

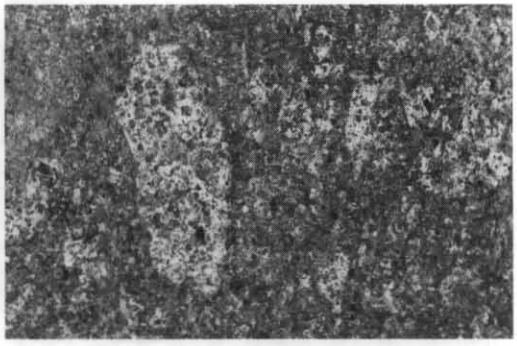

Plate 22. *Eutaxitic style of texture in probably rhyolitic material collected from float near FQ034030. The largest fragment is 70 mm long.*

surroundings. Deep weathering of outcrop surfaces causes the fragments to be obscured.

The shapes of the fragments resemble those of compacted pumice fragments, that is, they are predominantly discoids with ragged indented rims. Where they are abundant the fragments impart an eutaxitic texture (plate 22). In cross-section individual fragments range from less than 30 mm long with length:breadth ratios of about 10:1 to occasional fragments 100 mm long with length:breadth ratios of 3:1. The variation in length:breadth ratios suggests that the small fragments were more highly vesiculated (Ragan and Sheridan, 1972).

THE SOUTH-WESTERN CONTACT AND ADJACENT INTRUSIVE ROCKS

At the time of mapping there was a small artificial exposure of the south-western contact of the St Marys Porphyrite in a quarry beside the Tasman Highway at EP997965. The exposure showed the contact at this locality to be intrusive and to dip at 75° towards 243°(true) beneath thermally metamorphosed Mathinna Beds. North-west of the quarry the thermal metamorphic aureole in the Mathinna Beds is at least 1·5 km wide whereas south-east of the quarry in the vicinity of Irish Town [FP010955] the aureole has a width of only about 150 m (fig. 11). The reason for this considerable discrepancy in aureole width is unclear. In both areas boundaries were mapped on the basis of rubble rather than outcrop and some uncertainty exists as to the exact position of the aureole boundary near Irish Town. However, coverage was sufficiently detailed to determine that the aureole width does not exceed 400 m. The variation in width may be due to change in dip of the contact but no reliable measurements or estimates or the contact dip were made other than the measurement made in the quarry. A similar constriction in width occurs in the aureole of the Piccaninny Creek granite near FP048858 on a similarly trending segment of contact. This constriction may be due to faulting and is discussed in a later section on structure.

The St Marys Porphyrite adjacent to the south-western contact consists of abundant phenocrysts in a dark-grey aphanitic groundmass. Grain size of the phenocrysts ranges up to 15 mm and they are less disrupted than phenocrysts in rocks occurring at distances of more than a few metres from the contact. The phenocrysts consist of the same minerals in the same general order of abundance (table 2; McNeil, 1965) as the porphyrite near the northern contact. In keeping with its relatively high SiO_2 content (table 3, fig. 12) sample 83/33 from adjacent the south-western contact contains relatively more potash feldspar phenocrysts. Pyroxene in the same sample is relatively sparse, having mostly been altered to hornblende. It appears that this alteration was intramagmatic rather than subsolidus because the very fine grain size of the matrix indicates that the contact rocks probably cooled too quickly for significant subsolidus reaction to have occurred. The matrix is aphanitic and the presence of snowflake texture implies that it is incipiently recrystallised glass.

The lateral extent of the 'chilled' margin in which the matrix is aphanitic is only a few metres. Further from the contact the matrix is phaneritic and coarser grained than it is near the northern basal contact (fig. 13). Potash feldspar, quartz and plagioclase are the principal matrix minerals. Tiny flakes of biotite may be present and show an alignment which is deflected by coarser grains but the degree of deflection is slight compared with some rocks in the northern, basal zone. The alignment is parallel to a very weak and patchily discernible macroscopic fabric that is defined by aligned, relatively coarse biotite flakes (e.g. FP004957) sometimes accompanied by a felsic streakiness in the matrix (e.g. EP997970). Strike of the macroscopic fabric follows the varying strike trends of the contact which is consistent with the fabric being a flow-related phenomenon.

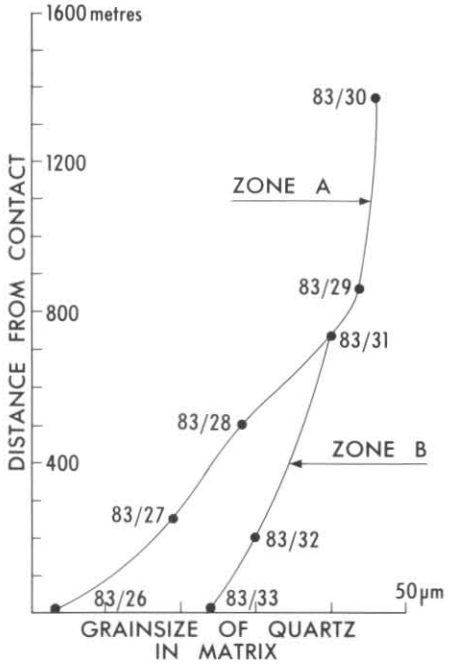

Figure 13. *Variation in the average size of matrix quartz grains in samples of St Marys Porphyrite. In samples 83/27 and 83/28 thirty grains were measured. In other samples 60 grains were measured. Co-ordinates of the sample sites are given in Table 3. Results for the intrusive part of the porphyrite (*Dpm, *Zone B in fig. 11) are plotted against distance from the south-western contact. Results for the extrusive part (*Dpr, *Zone A in fig. 11) are plotted against the estimated heights of samples above the base of the sheet.*

5 cm

BOUNDARY BETWEEN EXTRUSIVE AND INTRUSIVE ROCKS

The weak to distinct biotite foliation that appears to be a compaction foliation in the northern, basal rocks persists beyond the basal zone and maintains a shallow orientation over a wide area (fig. 11). However, south-west of a line that extends south-east through St Patricks Head there is a very weak biotite foliation which trends parallel to the steeply dipping 'flow' foliation near the south-western contact. This line through St Patricks Head appears to be the only structural discontinuity in the St Marys Porphyrite and is interpreted as a fault because it coincides approximately with the extrapolated position of a major fault which forms the eastern edge of Catos dyke (fig. 11).

Rocks south-west of the fault (Zone B of fig. 11) are considered to be vesiculated intrusives in the upper part of the feeder system of the porphyrite whilst rocks north-east of the fault (Zone A of fig. 11) are interpreted as a thick pile of compacted tuff. There is relatively little textural difference in porphyrite from either side of the fault and there is little difference in the morphology of the foliations. This is analogous with situations described by Almond (1971) and Fiske *et al.* (1963) in which steeply foliated intrusive rocks with pyroclastic texture occupy the upper levels of feeders to sheets of welded tuff.

THICKNESS OF THE EXTRUSIVE ROCKS

The thickness of the extrusive part of the porphyrite body was estimated for the section between FQ032032 on the northern contact west of Tasman Highway and FP030980 north of St Patricks Head near the boundary with the intrusive zone. An apparent dip for the base of the extrusives along the line of section was determined using data from a diamond drill hole at FQ032014 together with the distance and change in elevation between the drill collar and FQ032032. A value of 17° was obtained which is consistent in magnitude with dips of 5°–23° inferred from the intersection of the basal contact with the topographic contours. Assuming the value of 17° remains constant over the entire distance to St Patricks Head, the apparent thickness of extrusives in the section is 1 780 m. This figure reduces to 1 440 m when compensation is made for the effect of post-Palaeozoic faulting which produced a total of 340 m of north-side-down movement. The amount of movement is indicated by the relative elevation of a particular Permian unit (Pc) on St Patricks head (430 m elevation) and its correlate at FQ026029 (90 m elevation). The fault(s) causing the displacement was not located.

VARIATIONS IN MATRIX TEXTURE

Figure 13 illustrates the variation in average size of matrix quartz grains in a series of samples collected across the porphyrite from its northern contact near FQ032032 to FP030980 near St Patricks Head thence to the south-western contact. The sample interval is wide but the grain size trends are supported by field inspection which revealed no finer grained intervals between sample sites. North-east of St Patricks head grain size increases progressively with increasing height above the base of the porphyrite body. It decreases a little to the south-west of St Patricks head and shows relatively little variation with distance from the south-western contact.

Accompanying the changes in grain size are other changes in matrix texture. The mainly incipiently recrystallised matrix in the basal zone (plate 23*a–b*) changes upwards quickly to become a fine-grained, equigranular mosaic of evenly distributed, equant grains of potash feldspar, quartz and plagioclase (plate 23*c*). With increasing height the potash feldspar coalesces to form finely granular aggregates which surround and isolate other matrix grains (plate 23*d–e*). In the highest levels north-east of St Patricks Head large, optically continuous patches of potash feldspar also occur and substantial overgrowths appear on original, ash-sized grains of potash feldspar (plate 23*g*). The boundaries of mineral grains in the coarse fraction become progressively more pitted and irregular as the matrix changes and pyroxene grains are largely replaced by hornblende. Textures in rocks south-west of St Patricks Head are similar to those in the higher levels to the north-east, except in the chilled margin (plate 23*f*).

Overall the textural variations in the matrix of the St Marys Porphyrite north-east of St Patricks Head correspond to the stages of recrystallisation of glass outlined by Lofgren (1971). The variations are consistent with this part of the porphyrite body being a thick sheet of pyroclastics which cooled as a single unit and thus experienced high temperatures for progressively longer periods at higher levels in the sheet. With the exception of their chilled margin the rocks south-west of St Patricks Head appear to have cooled more uniformly.

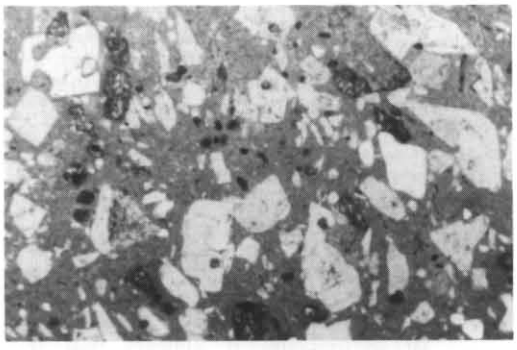

(a) *dacitic material collected at a height of less than 2 m above the northern basal contact of the St Marys Porphyrite at FQ032032 (83/25).*

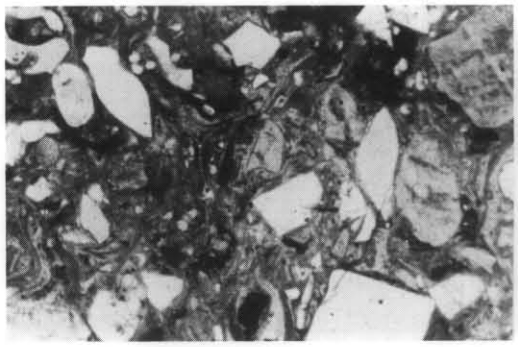

(b) *rhyolitic material collected at a height of less than 2 m above the base of the St Marys Porphyrite at FQ024031 (83/24).*

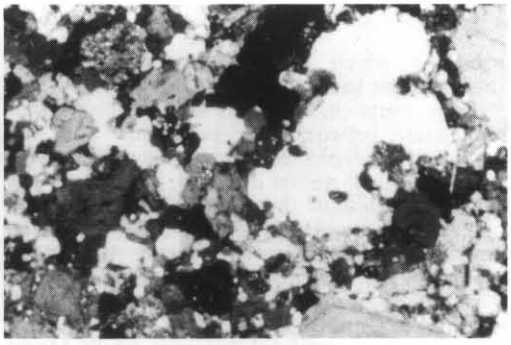

(e) *dacitic material - 1360 m above the base at FP030983 (83/30).*

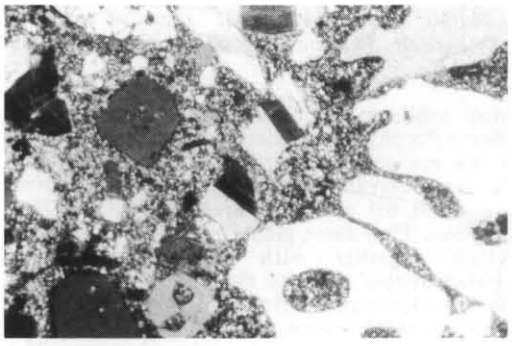

(c) *dacitic material - 230 m above the base at FQ034020 (83/27).*

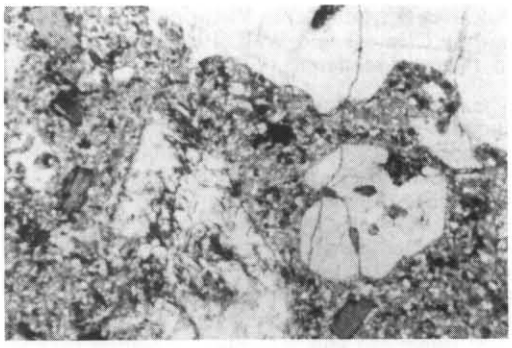

(f) *dacitic material from 'chilled', south-western margin of the St Marys Porphyrite at FP004957 (83/33).*

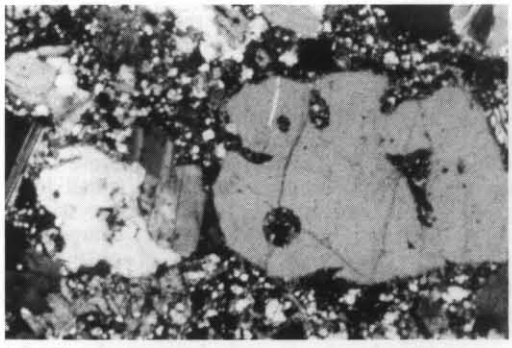

(d) *dacitic material - 850 m above the base at FP027998 (83/29).*

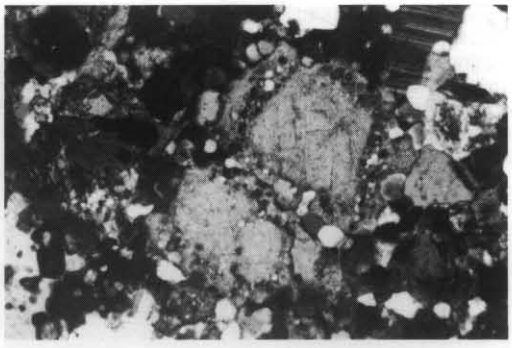

(g) *Enlargement of part of* e *showing inclusion-rich overgrowths on the original potash-feldspar grain south-west of the centre of the photograph.*

Plate 23. *Photomicrographs illustrating the variation in matrix grain size through the St Marys Porphyrite. For* a, b *(plane-polarised light),* c, d, e, *and* f *(crossed nicols) the width of the field of view is 4.2 mm. For* g *(crossed nicols) the width of the field of view is 1·55 mm.*

SCHLIEREN

Inclusions which are porphyritic and which consist of the same minerals as their host occur in both parts of the St Marys Porphyrite. Boundaries between the inclusions and the surrounding porphyrite tend to be diffuse over an interval of some 10 mm and thus the inclusions resemble schlieren. Where outcrop surfaces are deeply etched by weathering the presence of schlieren is difficult to detect. However, they are known to occur widely, being present in most coastal outcrops, in some creek outcrops (e.g. parts of Devils Creek, Ferntree Glen Creek), in artificial outcrops on St Marys Pass and in outcrops with relatively fresh surfaces which are scattered sporadically through the intrusive zone of the porphyrite body. Similar inclusions have been described from Devonian volcanics (rhyodacite) in Victoria by Birch (1978) and by Clemens and Wall (1984) who also refer to them as schlieren.

The groundmass grain size in the schlieren is similar to that in the porphyrite but the phenocrysts are larger and apparently less disrupted than the coarser grains in the porphyrite. The volumetric proportion of coarse grains is less in the schlieren but the difference is minor compared with the difference displayed by the igneous inclusions in the basal zone of the porphyrite. A conspicuous feature of the schlieren is that they are more felsic than their host (plate 24) and individual examples may be particularly distinctive due to the presence of a gneissic fabric (plate 25) defined by elongate patches of felsic groundmass, feldspars, strings of biotite grains and occasional, elongate, metasedimentary xenoliths. The xenoliths display coarser recrystallisation than metasedimentary fragments in the surrounding tuff. Inspection of an orthogonally-sectioned schlieren sample collected at FP046950 showed the gneissic fabric to consist of a strong linear component within a planar component.

Plate 24. *Felsic schlieren in St Marys Porphyrite cropping out on the shoreline east of Mt Elephant. The diameter of the lens cap is 49 mm.*

Plate 25. *Large and small felsic schlieren at FP084897 at the same locality as Plate 24. Note the gneissic style of internal foliation with aligned melanocratic xenoliths in the large schlieren that occupies the upper right segment of the photograph. The diameter of the lens cap is 49 mm.*

Most schlieren in the extrusive part of the St Marys Porphyrite are discoidal in shape although a few are equant or irregular. In cross-section the length:breadth ratios of the discoidal forms are about 6:1 and their average length is 200–300 mm. They show planar preferred orientation which together with the general shape characteristics suggests that the schlieren may be flattened pumice fragments. However, their length:breadth ratios are far exceeded by the maximum length:breadth ratio of nearly 25:1 cited by Ragan and Sheridan (1972) for compacted pumice in the Bishop Tuff. Possibly the degree of vesiculation of the schlieren in the St Marys Porphyrite was relatively low, that is, the schlieren may have resembled lava or vesicular lava rather than pumice. Birch (1978) suggested that schlieren in rhyodacite may have been lumps of magma which did not undergo disaggregation during eruption and emplacement and which underwent compaction during cooling. Clemens and Wall (1984) describe discoid felsic inclusions (schlieren) in rhyodacite which have planar arrangement with biotite phenocrysts and they interpret this fabric as a compaction foliation. They note that the proportion of potash feldspar phenocrysts is higher in the schlieren and suggest that they are derived from a less evolved magma than their host. No precise comparison has been made between the modal and chemical compositions of the St Marys Porphyrite and its schlieren, thus the interpretation of Clemens and Wall (1984) may or may not apply.

LITHIC-RICH LAYERS (Dprl) — PROBABLE ASH-FLOW UNITS

Layers containing abundant metasedimentary lithic fragments are present in rocks with a strongly recrystallised matrix east of Mt Elephant (fig. 11, plate 26). The fragments are mainly fine-grained metapelite containing a mineral

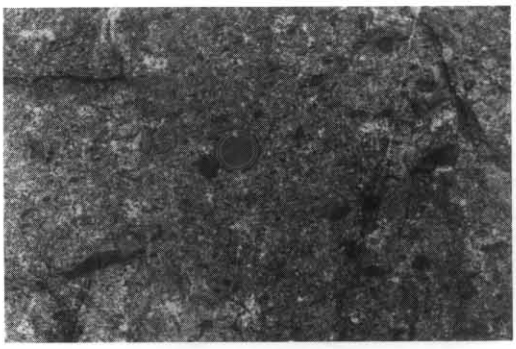

Plate 26. *Part of the zone rich in metasedimentary lithic fragments that crops out on the shoreline east of Mt Elephant at FP094897. The diameter of the lens cap is 49 mm.*

assemblage of quartz, biotite and potash feldspar but micaceous quartzite is also common and there are rare, small granite fragments. Most fragments are less than 60 mm across although there are uncommon examples up to 500 mm across. Shapes are angular but in cross-section very small fragments may have lenticular forms with whispy ends. Schlieren are also present in the layers.

There are substantial lateral thickness variations in the lithic-rich layer that was fully mapped out. It ranges from possibly 30 m thick to about 100 m thick. Within the layer the concentration of metasedimentary lithic fragments varies vertically such that it is least in the upper part, intermediate in the lower part and greatest in the central part where it ranges up to about 30% by volume. Schlieren are uncommon in the lower and middle part and common in the upper part. This partial segregation of schlieren and metasedimentary lithic fragments is comparable with the segregation of pumice and lithic fragments in pyroclastic flows which is attributed to differential buoyancy during transport (Sparks, 1976) and on this basis the layer is tentatively identified as a single flow unit or the base of a flow unit. It seems most likely that the metasedimentary lithic fragments accumulated as ground lag near the base of a thick flow unit.

There are other lithic- and schlieren-rich parts in the extrusive part of the St Marys Porphyrite but their lateral extents were not established. With very detailed mapping the distribution of lithics and schlieren may provide a basis for the stratigraphic subdivision of the extrusive sheet. Schlieren and lithics are present in the intrusive rocks south-west of St Patricks Head but they are sparsely scattered.

ORIENTATION FABRICS PROBABLY RELATED TO FLOW AND COMPACTION

Measurement and types

Fabrics due to the preferred orientation of constituents in the porphyrite are commonly weakly developed and difficult to discern. In most cases their orientation was determined by measuring their intersection lineations on several differently oriented surfaces of individual outcrops and plotting the lineations on a Lambert net. Orientations shown on the 1:50 000 map all represent single outcrops and the representativeness of most readings was tested by taking a considerable number of additional measurements in the same vicinity. Good consistency was found.

Several different types of fabric are present in the porphyrite.

They are defined by:

(1) biotite flakes;

(2) external shapes of igneous inclusions (pumice-like fragments in the northern, basal zone and schlieren);

(3) gneissic style of foliation inside some schlieren;

(4) external shapes of metasedimentary lithic fragments.

Relationships shown by these various fabrics differ in different parts of the porphyrite body. Although this report provides a substantial body of new information on those relationships, it should be regarded as a preliminary indication of the nature of what is clearly a complicated system. Further systematic work is necessary to fully describe and interpret the fabric of the St Marys Porphyrite.

RELATIONSHIPS IN THE INTRUSIVE ROCKS

Reference has already been made to the presence of a generally weakly-developed, steeply-dipping, biotite foliation in the intrusive part of the porphyrite body. The similarity between its orientation and the orientation of the contact implies a flow-related origin for the foliation. Unfortunately data relating to the orientation in the vertical plane of fabrics in much of the intrusive zone are sparse because most outcrops have little vertical relief thus making measurement of lineations on sub-vertical surfaces either impossible or imprecise in most localities. However, many measurements were made of the trend of fabrics on sub-horizontal outcrop surfaces.

At EP996989 near the north-western end of the zone there is sufficient outcrop relief to measure orientations in the vertical plane (fig. 14). Biotite

5 cm

flakes, schlieren shapes, schlieren-internal foliation and shapes of metasedimentary lithic fragments all have a roughly similar, steep orientation. However, at FQ046950 near the boundary with the extrusive rocks at the south-eastern end of the intrusive zone there is strong discordance between a shallow-dipping, schlieren-shape foliation and a steeply-dipping, schlieren-internal foliation (fig. 15). This locality is probably inside the intrusive zone because the boundary with the extrusive zone is only approximately positioned and in nearby rocks that are confidently regarded as part of the extrusive zone there is little evidence of steeply dipping fabric (e.g. fig. 16). Elsewhere in the intrusive zone individual schlieren may show discordance between their shape and their internal foliation and some internally foliated schlieren are without regular external shape. The significance of these variations of the external shape and shape-orientation of the schlieren in the intrusive zone is not understood and requires

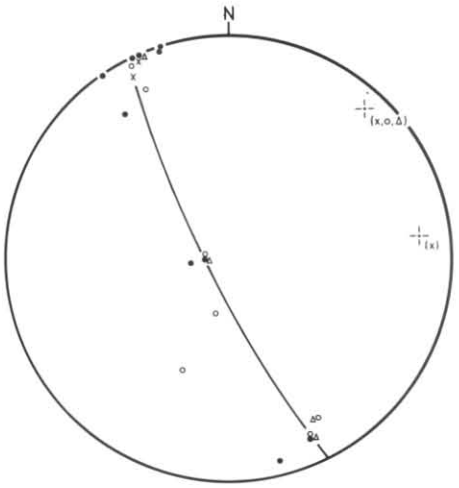

Figure 14. *Lambert projection of measurements of fabric elements in a small area near EP996989 at the north-western end of the intrusive part* (Dpm) *of the St Marys Porphyrite. The diagram shows roughly coplanar, steeply-dipping biotite flakes, elongate schlieren, elongate metasedimentary lithic fragments and internal fabric in schlieren. The following list provides a key to the symbols used in this figure and in Figures 15, 16, 18, 19, 20, 21, 23, 24.*

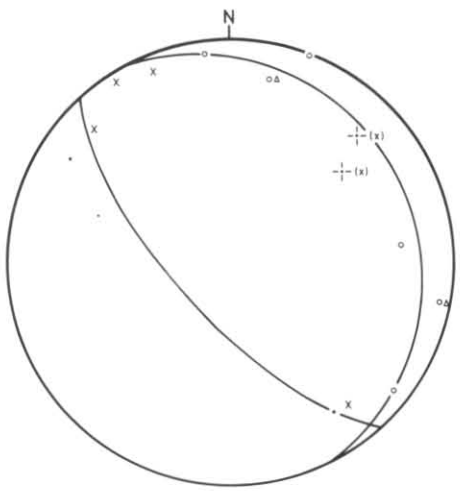

Figure 15. *Lambert projection of measurements of fabric elements in an area near the boundary between the extrusive* (Dpr) *and intrusive* (Dpm) *parts of the St Marys Porphyrite at the south-eastern end of the intrusive zone near FP046950. See Figure 14 for the key to symbols used. The figure shows shallowly-dipping, roughly coplanar, schlieren and metasedimentary lithic fragments and discordant, steeply-dipping schlieren internal fabric.*

- • Apparent lineation due to alignment of biotite flakes.
- ○ Apparent lineation due to alignment of elongate schlieren.
- △ Apparent lineation due to alignment of elongate metasedimentary lithic fragments.
- × Apparent lineation due to an internal fabric of gneissic style in some schlieren.
- ◇ Unspecified apparent lineation.

Measured pole of foliation. The type of foliation is indicated by symbols in parentheses:

- (×) Pole to internal fabric in schlieren.
- (•,○,△) Pole to coplanar biotite flakes, elongate schlieren, elongate metasedimentary lithic fragments.
- (c) Pole to approximately planar segment of the basal contact of the St Marys Porphyrite. Orientation estimated from the trace of the contact on the topography.
- (e) Pole to approximately planar segment of the lithic-rich layer east of Mt Elephant. Orientation estimated from the trace of the layer on the topography.
- ■ Pole to cleavage in breccia in Dsb.

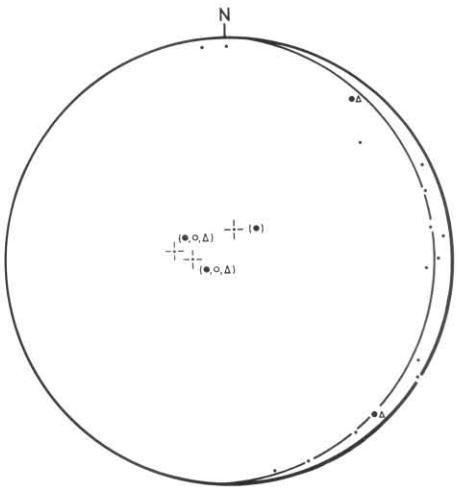

Figure 16. *Lambert projection of measurements of fabric elements in the extrusive part* (Dpr) *of the St Marys Porphyrite just north-west of St Patricks Head near FP025975. See Figure 14 for the key to symbols used. The figure shows shallowly-dipping, roughly coplanar biotite flakes, metasedimentary lithic fragments and schlieren.*

LEGEND FOR FIGURE 17

- Inferred fault
- Intrusive contact with metamorphosed Mathinna Beds
- Direction and angle of dip of contact.
- Foliation due to biotite flakes, apparent lineation on subhorizontal outcrop surface.
- Foliation due to schlieren shape
- Foliation due to schlieren internal fabric, apparent lineation on subhorizontal outcrop surface

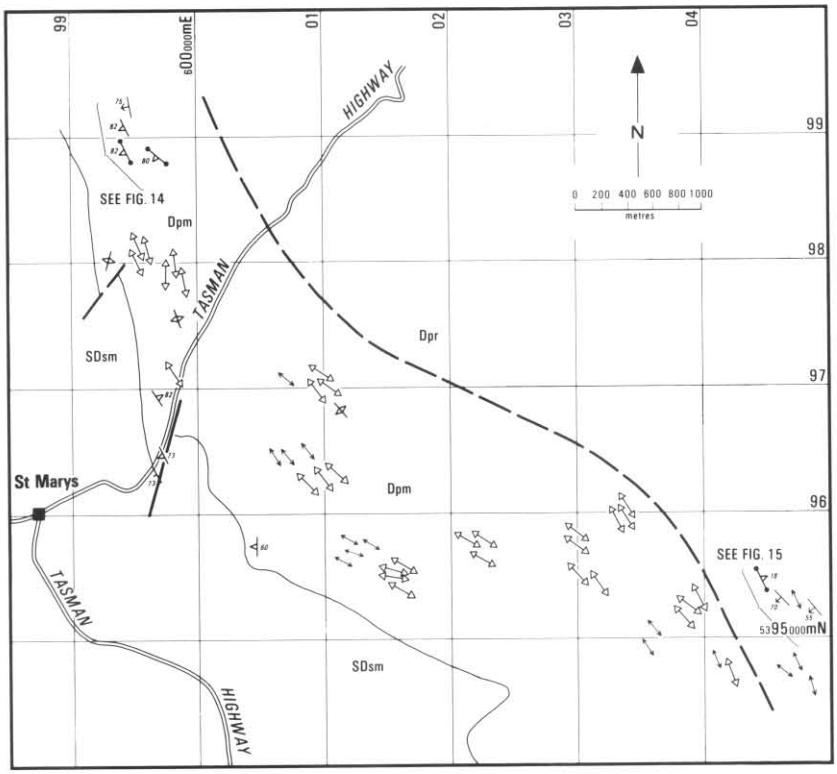

Figure 17. *Map showing fabric measurements made in the intrusive part* (Dpm) *of the St Marys Porphyrite. The figure shows the general trend of fabric elements sub-parallel to the contact.*

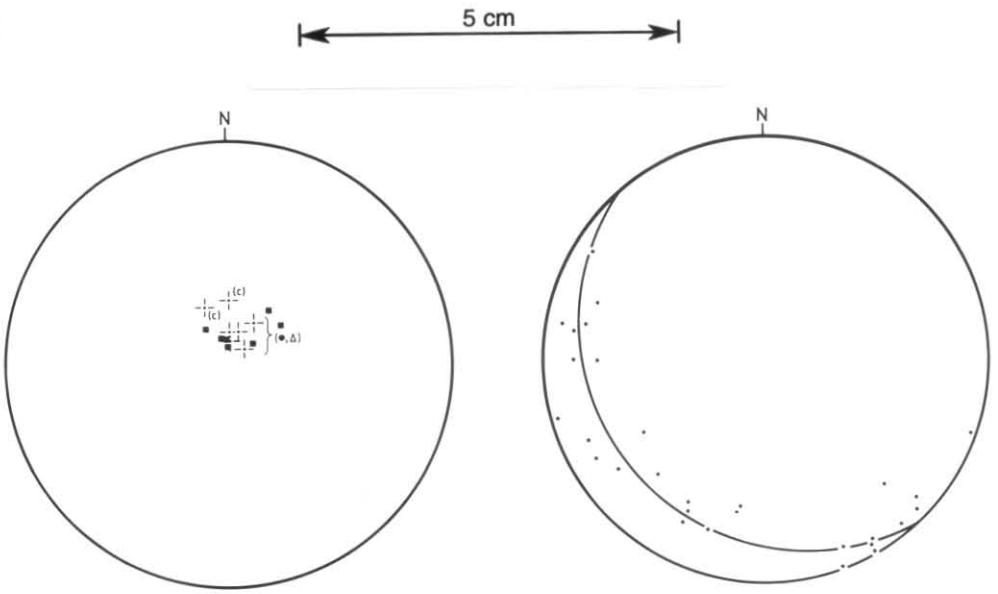

Figure 18. *Lambert projection of measurements made near the northern basal contact of the St Marys Porphyrite between EQ999041 and FQ008043. See Figure 14 for the key to symbols used. The figure illustrates that the foliation in the St Marys Porphyrite dips more shallowly than the basal contact of the body and is of similar orientation to shallowly dipping cleavage (?due to loading) in breccia in* Dsb.

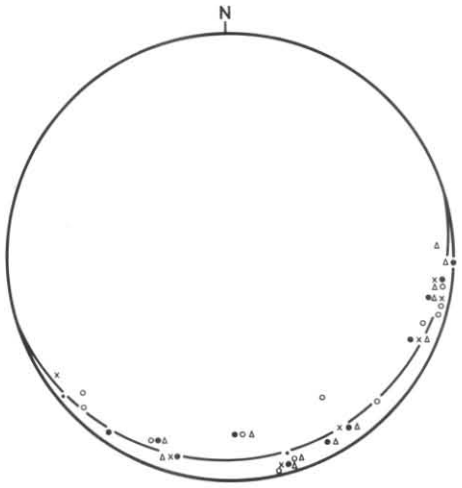

Figure 19. *Lambert projection of measurements of fabric elements in the extrusive part* (Dpr) *of the St Marys Porphyrite in Ferntree Glen Creek between FQ034021 and FQ025010. See Figure 14 for the key to symbols used. The figure shows roughly coplanar, shallowly-dipping biotite flakes, schlieren, metasedimentary lithic fragments and schlieren internal foliation.*

Figure 20. *Lambert projection of undifferentiated fabric elements in the extrusive part* (Dpr) *of the St Marys Porphyrite at Mariposa Point [FQ069206]. The figure illustrates the absence of significantly discordant elements.*

better description. The apparent consistency of orientation of the schlieren-internal foliation throughout the intrusive zone implies that the foliation developed *in situ*. This and its concordance with the biotite foliation (fig. 17) implies that its development was related to flow. Thus, it seems that the schlieren in the intrusive zone represent relatively unfragmented inhomogeneities in which a flow foliation is often better preserved than it is in the surrounding fragmental (extensively vesiculated?) porphyrite.

RELATIONSHIPS IN THE EXTRUSIVE ROCKS

The presence in the northern, basal zone of a gently dipping foliation probably due to compaction was referred to previously. The foliation is defined by groundmass microtextures, biotite flakes and the shapes of igneous inclusions and metasedimentary lithic inclusions. At FQ009042 (inset in fig. 11) and between FQ999042 and FQ009044 (fig. 18) the foliation is discordant with the basal contact and more shallowly dipping (c. 12° cf c. 22°). Similarly the shallowly dipping biotite foliation in the lower part of Ferntree Glen Creek (fig. 19) dips by about 10° more shallowly than the dip of the basal contact (17°) in the same vicinity, the latter dip having been determined by drilling at FQ032014. The biotite foliation in this area and the gently dipping, biotite foliation elsewhere in the extrusive zone are regarded as equivalent and both are considered equivalent to the foliation in the less extensively recrystallised basal zone.

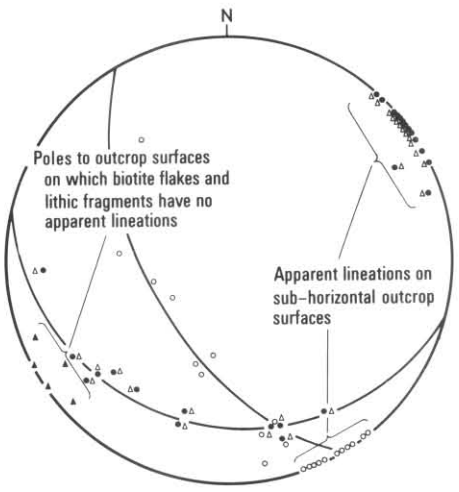

Figure 21. *Lambert projection of measurements of fabric elements in the extrusive part* (Dpr) *of the St Marys Porphyrite on the coast east of Mt Elephant at 093897. The data were collected along a 120 m traverse that crossed the more southerly of the layers rich in metasedimentary lithic fragments* (Dprl). *See Figure 14 for the key to the symbols used. The figure illustrates discordance between a shallowly-dipping foliation defined by coplanar biotite flakes and metasedimentary lithic fragments and a more steeply-dipping foliation defined by schlieren-shape. There is a prominent linear component in the biotite/lithic fragment fabric. Because of bias in the orientation of outcrop surfaces and the shallow dip of the biotite/lithic fragments fabric, this lineation was generally measured on subhorizontal outcrop surfaces. In some places the fabric is entirely linear with no evidence of a planar component intersecting surfaces normal to the lineation.*

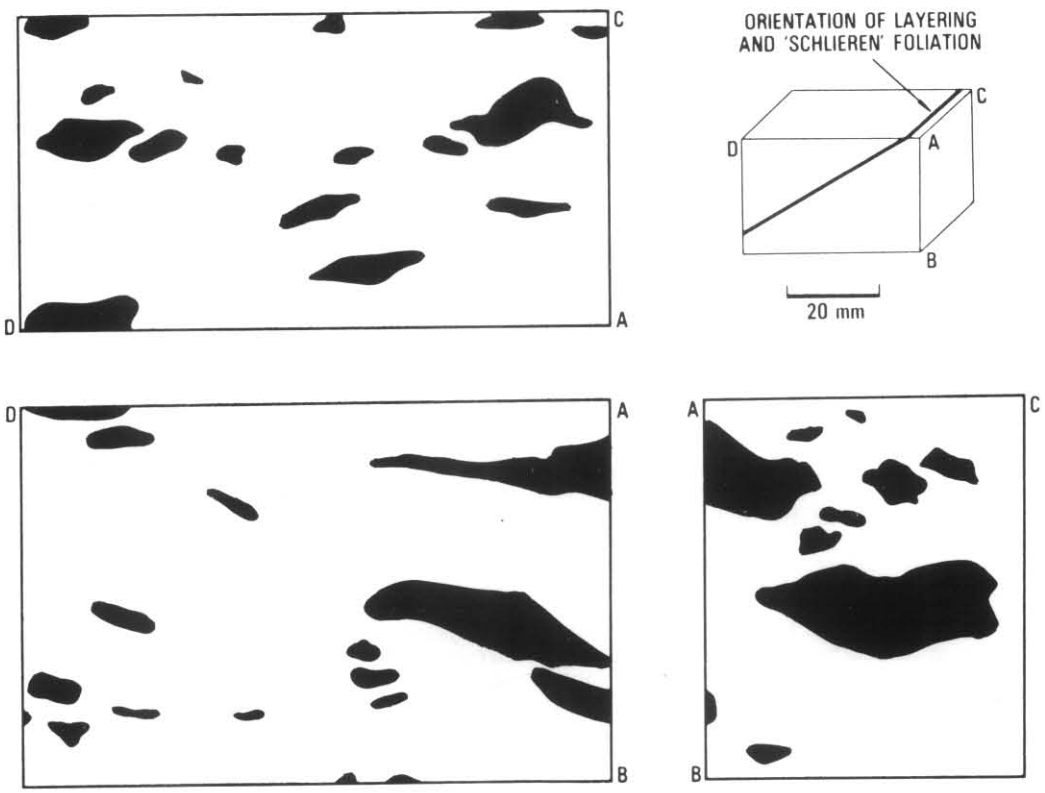

Figure 22. *Tracing of outlines of metasedimentary lithic fragments on orthogonally cut surfaces of a block from the same locality as Figure 21 [FP093897]. The figure shows the combination of foliation and lineation in the shape fabric of these fragments.*

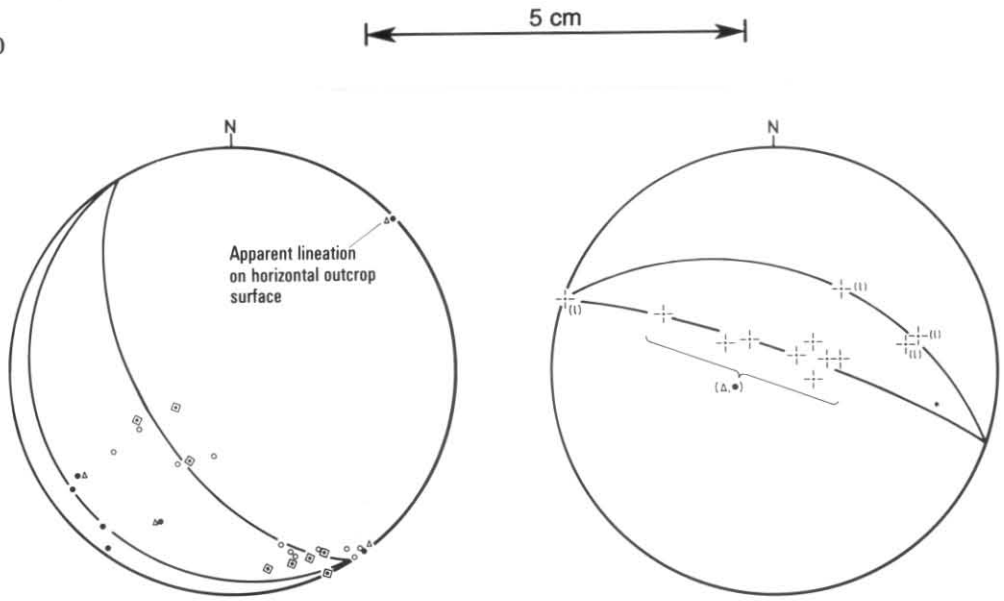

Figure 23. *Lambert projection of measurements of fabric elements in the extrusive part* (Dpr) *of the St Marys Porphyrite on the coast east of Mt Elephant at FP098917. The data were collected along a traverse of about 60 m length that crossed northwards out of the more northerly of the layers rich in metasedimentary lithic fragments into the adjacent normal porphyrite. See Figure 14 for the key to the symbols used. The figure illustrates that the foliation due to schlieren shape is roughly coplanar with the boundary of the layer. Also the orientation of the biotite/metasedimentary lithic fragments is much shallower.*

Figure 24. *Lambert projection of measurements of fabric elements defining the complex synclinal structure in the St Marys Porphyrite north-east of Mt Elephant. See Figure 14 for the key to the symbols used. The figure shows two girdles with axes of different plunge but of the same trend. Poles to foliations defined by biotite flakes and metasedimentary lithic fragments lie on a very shallowly-plunging girdle whereas poles to the boundaries of the layer rich in metasedimentary lithics lie on a more steeply-plunging girdle.*

In lower Ferntree Glen Creek the biotite fabric and the various other types of fabric all show a similar, shallowly dipping orientation. At Mariposa Point [FQ068026] on the coast south of Falmouth the various types of fabric are again shallowly dipping and there is little evidence in the data obtained (fig. 20) of either steeply dipping fabrics or discordant fabrics. A few kilometres further south discordance becomes evident between the very shallowly dipping biotite foliation and the shallowly dipping schlieren-shape foliation (fig. 11). This discordance is evident at places along the rest of the coastline to the south.

Figures 21–23 illustrate that the schlieren-shape foliation in the lithic-rich layers east of Mt Elephant dips more steeply than the fabric defined by alignment of both biotite flakes and small metasedimentary inclusions. The latter fabric is compound, containing a planar and linear component which reflect the often roughly triaxial shape of the small metasedimentary lithic fragments (fig. 22). At least some of these small inclusions appear to have undergone shape modification since they display lenticular forms with whispy, drawn-out tails. Intensity of the linear component of the fabric is variable, being pronounced in places yet difficult to detect only a few metres away. It is present both inside and outside the lithic-rich layers.

The fabric defined by biotite flakes and metasedimentary inclusions is younger than the schlieren-shape foliation and is expressed within schlieren by alignment of biotite grains. It is not equivalent to the gneissic schlieren-internal foliation which is very well developed in a large (0·6 m), fairly equant schlieren at FP094897 (plate 24) where it is oriented parallel to the general schlieren-shape foliation.

In coastal outcrops east of Mt Elephant the schlieren-shape foliation and the lithic-rich layers are oriented similarly (fig. 21, 23). Variations in the orientation of the schlieren-shape foliation in adjacent inland areas were not established, largely because of unsuitable outcrop. However, one of the lithic-rich layers was traced out and its orientation estimated from its intersection with topographic contours. The layer forms a syncline with a moderately dipping eastern limb and an apparently sub-vertical western limb.

The axial surface trace of the syncline coincides with the axial surface trace of a more open (fig. 24) syncline defined by the biotite foliation. In both the western and eastern limbs the biotite foliation dips more shallowly than the layering.

An explanation of the discordance in the coastal belt of the St Marys Porphyrite between the layering and schlieren-shape foliation on the one hand and the fabric defined by biotite flakes and small metasedimentary inclusions on the other hand may be developed by invoking essentially two phases of compaction with the latter phase accompanied by folding. Much of the compaction fabric evident in pyroclastic flows is generated by deflation which occurs shortly after emplacement (Ragan and Sheridan, 1972; Wolff and Wright, 1981). In thick, rapidly emplaced pyroclastic piles a long cooling period ensues (Riehle, 1973). Thus, further compaction may occur progressively through gradual loss of residual volatiles and constant volume deformation until the temperature of the pile falls below some limiting value. If during this late phase the pyroclastic pile underwent relatively rapid folding the fabric generated by the early compaction could be inclined well away from the horizontal before compaction ceased. In the case of the St Marys Porphyrite the schlieren-shape foliation may represent early deflation whilst the layering in the pyroclastics was still sub-horizontal and the generally weakly developed biotite and metasedimentary inclusion fabric may have been the result of subsequent compaction during folding. The linear component in the latter fabric may reflect shear in the plane of the foliation.

Folding during the cooling period of the extrusive sheet was perhaps due to subsidence along basement fractures related to the regional lineament that includes Scamander Tier dyke and the contacts at Piccaninny Point and Long Point (fig. 11). However, there is evidence of regional folding having affected the north western edge of the porphyrite body (see later section) and it may also have affected the coastal belt. The asymmetric form of the syncline formed by the layering in the porphyrite is similar to the asymmetry shown by folds in the Mathinna Beds on Elephant Pass.

Major Devonian granitic intrusions

N. J. Turner

PORPHYRITIC MICROGRANODIORITE (Dapl)

Part of a body of porphyritic, biotite-hornblende microgranodiorite crops out in the region of Catos Creek [EQ970040] near the northern edge of the map sheet. The body is a dyke of asymmetric form and is called Catos Creek dyke. It has a steeply dipping eastern contact against thermally unmetamorphosed Mathinna Beds whereas its western margin dips moderately (about 45°) beneath an extensive thermal metamorphic aureole. The contacts of the dyke are considered to extend south beneath the younger sedimentary rocks of the Parmeener Super-Group to reappear near St Marys as the boundaries of the intrusive part of the St Marys Porphyrite. Chemical and isotopic data support this contention by indicating that the rocks in the dyke and those in the St Marys Porphyrite are derived from the same magma (Turner *et al.*, in 1986).

There is clear evidence that the eastern contact of the dyke is a fault at EQ984034 and further north at Catos Road in St Helens quadrangle. In the former locality there is a band about 300 mm wide adjacent the contact of intensely shear-foliated country rock in which anastomosing, closely spaced and polished foliation surfaces are parallel to the contact. The igneous material adjacent to the contact is also deformed. It is foliated but massive and unfractured thus implying that the deformation was ductile not brittle. A proportion of intact quartz and feldspar phenocrysts are present but most grains are shattered. In particular quartz grains are strewn out into lenticules containing highly strained, partially annealed fragments. Alteration of feldspar grains to sericite is extensive but, surprisingly, biotite shows no chlorite alteration.

Despite evidence that the eastern contact of the dyke is a fault, the rocks adjacent to the contact are chilled which indicates that the fault may coincide with an intrusive contact. Other movement on the contact predating emplacement of the microgranodiorite is indicated by the presence of an early breccia phase which is generally very poorly preserved along the main eastern contact of the dyke between Catos Creek in St Marys Quadrangle and Catos Road in St Helens Quadrangle. The breccia is well preserved around the edges of the apophysis at EQ986036, particularly at the northern edge where it forms an interval about 10 m wide. It comprises small, blocky poorly-rounded fragments of country-rock and plastically moulded lumps of porphyry set in a matrix of disaggregated country-rocks and magma constituents (plates 27, 28). The igneous material is relatively rich in potash feldspar phenocrysts and is probably rhyolitic. The igneous component in the matrix displays snowflake texture indicating that it is recrystallised glass. At the northern contact of the apophysis the breccia contains a one metre interval in which there is steeply dipping flow-banded material that is probably oriented approximately parallel to the contact. The bands range in width from less than 5 mm to about 30 mm and are discontinuous. There are two types of material involved: porphyry with little incorporated country rock, and mixed porphyry and finely comminuted country rock (plate 29). Similar banded material is present near other contacts of the apophysis. The interpretation of the breccia is that it represents an explosive pulse of igneous material which escaped as the country rock initially fractured. The banded material probably corresponds to a zone in which ductile behaviour persisted at a relatively slower rate as a result of more igneous material being present.

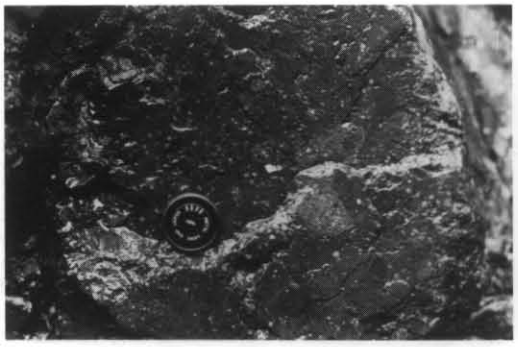

Plate 27. *Breccia that consists of igneous fragments (pale colour) and fragments of dark-coloured Mathinna Beds set in a dark-coloured matrix of disaggregated igneous and Mathinna Beds material. The breccia is located at the northern edge of the apophysis on Catos Creek dyke at EQ986036. The lens cap is 49 mm across.*

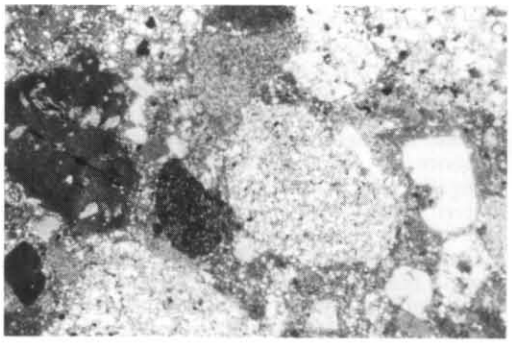

Plate 28. *Photomicrograph (crossed nicols) of a sample of breccia from the same locality as Plate 26, showing sub-rounded to angular fragments of Mathinna Beds sandstone and pelite together with relatively large quartz and feldspar grains and lithic fragments of igneous derivation. The very fine-grained matrix is mainly of igneous derivation with some disaggregated Mathinna Beds. The width of the field of view is 3.4 mm.*

The porphyritic microgranodiorite that forms the main intrusive phase in Catos Creek dyke is chilled against the breccia phase in the apophysis (plate 30) and is generally fine grained within 20 m of the eastern contact. Beyond the contact zone the groundmass grain size is variable but relatively coarse *c.* 160 um). Phenocrysts in the dyke are much less disrupted than those in the St Marys Porphyrite. In the chilled eastern margin plagioclase and biotite are subhedral to euhedral and quartz grains are mostly modified by absorption. Biotite and other grains may be oriented parallel to the contact in the chilled margin but no foliation was recognised elsewhere in the part of the dyke that is within St Marys

Plate 29. *A banded zone within the breccia at the same locality as Plates 27 and 28. The pale-coloured, lenticular bands consist mainly of igneous material whereas the dark bands contain abundant relatively finely comminuted material derived from the Mathinna Beds. The diameter of the lens cap is 49 mm.*

Plate 30. *A chilled, intrusive contact between pale-coloured microgranodiorite and dark-coloured breccia at the same locality as Plates 27 and 28. The microgranodiorite is equivalent to the main intrusive phase in Catos Creek dyke* (Dapl). *Note the stoped-off slivers of breccia within the microgranodiorite and the finely sinusoidal form of the contact. The diameter of the lens cap is 49 mm.*

Quadrangle. However, biotite grains are often bent or kinked indicating that the rocks have not been free of deformation processes.

The constituent minerals of the dyke are similar to those in the porphyrite. Phenocrysts are mainly zoned plagioclase, quartz and biotite. Potash feldspar is minor but unlike the porphyrite there are large phenocrysts up to 30 mm long sparsely distributed through the dyke. Pyroxene is sparse and both clinopyroxene and orthopyroxene are present. All grains are rimmed by amphibole and many amphibole grains have inhomogeneously coloured cores suggesting that they are after pyroxene. Pyroxene is most common in some of the chilled rocks near the

eastern boundary where the grains have rims of colourless fibrous amphibole which in turn have thin rims of hornblende. In the central part of the dyke a little clinopyroxene is preserved as cores in hornblende laths. A little fibrous amphibole is similarly preserved. Most hornblende occurs in clusters of grains in association with minor biotite rather than as single laths. Several fragments comparable with the norite and gabbro fragments in the volcanic rocks were found in thin sections of the dyke rocks but they contain hornblende rather than pyroxene. Although some biotite occurs in clusters with hornblende, most occurs as single grains. Accessory minerals include green chlorite as an alteration product of biotite. Muscovite is an alteration product of cores of some plagioclase grains. A little calcite, epidote and colourless chlorite occur in some rocks. Pyroxene occurs as inclusions in some plagioclase grains. Zircon, apatite and opaques are inclusions in biotite.

Sparse metasedimentary xenoliths are disseminated through the dyke but no schlieren were recognised. A few irregularly shaped xenoliths of fine-grained quartz diorite are present and can be several metres across. They consist of about 55% ferro-magnesians with abundant laths of plagioclase and subordinate quartz and potash feldspar. The ferromagnesians are predominantly fibrous amphibole, relict orthopyroxene, biotite and chlorite. Metasedimentary xenoliths occur in the diorite as well as a small proportion of euhedral phenocrysts rich in pyroxene inclusions.

BIOTITE-HORNBLENDE ADAMELLITE (Daec) AND DIORITE (Ddx)

A small plutonic granitoid with a marginal dioritic phase is in contact with the St Marys Porphyrite east of Mt Elephant. The body is called the Piccaninny Creek Adamellite (McNeil, 1965) although the rock type is granite in the nomenclature of Streckeisen (1973). The body transects compositional banding in the St Marys Porphyrite and is therefore regarded as being younger. Its isotopic age is indistinguishable from the isotopic age of the porphyrite body but the adamellite is apparently not derived from the same magma (Turner *et al.*, 1986) because it shows different compositional trends in major elements (*e.g.* Mg), trace elements (*e.g.* Ba, La, Zr) and rare earth elements.

The adamellite is equigranular and generally coarse grained although there is a decrease in grain size near the country-rock contact and in the northern (?higher) part of the body. Mineralogical composition varies with hornblende being less abundant in the southern part of the body. Microtexture is typically granitic with orthoclase grains commonly having optically continuous extensions between adjacent grains and into embayments in quartz grains. Undulose extinction is a feature of quartz grains and they are commonly recrystallised. Plagioclase grains are subhedral and zoned. Biotite occurs as individual subhedral flakes and in clusters with green hornblende, either intermixed with the hornblende grains or as selvages around composite grains. A little clinopyroxene is preserved as cores in grains of hornblende and a little colourless, fibrous amphibole has the same mode of occurrence. No relationship between fibrous amphibole and pyroxene was observed. Unlike the Scamander Tier dyke in St Helens Quadrangle and Catos Creek dyke, the Piccaninny Creek Adamellite contains very few potash feldspar megacrysts and those that are present are anhedral rather than tabular euhedral. Alteration in the adamellite is slight except in shear zones and is confined to minor chloritisation of biotite and alteration of plagioclase cores.

Only a few xenoliths are present in the adamellite. They are fine grained and mafic with rounded sections up to 150 mm across. A few microxenoliths comparable with the norite and gabbro inclusions in the volcanics were observed in thin section. They contain over 50% zoned plagioclase with hornblende, minor biotite and trace orthoclase.

Along part of the north-eastern contact of the adamellite there is a marginal phase of richly xenolithic, slightly porphyritic, medium grained quartz diorite (Ddx) that is transitional through xenolithic, coarse-grained granodiorite to normal, xenolith-poor adamellite. The diorite consists of grains of zoned plagioclase, biotite and hornblende enclosed poikilitically in quartz. Only trace potash feldspar is present. Both orthopyroxene and clinopyroxene are common within hornblende and there are a few pyroxene grains which show very little alteration. Quartz diorite also comprises most of the xenoliths but it is fine grained. Sparse hornfels xenoliths are also present.

Thin, fine- to medium-grained intrusions of aplite and leucogranite occur in the adamellite and are particularly abundant in the southern part of the body. Some of these intrusions contain thin seams of pegmatite.

BIOTITE-HORNBLENDE GRANODIORITE (Dg)

Granodiorite at each of the Long Point and Piccaninny Point localities is similar and the contact at Piccaninny Point lies near the line of extrapolation of the Long Point contact, therefore the granodiorite in each locality is considered to be part of the same body. No field relationships between the granodiorite and the Piccaninny Creek adamellite have been established. Both rock types have similar mineralogy apart from the feldspar ratio and each is fairly coarse-grained and fairly even-grained. However, they are compositionally distinct with the granodiorite being readily

distinguished on the basis of major elements (e.g. Mg), trace elements (e.g. Ba, La, Zr) rare earth elements (Eu anomaly) and initial Sr ratio (Turner *et al.*, 1986). The isotopic age of the granodiorite is indistinguishable from the age of the adamellite. However, the granodiorite may be older because the adamellite transects a regional lineament which involves the granodiorite contacts at Long Point and Piccaninny Point together with the axial surface trace of the syncline in the coastal part of the St Marys Porphyrite and Scamander Tier dyke (fig. 11).

The granodiorite ranges from coarse, even-grained to medium-grained and slightly porphyritic. Plagioclase is zoned and subhedral. Biotite occurs as individual flakes and in clusters with hornblende. Clinopyroxene is present as remnant cores in a few hornblende grains. Orthoclase is late formed and intergranular whilst quartz textures imply extensive recrystallisation. Alteration is slight and involves partial chloritisation of biotite and saussuritisation of plagioclase cores.

Xenoliths are very common at both Long Point and Piccaninny Point. Rounded, fine- to medium-grained, mafic types predominate over sparse hornfels. They vary in cross-sectional shape from elliptical to quite irregular and are commonly about 0·2 m across. Those with elongate shapes generally lie parallel to the foliation. Relationships in a 40 m interval of compositional banding at FP092777 on Long Point indicate that the elongate shapes are due to flattening. Most bands in the interval are defined by different proportions of ferromagnesian minerals, whilst a number are characterised by abundant mafic xenoliths (plate 31). Interfaces between some bands appear to be erosional therefore the bands are thought to result from intrusion of discrete pulses of magma. Flow alignment of xenoliths could thus be expected to be of similar orientation to the bands. However, elongation of xenoliths is at a high angle to the layering and parallel to the foliation thus indicating that both elongation of xenoliths and foliation are due to flattening. The considerable variation in shape of the xenoliths throughout the granodiorite implies that they had variable initial shapes.

Plate 31. *Part of the banded zone in the granodiorite* (Dg) *which crops out near FP083776 on the shoreline at Long Point. The photograph shows possible erosional features at the base of the felsic band in the foreground. It also shows xenoliths in the band of fairly normal granodiorite in the middle ground which are elongate perpendicular to the banding and parallel to the foliation. The length of the head of the geological pick is 180 mm.*

Quartz diorite occurs at Piccaninny Point but differs from diorite in the marginal phase of the Piccaninny Creek adamellite by being relatively poor in xenoliths. It is a very minor rock type and occurs in a band less than one metre thick in a dyke contiguous with the main granodiorite mass (McNeil, 1965). There are several compositional bands in the dyke and Gee and Groves (1974) cite instances of one band transgressing another. They conclude that the bands represent sequential intrusions of magma of different compositions.

Thin sheets of aplite and leucogranite are common at both Long Point and Piccaninny Point. Commonly they dip gently to the north.

Minor Devonian granitic intrusions

N. J. Turner

QUARTZ-FELDSPAR PORPHYRY (Dmp)

At FP064864 near Chain of Lagoons there is a thin (30 m wide) porphyritic dyke which intrudes the Piccaninny Creek adamellite along sharp, planar boundaries. The dyke rock contains stubby, euhedral feldspar phenocrysts up to about 15 mm long and euhedral to rounded quartz phenocrysts up to about 5 mm across. There are also phenocrysts of biotite and subordinate hornblende, commonly with small biotite grains adhering. The very fine, even-grained groundmass comprises about 60% by volume of the porphyry and consists of quartz, feldspar and biotite.

COARSE-GRAINED GRANITE (Dgpc)

Along part of the south-western contact of the St Marys Porphyrite [FP000966–FP004957] east of St Marys and again near the south-western contact at FP022942 there are small patches of coarse-grained rocks within the porphyrite. These patches may be minor intrusions or rafts. The possibility that they are rafts is raised by the presence of EP993988 of an apparent raft of Mathinna Beds over 100 m long.

The coarse-grained rocks are porphyritic with K-feldspar, zoned plagioclase, quartz, biotite and hornblende phenocrysts. K-feldspar

phenocrysts are euhedral, tabular and commonly contain numerous biotite inclusions. Their proportion varies considerably, ranging up to greater than 50% by volume of the rock. Their maximum length ranges from 30–40 mm and they may show strong parallelism of their 010 faces. Phenocrysts of other minerals are substantially smaller, for example quartz grains range up to about 15 mm. The groundmass is fine grained (*c.* 1 mm) and consists of quartz, feldspar and biotite.

Triassic basalt

J. L. Everard

SUMMARY (for detailed discussion of petrology see Appendix A; for stratigraphy, see above)

The Middle Triassic basalts (233 ± 5 Ma) comprise two units each up to 30 m thick and include both flows and shallow intrusives.

Mineralogically they may be classified as leucobasalts and chemically as trachybasalts. When fresh, they consist mainly of a fine, intergranular to subophitic feldspar-rich groundmass of plagioclase (mostly labradorite) laths, titanaugite, interstitial sanidine, and olivine, with abundant accessory apatite, ilmenite and ulvospinel.

Plagioclase megacrysts are present in the lower unit but absent in the upper unit, whilst olivine phenocrysts, probably xenocrysts, are abundant in the upper unit but very rare in the lower unit. Chemically they are slightly *ne*-normative but strongly differentiated alkali olivine basalts with low 100 Mg/Mg + Fe* and CaO and high Al_2O_3, TiO_2, P_2O_5 and K_2O. However, they plot within, although near the limit of, the compositional field of Tasmanian Tertiary basalts, at least with respect to major elements.

The lower basalt unit could have been produced by about 9% partial melting of a garnet lherzolite source (pyrolite composition), at depths of 55 km, followed by fractionation of about 30% clinopyroxene and olivine at (15)–30–(35) km. The plagioclase megacrysts probably represent the low pressure liquidus phase, and were fairly buoyant as the lower unit erupted. Continued cooling of the remaining liquid in the magma chamber caused iron-titanium oxides to fractionate, lowering the magma density and causing plagioclase to settle.

Recharge and mixing by a new, more primitive magma containing olivine phenocrysts probably caused another eruption, producing the upper basalt unit. Some *in situ* settling of olivine xenocrysts in the upper unit occurred. Both units were later enriched in Ba by secondary processes. Alteration was a process of net mass loss, involving addition of H_2O and CO_2 and depletion of Na_2O, SiO_2 and, to a lesser extent, Cr, V and Co.

Jurassic dolerite (Jdl)

C. R. Calver

TYPES AND DISTRIBUTION

INTRODUCTION

Widespread dolerite intrudes Triassic and older rocks on St Marys Quadrangle, part of the massive complex of Jurassic (McDougall, 1961; Schmidt and McDougall, 1977) intrusions that crop out over most of central and eastern Tasmania.

Nearly all the dolerite on the map sheet makes up an essentially horizontal, single thick sheet that probably once extended over the entire quadrangle. Its base is usually 200–300 m above the base of the Upper Parmeener Super-Group. In the northern half of the quadrangle, the sheet has been extensively eroded, leaving as prominent outliers the Nicholas Range, St Patricks Head and Mt Elephant. In the southern half, the sheet remains largely intact, comprising the elevated plateau of Fingal Tier. Roof rocks of the intrusion have been entirely removed by erosion. The remaining thickness of the sheet exceeds 400 m in several drill holes (67, 68, 69, GY13, GY15).

The shape of the intrusion in the subsurface is described in a later section. In spite of the apparent multiplicity of feeders, there is no field evidence, such as compositional variation or internal chilled margins, to suggest that more than one major phase of intrusion is present. The dolerite appears to be uniform across the quadrangle, apart from chilled margins and rather subtle changes associated with post-emplacement differentiation. The sole exception is the occurrence, within the intrusion, of minor late dykes described below.

Textural variation is sufficient to allow the recognition of a number of intergrading dolerite types in the field and in drill core. During mapping of the St Marys sheet, coarse-, medium- and fine-grained types were recognised on the basis of approximate grain size limits of >1·5 mm, 1·5–0·7 mm and <0·7 mm, respectively. These limits refer to the average grain size of equigranular rocks and the average phenocryst size of porphyritic rocks. Field determinations of grain size have not always been consistent, as well-developed ophitic textures tend to mask the coarse grain sizes. Coarse-, medium- and fine-grained dolerites indicated on the map will therefore be mostly, but not all, approximately equivalent to the categories described below, which are based primarily on petrography. Porphyritic glassy dolerites and localities with late dykes are also indicated on the map. Dolerite types other than coarse and medium appear to be volumetrically insignificant.

The observations cited below on the zonation of dolerite types in drill core are based on

5 cm

examination of core from boreholes 42, 56, 57, 67, 68, 72 and 74, all on the western part of the Fingal Tier. Petrographic descriptions of the various dolerite types given below are synthesised from about 80 thin sections, mostly from widespread outcrops on the Fingal Tier, and many from boreholes. Most of the samples were collected by R. H. Castleden. The geochemistry of each dolerite type, and the differentiation of the intrusion, are discussed in Appendix B.

PORPHYRITIC GLASSY DOLERITES

This type occurs in two areas near the summit of Bare Rock (around EP965872 and EP963884), at EP851819, and in the top 30 m of borehole 67 [EP842820]. It is the most differentiated of the dolerite types encountered, although less differentiated than the granophyres recorded elsewhere in Tasmania (e.g. Edwards, 1942; McDougall, 1962, 1964).

In hand specimen the porphyritic glassy dolerites consist dominantly (50–90%) of a black aphanitic groundmass, the remainder being euhedral pyroxene and plagioclase laths 1–4 mm long. In outcrop they are massive to poorly jointed; but at EP851819 vertical polygonal columnar jointing is developed (R.H.C.). At the Bare Rock localities, agate-filled amygdales up to 40 mm in diameter are locally abundant, not exceeding a few percent of the rock volume. There is a minor pegmatitic variation with lath-like to acicular phenocrysts 10–20 mm long, and a somewhat higher proportion of amygdaloidal chalcedony. The porphyritic glassy dolerites grade laterally over many metres, or downwards over several metres in borehole 67, with an increase in crystallinity into normal coarse dolerites.

Thin sections from Bare Rock typically show blocky euhedral to subhedral phenocrysts of calcic plagioclase (300μm–1 mm) and of very pale yellow, often twinned, pigeonite and augite (1–4 mm). Plagioclase often has prolonged skeletal terminations (plate 32). The phenocrysts are usually clumped together and ophitically intergrown, a feature better developed in the more densely crystalline examples (plate 33). The groundmass characteristically consists of complexly intergrown arrays of trichites up to 3 mm long, set in a matrix of uniform dark grey-brown to black glass. In some samples, the trichites are straight and arranged in parallel arrays (plate 34); in others they are curved, and arrayed in radiating, fan-shaped plumose sheaves. Numerous tiny opaque blebs (<1–20 μm) are abundant in the glass in several samples, and opaques (ilmenite) may also occur as larger (up to 250 μm) grains. Chalcedony and a zeolite fill rare small amygdules. In 67/15, from bore hole 67, the groundmass contains abundant sheaf-like aggregates of bladed to acicular clinopyroxene.

Plate 32. *Thin section of sample M363 from Bare Rock, Fingal Tier [EP964872]. Glassy porphyritic dolerite, showing clinopyroxene phenocrysts, ophitically intergrown with plagioclase laths, lying in a groundmass of dark brown glass containing incipiently crystalline trichites. Hyalophitic texture. Crossed nicols, field of view 4·3 × 2·9 mm.*

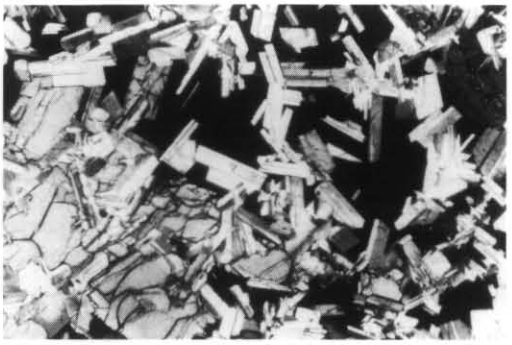

Plate 33. *Thin section of sample M364 from Bare Rock, Fingal Tier [EP964872]. Glassy porphyritic dolerite similar to Plate 32, but containing less abundant, almost black, glass, without trichites in the area shown. Ophitic to intersertal texture. Crossed nicols, field of view 4·3 × 2·9 mm.*

Despite the relatively high silica content (M363, M364: see Appendix B) X-ray diffraction shows that quartz is absent, and evidently normative *Q* is represented within the glass (J. L. Everard, pers. comm.).

Transitional rocks appear to be normally crystalline coarse-grained dolerites in hand specimen, but have a mesostasis very similar to the groundmass phase described above. One transitional dolerite, M361, has a mesostasis entirely consisting of a yellow poorly crystalline to botryoidal mineral, probably palagonite or a zeolite.

The sudden quenching indicated by the groundmass texture suggests that the porphyritic glassy dolerites formed near the top of the intrusion. At bore hole 67 and Bare Rock they

Plate 34. *Thin section of sample 79/16 from Bare Rock, Fingal. [EP964884]. Groundmass of sparsely porphyritic glassy dolerite. Interwoven arrays of trichites in pale brown glass.* × *40.*

Plate 35. *Thin section of sample from borehole 68, depth 58·7 m, Fingal Tier. Coarse-grained, moderately differentiated dolerite, showing ophitic to subophitic intergrowth of clinopyroxenes and plagioclase, grading into a finer feldspar-rich mesostasis. Crossed nicols, field of view 4·3* × *2·9 mm.*

Plate 36. *Thin section of sample from borehole 68, depth 214·8 m, Fingal Tier. Coarse-grained slightly differentiated dolerite, showing intergrown equant to columnar clinopyroxene crystal and finer feldspar-rich mesostasis. Texture intergranular to poorly-developed subophitic. Crossed nicols, field of view 4·3* × *2·9 mm.*

occur above relatively thick (400 m) parts of the sheet. Granophyres at Great Lake described by McDougall (1964) are texturally similar to these rocks, having an abundant mesostasis exhibiting textures suggestive of rapid cooling. An alternative possibility (McDougall, 1964) is that crystallisation was inhibited by a sudden increase in viscosity due to rapid ebullition of volatiles, perhaps caused by fracturing of the roof rocks of the intrusion.

COARSE-GRAINED DOLERITES (>1·5 mm)

Coarse-grained dolerites comprise the bulk of the sheet on Fingal Tier, passing downwards into medium-grained dolerites at a level 100–150 m above the basal contact of the sheet.

In outcrop, the rock typically displays close-spaced (10–50 mm) sub-parallel vertical joints that in plan view tend to be curved, forming fan-shaped or spindle-shaped sets. The sets persist laterally for only a metre or two; adjacent sets, rarely overlapping, are of widely differing directions.

In thin section (plates 35, 36) the typical coarse dolerite consists of columnar to equant clinopyroxene crystals, 2–4 mm long, surrounded by a meshwork of stubby, frequently zoned, plagioclase laths 200 μm–1 mm in length. Clinopyroxene (including both augite and pigeonite in approximately equal proportions) is less abundant than plagioclase. The abundant (10–30%) mesostasis is composed of plagioclase and finely intergrown quartz and alkali feldspar. Scattered angular opaques, ranging from fine dust to jagged grains of ilmenite 200μm across are disseminated through the rock.

The degree of ophitic intergrowth is variable. When ophitic textures are absent or poorly developed, the pyroxenes appear as distinct phenocrysts in hand specimen. On wetted drill-core, the pyroxene phenocrysts are pale pinkish-brown, in a darker olive-grey groundmass. Conversely, well developed ophitic intergrowth tends to disguise the larger grain size of the pyroxenes in hand specimen.

Some samples are a distinctly lighter colour in hand specimen, apparently due to a lower proportion of mesostasis (E54, 79/8, 67/272). In borehole 67, such medium to light grey rocks comprise the lowest 75 m of the coarse dolerite, but elsewhere are found at higher levels in the intrusion.

Patches of pegmatitic dolerite, a few centimetres to a few metres wide, are occasionally seen in drill core within coarse dolerite. Sample 72/115 contains columnar clinopyroxene euhedra and plagioclase laths 8–10 mm long, in places micrographically intergrown, and an abundant mesostasis.

The coarse dolerites are very similar in appearance and distribution to McDougall's (1964) and Spry's (1958) 'central zone' dolerites.

There is only a slight downward decrease in grain size of the pyroxene phenocrysts through the 300 m or so thickness of the coarse dolerite zone in drill core. The downward transition into medium-grained dolerite occupies an interval of only 10–30 m, at a distance between 100 and 150 m above the base of the intrusion in the eight boreholes examined.

MEDIUM-GRAINED DOLERITES (1·5–0·7 mm)

Medium-grained dolerites in outcrop have a similar pattern of jointing to the coarse dolerites. In hand specimen the rock appears even-grained.

Clinopyroxenes are $<1{\cdot}5$ mm, usually about one millimetre in length, and in thin section the texture is seen to be more or less equigranular, and subophitic to intergranular; and no clear distinction between phenocrysts and groundmass can be made. Clinopyroxene (again including both augite and pigeonite) equals or exceeds plagioclase in abundance. Some clinopyroxenes display very narrow (a few micrometres), closely-spaced lamellae, which probably represent pigeonite exsolution from augite, and *vice versa* (Edwards, 1942; McDougall, 1961). Minor orthopyroxene may be present as rounded anhedra rimmed by either augite or pigeonite (plate 37). Unlike the fine-grained dolerites, orthopyroxene is generally not discernible in hand-specimen.

Plagioclase occurs as narrow laths or more equant subhedra and anhedra (200μm–1 mm long), both interstitial between, and interlocking with pyroxene crystals. Scattered, angular but roughly equant opaques are mostly 20–100μm across.

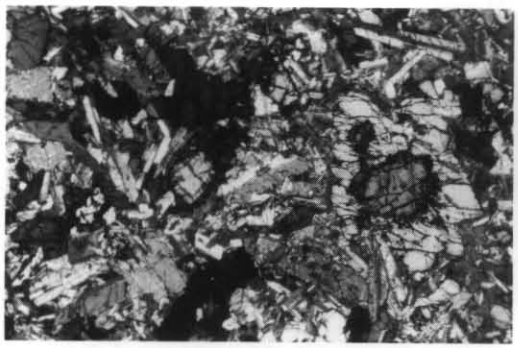

Plate 37. *Thin section of sample from borehole 68, depth 361·95 m, Fingal Tier. Medium-grained. pyroxene-rich dolerite with more or less equigranular subophitic texture, showing an orthopyroxene crystal enclosed by pigeonite (centre right). Crossed nicols, field of view 4·3 x 2·9 mm.*

X-ray diffraction and electron microprobe work show that minor quartz and potash feldspar are present (J. L. Everard, pers. comm.).

This dolerite type is very similar to Spry's (1958) and McDougall's (1964) 'lower zone' dolerites.

FINE-GRAINED DOLERITES (<0·7 mm), EXCLUDING CHILLED MARGINS

Medium-grained dolerites grade over several metres into fine-grained dolerites that comprise the lowest 10–40 m of the intrusion in drill core, and observed in similar proximity to contacts in the field. Excluding chilled margins, this rock type is black in hand specimen, and in outcrop exhibits closely spaced, randomly orientated 'hackly' jointing.

In thin-section fine-grained dolerite has an intergranular to intersertal fabric, with anhedral clinopyroxene and narrow to acicular plagioclase laths, and an abundant dark glassy mesostasis. Small, euhedral to subhedral phenocrysts of orthopyroxene, up to one millimetre long, comprise a few per cent of the rock. They are dark green to black in hand specimen, and are usually conspicuous on the outer surface of drill core. The orthopyroxene is often partly serpentinised.

In some slides, with particularly abundant mesostasis (e.g. 78/533, E261) the crystals aggregate into ill-defined rosettes or clots about one millimetre in diameter, often centred on a corroded orthopyroxene, partly merging together and partly surrounded by dark glassy mesostasis (plate 38).

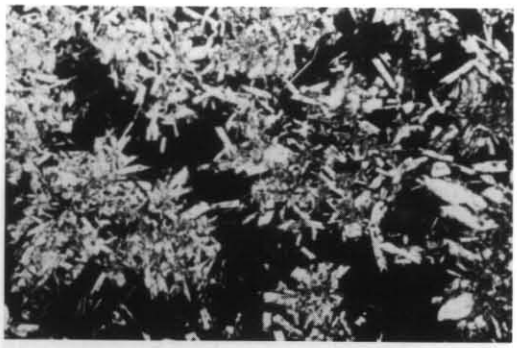

Plate 38. *Thin section of sample 78/533 from EP858830. Fine-grained dolerite, plane-polarised light, × 6·8. Aggregates of intergranular plagioclase and clinopyroxene surrounded by dark, glassy, mesostasis.*

CHILLED MARGINS

Contacts are rarely seen in the field. Chilled margins, here referring to the adjacent metre or so of dolerite, are closely jointed, greenish-grey in colour, and aphanitic except for sparse small phenocrysts.

A thin section from 600 mm above the contact in borehole 68 (sample 68/451·96) contains sparse phenocrysts (500 μm–1 mm long) of orthopyroxene, augite and plagioclase, in an abundant fine-grained, holocrystalline, intergranular to rarely subophitic groundmass (plate 39). Some phenocrysts are clumped together as small (2–3 mm) subophitic glomerocrysts. A few glomerocrysts also contain pigeonite. The groundmass consists of narrow to acicular, randomly oriented plagioclase laths (typically 50–200 μm by 20–40 μm), between which are anhedral granules of clinopyroxene (typically 50 μm across). Small, irregular, equant opaques, ranging from 15 μm across to dust, are lightly disseminated throughout the rock. Rare, irregular amygdales up to 500 μm across are filled with calcite and quartz.

X-ray diffraction and electron microprobe work indicate that the groundmass pyroxene is probably an intergrowth of augite and pigeonite (J. L. Everard, pers. comm).

The 20 mm of dolerite immediately adjacent to the contact contains a few per cent small phenocrysts (to 1 mm) of euhedral orthopyroxene, and a few per cent phenocrysts of clinopyroxene and plagioclase up to 0·5 mm in size. The latter usually occur as monomineralic aggregates or rosettes of several crystals, but some plagioclase-pyroxene glomerocrysts are present, displaying subophitic intergrowth. Smaller, acicular plagioclase microphenocrysts have swallowtail terminations. The groundmass is turbid, and uniformly cryptocrystalline within 10 mm of the contact; further away, an incipient fibrous, plumose texture is developed. Sample 8055·3 contains sparse spherical amygdules, up to 0·2 mm in diameter, filled with quartz and calcite.

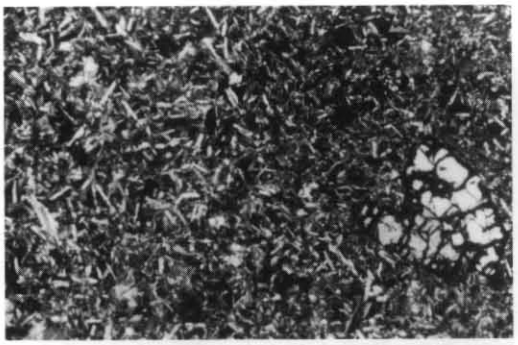

Plate 39. *Thin section of sample from borehole 68, depth 451·96 m, Fingal Tier. Chilled dolerite, about 0·6 m above lower contact, showing a glomerocryst of two orthopyroxene microphenocrysts (lower right) in a fine, dominantly intergranular groundmass of clinopyroxenes, feldspars, quartz and minor opaques. Crossed nicols, field of view 4·3 × 2·9 mm.*

LATE DYKES

At seven widespread localities, late-stage dykes or veins intrude the dolerite. All are indicated on the 1:50 000 geological map sheet except for an occurrence at EP858830. The occurrence at EP959871, near Bare Rock, is compositionally distinct and will be described separately.

At each of the other localities, the dolerite is intruded by a number of irregular dykes up to one metre wide, of pale grey, aphanitic dolerite with sparse small phenocrysts. The dyke rocks weather to a distinctly lighter colour than the surrounding rock, except for black glassy selvedges a few millimetres wide. The dykes may be irregular, sinuous or branching. The host rock usually shows evidence for brittle fracture at the time of intrusion of the dykes, which appear to be dilatational with matching opposite sides. At EP899811, a later dyke cuts earlier ones (R.H.C.). Generally speaking, dykes intrude fine-grained dolerite host rock and occur near contacts.

They are very similar petrographically to the chilled margins of the main intrusion described above, with euhedral phenocrysts of orthopyroxene and aggregates of plagioclase and clinopyroxene scattered through a murky brown cryptocrystalline groundmass. There may be small xenoliths derived from the host rock. TCE6, collected from the glassy selvedge of a dyke, has a groundmass of devitrified brown glass (plate 40).

The chemical composition of the dyke rocks is also very close to that of the chilled margins of the main intrusion (table B3).

At the Bare Rock locality [EP959871], veins of a different, felsic composition intrude coarse-grained dolerite (R.H.C.). These veins, 5–20 mm wide, are composed of a fine-grained mesh of acicular feldspar rods enclosing abundant

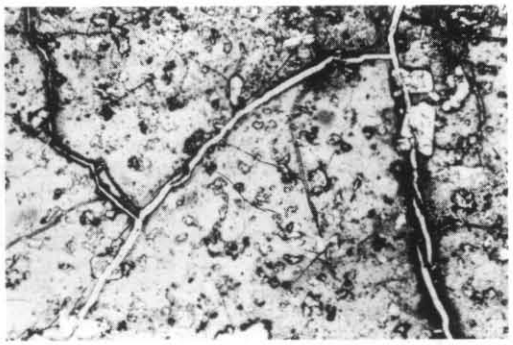

Plate 40. *Thin section of glassy selvedge of a late dolerite dyke. Sample TCE6, from EP899813. Larger phenocrysts of orthopyroxene, and smaller aggregates of clinopyroxene and plagioclase, in brown glass; zeolite veinlets. Plane-polarised light, × 6·8.*

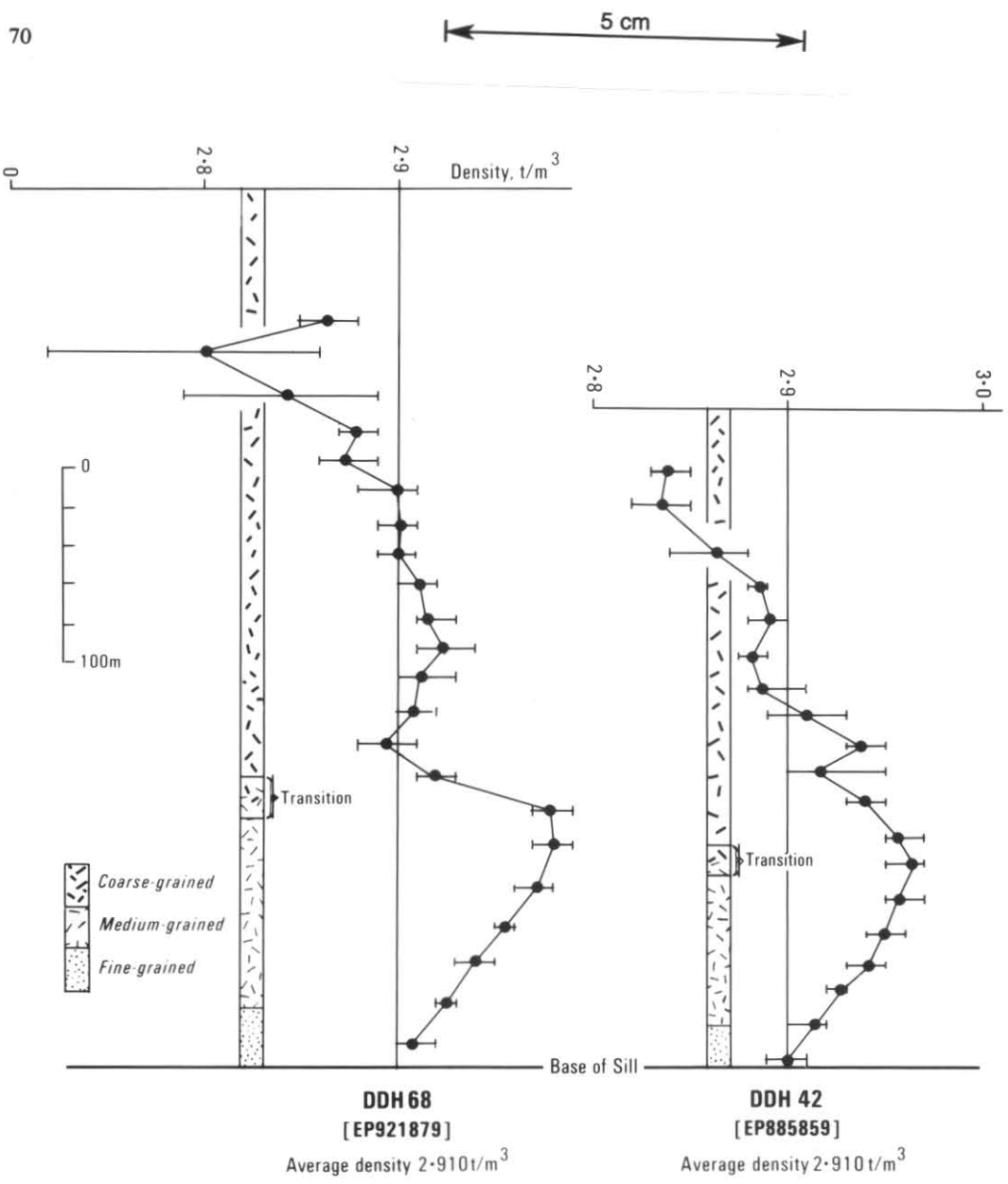

Figure 25. *Variation in dolerite density, and distribution of dolerite types, in two diamond drill holes on Fingal Tier. Each plotted point is averaged from five samples. The range of variation is also shown.*

intergranular quartz and potassium feldspar, including sanidine. They occur in proximity to porphyritic glassy dolerites and are probably residual differentiate.

DENSITY TRENDS

Systematic density determinations were made of dolerite from two boreholes, 68 and 42. Samples, weighing 200–600 g, were taken approximately every 3 m and their densities calculated from their weights in air and in water. The results are plotted in Figure 25 against height above the base of the intrusion. Each point is averaged from five adjacent samples. Treatment of data thus follows previous work (Jaeger, 1964).

The results closely follow the 'standard' pattern of density variation sills established by Jaeger and Green (1958) and Jaeger (1964). As in the 'standard' pattern the lowest densities occur in the upper part of the sheet, and density increases downwards to a maximum 100 m or so above the base of the intrusion. Thereafter there is a

linear decrease to a value, at the basal contact, of 2·90–2·91 t/m³. This value, representing undifferentiated dolerite, approximates the average density through the whole sheet.

The trends in borehole 68 are slightly unusual in that the downward increase to the peak density is relatively abrupt.

In the Great Lake sill, of similar thickness to the dolerite in borehole 68, the minimum density values were obtained about 100 m below the top of the sill (Jaeger, 1964) suggesting that borehole 68 was collared not far below the (now removed) top of the sill (note that the sampled interval begins 60 m below the collar of the hole).

Also shown in Figure 25 are graphic logs of dolerite types in the two holes. Significantly, the transition between medium- and coarse-grained types coincides with the interval immediately above the density maximum in both cases. Thus, the coarse-grained dolerite, with an average density of about 2·89t/m³ has an irregular trend but tends to become denser with depth; while the underlying medium-grained type, with an average density of about 2·95 t/m³, displays a clear-cut trend of density decreasing with depth.

The textural and density trends thus have predictive qualities that may be of value in coal exploration, but considerably more data are required to confirm these trends.

Leaman and Richardson (1981) report an average dolerite density of only 2·83 t/m³ from 123 determination from bore holes 17, 20 and 23. No systematic trends, or higher density lower zone, were discerned. The value 2·83 t/m³ for dolerite was used in the interpretation of the results of the East Coast gravity survey.

If the densities in bore holes 68 and 42 are more characteristic of the region, then some aspects of the gravity survey may require reinterpretation. Substituting the higher average density value of 2·91 t/m³ gives substantially lower estimates for the thickness of the dolerite, other factors being equal.

Discussion

The similarity of the density trends in boreholes 68 and 42 with those observed in the Mt Wellington and Great Lake sills (Jaeger and Green, 1958; Jaeger, 1964), and the similar values obtained for lower chilled margin densities, support Edwards' (1942) conclusion that composition and differentiation of the dolerite magma were remarkably uniform across the State. This is also supported by geochemical comparisons (see Appendix B).

Some dolerite types described above also correspond well, as remarked previously, with those of Spry (1958) and McDougall (1964). However, neither granophyres nor 'upper zone' dolerites were recognised in St Marys Quadrangle, and no rocks quite like the porphyritic glassy dolerites have yet been described outside the St Marys Quadrangle.

Chilled margin rocks from Fingal Tier contain phenocrysts that are larger and more abundant than is typical elsewhere in Tasmania. Edwards (1942) noted a similar phenomenon in a sample from the Nicholas Range, and remarked that crystallisation must have been slightly more advanced prior to emplacement. This factor, together with the presence of amygdules in some chilled lower margins and some porphyritic glassy dolerites, tend to suggest that these dolerites were part of a relatively high-level intrusion.

Tertiary basalt

J. L. Everard

SUMMARY (for detailed discussion of petrology see Appendix C)

Quartz normative tholeiitic basalt occurring 16 km WNW of St Marys consists mainly of resorbed olivine (Fo_{74-77}), augite, plagioclase and black glass, and belongs to the intergranular-intersertal Bridgewater textural type. Chemically the basalt is similar to other Tasmanian Tertiary tholeiites, but is more strongly differentiated, with lower MgO and higher SiO_2. The basalt probably evolved from an original parental olivine tholeiite, formed by about 33% partial melting of mantle, by low pressure (< 5 kb) fractionation of olivine, clinopyroxene and plagioclase.

THERMAL METAMORPHISM

Associated with Devonian plutonic rocks

N. J. Turner

McNeil (1965) recorded a thin (<25 mm) zone of metamorphosed Mathinna Beds abutting against the granodiorite at Piccaninny Point in which there is a thermal metamorphic assemblage of sillimanite, corundum, biotite, microcline, quartz, cordierite and muscovite. More commonly the thermal metamorphic assemblage is biotite, quartz, microcline and cordierite with muscovite, epidote, albite and chlorite.

The very high rank rocks present at Piccaninny Point have not been detected in the aureole of the Piccaninny Creek adamellite. Based on its intersection with the topographic contours, the western contact of the adamellite dips 45°W beneath the Mathinna Beds. On the same basis, the outer edge of the thermal aureole has a similar dip thus indicating a thickness of about 350 m for the aureole. This is substantially less than the thickness of metamorphic aureoles in the Ringarooma and Boobyalla Quadrangles (Turner *in* McClenaghan *et al.*, 1982) which presumably is an indication that the Piccaninny Creek adamellite is volumetrically small. The

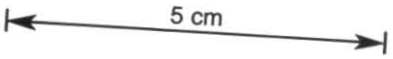

widening of the aureole in the Piccaninny Creek area suggests that this is a 'roof' zone. Possibly the abundance of aplite in the southern part of the adamellite body is a related feature.

Associated with the St Marys Porphyrite and Catos Creek dyke

N. J. Turner

The aureole of the intrusive part of the St Marys Porphyrite was not extensively sampled so the variation in thermal metamorphic assemblages from point to point on the contact is unknown. In a small quarry [EP996964] beside the Tasman Highway east of St Marys the pelitic rocks in the Mathinna Beds are poorly recrystallised and contain muscovite and biotite as the thermal assemblage. At EP982993, across the major fault west of the German Town Road, the extent of thermal metamorphic recrystallisation is apparently much greater. Adjacent the western contact of Catos Creek dyke north of Mt Nicholas the pelitic rocks in the Mathinna Beds are completely recrystallised and contain andalusite, cordierite, biotite, muscovite, quartz, tourmaline and ?feldspar.

Associated with Jurassic dolerite

C. R. Calver

Contact metamorphism of the country rock is restricted to a zone a few metres wide, usually less; and is not commonly seen in outcrop due to talus deposits mantling the lower slopes of the dolerite escarpments. Baked mudstones are darkened, hardened, closely-jointed, and usually become hornfels within a few centimetres of the intrusion. Carbonaceous material becomes oxidised, and sandstone at contacts may become partly replaced by zeolites.

Subtle effects on coal in the form of removal of volatiles are detectable at much greater distances (30–50 m) from contacts (Bacon, 1979); and miospore preservation appears to be adversely affected at similar distances (S. Forsyth, pers. comm.).

Some localities with baked sedimentary rocks are distant from known intrusions [FP059779, EP996907, EQ933013].

STRUCTURE

Mathinna Beds

N. J. Turner

INTRODUCTION

The structure of the Mathinna Beds in four areas is discussed. These areas include a small area at Piccaninny Point and relatively large areas south of Mt Elephant (Elephant Pass area), around St Marys (St Marys area) and near the northern edge of the map sheet east of Catos Creek dyke (northern area). Very little structural data were collected in the relatively large tract of Mathinna Beds west of Catos Creek dyke. Where there appears to be correspondence between structural features in the Mathinna Beds and structural features in adjacent igneous bodies the relationships are outlined in this section.

PICCANINNY POINT

A compass and pace traverse was conducted across the Mathinna Beds to the south-west of the granodiorite dyke at the southern end of Piccaninny Point. Bedding in the section shows a preponderance of westerly dips (fig. 26) with

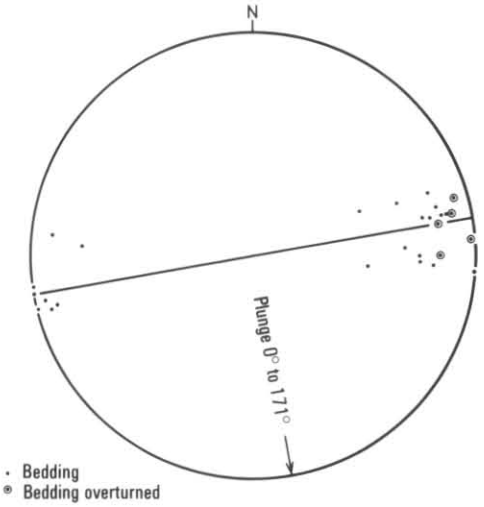

Figure 26. *Lambert projection of bedding in the Mathinna Beds south of Piccaninny Point near FQ073029.*

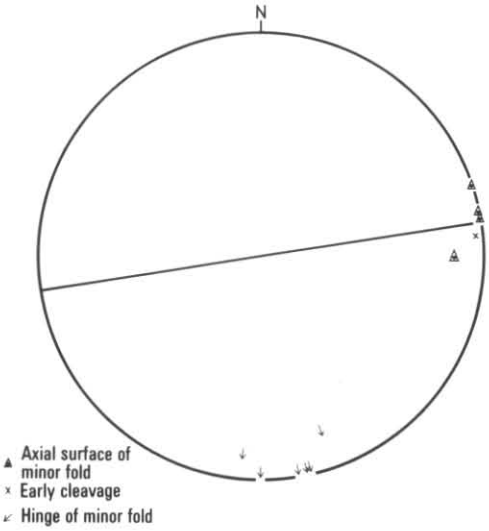

Figure 27. *Lambert projection of axial surfaces and hinges of minor folds and cleavage in the Mathinna Beds south of Piccanniny Point near FQ073029.*

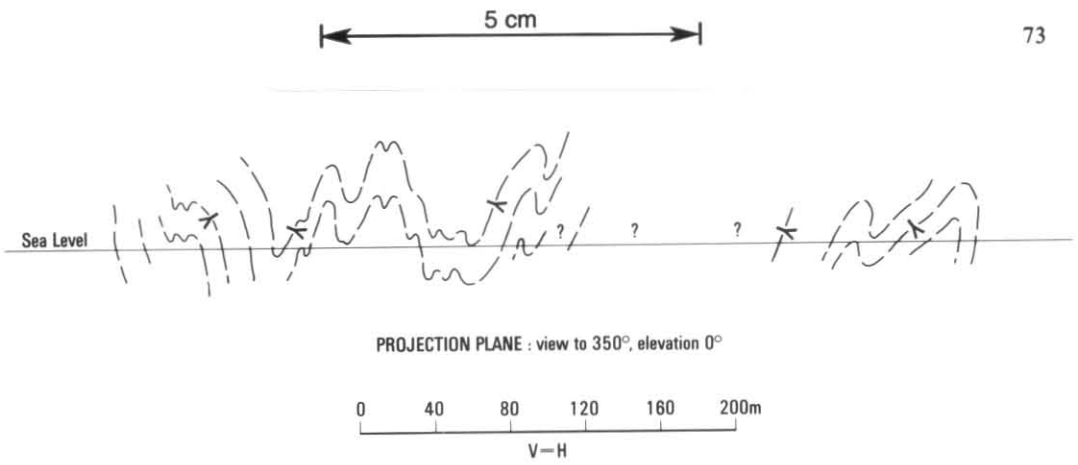

Figure 28. *Fold profile south of Piccaninny Point near FQ073029, derived from a compass and pace traverse.*

some overturning of easterly facing beds. A statistical fold axis of plunge 0° to 171° is indicated and is consistent with the orientations of minor folds measured in the field (fig. 27). Cleavage is difficult to measure, probably because of changes in the fabric of the rocks in the section due to thermal metamorphic recrystallisation.

Overall the folds in the section are upright to steeply overturned (fig. 28). Their dihedral angles are in the range 45–90. There are several orders of folds, including outcrop-scale structures with wavelengths of a few metres and larger scale structures with wavelengths of about 80 m. The major order structure is not clearly defined but the suggested vergence in the section is easterly.

ELEPHANT PASS AREA

This area includes Elephant Pass itself which is the route of the Tasman Highway as it descends south thence south-east from Mt Elephant. Also included is the area east and north of the highway and areas to the west and south along Wardlaws Creek and Piccaninny Creek. The description of the structural features of the Elephant Pass area presented here extends earlier detailed work by McNeil (1965).

The area has been subdivided into four sub-areas (fig. 29) on the basis of markedly different fold trends. In Sub-area 1 near Piccaninny Creek the Mathinna Beds are essentially west-dipping and west-facing with very few parasitic structures. The statistical fold axis for the sub-area is poorly defined by the bedding projection (fig. 30) but has an approximately northerly trend. In Sub-area 3 a predominance of west-dipping and west-facing beds is again evident (fig. 32). This indication of overall easterly vergence in the sub-area is substantiated by the structural profile along Elephant Pass which has been included as an inset on the 1:50 000 map sheet. McNeil (1965) obtained a very similar profile. The profile shows small scale folds with wavelengths of up to about 10 m and larger scale folds with half wavelengths of 50–100 m. The latter verge to the east, being parasitic on a major west-dipping limb which extends down dip for at least the width of Sub-area 3, that is, about 3 km. Dihedral angles of minor folds are in the range 45° to 90° and the folds are steeply overturned to the east. Axial surface cleavage is associated with the folds and its predominantly steep westerly dip in pelite and siltstone (fig. 33) reflects the steeply overturned attitude of the folds. Cleavage in sandstone beds generally fans around fold closures. The shallow, northerly plunge of the statistical fold axis for Sub-area 3 (fig. 32) is similar to the orientations of minor folds measured in the field and lies within the approximate statistical plane of cleavage (fig. 32).

In Sub-area 2 which lies between Sub-areas 1 and 3 there is considerable rotation of structures with bedding (fig. 31), cleavage and minor fold hinges (fig. 33) all trending north-westerly. A predominance of south-westerly dips and facings implies north-easterly vergence in the sub-area and supports the conclusion that the sub-area is a rotated part of the same major limb that underlies Sub-areas 1 and 3. Unfortunately there are no marker horizons in the Mathinna Beds so the exact relationship between the successions in each sub-area is unknown.

The boundary between Sub-areas 1 and 2 is largely obscured by younger rocks. However, near its north-eastern end adjacent the Piccaninny Creek adamellite there is a transitional change in bedding trend (fig. 29) which suggests that the boundary coincides with the trace of a fold axial surface which trends somewhere between 60° and 90°. The boundary between Sub-areas 3 and 4 may occupy a similar structural position but it is even more poorly defined than the boundary between Sub-areas 1 and 2. In contrast the boundary between Sub-areas 2 and 3 can be traced over a distance of 3–4 km. It corresponds to a generally sharp change in structural trend.

Since the contact between the Piccaninny Creek adamellite (Daec) and the Mathinna Beds shows

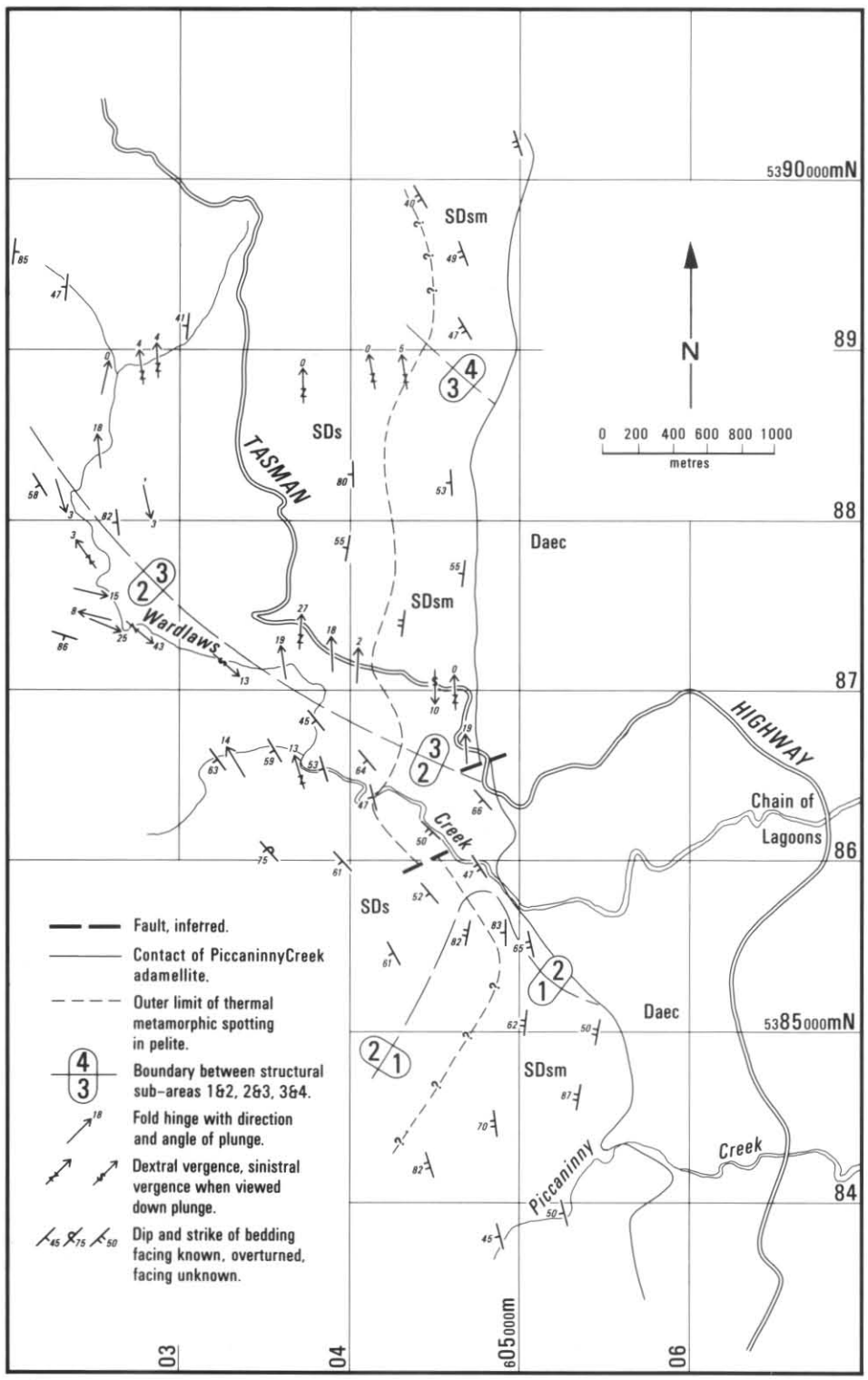

Figure 29. *Structural trends and sub-areas in the Elephant Pass area of Mathinna Beds. The sub-areas are numbered 1 to 4 from the south and the numbers are shown at their boundaries.*

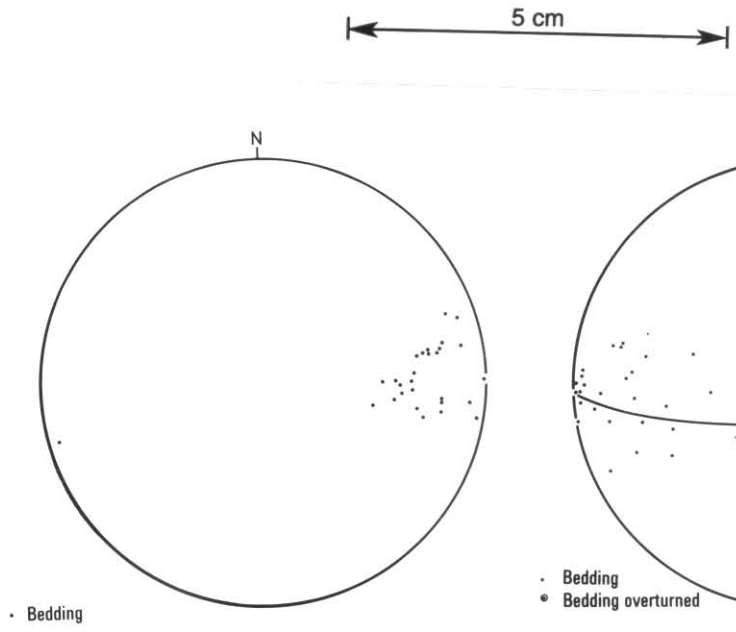

Figure 30. *Lambert projection of bedding measurements in Sub-area 1 of the Elephant Pass area.*

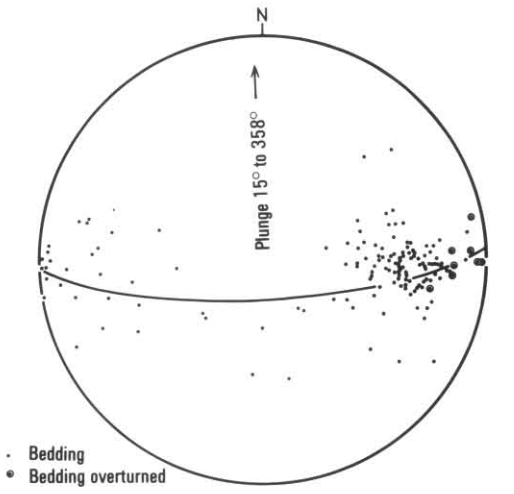

Figure 32. *Lambert projection of bedding measurements in Sub-area 3 of the Elephant Pass area including measurements made along the Tasman Highway.*

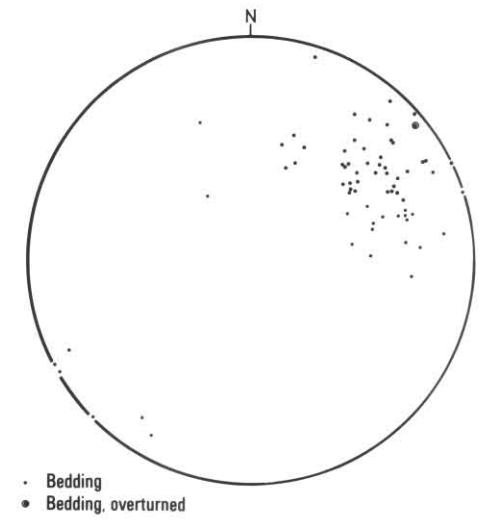

Figure 31. *Lambert projection of bedding measurements in Sub-area 2 of the Elephant Pass area.*

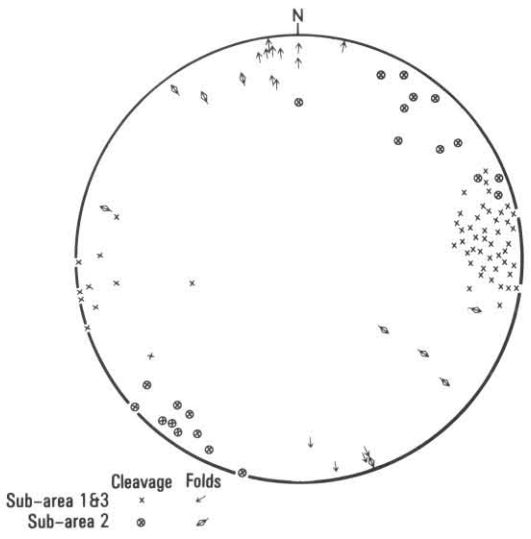

Figure 33. *Lambert projection of measurements of fold hinges and cleavage in Sub-areas 1, 2 and 3 of the Elephant Pass area.*

no change in trend corresponding to the boundary between Sub-areas 3 and 4, it appears that the event which caused the relative rotation of the sub-areas occurred prior to emplacement of the adamellite. It seems likely that the timing of the event which caused similar relative rotation in Sub-area 2 would have been the same. However, uncertainty as to the timing of this event arise from the presence of structures involving the adamellite which may correspond to structures in Sub-area 2. For example, where the igneous contact is contiguous with Sub-area 2 there is a change in attitude from apparently uniform, moderate dip (45°W) to the north to apparently shallow dip near Piccaninny Creek. There is also a marked constriction of the thermal metamorphic aureole of the adamellite. In addition, the igneous contact south of Wardlaws Creek has the same general trend as the northern boundary of Sub-area 2. These various features of the adamellite contact together with the changes in structural trend

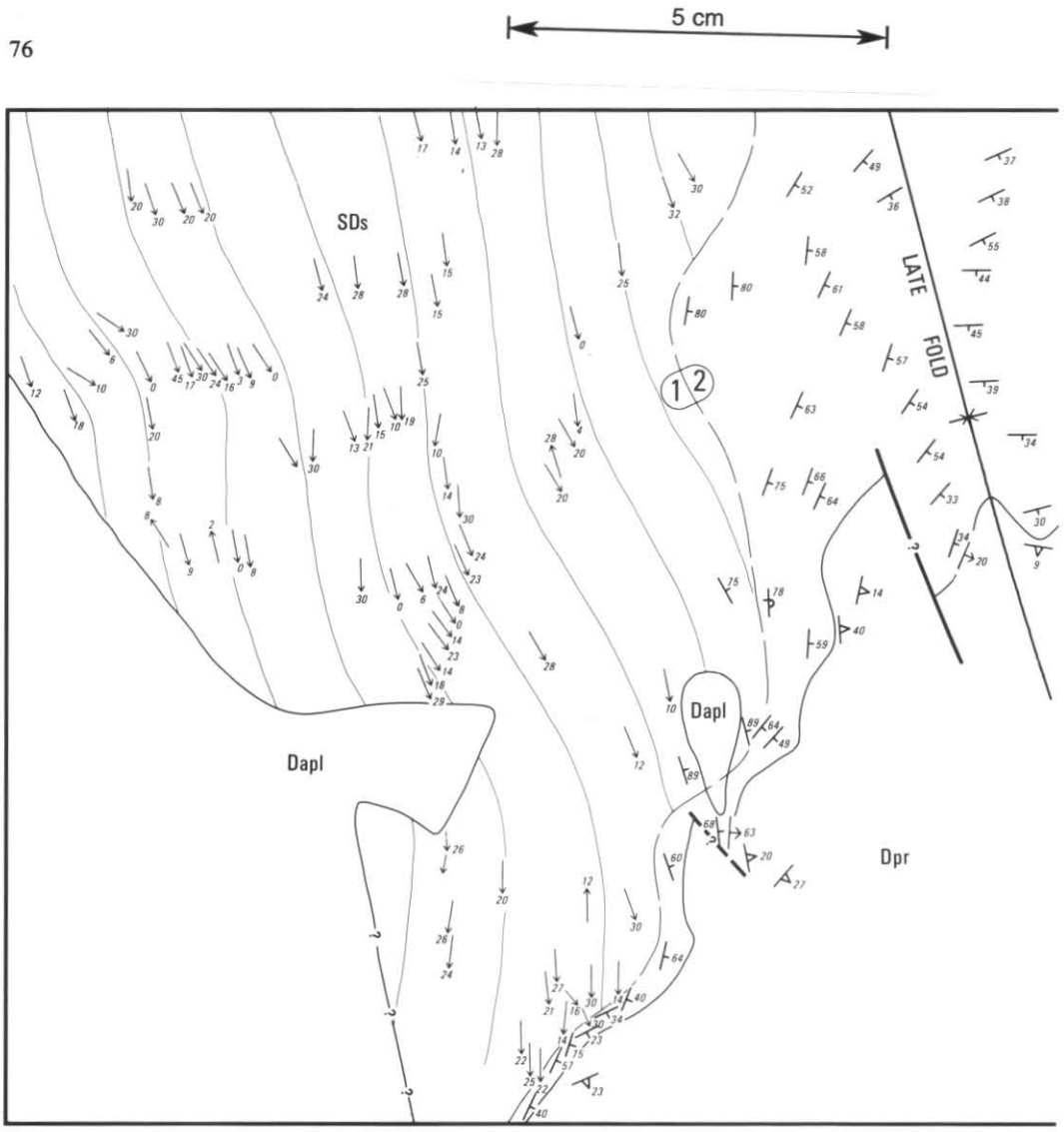

Figure 34. *Structural trends and sub-areas in the northern area of Mathinna Beds, around the basal contact of the St Marys Porphyrite. The sub-areas are numbered 1 to 3 from the west and the numbers are shown at their boundaries. Fold hinges shown in Sub-area 1 include hinges measured in the field but were mainly derived by plotting adjacent, oppositely dipping bedding measurements on a Lambert projection and determining the pole to the girdle.*

between Sub-areas 1, 2 and 3 in the Mathinna Beds suggest that major fault movement has occurred. Specifically, the sense of rotation of structures in the Mathinna Beds and the sense of offset on the adamellite contact suggest a major line of sinistral movement trending WNW to north-west and corresponding to the contact south of Wardlaws Creek and to the northern part of Sub-area 2. However, the adamellite contact is observably intrusive at EP650856 and therefore the contact south of Wardlaws Creek does not correspond to a major post-emplacement fault. None-the-less, the possibility of transverse movement in the northern part of Sub-area 2 is supported by the occurrence on outcrop scale of small faults of north-westerly trend and sinistral transverse movement. Several examples of these structures were observed in Wardlaws Creek and tributaries but no major mylonite zones were recognised. Calcite which is very unusual in the Mathinna Beds occurs as a secondary mineral associated with one of these small faults near EP628873 in Wardlaws Creek. No control on the time of development of the

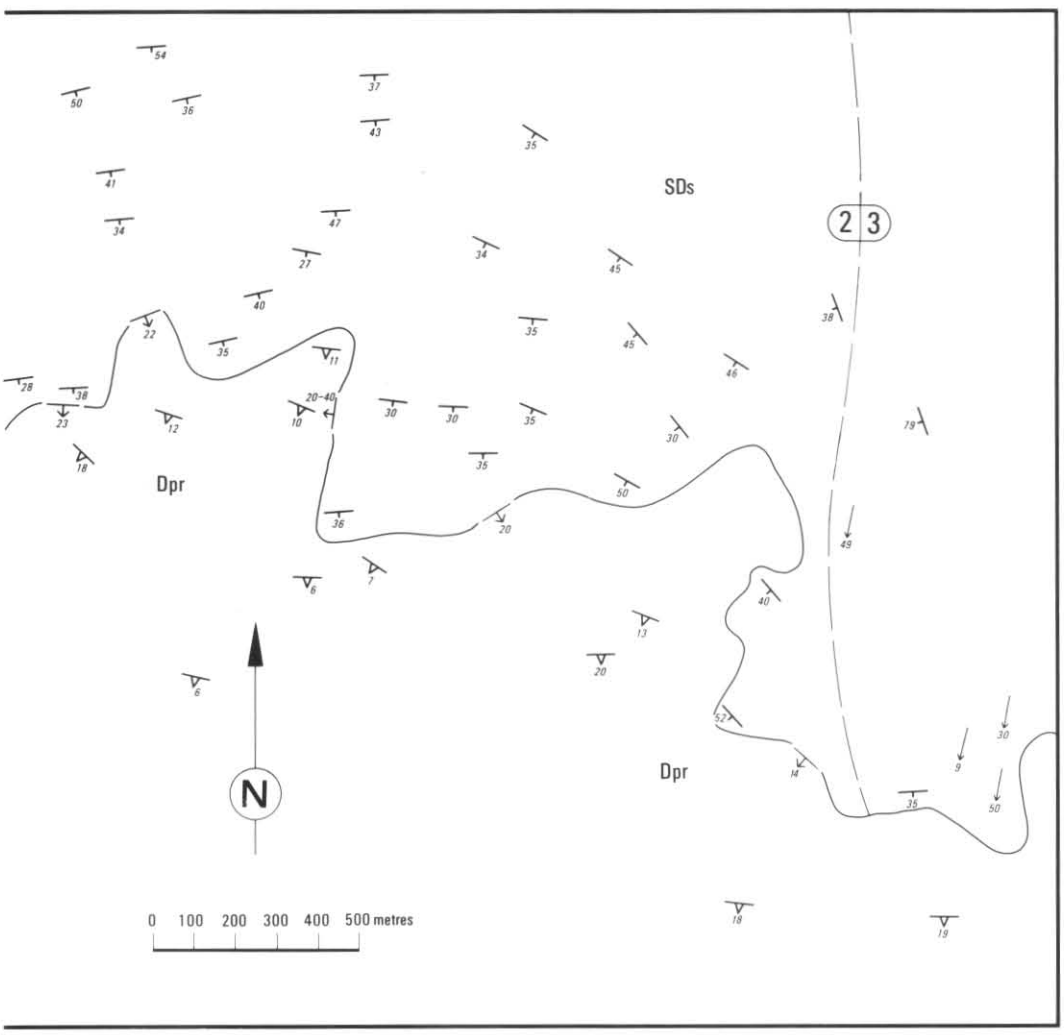

Trend lines
Geological boundary
Fault, inferred
Sub-area boundary
Strike and dip of bedding, facing known, overturned
Foliation (?due to compaction) in St Marys Porphyrite
Fold hinge, with amount and direction of plunge
Strike and dip of the basal contact of Dpr given by the trace of the contact on the topography

small faults was recognised and they may have occurred either before or after emplacement of the Piccaninny Creek adamellite.

Post-emplacement movement in the Piccaninny Creek adamellite is demonstrated by the presence of thin seams of mylonite which are locally common in the vicinity of the contact with Sub-area 2, occurring on Tasman Highway and in Wardlaws Creek. They are also common at EP665843 which is 'along strike' to the south-east. The seams have variable orientation and range in width from less than one millimetre to over 40 mm. They consist of finely comminuted adamellite in which the feldspars have been extensively sericitised and the ferromagnesian minerals chloritised. Figure 40 summarises measurements of the trends of mylonitic seams at a small locality in Wardlaws Creek. There is a strong NW-NNW maximum and a subsidiary maximum trending WNW. At Piccaninny Point Gee and Groves (1974) described a post-intrusive system of small, vertical conjugate faults (fig. 11) of similar

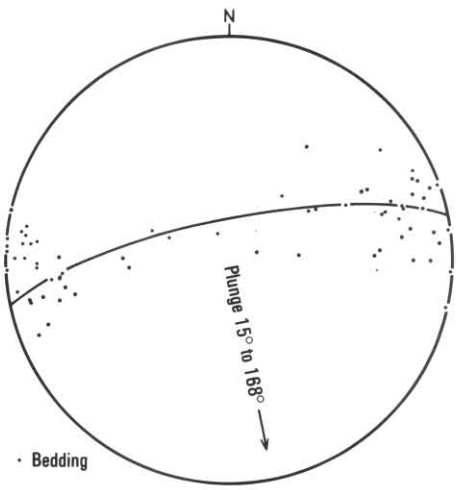

Figure 35. *Lambert projection of measurements of bedding in the St Marys area of Mathinna Beds.*

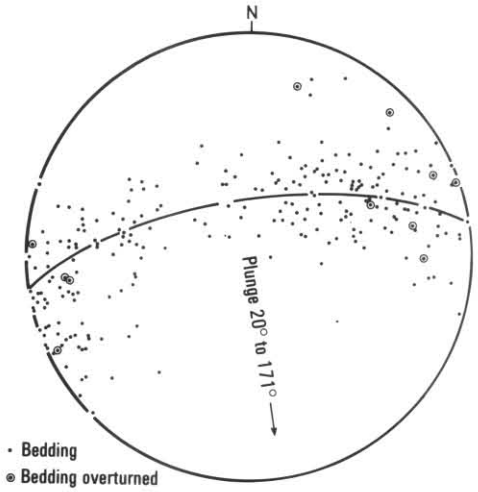

Figure 36. *Lambert projection of bedding measurements in Sub-area 1 of the northern area.*

orientation to the maxima of the mylonitic seams in Wardlaws Creek. One set of faults trends north-west and is sinistral whilst the other trends a little north of east and is dextral. They related the conjugate pair to the same compressive field that they inferred as the cause of the northerly trending foliation in the granodiorite.

Despite evidence of post-emplacement movement of north-west trend within the Piccaninny Creek adamellite and apparently sympathetic movement in the granodiorite at Piccaninny Point there appears to be no corresponding dislocation of the adamellite contact of any significant extent.

Thus, if the rotation in the Mathinna Beds is due to NW-trending, sinistral movement it either preceded or accompanied emplacement of the adamellite. The possibility that it may have accompanied emplacement is raised by the variation evident in the width of the thermal aureole. This variation seems greater than would be expected from simply a change in orientation of the contact (see Turner *in* McClenaghan *et al.*, 1982). It could not be confidently attributed to post-emplacement faulting since both the contact and outer edge of the aureole are unfaulted and no faults of sufficient magnitude were identified within the aureole. A possible scenario is that the contact segment south of Wardlaws Creek was an active fault during emplacement but major movement ceased before the adamellite consolidated, thus giving rise to an intrusive contact. Minor subsequent movement in the zone gave rise to mylonite seams in the adamellite and the small faults at Piccaninny Point.

There is a similar reduction in width of the thermal metamorphic aureole associated with the intrusive part of the St Marys Porphyrite east of St Marys. The trend of the contact is roughly similar to the trend of the contact of the Piccaninny Creek adamellite south of Wardlaws Creek and there is some evidence of rotation of bedding in a similar sense to the rotation in Sub-area 2 of the Elephant Pass area. Possibly both areas were subjected to similar north-west trending, sinistral movement during igneous emplacement.

ST MARYS AREA

Little structural detail was obtained from the St Marys area because of generally poor outcrop. The bedding projection for the area (fig. 35) indicates a N-S trend for the statistical fold axis with possibly a shallow southerly plunge. Cleavage is commonly difficult to detect in the area.

NORTHERN AREA

This area extends east from Catos Creek dyke across S Road and around the northern edge of the St Marys Porphyrite to the Tasman Highway near Falmouth. As is the case in the Elephant Pass area there is correspondence between Mathinna Beds structure and structural features of the igneous bodies. There is also the same problem of relative timing of events.

The area has been divided into three sub-areas (fig. 34) which reflects the striking variation in structural style across the area. Sub-area 1 is characterised by an abundance of short wavelength folds but there is little evidence of an overall vergence in the bedding projection (fig. 36). Folds with easterly vergence outcrop on S Road at EP989043. The statistical fold axis is consistent with fold hinges measured in the field (fig. 39) and with cleavage which is commonly difficult to detect. Fold closures

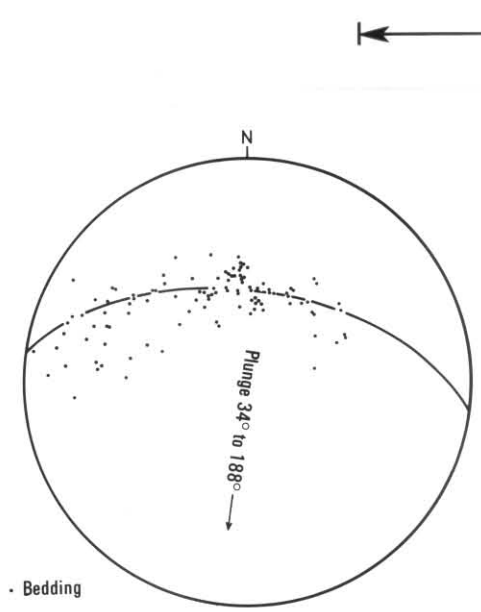

Figure 37. *Lambert projection of bedding measurements in Sub-area 2 of the northern area.*

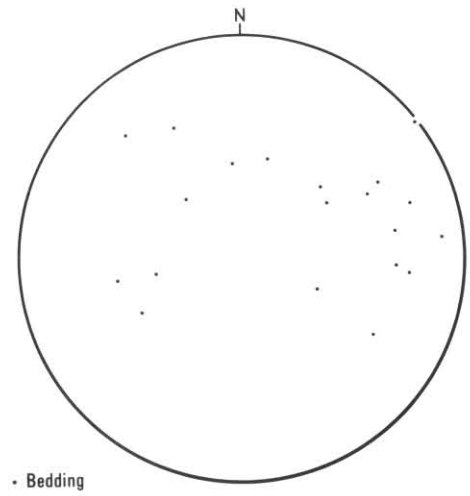

Figure 38. *Lambert projection of bedding measurements in Sub-area 3 of the northern area.*

generally have dihedral angles in the range 45–90°. Sub-area 2 is underlain by a single large syncline free of parasitic structures. Sub-area 3 contains folds of short wavelength but outcrop is poor and insufficient data were obtained for satisfactory interpretation (see fig. 38).

The syncline in Sub-area 2 sweeps around the north-western and northern edges of the St Marys Porphyrite and extends east as far as Yorkys Creek, thus giving the structure a width of about 3 km. No parasitic structures were found within the syncline and cleavage is generally difficult to discern. The bedding projection (fig. 37) indicates that the statistical fold axis trends south to SSW and plunges at about 34°. The syncline is transected by the breccia-bearing zone, Dsb, and is overlain with observable angular unconformity by Ds, the thin, laterally restricted bedded interval in Dsb. Thus, formation of the syncline preceded the development of the breccia-bearing zone and the emplacement of the overlying St Marys Porphyrite. However, the breccia-bearing zone, the basal contact of the porphyrite body and the foliation within the porphyrite all sweep around in a broad synclinal structure that is superimposed on the structure in the Mathinna Beds. The best estimate of the position inside the St Marys Porphyrite of the trace of the axial surface of the younger structure corresponds in part to a region in which mylonitic fractures are particularly numerous (fig. 34). These fractures are generally less than 10 mm wide and consist of finely comminuted, chloritised and ?albitised porphyrite. They closely resemble mylonitic fractures in the plutonic rocks in the Elephant Pass area and are of widespread occurrence in the St Marys Porphyrite.

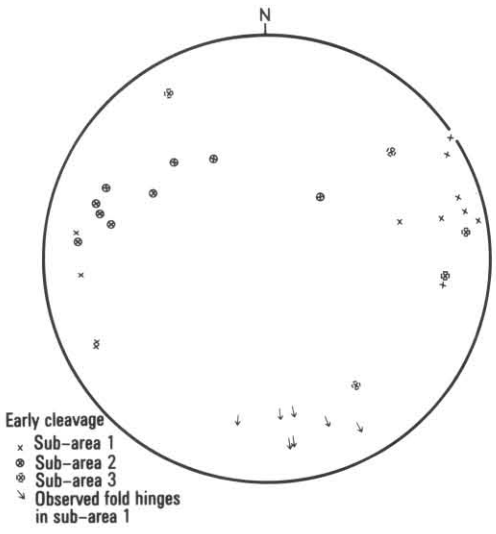

Figure 39. *Lambert projection of measurements of cleavage and fold hinges in Sub-areas 1, 2 and 3 of the northern area.*

In the Mathinna Beds the axial surface trace of the syncline formed by the younger rocks is expressed as a NNW-trending flexure in the western limb of the broad syncline of Sub-area 2. This flexure trends parallel to the trend of hinges of the parasitic folds in Sub-area 1. It may thus reflect tightening of the broad synclinal structure during the deformational event which produced the short wavelength folds. Such an interpretation implies that a large part of the shortening evident in the Mathinna Beds occurred *after* emplacement of the St Marys Porphyrite.

This is consistent with the widespread presence of folds and mylonitic fractures in the porphyrite body. The chlorite-bearing assemblage in the mylonite indicates that the fractures formed after the porphyrite had cooled substantially but the possibility of the assemblage having regressed from an earlier, higher-rank assemblage exists. This point is relevant in view of the conclusion in an earlier section of this report that folding in the coastal belt of the St Marys Porphyrite had an extended history, commencing whilst the volcanic pile was still very hot and either continuing or recurring after it had cooled substantially. However, the identification of early folding in the coastal belt is a consequence of the presence of discordant compaction fabrics and such discordancy appears to be absent elsewhere in the body. Therefore, it seems likely that most of the regional deformation in the St Marys Porphyrite occurred late in the cooling history of the body when it would have been a fairly competent unit. In the cases of the two largest folds affecting the body, namely the syncline in the coastal belt and the syncline that extends into the Mathinna Beds in Sub-area 2 of the northern area, the end result of early and late folding was to generate structures with the same asymmetry as synclines in the Mathinna Beds. Specifically, their western limbs dip steeply compared to their eastern limbs.

A separate line of evidence bearing on the relative timing of deformation and igneous emplacement of the St Marys Porphyrite and Catos Creek dyke is provided by the pattern of folding in relation to the positions of igneous features. For example, the boundary between Sub-areas 1 and 2 in the northern Mathinna Beds area marks the outer limit of an envelope around and under the shallowly dipping northern edge of the St Marys Porphyrite. The envelope was apparently structurally protected by the competent porphyrite body during post-emplacement deformation. The envelope's boundary is exposed at EQ994037 and corresponds to a thin breccia interval. Other evidence of the influence of the igneous bodies on the pattern of folding is provided by variations in the trend of the short wavelength folds in Sub-area 1 which are consistent with the folds having been deflected by the apophysis on Catos Creek dyke and at the boundary between Sub-areas 1 and 2.

In conclusion, the favoured interpretation is that the short wavelength folds in Sub-area 1 were formed after emplacement of the St Marys Porphyrite and Catos Creek dyke. This is supported by:

(1) Abundant evidence of deformation within the St Marys Porphyrite although equivalent deformation is yet to be demonstrated in Catos Creek dyke.

(2) Continuity from Mathinna Beds into St Marys Porphyrite of a fold whose axial surface trend is parallel to the trend of the short wavelength folds.

(3) Influence by the igneous bodies on the trend and pattern of distribution of the short wavelength folds.

Devonian igneous rocks

INTRODUCTION

There are a number of previously published works relating to igneous structure in the St Marys Quadrangle. These include McNeil (1965), Gee and Groves (1971, 1974) and Williams and Groves (1967). The relevant material contained in each of these works relates either primarily or entirely to structures in the granodiorite at Piccaninny Point.

New information on various aspects of the structure of the igneous rocks in the quadrangle has been covered in other sections of this report. Features in the St Marys Porphyrite that are thought to be related to either flow or compaction are covered in the section which deals with the porphyrite. Folds in the porphyrite are covered in the same section also in the subsection dealing with the structure of the northern Mathinna Beds area where there appear to be corresponding folds. Some aspects of the structure of the Piccaninny Creek adamellite (Daec) and the granodiorite (Dg) at Piccaninny Point are covered in the subsection on the structure of the Mathinna Beds in the Elephant Pass area again because there appears to be a correspondence of structures. Rather than repeat these discussions it is the aim of this section to provide a brief summary of the main structural features in the principal igneous bodies.

ST MARYS PORPHYRITE (Dpr, Dpm)

(1) Little evidence of stress-related recrystallisation of quartz was recognised in the porphyrite.

(2) Coastal belt:

East of Mt Elephant there is a relatively tight syncline defined by a layer rich in metasedimentary lithic fragments. The structure is 2–3 km across and asymmetric.

The schlieren shape foliation is approximately parallel to the layering in the coastal outcrops and probably around the syncline. This foliation is interpreted as a deflation fabric which formed at the time of emplacement of the pyroclastics.

Superimposed on the syncline in the layering is a more open, asymmetric structure defined by the biotite foliation. The axial surface of this syncline can be traced from east of Mt Elephant to near Falmouth.

The biotite foliation is thought to represent residual compaction and to have developed progressively whilst the hot volcanic pile was undergoing relatively rapid subsidence. The syncline defined by the foliation is thought to have formed after cooling proceeded beyond a point where compaction could occur.

(3) Inland area:

Unlike the coastal belt there appears to be no discordance between the various fabric elements in the porphyrite.

The fabric is gently folded on northerly trends.

Thin seams containing chloritic mylonite are widespread being particularly conspicuous in drill-core obtained at EQ632014.

(4) North-western and northern area:

An open, asymmetric syncline is defined by Dsb, the basal contact of the porphyrite and the foliation within the porphyrite.

The axial surface of the syncline corresponds in part to an area in which seams of chloritic mylonite are very numerous. This correspondence suggests that the fold and mylonite seams are related strains.

CATOS CREEK DYKE (Dapl)

Little evidence of deformation was observed in Catos Creek dyke except near the faulted eastern contact.

PICCANINNY CREEK ADAMELLITE (Daec)

(1) Quartz grains in Daec are highly strained and mostly recrystallised.

(2) Measurements of a weakly developed, northerly-trending, mineral alignment were made at a number of localities but the fabric is not generally discernible. It is expressed as a weak alignment of flakes and patches of biotite although, feldspar grains are sometimes aligned (e.g. EP669882). The fabric is probably a foliation but only measurements of its apparent lineation on subhorizontal outcrop surfaces were made.

(3) Chloritic mylonite occurs in thin seams in Daec near the Mathinna contact in Wardlaws Creek and on Tasman Highway and in outcrops to the south-east. Figure 40 illustrates the trends of seams at EP649858.

GRANODIORITE (Dg)

(1) Strain is ubiquitous in quartz grains in the granodiorite. Remnants of coarse primary grains are present which are optically continuous but which show lamellar structure when close to extinction. Most of this early population is annealed and forms patches of smaller subgrains which are themselves highly strained and have sutured interfaces. Where foliation is particularly intense both the subgrains and the patches formed by them are aligned.

(2) Petrofabric analyses by McNeil (1965) show that biotite flakes dip steeply and strike 316–38°. Visual estimates of foliation orientation correspond to about the mid-point of this range.

(3) Xenoliths are common in the granodiorite and vary in cross-sectional shape from elliptical to quite irregular. Those with elongate shapes mostly trend parallel to the foliation. In a zone at Long Point both shapes and foliation are highly oblique to layering (plate 31).

(4) Late aplite and leucogranite dykes often contain mineral alignment parallel to that in the granodiorite. However, deformation was well advanced prior to the emplacement of some of these bodies (plate 41).

After investigating dykes of granodiorite in Mathinna Beds at Piccaninny Point Williams and Groves (1967) concluded that the dykes were dilational and implied that the foliation in them developed as the dykes opened.

(5) Gee and Groves (1974) identified a system of late, conjugate, transverse faults at Piccaninny Point. Small, sinistral faults trend north-west and small dextral structures trend ENE. They related the system to the same stress-field which generated the NNW-N trending foliation.

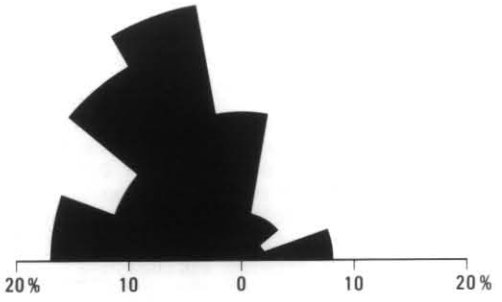

Figure 40. *130 measurements of trends of thin mylonitic shears on a sub-horizontal outcrop surface of the Piccaninny Creek adamellite* (Dbaec) *at EP949858 in Wardlaws Creek. Inspection of two subvertical surfaces indicated a subvertical orientation for the fractures. The measurements have been grouped over 20° intervals and the number in each interval calculated as a percentage of the total number of measurements.*

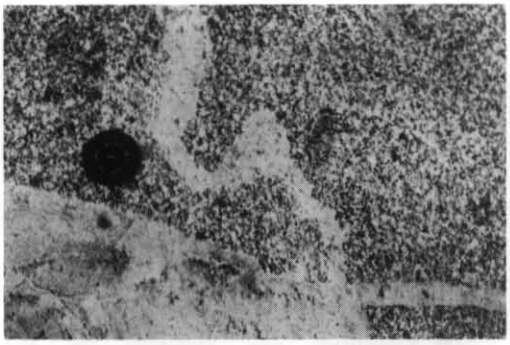

Plate 41. *A folded leucocratic vein in foliated granodiorite at Long Point. The fold is juxtaposed with an unfolded aplite dyke. The lens cap is 49 mm across.*

Timing and regional nature of Devonian deformation

The RB-Sr isotopic age of the St Marys Porphyrite (388 ± 1 Ma — Turner *et al.*, in press) together with the age of a graptolite in the Mathinna Beds (late Siegenian — Rickards and Banks, 1979) indicate that the phase of deformation which preceded emplacement of the porphyrite body probably occurred in Emsian times (Harland *et al.*, 1982). This deformation would have only shortly preceded emplacement of the St Marys Porphyrite.

Apparent continuity between a synclinal structure in the St Marys Porphyrite and a subordinate fold structure in Sub-area 2 of the northern Mathinna Beds area indicates that some folds in the Mathinna Beds are younger than the St Marys Porphyrite. Short wavelengths folds in Sub-area 1 of the northern Mathinna Beds area may belong to this phase because their trends is parallel to the subordinate fold in Sub-area 2 and their distribution appears to be influenced by the shape and extent of both the porphyrite body and Catos Creek dyke.

Folding in the coastal belt of the St Marys Porphyrite seems to have preceded emplacement of the Piccaninny Creek adamellite because the contact between the two bodies appears to be unaffected by the folds. The folds apparently developed shortly after emplacement of the porphyrite body because the indistinguishable Rb-Sr isotopic ages of the adamellite and porphyrite imply that little time elapsed before emplacement of the adamellite. Such rapid onset of folding is supported by the independent conclusion that much of the deformation in the coastal belt of the St Marys Porphyrite occurred whilst the body was still hot.

Despite being apparently younger than the folds in the St Marys Porphyrite, the Piccaninny Creek adamellite contains a weakly developed fabric of similar trend to the folds. The more strongly developed fabric in the Long Point–Piccaninny Point granodiorite is also of similar trend but no direct evidence was recognised which determines the time of its development relative to either the folds in the porphyrite body or the fabric in the adamellite. It may follow from observations by Williams and Groves (1969) that foliation in granodiorite dykes in Mathinna Beds at Piccaninny Point developed as the dykes opened. Gee and Groves (1974) relate the opening of the dykes to the same stress field which caused the foliation, but they assign a slightly later timing to foliation development in order to account for flattening of dyke wall irregularities and for extensive micro-deformation and quartz recrystallisation in the granodiorite.

Gee and Groves (1974) postulate intrusive pressure as the cause of deformation but the evidence of the regional mapping is that comparably oriented strain is not localised at the granodiorite contact but is of regional extent. Strains in the Mathinna Beds, the St Marys Porphyrite and the Piccaninny Creek adamellite share the same general orientation which implies the repeated application of a regional stress pattern in which the maximum principal stress is oriented approximately E-W.

The late small conjugate faults at Piccaninny Point are consistent with this pattern (Gee and Groves, 1974) and appear to be one expression of a temporally extended movement pattern which is also represented by the sinistral rotation of structures in Sub-area 2 of the Elephant Pass area of Mathinna Beds, by mylonitic seams in the Piccaninny Creek adamellite and possibly by the contact of the adamellite south of Wardlaws Creek.

The Rb-Sr isotopic ages of all the major igneous bodies in the St Marys Quadrangle are very similar and it has been suggested that they were all emplaced in an interval of possibly 3 million years (Turner *et al.*, in press). It seems that the entire history of deformation and igneous activity in the St Marys Quadrangle was of short duration, perhaps less than 10 million years.

Parmeener Super-Group

C. R. Calver

The Parmeener Super-Group is essentially flat-lying, and rests with landscape unconformity upon pre-Carboniferous deformed basement rocks. Details of basement topography and shapes of lithosomes within the sequence are included in the Stratigraphy section.

The Parmeener Super-Group has a regional dip of about one degree to the south-east. Substantially steeper dips were recorded, mostly near known faults.

Faults affecting the Parmeener Super-Group (and presumably also the Jurassic dolerite, although

this cannot usually be proved) are shown in Figure 41. Faults known from surface mapping, or from underground coal mine workings are mostly accurately located and are shown with solid lines. Those faults inferred from borehole data, whose position and trend is constrained only by the position of the boreholes (indicated on Figure 41) are shown with dashed lines. Approximate throws of the faults are also indicated. Faults with displacements of less than 10 m are usually beyond the resolution of mapping at this scale, and also beyond the resolution of subsurface interpretation with boreholes at the present gridded interval. A greater fault density than that shown is therefore probable, a factor likely to adversely affect recoverable coal reserves.

The predominant trend is N-S, with the rocks being thrown into a series of shallow meridional

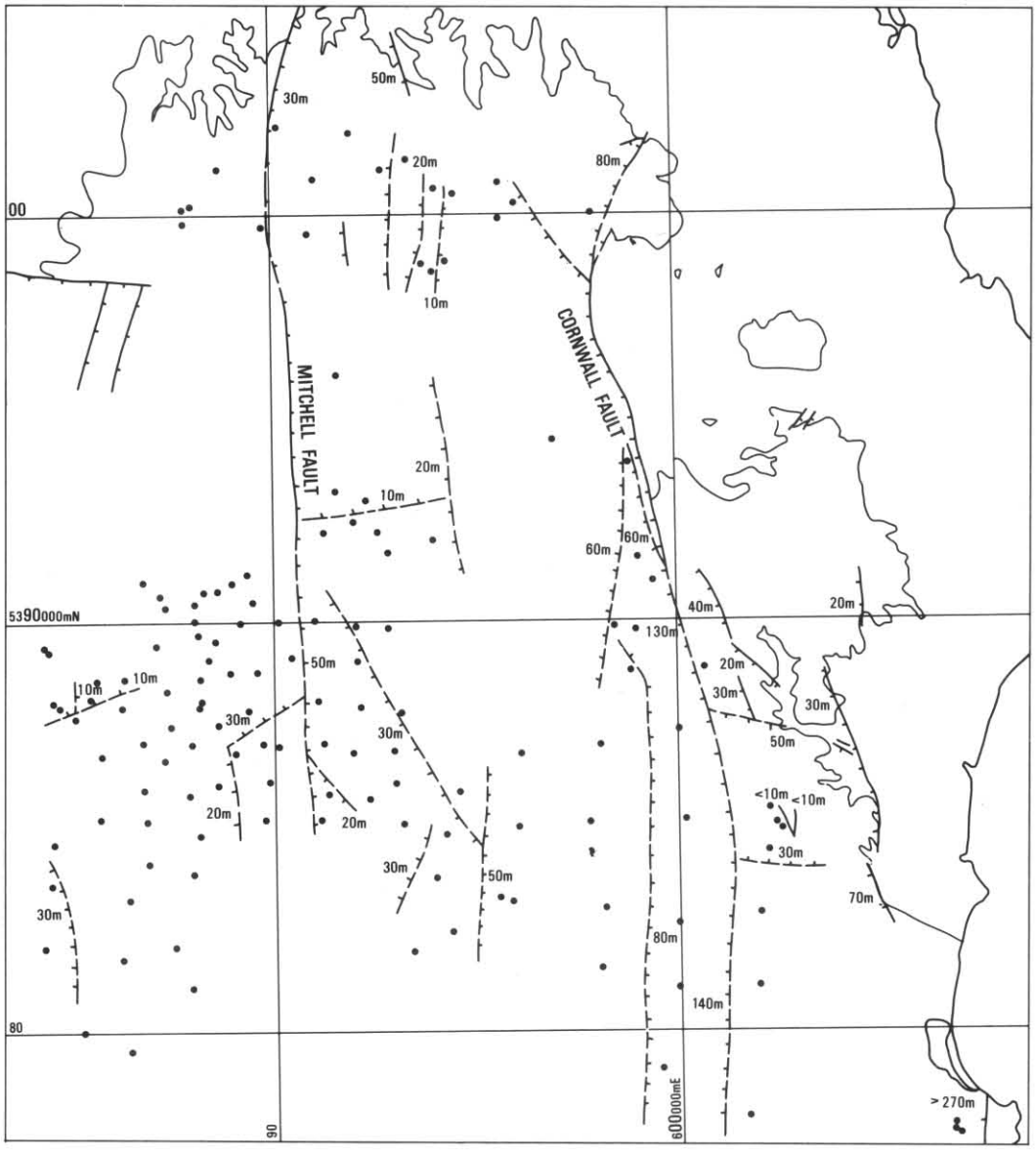

Figure 41. *Known faults affecting the Parmeener Super-Group. Dashed lines are faults inferred from bore hole information (bore hole locations are indicated). Solid lines are faults located by surface mapping and underground mining operations. Downthrown side indicated by ticks. Approximate throws given in metres.*

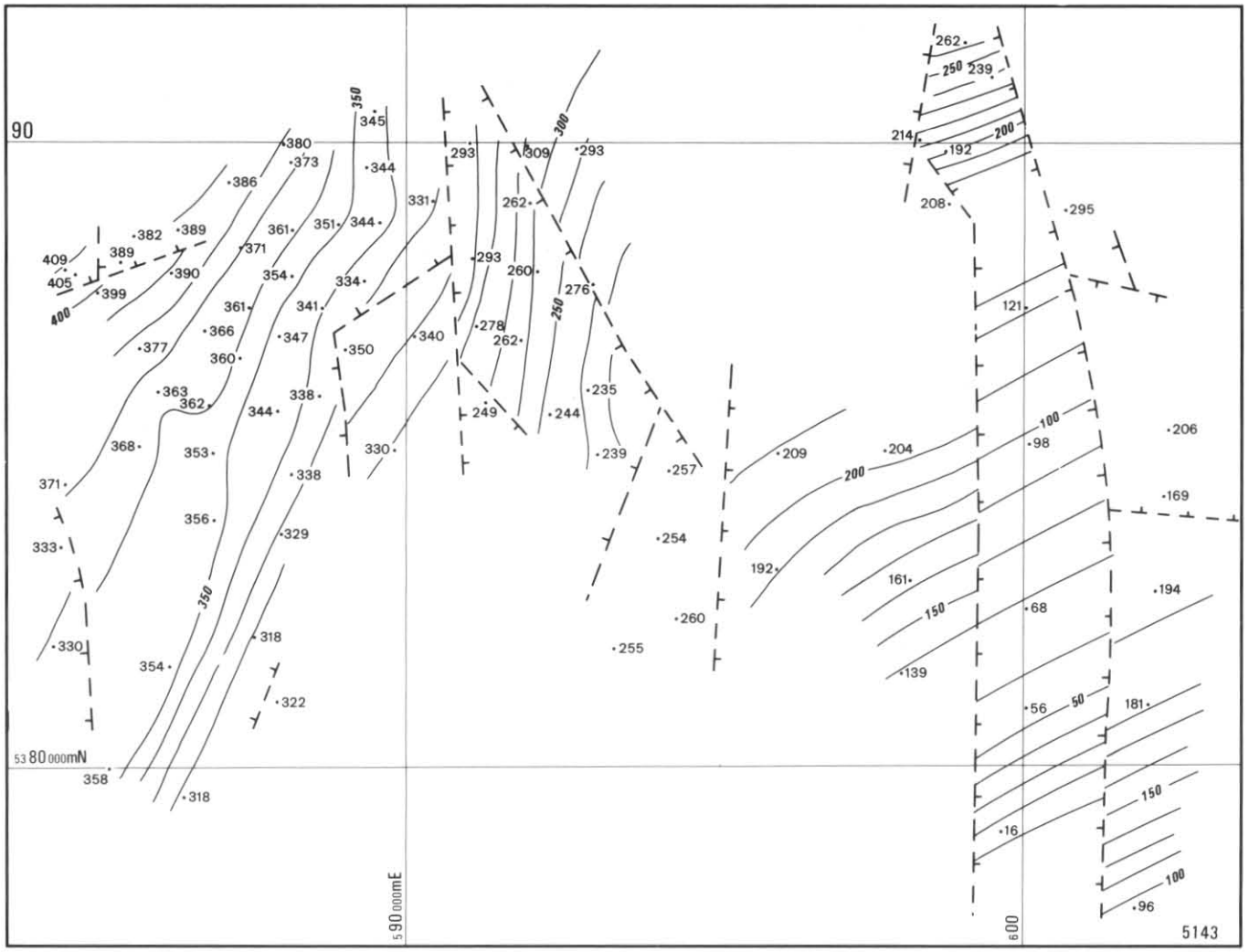

Figure 42. *Structure contours of base of Gl seam and correlates (metres above sea-level).*

horsts and grabens. Three faults have relatively large throws. A fault with a vertical displacement of at least 270 m crosses Long Point [FP083778], where granite to the east is juxtaposed against Upper Parmeener Super-Group rocks to the west. The Cornwall Fault (Hills, *et. al.*, 1922) passes through the St Marys township, and to the north splits into two divergent faults, the easterly one being known as Goulds Fault (*ibid.*). Southwards, the Cornwall Fault appears to split into several structures. The fault comprising the eastern edge of the N-S graben in the Thompsons Marshes area appears to be the main southward continuation of the Cornwall Fault. The Mitchell Fault (Threader and Bacon, 1983) is well substantiated by borehole and field data. Its throw appears to decrease to the north.

Figure 42 is a structure contour diagram of the base of the G seam (the lowest widely correlative seam in the Upper Parmeener Super-Group, see fig. 6) or, where present, the lower split of the G seam. The gentle south-easterly dip is apparent, as are variations that represent gentle monoclines or perhaps minor faults.

Jurassic dolerite

C. R. Calver

As previously described, nearly all the dolerite on St Marys Quadrangle is contained in a thick, unroofed sheet, probably once continuous over the whole quadrangle, its base usually 200–300 m above the base of the Upper Parmeener Super-Group.

The thickness and configuration of the dolerite are crucial to coal exploration in the Upper Parmeener Super-Group, and have been the main focus of a regional (central-eastern Tasmania) gravity survey (Leaman and Richardson, 1981). The Fingal Tier on St Marys Quadrangle has been the area of most concentrated investigation, with closer station spacing and higher resolution. Other geophysical work, primarily magnetics, have provided subsidiary information on the structure of the dolerite (Leaman and Richardson, 1980; Leaman, 1980, Richardson and Leaman, 1981). Ground magnetometer traverses have been used at a few localities to locate edges of dolerite outcrop concealed under talus (see p. 43). Numerous boreholes on Fingal Tier penetrate the sheet to reach the underlying coal measures.

This information has provided a broad picture of the configuration of the base of the intrusion over most of the map sheet.

The thickest known preserved section of dolerite occurs near Bare Rock, where bore hole GY13 [EP961867] intersected 458 m without reaching the base of the intrusion. Bore hole 67 [EP842820] reached the base after penetrating 433 m of dolerite; bore hole 68 after 453 m. Evidence discussed previously suggests that these holes were all collared not far below the (now removed) top of the sheet.

An isostrat (Carey, 1958) diagram of the base of the sheet, using drill hole data with the stratigraphic framework established above for the Upper Parmeener Super-Group, was constructed for Fingal Tier (fig. 43). This shows the shape of the base of the sheet relative to major coal seams, and reflects the pre-faulting configuration of the intrusion. The base of the sheet tends to recur at particular horizons, specifically coal seams G, F, D, and particularly C; and at and above the Dalmayne Conglomerate. Over most of the area, the base of the sheet is essentially concordant with relatively abrupt, probably step-like changes of level. Coal-lutite intervals evidently acted as planes of weakness that opened up to admit the intrusion.

In addition to the sheet-like part of the intrusion, there are several large (1–10 km^2) areas of anomalously thick or low-lying dolerite around the edge of the Fingal Tier, whose form is known partly from surface mapping and partly from the gravity survey (Leaman and Richardson, 1981). The main relevant conclusions of the gravity survey are incorporated in the following discussion of these features.

The +1 mgal Bouguer anomaly contour, considered by Leaman and Richardson (1981) to approximately delineate zones of thickened dolerite, is shown on Figure 43. Also indicated are areas of low-lying dolerite determined from field mapping. There is rough agreement, with thickened dolerite zones indicated around Fingal Rivulet [EP835880], Bare Rock [EP960880], Bedggood Hill [FP035790], and Mt Puzzler [EP900780].

Computer modelling of downward continuations of the gravity field have suggested the form and areal extent of smaller features (pipes, dykes, etc.) at depth, and these are also indicated on Figure 43. The general form implied for the zones of thickened dolerite is asymmetric funnel-shaped feeder structures, tapering at depth and sometimes dividing into two or more pipes or dykes.

The Fingal Rivulet zone is associated with pronounced Bouguer anomalies, but detailed analysis indicated that much of the mass has been removed by the ravine of the rivulet, and that the pipe is relatively small.

Spion Kop [EP863903] is the summit of a roughly circular boss of dolerite, about one kilometre in diameter, with steeply transgressive contacts, indicated by surface mapping, on its eastern and western sides. An offshoot to the south-west is in the form of a discontinuous, dyke-like body that reaches almost as far as the Duncan Mine portal [EP845893]. Mine workings confirm that both dyke and boss have near-vertical contacts at depth.

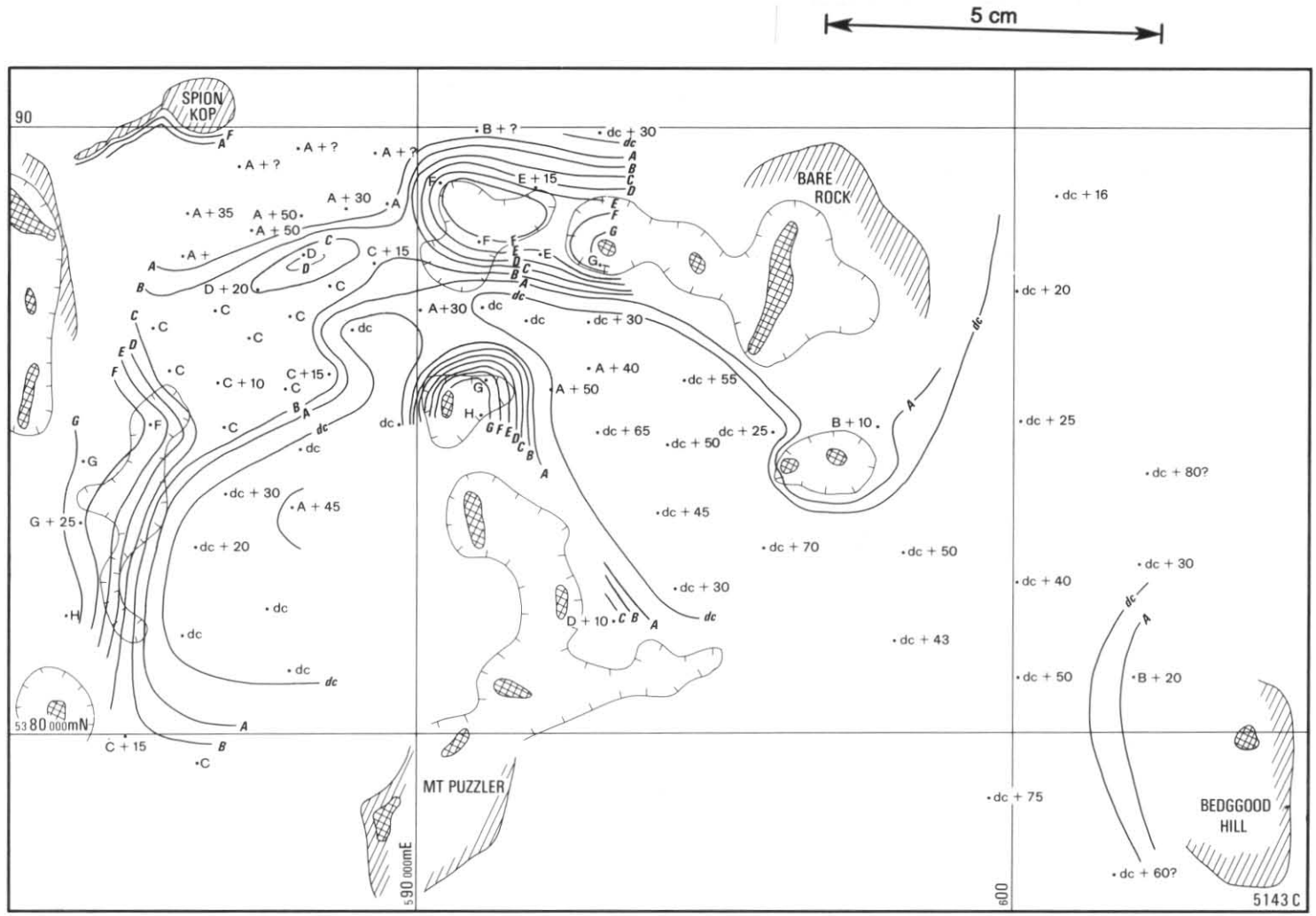

Figure 43. *Structure of dolerite sheet, Fingal Tier. Isostrats inferred from bore hole data (Threader and Bacon, 1983), gravimetric information (Leaman and Richardson, 1981) and surface mapping. Isostrats drawn at inferred contacts of dolerite with coal seams (A, B, C, etc.) and the Dalmayne Conglomerate (dc). See Figure 42 for stratigraphy. Data points indicate approximate level of dolerite intrusion in metres above horizon indicated. Also shown are the 1 mgal contour and major feeder structures determined from gravity survey (cross-hatching), and areas of low-lying dolerite determined from surface mapping (diagonal lines).*

The Bare Rock area, and the zone extending north from Mt Puzzler, have the most pronounced Bouguer anomalies, and each splits up at depth into several major feeders. Substantial gradients around the anomalies suggest that the lower contact of the intrusion has significant dips about these centres.

A number of smaller gravity anomalies, not included on Figure 43, probably reflect isolated small dykes or pipes. None of these is considered likely to exceed 75–100 m in thickness or diameter.

Small, low-lying bodies of dolerite, elongate in plan view, were mapped at a few places [EP858919, FP030830, FP034879). They are probably the eroded remnants of feeders. A positive Bouguer anomaly is centred on the first of these.

On the Nicholas Range, the dolerite appears mostly concordant, with the base of the sill at about 550 m a.s.l. around Mt Durham, and 650 m a.s. l. along the spine of the range as far east as South Sister. Huntsmans Cap, North Sister and Cheeseberry Hill are nearby prominent outliers that intrude at a lower level. No positive Bouguer anomalies are associated with them, suggesting that they do not overlie substantial pipes or feeders. They may instead be remnants of a downward-transgressing sheet. Baked mudstone at EQ933014 also suggests that the Nicholas Range sheet transgressed downwards to the north.

Dolerite on St Patricks Head is slightly transgressive, intruding Permian and lowermost Triassic strata. Here also there is no positive gravity anomaly, so the same conclusion can be drawn.

Mt Elephant appears to be simply the eroded remnant of the base of a sill intruding 250–280 m above the base of the Upper Parmeener Super-Group.

The linear, ridge-like form of most of these outliers suggests a structural (jointing?) control on their morphology.

Small dolerite bodies, some dykes, intrude pre-Parmeener basement rocks at FP988038 and vicinity, and at FP077980.

REFERENCES

ANDERSON, A. T. 1968. The oxygen fugacity of alkaline basalt and related magmas, Tristan da Cunha. *Am. J. Sci.* 266:704–727.

BACON, C. A. 1979. *Regional geology of the Apsley River area.* B.Sc. thesis [Part A], University of Tasmania : Hobart.

BACON, C. A.; EVERARD, J. L. 1981. Pyroclastics in the Upper Parmeener Super-group, near Bicheno, eastern Tasmania. *Pap. Proc. R. Soc. Tasm.* 115:29–36.

BOTTINGA, Y.; WEILL, D. 1970. Densities of liquid silicate systems calculated from partial molar volumes of oxide components. *Am. J. Sci.* 269:169–182.

BOTTINGA, Y.; WEILL, D.; RICHET, P. 1982. Density calculations for silicate liquids. I. Revised method for aluminosilicate compositions. *Geochim. cosmochim. Acta.* 46:909–919.

BROOKS, C. K. 1976. The Fe_2O_3/FeO ratio of basalt analyses: an appeal for a standard procedure. *Bull. geol. Soc. Denmark* 25:117–120.

BROWN, A. V.; MCCLENAGHAN, M. P. 1982. Tertiary basaltic rocks, *in* MCCLENAGHAN *et al.*, Geology of the Ringarooma–Boobyalla area. *Bull. geol. Surv. Tasm.* 61:92–114.

BROWN, G. E. 1982. Olivines and silicate spinels, *in* RIBBE, P. H. (ed.), Orthosilicates. *Rev. Mineral., Mineral. Soc. Am.* 5:275–381. ed.]

BUDDINGTON, A. F.; LINDSLEY, D. H. 1964. Iron-titanium oxide minerals and synthetic equivalents. *J. Petrology* 5:310–357.

BURNHAM, C. W.; HOLLOWAY, J. R.; DAVIS, N. F. 1969. Thermodynamic properties of water to 1000° and 10 000 bars. *Spec. Pap. geol. Soc. Am.* 132:1–96.

CARMICHAEL, I. S. E.; TURNER, F. J.; VERHOOGEN, J. 1974. *Igneous petrology.* McGraw Hill : New York.

COOMBS, D. S.; WILKINSON, J. F. G. 1969. Lineages and fractionation trends in undersaturated volcanic rocks from the East Otago volcanic province (New Zealand) and related rocks. *J. Petrology* 10:440–501.

COX, K. G.; BELL, J. D.; PANKHURST, R. J. 1979. *The interpretation of igneous rocks.* Allen and Unwin : London.

DEER, W. A.; HOWIE, R. A.; ZUSSMAN, J. 1963. *Rock-forming minerals minerals. Vol. 4. Framework silicates.* Logmans : London.

DUKE, J. M. 1976. Distribution of the period four transition elements among olivine, calcic clinopyroxene and mafic silicate liquid: experimental results. *J. Petrology* 17:499–521.

EDWARDS, A. B. 1941. The crinanite laccolith of Circular Head. *Proc. R. Soc. Vict.* 53:403–415.

EDWARDS, A. B. 1950. The petrology of the Cainozoic rocks of Tasmania. *Proc. R. Soc. Vict.* 62:97–120.

EVERARD, J. L. 1984. Petrology of Tertiary basalt, altered dolerite and tuff samples, *in* GULLINE, A. B. Geological atlas 1:50 000 series. Sheet 83(8412N). Sorell. *Explan. Rep. geol. Surv. Tasm.*

FINNERTY, A. A.; BOYD, F. R. 1978. Pressure dependent solubility of calcium in forsterite coexisting with diopside and enstatite. *Yb. Carnegie Inst. Wash.* 77:713–717.

FLOYD, P. A.; WINCHESTER, J. A. 1975. Magma type and tectonic setting discrimination using immobile elements. *Earth planet. Sci. Lett.* 27:211–218.

FORSYTH, S. M. 1980. Preliminary palynological report on Upper Parmeener Super-Group rocks interbedded with basalt at Webber Falls. *Unpubl. Rep. Dep. Mines Tasm.*

FREY, F. A.; GREEN, D. H.; ROY, S. D. 1978. Integrated models of basalt petrogenesis: a study of quartz tholeiites to olivine melilitites from south eastern Australia utilizing geochemical and experimental petrological data. *J. Petrology* 19:463–513.

FRONDEL, C. 1969. Scandium, *in* WEDEPOHL, K. H. (ed.) *Handbook of geochemistry. Vol. II/2. Elements Si(14) to V(23).* Springer-Verlag : Berlin.

FULLER, R. E. 1939. Gravitative accumulation of olivine during the advance of basaltic flows. *J. Geol.* 47:303–313.

GEE, R. D. 1971. Geological atlas 1 mile series. Sheet 22(8016S). Table Cape. *Explan. Rep. geol. Surv. Tasm.*:35-39.

GREEN, D. C. 1980. Barium-bearing heulandite from DDH 55, Fingal. *Unpubl. Rep. Dep. Mines Tasm.* 1980/27.

GREEN, D. H.; RINGWOOD, A. E. 1967. The genesis of basaltic magmas. *Contrib. Mineral. Petrology* 15:103–190.

GRUNDY, H. D.; BROWN, W. L. 1974. A high-temperature X-ray study of low and high plagioclase feldspars, *in* MACKENZIE, W. S.; ZUSSMAN, J. *The feldspars*:162–173. Manchester University Press.

HAGGERTY, S. E. 1976. Opaque mineral oxides in terrestrial igneous rocks, *in* RUMBLE, D. (ed.). Chapter 8. Oxide minerals. *Short Course Notes, Mineral. Soc. Am.* 3.

HALE, G. E. 1962. Triassic system, *in* SPRY, A. H.; BANKS, M. R. (ed.). The geology of Tasmania. *J. geol. Soc. Aust.* 9(2):217–231.

JOPLIN, G. A. 1963. Chemical analyses of Australian rocks. Part I: Igneous and metamorphic. *Bull. Bur. Geol. Geophys. Aust.* 65.

KUNO, H. 1960. High-alumina basalt. *J. Petrology* 1:121–145.

LE MAITRE, R. W. 1979. A new generalized petrological mixing model. *Contrib. Mineral. Petrology* 71:133–137.

MACDONALD, G. A. 1960. Dissimilarity of continental and oceanic rock types. *J. Petrology* 1:172–177.

MACDONALD, G. A.; KATSURA, T. 1964. Chemical composition of Hawaiian lavas. *J. Petrology* 5:82–133.

MCNEIL, R. D. 1965. The geology of the Mt Elephant, Picanniny Point area, Tasmania. *Pap. Proc. R. Soc. Tasm.* 99:27–49.

MANSON, V. 1967. Geochemistry of basaltic rocks: major elements, *in: The Poldervaart treatise on rocks of basaltic composition.* 1:215–269. Wiley : New York.

MATHEWS, W. H.; THORARINSSON, S.; CHURCH, N. B. 1964. Gravitative settling of olivine in pillows of an Icelandic basalt. *Am. J. Sci.* 262:1036–1040.

MYSEN, B. O.; KUSHIRO, I. 1979. Pressure dependence of nickel partitioning between forsterite and aluminous silicate melts. *Earth planet. Sci. Lett.* 42:383–388.

PEARCE, J. A.; CANN, J. R. 1973. Tectonic setting of basic volcanic rocks determined using trace element analyses. *Earth planet. Sci. Lett.* 19:290–300.

PEARCE, J. A.; NORRY, M. J. 1979. Petrogenetic implications of Ti, Zr, Y and Nb variations in volcanic rocks. *Contrib. Mineral. Petrology* 69:33–47.

RINGWOOD, A. E. 1966. The chemical composition and origin of the earth, *in* HURLEY, P. M. (ed.). *Advances in earth science.* MIT Press : Cambridge, Mass.

ROBINSON, P. 1980. The composition space of terrestrial pyroxenes — internal and external limits, *in* PREWITT, C. T. (ed.). *Pyroxenes. Reviews in mineralogy* 7(9):419–494.

SATO, H. 1977. Nickel content of basaltic magmas: identification of primary magmas and a measure of the degree of olivine fractionation. *Lithos* 10:113–120. SIMKIN, T.; SMITH, J. V. 1970. Minor element distribution in olivine. *J. Geol.* 78:304–325.

SMITH, J. V. 1974*a*. *Feldspar minerals. I. Crystal structure and physical properties.* Springer-Verlag : Berlin.

SMITH, J. V. 1974*b*. *Feldspar minerals. II. Chemical and textural properties.* Springer-Verlag : Berlin.

SPARKS, R. S. J. 1983. Mixed-up magmas. *Nature, Lond.* 306: 315–316.

SPEIDEL, D. H. 1970. Effect of magnesium on the iron-titanium oxides. *Am. J. Sci.* 268:341–353.

SPRY, A. H. 1962. Igneous activity, *in* SPRY, A. H.; BANKS, M. R. (ed.). The geology of Tasmania. *J. geol. Soc. Aust.* 9(2):255–284.

STRECKEISEN, A. 1967. Classification and nomenclature of igneous rocks. *Neues Jb. Mineral., Abh.* 107:144–240.

STRECKEISEN, A. L. 1978. Classification and nomenclature of volcanic rocks, lamprophyres, carbonatites and melilitic rocks. *Neues Jb. Miner., Abh.* 134:1–14. SUTHERLAND, F. L. 1969*b*. A review of the Tasmanian Cainozoic Province. *Spec. Publ. geol. Soc. Aust.* 2:133–144.

SUTHERLAND, F. L. 1976. Cainozoic volcanic rocks, *in Leaman, D. E.* Geological atlas 1:50 000 series. Sheet 82(8312S). Hobart. *Explan. Rep. geol. Surv. Tasm.*:35–56.

SUTHERLAND, F. L. 1977. Cainozoic volcanic rocks, *in Leaman, D. E.* Geological atlas 1:50 000 series. Sheet 75(8312N). Brighton. *Explan. Rep. geol. Surv. Tasm.*:25–37.

SUTHERLAND, F. L. 1984. Cainozoic basalts, *in* FORSYTH, S. M. Geological atlas 1:50 000 series. Sheet 68(8313S). Oatlands. *Explan. Rep. Dep. Mines Tasm.*:103–120.

SUTHERLAND, F. L. 1985. Cainozoic volcanic rocks, *in* FARMER, N. Geological atlas 1:50 000 series. Sheet 94(8311N). Kingborough. *Explan. Rep. geol. Surv. Tasm.*:73–83.

SUTHERLAND, F. L.; KERSHAW, R. C. 1971. The Cainozoic geology of Flinders Island, Bass Strait. *Pap. Proc. R. Soc. Tasm.* THREADER, V. M. 1968. An interim report on the geology and coal resources of the northeast coalfields of Tasmania. *Unpubl. Rep. Dep. Mines Tasm.*

VOGT, J. H. L. 1923. Nickel in igneous rocks. *Econ. Geol.* 18:307–353.

WALKER, J. A. 1984. Volcanic rocks from the Nejapa and Granada cinder cone alignments, Nicaragua, Central America. *J. Petrology* 25:299–342.

WALKER, K. R. 1957. The geology of the St Helens–Scamander area, Tasmania. *Pap. Proc. R. Soc. Tasm.* 91:23–39.

WINCHESTER, J. A.; FLOYD, P. A. 1976. Geochemical magma type discrimination: application to altered and metamorphosed basic igneous rocks. *Earth planet. Sci. Lett.* 28:459–469.

YODER, H. S. 1976. *Generation of basaltic magma.* National Academy of Sciences : Washington.

YOUNG, H. D. 1962. *Statistical treatment of experimental data.* McGraw-Hill : New York.

APPENDIX A
Petrology of the Triassic basalt

CONTENTS

LIST OF PLATES

LIST OF FIGURES

LIST OF TABLES

Table A1
SPECIMEN LOCALITIES OF TRIASSIC BASALTS

Field no.	Analysis no.	Unit	Stratigraphic position	Coordinates
Slab Hut Creek				
M240	802966	Lower?		EQ913032
Huntsmans Creek				
M154	-	Lower	0·5 m above lower contact	EQ952021
M130	800265	Lower	Middle of unit	EQ952021
M151(P) .... [radiometrically dated]		Lower	Near upper contact (no thin section available)	EQ953031
M153	-	Lower	Boulder, bottom of waterfall	EQ952021
Webber Falls (Scales Creek)				
M134	-	Lower	Altered portion near lower contact	EQ962019
M209	-	Lower	0·4 m above lower contact	EQ962019
M211(P)	802960	Lower	6 m above lower contact	EQ962019
M212	-	Lower	3 m below upper contact	EQ962018
M205	-	-	Clast in mudstone, between units	EQ962018
M208	-	Upper	0·4 m above lower contact (tributary)	EQ963019
M213	802961	Upper	Middle of unit	EQ962018
M214	802962	Upper	Near upper contact	EQ962018
M41	-	Upper	Upper contact	EQ962017
M133	-	Upper?	Boulder	EQ962018
Catos Rivulet				
M250(P)	802967	Upper	8 m below upper contact	EQ970022
M249	-	Upper	Near upper contact	EQ970022
M251	-	Upper?	Boulder	EQ969023
M155(P)	-	Upper?	Boulder	EQ970024
North of North Sister (small gully, eastern flank of Catos Rivulet)				
M253	802968	Lower	Near lower contact	EQ979030
M254	802969	Upper	Near lower contact	EQ975030
Binns Creek				
M232(P)	802963	Lower	2 m above lower contact	EQ984029
M139(P)	-	Lower	Middle of unit	EQ984027
M233	-	Lower	5 m below upper contact	EQ983028
Scamander Road				
M200	800266	Upper?	(Very altered; no thin section available)	EQ986023
Yorkys Creek/Germantown area				
M239	802964	Upper	Lower part of unit	EQ990012
M238	802965	Upper	Middle of unit	EQ990012
M36	-	Upper	Upper part of unit	EQ988011
M220	-	-	Clast from agglomerate	EQ990016
Near the 'Rosegarland' property				
PM9	-	Upper?	Near upper contact	EP968991
PM11	-	Upper?		EP968990
PM12	-	Upper?		EP970987
PM13	-	Upper?		EP973985
PM14	-	Upper?	Float	EP973985
Near Cornwall				
PM15	-	Upper?		EP951982
West of St Patricks Head				
M87	-	Upper		FP024967

(P) denotes polished thin section prepared for electron microprobe analysis.
Specimens prefixed by M were collected by C. R. Calver, those prefixed by PM were collected by P. W. Baillie.

APPENDIX A

Petrology of the Triassic basalt

J. L. Everard

PREVIOUS WORK

During regional mapping of the St Marys quadrangle, the basalts were mapped by C. R. Calver, who demonstrated a Triassic age first from field relationships, and P. W. Baillie. The following account results from this work, some of which has been reported more briefly previously (Calver 1980, 1982; Calver and Castleden 1981; Baillie, 1980).

Basalt has been known from the vicinity of St Marys for many years, but was previously assumed to be of Tertiary age (McNeil, 1965; Threader, 1968) or apparently confused with Jurassic dolerite (Walker, 1957). In a stratigraphic section from the Triassic at Mt Nicholas, Hale (1962, p. 227) shows a thin basalt layer, but does not discuss it further or explicitly state a Triassic age or an extrusive origin.

AGE

Sample M151, from the lower basalt unit at Huntsmans Creek, was selected and submitted, with the assistance of the Bureau of Mineral Resources, to the Australian Mineral Development Laboratories (Amdel) for radiometric dating (Report AC5195/80). The analytical data (table A2) indicate a whole rock potassium-argon age of 233 ± 5 Ma ($\pm 1\%$, analytical error only), as reported by Calver and Castleden (1981). Due to slight alteration of the sample, this should be regarded as a minimum age.

Well preserved spore assemblages with Middle Triassic (Ladinian or possibly Anisian) affinities were obtained from sedimentary rocks below the lower basalt unit and between the two units at Webber Falls (Forsyth, 1980, pers. comm.).

Table A2
RADIOMETRIC AGE OF SAMPLE M151

Analytical data

K	=	1·565% (1·885% K_2O)
		1·563% (1·883% K_2O)
	average:	1·564% (1·884% K_2O)
$^{40}Ar^*$	=	$6{\cdot}7473 \times 10^{-10}$ mol/g
$^{40}Ar^*/^{40}Ar$ total	=	0·958

Constants

K	=	*39·098 a.m.u.*
$^{40}K/K$	=	$1{\cdot}167 \times 10^{-4}$ *(atomic ratio)*
λ_β	=	$4{\cdot}963 \times 10^{-10} a^{-1}$
λ_ϵ	=	$0{\cdot}5811 \times 10^{-10} a^{-1}$

Equation

$t = (1/\lambda_\epsilon + \lambda_\beta)\ln[(\lambda_\epsilon + \lambda_\beta/\lambda_\epsilon)(^{40}Ar^*/^{40}K) + 1]$
$= 233.0$ Ma

PETROGRAPHY

Approximately 35 specimens of the Triassic basalts were collected from all main areas of outcrop by C. R. Calver and P. W. Baillie (table A1).

In hand specimen, the basalts are mostly rather featureless, fine-grained dark grey rocks in which small, often iddingsitised phenocrysts of olivine and tiny plagioclase laths may be visible. Large plagioclase crystals, here termed megacrysts, are common in the lower unit but absent in the upper unit. The plagioclase megacrysts are commonly rounded or embayed, equant or shortly elongate anhedra, subhedra or euhedra, up to 30 mm but more commonly a few millimetres across. The basalts become finer grained, more altered and more amygdaloidal towards their contacts. There are only minor petrographic differences between the two units. The lower unit contains about 0.9 vol.% plagioclase megacrysts and only 0·1% olivine phenocrysts (measured abundance in thin sections), whilst the olivine phenocryst abundance in the upper unit, although variable, is typically about 5–10%. Titanaugite is more strongly coloured (pinkish-brown) and more titaniferous in the lower unit. Textures range from ophitic to intergranular but there is no consistent textural distinction between units, or clear lateral or vertical textural trend within either unit. Specimens from only one locality (Huntsmans Creek) contain probable intersertal devitrified glass. Flow texture ranges from well developed to absent, but this is probably partly a function of section orientation.

In the following descriptions, a typical, relatively fresh representative specimen from each flow is described in detail.

Comparative notes are given on the other specimens.

LOWER BASALT UNIT

M232 (analysis 802963) – 2 m above base of lower unit, Binns Creek [EQ984029]

The thin section is of a moderately altered fine-grained basalt, consisting of rare altered olivine phenocrysts and scattered plagioclase megacrysts, in an intergranular to subophitic groundmass of plagioclase, alkali feldspar, titanaugite, opaques, accessory acicular apatite, and abundant orange-brown to green alteration products, probably partly derived from groundmass olivine.

Olivine phenocrysts, which are altered to dirty-green chlorite, range from euhedral rhombs (1·5 mm) to smaller equant subhedra (500 μm).

Plagioclase megacrysts (mostly 2–4 mm) include a large, rounded rhomb, but most are embayed, equant to irregular subhedra. No zoning is detectable in thin section, but electron microprobe analyses (discussed below) suggest slight reverse zoning, from sodic labradorite to more calcic labradorite at the extreme rim.

In the groundmass, laths (100–300 μm) of sodic labradorite (table A9c) tend to be aligned to produce a moderately developed flow lamination, somewhat inconsistent in direction. Untwinned interstitial feldspar is probably sanidine. Angular titanaugite granules (>100 μm) are deep pink to almost crimson, consistent with a very high (up to 4·4%) TiO_2 content (table A9f). Pleochroism is weak to moderate. Opaques range from equant, irregularly jagged grains (<100 μm) to more elongate grains, and include both rhombohedral (ilmenite series) and spinel (titanomagnetite series) phases. Alteration products range from microcrystalline pale green chlorite to more oxidised iddingsitic material. Finely fibrous length-slow material occasionally rimming titanaugite may be secondary amphibole.

M139 – middle of lower unit, Binns Creek [EQ984027]

The section shows part of a large, slightly embayed plagioclase glomerocryst more than 20 mm long, consisting of two slightly intergrown megacrysts. The altered groundmass consists mainly of crudely aligned plagioclase laths (100-400 μm) and intergranular, orange-brown completely iddingsitised mafic granules (<200 μm), together with opaques and secondary chlorite.

M233 – 5 m below top of lower unit, Binns Creek [EQ983028]

This strongly altered sample contains no phenocrysts, and possible plagioclase megacrysts have not survived section preparation. The rock consists of vaguely aligned plagioclase laths, intergranular completely altered mafic granules, turbid interstitial alkali feldspar, opaques, and fuzzy pale green-brown chloritic alteration.

M253 (analysis 802968) – gully north of North Sister [EQ979030]

This sample is very similar to M232. A single, completely altered olivine phenocryst (1·5 mm) and a few, small (<1 mm) anhedral to lath-like plagioclase megacrysts lie in an altered intergranular to subophitic, flow-laminated groundmass, consisting mainly of feldspar, deep pink titanaugite, opaques and secondary chlorite.

M134 – altered zone at base of lower unit, Webber Falls [EQ962019] This extremely altered sample is recognisable only from the ghost texture, and consists of chlorite, carbonate and low-birefringence clay minerals. A possible euhedral pseudomorph of olivine consists of pale green chlorite and carbonate, and laths of former plagioclase define a weak flow lamination. Amygdales filled with chlorite and carbonate are present.

M209 – 0·4 m above base of lower unit, Webber Falls [EQ962019]

No original mafic minerals remain in this strongly altered fine-grained basalt, which consists of strongly aligned plagioclase laths (50–150 μm), equant jagged opaques (20–60 μm) and abundant pale green chlorite and formless secondary carbonate. No olivine or former olivine phenocrysts are present, but a glomerocryst is formed by two slightly interlocking, embayed elongate plagioclase megacrysts (3 mm x 1-1·5 mm). Veinlets and a round (2 mm) amygdale of carbonate are present.

M211 (analysis 802960) – 6 m above base of lower unit, Webber Falls [EQ962019]

This nearly fresh, fine-grained ophitic basalt consists of aligned plagioclase laths (400–150 μm x 15–40 μm), interstitial alkali feldspar, deep pink titanaugite grains (200–500 μm) deeply dissected by plagioclase equant opaques (50–200 μm), acicular apatite (typically 100 μm x 5 m) and patchy dirty green chloritic alteration. No phenocrysts or megacrysts are intersected by the section. A large (4 mm) round amygdale of carbonate and the adjacent groundmass are stained deep yellow-green.

M212 – 3 m below top of lower unit, Webber Falls [EQ962018]

This strongly altered, flow-laminated basalt is similar to but somewhat coarser than M209. A single olivine pseudomorph (1 mm) is replaced by carbonate. Several anhedral to subhedral plagioclase megacrysts are present.

M154 – 0·5 m above base of lower unit, Huntsmans Creek [EQ952021]

This specimen (plate A1) is another strongly altered, flow-laminated basalt with several plagioclase megacrysts (2–4 mm), very similar to M209 and M212. One irregular, deeply embayed megacryst consists of a clear homogeneous core, surrounded by a broad very mottled zone with numerous inclusions of skeletal opaques, fine secondary carbonate, and pale green chlorite and/or devitrified glass (similar minerals to the altered groundmass). This is partly mantled by a narrow discontinuous rim of clear feldspar. This texture is interpreted as the result of partial internal melting of the megacryst and exchange with the surrounding melt, followed by quenching to glass or cryptocrystalline material and subsequent devitrification or alteration.

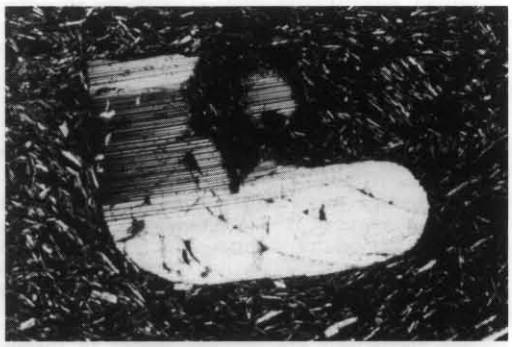

Plate A1. *Sample M154, lower unit of Triassic basalts, showing a deeply embayed plagioclase megacryst. The strongly altered groundmass consists of aligned plagioclase plagioclase laths, opaque minerals, chlorite and carbonate. Crossed nicols, field of view 4·3 × 2·9 mm.*

M130 (analysis 800265) – middle of lower unit, Huntsmans Creek [EQ952021]

This sample and M153 differ from all other fresh samples in containing very little pyroxene.

The thin section shows a fine-grained, only slightly altered basalt very rich in plagioclase laths (100–300 μm x 10–40 μm) which are vaguely aligned to define a weak flow lamination. Olivine (colourless, biaxial negative) is a subordinate consistent, ranging from intergranular equant granules (>40 μm) to euhedral

and subhedral microphenocrysts and phenocrysts (< 2 mm), frequently riddled with inclusions of plagioclase laths (ophitic texture). Olivine displays slight to partial alteration to fine dirty green chlorite. Opaques are abundant, both as equant, jagged irregular grains (20–100 μm) and as more elongate to acicular material. Some interstitial, anhedral, untwinned, zoned feldspar is probably sanidine. In contrast to most other samples, apatite is rare.

In addition, minor cryptocrystalline fuzzy grey material, probably altered devitrified glass, is present in interstices between plagioclase laths. Tiny, barely birefringent pinkish forms within this material are probably incipient titanaugite.

Two rounded to embayed, ovate to elongate anhedral megacrysts (2·5, 3·5 mm) of plagioclase are present in the section. In addition to the usual albite twinning, one also shows ?pericline twinning.

M153 – boulder, bottom of falls, Huntsmans Creek [EQ952021]

This basalt is similar to, but more altered than M130. Olivine granules and microphenocrysts are commonly partly or wholly altered to iddingsite and/or chlorite. Aligned plagioclase laths define a good flow lamination. Several plagioclase megacrysts are present.

M240 (analysis 802966) – Slab Hut Creek [EQ013032]

This moderately altered basalt consists of very sparse, completely iddingsitised olivine phenocrysts (< 1 mm) in a very feldspar-rich, intergranular groundmass which lacks any flow lamination. This consists of plagioclase laths (100–300 μm), interstitial zoned alkali feldspar, small intergranular pinkish brown titanaugite granules (< 50 μm), abundant equant (< 50 μm) to less commonly acicular opaques, and relatively abundant fine acicular apatite. Fine, isotopic dirty-green chlorite and patches of carbonate are alteration products. No plagioclase megacrysts are present.

UPPER BASALT UNIT

M250 (analysis 802967) – 8 m below upper contact, Catos Rivulet [EQ970022]

In thin section (plate A2) this nearly fresh basalt consists of scattered olivine phenocrysts, comprising only a few per cent of the rock, in a nearly unaltered intergranular groundmass of plagioclase, alkali feldspar, titanaugite and olivine. Opaques and apatite are abundant accessory minerals.

Olivine phenocrysts are typically equant to slightly elongate subhedra and euhedra, 200 μm–1·5 mm long, occurring either isolated or in small glomerocrysts of a few crystals. A few phenocrysts are slightly zoned. Although crystal outlines are often rounded and partly obscured by alteration or abutting phenocrysts, none show any clear evidence of resorptional embayment in this or other specimens. The mineral is colourless and biaxial negative. Alteration is limited to incipient development of iddingsite around rims and internal fractures. In contrast, groundmass olivine occurs typically as colourless anhedral granules less than 100 μm across.

Titanaugite granules, mostly 50–200 μm across, are equant to moderately elongate subhedra and anhedra. Their characteristic pale pinkish-brown colour readily distinguishes them from olivine. Pleochroism is barely detectable.

Plagioclase (sodic labradorite) occurs as randomly oriented subhedral oblongs and splinters 50–200 μm long. Untwinned, strongly zoned, turbid, alkali feldspar occurs as interstitial anhedra.

Opaques are mostly equant, irregularly polygonal grains 50-100 μm across but both finer blebs and narrow, jaggedly elongate to almost acicular opaques are also present.

Apatite is abundant but inconspicuous throughout the rock as colourless needles with high relief, commonly several hundred micrometres long but only 5–10 μm across. However, rare nearly isotropic basal sections are present (one 60 μm across).

Alteration is minor. Scattered, formless patches of isotropic green-brown secondary chlorite are present, and a slight cloudiness has developed in much of the feldspar.

M155 – Catos Rivulet [EQ970024]

M251 – Catos Rivulet [EQ969023]

These samples, from loose boulders down slope from M250, are indistinguishable from it, except for a greater cloudiness of feldspar particularly in M155. Neither sample has any apparent flow lamination in thin section.

M249 – near upper contact, Catos Rivulet [EQ970022]

In this rather altered sample, the groundmass is much coarser and richer in titanaugite than in M250, and the texture is subophitic rather than intergranular, with plagioclase laths (< 400 μm) partly enclosed by incipiently altered titanaugite (< 1 mm). Opaques are particularly abundant and also rather coarse (mostly 50–200 μm). Olivine phenocrysts and glomerocrysts, and possible groundmass olivine, are completely altered to reddish-brown iddingsite and/or green-brown chlorite. Again, no apparent flow lamination is present.

M208 – 0·4 m above base of upper unit, tributary of Scales Creek near Webber Falls [EQ963019].

This very altered sample contains scattered subhedral to euhedral olivine pseudomorphs (500 μm–1·5 mm) now replaced by carbonate and sometimes also chlorite, in a groundmass of plagioclase laths, minor relict intergranular pyroxene, formless carbonate and green

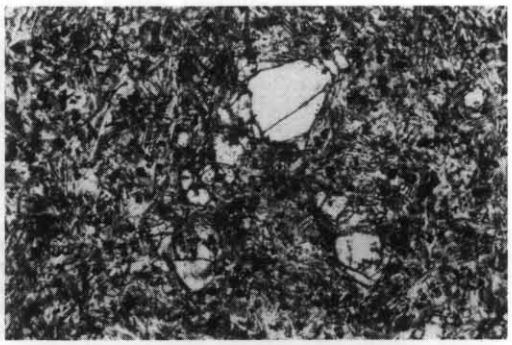

Plate A2. *Sample M250, Catos Rivulet. Upper unit of Triassic basalts, showing several subhedral phenocrysts in an intergranular groundmass of plagioclase laths, titanaugite granules, opaque minerals and interstitial alkali feldspar. Plane polarised light, fields of view 4·3 x 2·9 mm.*

nearly isotropic chlorite. Opaques and acicular apatite are accessories. Plagioclase laths are aligned to define a flow lamination (trachytic texture).

M213 (analysis 802961) – middle of upper unit, Webber Falls [EQ962018]

This sample is more altered than M250, but otherwise very similar. Rather abundant, completely iddingsitised phenocrysts of olivine (≤1·5 mm) lie in an intergranular groundmass containing fresh pinkish-brown titanaugite. Abundant pale green secondary chlorite may be at least partly derived from former groundmass olivine. There is no flow lamination.

M214 (analysis 802962) – near top of upper unit, Webber Falls [EQ962018]

Apart from coarser titanaugite (≤1 mm) and a generally subophitic rather than intergranular texture, this sample is very simple to M213. The presence of interstitial sanidine (apparently uniaxial, negative) was confirmed in this section.

M41 – top of Webber Falls [EQ962017]

Probably originally similar to M214, this sample is very altered and no igneous mafic minerals remain. Scattered, oblong to polygonal phenocrysts of former olivine (1–1·5 mm) have been altered to fine-grained, platy, colourless serpentine, which in turn has been largely replaced by carbonate. The groundmass consists of randomly oriented plagioclase laths (150–400 μm) interstitial alkali feldspar, opaques (50–100 μm) and acicular apatite, with abundant fine dull green secondary chlorite, formless carbonate and limonitic alteration. The original texture was probably subophitic. Several amygdales of carbonate and one large ovate amygdale (15 mm) of interlocking equant quartz anhedra are present.

M133 – loose boulder, Webber Falls [EQ962018]

This moderately altered subophitic basalt is similar to M214, but slightly finer and more altered.

M254 (analysis 802969) – gully north of North Sister [EQ975030]

Abundant, completely iddingsitised and/or chloritised polygonal euhedra and subhedra of olivine (≤1·5 mm) lie in a somewhat altered ophitic groundmass. Plagioclase laths (100–200 μm) are randomly oriented where they are intergrown with the rather large, irregular titanaugite grains (≤1 mm), but elsewhere are aligned to define a flow lamination. Turbid alkali feldspar, opaques, acicular apatite and traces of zircon, together with abundant secondary chlorite and iddingsite, are also present in the groundmass.

M239 (analysis 802965) – lower part of upper flow, Yorkys Creek [EQ990012]

This sample is very similar to M250 but slightly more altered. Abundant, equant olivine phenocrysts (typically 250 μm–500 μm) are only incipiently to partially altered along fractures and margins. The relatively fine, predominantly intergranular groundmass contains partly chloritised pinkish titanaugite. There is no flow lamination.

M238 (analysis 802964) – middle of upper unit, Yorkys Creek [EQ990012]

This sample is coarser than M239 from the same locality, and texturally is subophitic rather than intergranular. Olivine phenocrysts (≤1·5 mm) are completely altered, but the groundmass is relatively fresh. Veinlets and an amygdale of carbonate are present.

M36 – near top of upper unit, Yorkys Creek [EQ988011] Abundant, completely iddingsitised or chloritised, equant, crudely polygonal olivine phenocrysts (≤1·5 mm) lie in an intergranular groundmass of aligned feldspar laths (100–300 μm), titanaugite granules (≤40 μm), interstitial alkali feldspar, opaques and apatite, together with abundant secondary chlorite and some carbonate.

PM12 – near Rosegarland [EQ970987] *PM14* – float, near Rosegarland [EP973985] Numerous, completely iddingsitised, equant to shortly elongate phenocrysts and glomerocrysts of olivine (≤2 mm) lie in a subophitic, moderately altered groundmass of randomly oriented plagioclase (100–500 μm), zoned interstitial alkali feldspar, titanaugite granules (100–500 μm), equant and acicular opaques and fine acicular apatite. Patches of secondary chlorite are abundant and may be derived largely from groundmass olivine. In PM14 a carbonate amygdale is present.

The sample is very similar to many upper unit samples (*e.g.* M214, M254, M239) from north of the Nicholas Range, and is correlated with them.

PM13 – near Rosegarland [EP973985] No original mafic minerals remain in this altered basalt. Phenocrysts and glomerocrysts of former olivine (≤2 mm), lie in an originally intergranular to subophitic groundmass of randomly oriented plagioclase laths (100–300 μm), interstitial alkali feldspar, opaques (20–40 μm), acicular apatite, and secondary iddingsite and carbonate.

PM9 – near upper contact, near Rosegarland [EP968991] *PM11* – near Rosegarland [EP968990] Rare small phenocrysts (100–200 μm) are replaced by carbonate and lie in a fine altered groundmass of plagioclase laths (50–200 μm), aligned to define a flow lamination, alkali feldspar, opaques, apatite, and abundant secondary chlorite and carbonate.

PM15 – near Cornwall In this altered basalt, olivine phenocrysts are completely replaced by carbonate. The groundmass consists of randomly oriented plagioclase laths (100–300 μm), interstitial alkali feldspar, opaques, apatite and abundant olive-green secondary chlorite and fine carbonate.

M87–west flank of St Patricks Head [FP024967] Abundant completely iddingsitised, irregularly polygonal phenocrysts (1–1·5 mm) lie in a moderately altered intergranular to subophitic groundmass of randomly oriented plagioclase laths (150–200 μm), equant to elongate pinkish-purple titanaugite granules (≤200 μm), alkali feldspar, opaques and apatite, together with secondary iddingsite (after groundmass olivine), chlorite and carbonate. The sample is correlated on petrographic grounds with the upper basalt unit.

MISCELLANEOUS SAMPLES

M205 – Clast in mudstone between upper and lower units, Webber Falls [EQ963028] This extremely altered and oxidised mixture of clay minerals and limonitic material contains probably ghost outlines of plagioclase laths and is probably of basaltic origin. This suggests that the lower basalt unit is extrusive at this locality.

M220 – Clast agglomerate, near Yorkys Creek [EQ990016] This extremely altered basalt clast also now consists of clay minerals and limonitic material, but the ghost basaltic texture is quite clear. Numerous

Table A3
CHEMICAL ANALYSES OF TRIASSIC BASALTS (mass%)

	Lower basalt unit						Upper basalt unit							
Field no.	M253	M232	M240	M130	M211	Average	M254	M238	M239	M214	M250	M213	Average	M200 (altered)
Analysis no.	802968 (anomalous)	802963	802966	800265	802960		802969	802964	802965	802962	892967	802961		800266
SiO_2	47·32	45·12	45·20	45·7	45·24	45·31	47·30	46·27	46·77	46·07	47·36	46·07	46·64	43·9
TiO_2	2·43	3·34	3·65	3·6	3·63	3·56	2·51	2·47	2·45	2·48	2·39	2·38	2·45	2·6
Al_2O_3	15·55	16·27	16·18	15·4	16·32	16·04	15·63	14·77	14·73	14·86	14·57	14·57	14·86	16·0
Fe_2O_3	6·37	5·02	4·38	3·3	5·94	4·66	4·91	4·24	3·81	5·11	3·58	5·12	4·46	2·7
FeO	6·12	7·41	7·87	8·7	6·42	7·60	6·42	7·18	7·26	6·12	7·64	5·97	6·77	6·7
MnO	0·18	0·15	0·17	0·19	0·22	0·18	0·16	0·17	0·17	0·16	0·15	0·22	0·17	0·26
MgO	3·09	5·01	4·98	5·1	5·51	5·15	5·15	5·90	5·81	5·96	6·37	6·76	5·99	1·6
CaO	6·37	7·50	7·66	8·1	7·72	7·75	6·85	7·09	7·19	6·86	7·12	7·27	7·06	10·3
Na_2O	3·17	2·40	3·09	2·9	2·42	2·70	3·32	2·89	3·57	2·40	4·10	2·65	3·16	3·3
K_2O	2·60	2·03	1·99	2·0	1·75	1·94	2·32	2·37	2·33	2·35	2·12	2·07	2·26	2·5
P_2O_5	1·80	0·75	0·74	0·74	0·75	0·75	1·60	1·56	1·51	1·58	1·34	1·36	1·49	1·9
H_2O^+	2·43	3·15	2·67	2·3	2·84	2·74	2·74	2·74	2·60	3·39	2·59	3·18	2·87	1·8
H_2O^-	1·15	1·18	0·70	1·1	1·24	1·06	1·08	1·24	0·96	1·81	0·55	1·40	1·17	1·0
CO_2	0·50	0·23	0·18	0·03	0·35	0·20	0·18	0·36	0·18	0·20	0·19	0·22	0·22	5·1
SO_3	n.d.	n.d.	n.d.	0·04	n.d.	n.d.	n.d.	n.d.	n.d.	n.d.	n.d.	n.d.	n.d.	0·02
Traces as oxides	0·33	0·52	0·40	0·37	0·28	0·38	0·44	0·37	0·32	0·32	0·32	0·31	0·35	0·30
Total	99·41	100·08	99·86	99·60	100·63	100·02	100·61	99·62	99·66	99·67	100·39	99·55	99·92	100·00
Trace elements *(ppm)*														
Li	n.d.	n.d.	n.d.	10	n.d.	-	n.d.	n.d.	n.d.	n.d.	n.d.	n.d.	-	10
Sc	19	20	22	14	15	18	13	17	18	13	13	13	15	11
V	90	234	234	175	216	215	117	118	119	115	126	119	119	53
Cr	48	20	11	628*	21	(17)	148	155	169	141	197	186	166	53
Co	24	38	38	57	32	41	25	30	32	21	31	32	29	39
Ni	37	29	32	38	34	33	78	79	88	85	114	115	93	30
Cu	36	39	33	37	33	36	34	45	34	37	38	35	37	26
Zn	126	104	108	137	107	114	114	116	108	108	111	109	111	156
Ga	24	21	23	22	21	22	20	22	19	22	20	22	21	23
Rb	42	39	34	29	30	33	43	37	39	40	39	38	39	44
Sr	860	1037	947	901	849	934	738	815	688	736	710	725	735	822
Y	32	18	22	19	22	20	28	27	28	26	25	26	27	31
Zr	337	262	261	272	257	263	309	296	292	299	278	283	293	394
Nb	77	56	58	68	57	60	67	67	67	64	62	60	65	85
Ba	1060	2600	1560	591	681	1358	2040	1260	941	961	931	771	1151	723
Pb	20	13	9	11	12	11	20	16	19	16	14	10	16	15
Th	<4	<4	<4	<4	<4	<4	<4	<4	<4	<4	5	<4	-	<4
U	<5	<5	<5	<5	<5	<5	<5	<5	<5	<5	<5	<5	-	<5

n.d. – not determined; * – probable laboratory contamination

Table A4 CHEMICAL PARAMETERS

Field no.	Lower Basalt Unit						Upper Basalt Unit					
	M253	M232	M240*	M130	M211	Average	M254	M238	M239	M214	M250*	M213	Average
Analysis	802968	802963	802966	800265	802960		802969	802964	802965	802962	892967	802961	
100 Mg/Mg + Fe^{II}(a)	47·4	54·7	53·0	51·1	60·5	54·8	58·8	59·4	58·8	63·5	59·8	67·0	61·2
(b)	34·5	45·9	46·0	46·9	48·7	46·9	49·0	52·1	52·4	52·9	54·3	56·4	52·9
(c)	31·7	42·8	42·9	43·8	45·5	43·8	45·9	48·9	49·2	49·8	51·1	53·3	49·8
Al_2O_3/CaO	2·44	2·17	2·11	1·90	2·11	2·07	2·28	2·08	2·05	2·17	2·05	2·00	2·10
K_2O/Na_2O	0·820	0·846	0·644	0·690	0·723	0·726	0·699	0·820	0·653	0·979	0·517	0·781	0·715
K/Rb	514	432	486	573	484	493	448	532	496	488	451	452	481
K/Zr	64·0	64·3	63·3	61·0	56·5	61·3	62·3	66·5	66·2	65·2	63·3	60·7	64·0
Rb/Sr	0·049	0·038	0·036	0·032	0·035	0·035	0·058	0·045	0·057	0·054	0·055	0·052	0·053
Ti/Zr	43·2	76·4	83·8	79·3	84·7	81·0	48·7	50·0	50·3	49·7	51·5	50·4	50·1
Nb/Y	2·41	3·11	2·64	3·58	2·59	2·98	2·39	2·48	2·39	2·46	2·48	2·31	2·41
Zr/Y	10·5	14·6	11·9	14·3	11·7	13·1	11·0	11·0	10·4	11·5	11·1	10·9	10·9
Zr/P_2O_5	0·019	0·035	0·035	0·037	0·034	0·035	0·019	0·019	0·019	0·019	0·021	0·021	0·020

*—least altered samples (see text)
(a)—as analysed, atomic proportions; (b)—assuming $Fe_2O_3/FeO = 0{\cdot}15$ (Brooks, 1976)—atomic proportions; (c)—all iron calculated as Fe^{II} (minimum possible value)—atomic proportions.
All other ratios calculated on a mass basis.

phenocrysts (≤ 1 mm) of iddingsite lie in a groundmass showing outlines of randomly oriented laths (40–80 μm) of former plagioclase.

GEOCHEMISTRY

CHEMICAL ANALYSES

Major and trace element analyses of eleven relatively fresh specimens of the Triassic basalts are presented in order of increasing 100 Mg/Mg + Fe^{II} (table A3). Ten of these were originally reported by Calver (1982), apart from the determination of Fe_2O_3/FeO, but were only discussed very briefly. Selected chemical parameters are presented in Table A4. In calculating Mg numbers (atomic 100 Mg/Mg + Fe^{II}) and CIPW norms (table A5), the oxidation ratio of iron was recalculated assuming $Fe_2O_3/FeO = 0{\cdot}15$ as recommended by Brooks (1976). Electron probe microanalyses of iron-titanium oxides (tables A9g, h, fig. A13) suggest that this ratio is probably an overestimate. Rittmann norms (table A6) were calculated by computer programme. Another analysis (M200/800266) is clearly of a very altered rock and is not considered further.

All analyses show some evidence of alteration and oxidation, and most fall just outside Manson's (1967) 'basalt screen' on account of high loss-on-ignition (>4%), and, in one case, high Fe_2O_3 (>6%). A plot of Na_2O against loss-on-ignition (fig. A1) shows that Na_2O is progressively depleted during alteration, probably due to the breakdown of feldspars to cryptocrystalline epidote and/or sericite. Figure A1 also suggests that Na_2O was originally higher in the upper unit than in the lower unit. Loss of Na_2O increases the apparent silica-saturation state of the rock, causing *ne* to disappear and *hy* to appear in the CIPW norms (table A5). Attention is therefore focussed on the least altered analysed samples from each unit, M240/802966 and M250/802967.

As discussed below, alteration also has slightly affected other elements, the effect being masked by other causes of variation.

Chemically, these rocks are alkali basalts, rather than tholeiites. They plot in the alkalic field of the alkali-silica diagram (fig. A2) of Macdonald and Katsura (1964) and, when fresh, are slightly *ne* normative (table A5). Other distinctively alkalic features (*e.g.* Floyd and Winchester, 1975; Winchester and Floyd, 1976) are high TiO_2 (>1·8%) and P_2O_5 (>0·25%), high Nb/Y (>1) and low Zr / P_2O_5 (<0·06) (fig. A3). Petrographically the presence of olivine in the groundmass, as well as in phenocrysts, and pinkish-purple titanaugite is also characteristic.

PETROLOGICAL NOMENCLATURE

There are two basic approaches to the classification of igneous rocks: mineralogical and chemical.

Table A5
CIPW NORMS (mass%)

	Lower Basalt Unit										
Field no.	M253	M232	M240*	M130	M211	M254	M238	M239	M214	M250*	M213
Analysis	802968	802963	802966	800265	802960	802969	802964	802965	802962	892967	802961
or	16·21	12·62	12·26	12·37	10·82	14·26	14·75	14·41	14·81	12·95	12·98
ab	28·27	21·35	26·19	25·66	21·39	29·18	25·74	30·54	21·62	29·87	23·76
an	21·56	29·28	25·59	24·23	29·87	21·88	21·53	18·16	24·41	15·69	23·13
ne	-	-	0·57	-	-	-	-	0·55	-	3·22	-
c	0·07	-	-	-	-	-	-	-	-	-	-
di	-	4·83	8·08	10·94	4·58	2·83	4·48	7·68	1·15	10·09	5·05
hy	19·09	11·98	-	1·46	13·89	9·08	10·30	-	22·11	-	14·02
ol	2·98	8·96	15·86	13·94	8·00	11·65	12·07	17·82	4·62	17·99	10·62
mt	2·39	2·41	2·35	2·34	2·35	2·16	2·22	2·14	2·18	2·15	2·15
il	4·86	6·66	7·22	7·15	7·20	4·95	4·94	4·86	5·01	4·69	4·79
ap	4·48	1·86	1·82	1·83	1·85	3·92	3·87	3·72	3·97	3·26	3·40
z	0·07	0·05	0·05	0·05	0·05	0·06	0·06	0·06	0·06	0·05	0·06
cm	0·01	<0·01	<0·01	-	<0·01	0·03	0·03	0·04	0·03	0·04	0·04
py	-	-	-	0·03	-	-	-	-	-	-	-
Total	99·99	100·00	99·99	100·00	100·00	100·00	99·99	99·98	99·97	100·00	100·00
Fe/Fe+Mg(pyroxenes, olivine)	0·584	0·437	0·426	0·418	0·403	0·425	0·399	0·394	0·388	0·378	0·359
mol.% An (plagioclase)	41·7	56·2	47·8	47·0	56·7	41·2	43·9	35·4	51·4	33·0	47·7

* Least altered samples (see text).
Calculated assuming $Fe_2O_3/FeO = 0{\cdot}15$ (Brooks, 1976). Recalculated to 100 mass% anhydrous.
Sr and Ba distributed to *an*, Rb to *or*, Ni included with Mg, Mn included with Fe.

Table A6
RITTMANN NORMS (vol.%)

	Lower Basalt Unit					Upper Basalt Unit					
Field no.	M253	M232	M240*	M130	M211	M254	M238	M239	M214	M250*	M213
Analysis	802968	802963	802966	800265	802960	802969	802964	802965	802962	892967	802961
sanidine	23·2	14·2	14·4	14·8	11·2	18·9	19·7	20·5	18·5	17·5	16·0
plagioclase	52·1	56·2	57·9	52·8	57·9	53·6	49·3	50·4	49·2	49·1	50·5
nepheline	-	-	-	-	-	-	-	-	-	2·5	-
spinel	0·3	-	-	-	-	-	-	-	-	-	-
clinopyroxene+	-	16·8	8·9	12·3	18·1	12·5	15·4	9·0	21·7	10·7	19·3
orthopyroxene	18·1	-	-	3·2	-	-	-	-	-	-	-
olivine	0·5	5·5	11·4	8·9	5·3	6·9	7·5	12·3	2·3	13·0	6·7
magnetite	1·7	1·6	1·7	1·7	1·5	1·7	1·7	1·8	1·6	1·9	1·6
ilmenite	-	3·9	4·0	4·5	4·2	2·9	2·8	2·6	3·0	2·3	2·7
apatite	4·1	1·7	1·7	1·7	1·7	3·5	3·5	3·3	3·6	2·9	3·1
zircon, pyrite	0·1	-	-	0·1	-	-	-	-	-	-	-
Total	100·1	99·9	100·0	100·0	99·9	100·0	99·9	99·9	99·9	99·9	99·9
A	30·8	20·2	19·9	21·9	16·2	26·0	28·6	28·9	27·4	25·3	24·1
P	69·2	79·8	80·1	78·1	83·8	74·0	71·4	71·1	72·6	71·1	75·9
F	-	-	-	-	-	-	-	-	-	3·6	-
Colour index	20·6	27·9	26·1	30·6	29·2	24·1	27·5	25·7	28·7	28·0	30·4

* Least altered samples (see text).
\+ 802966, 800265, 802965 and 802967 are titanaugites; the remainder are pigeonites.
(Q):A:P:F = (quartz):alkali feldspar:plagioclase:feldspathoid, sum 100.
Colour index = sum of femic minerals (pyroxenes, olivine, magnetite, ilmenite, spinel).
Trace elements (except Zr) not included in program.

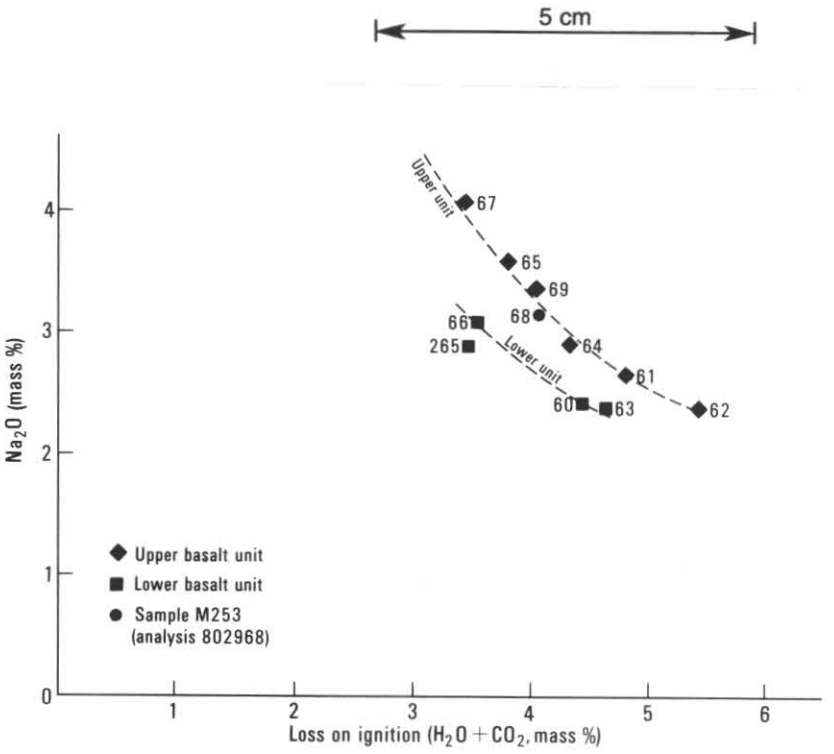

Figure A1. *Alteration and sodium depletion in Triassic basalts.*

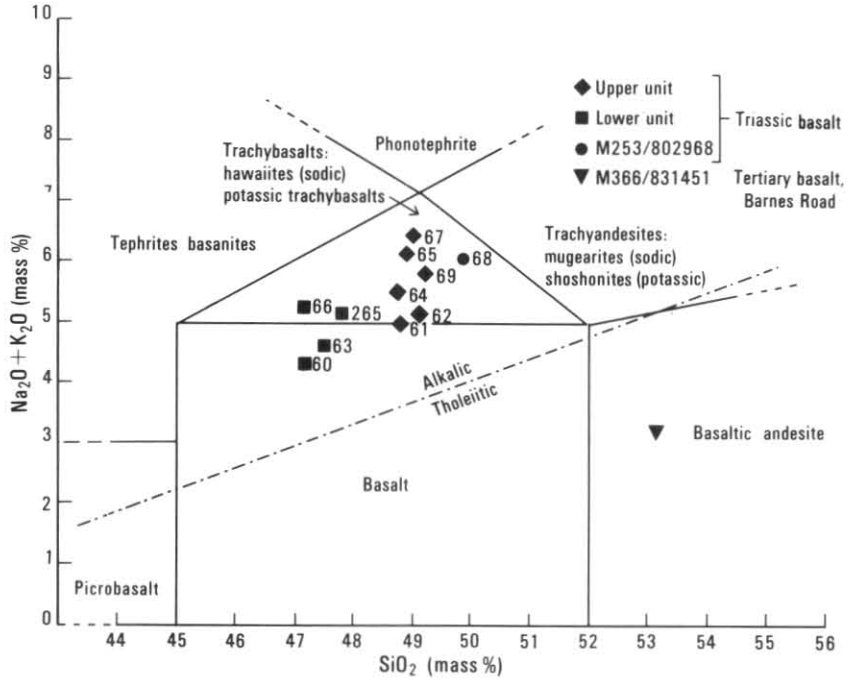

Figure A2. *Chemical classification of volcanic rocks from St Marys Quadrangle. After Le Maitre (1984). Analyses recalculated to 100% minor elements. Sodic if Na_2O–K_2O 1·5%, potassic if Na_2O–K_2O 1·5%. Boundary of tholeiitic and alkalic fields (Macdonald and Katsura, 1964) also shown.*

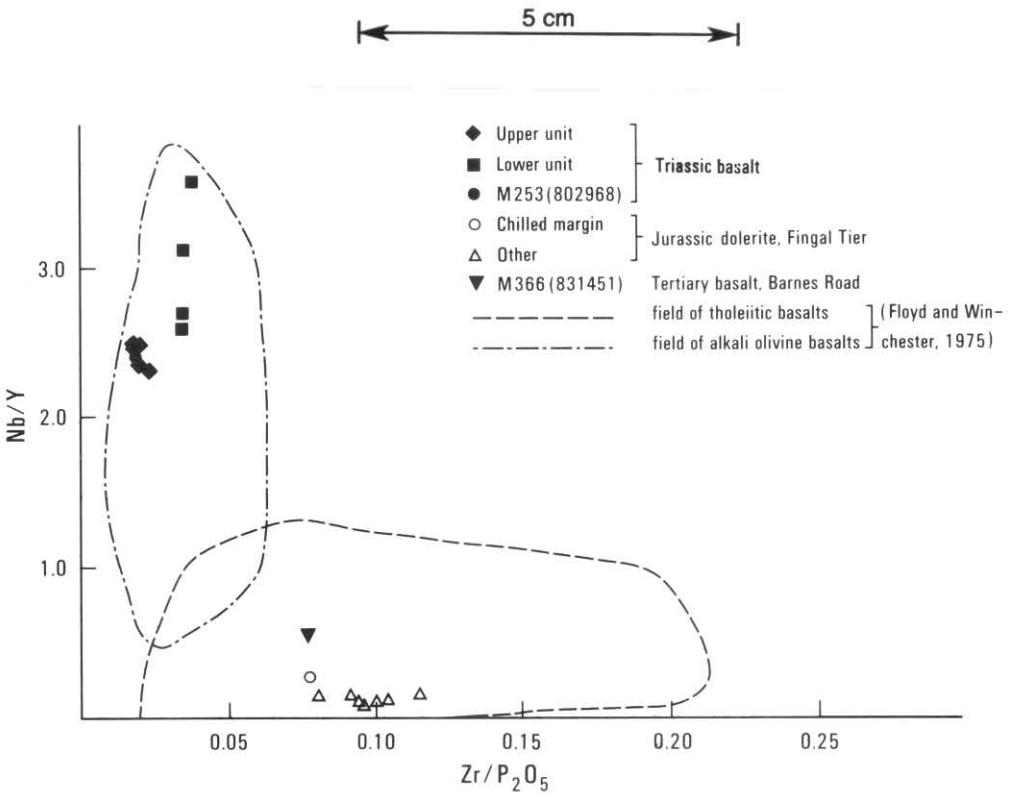

Figure A3. *Zr/P_2O_5–Nb/Y diagram for basaltic rocks from St Marys Quadrangle.*

The main drawback to the mineralogical approach, particularly for fine or glassy volcanic rocks, is the difficulty of accurately estimating mineral abundances. For these rocks we assume that the Rittmann norms (table A6) provide a good approximation to the mode. In the QAPF (quartz-alkali feldspar-plagioclase-foid) classification recommended by the I.U.G.S. Subcommission on the Systematics of Igneous Rocks (Streckeisen 1967, 1978) they are leucobasalts.

The chemical scheme of classification recommended by the I.U.G.S. (Le Maitre, 1984) is based on a total alkali/silica diagram, after recalculation of major element oxides to 100%. For these rocks this is complicated by sodium depletion caused by alteration (fig. A2). However, the least altered analyses of both upper and lower units (802967 and 802966) plot in the trachybasalt field. Probably the lower unit basalts could be termed potassic trachybasalts ($Na_2O - K_2O < 1{\cdot}5$ mass%), whilst the more sodic upper unit basalts (fig. A1, A2) are hawaiites.

The term hawaiite is often applied to moderately under-saturated alkali-olivine basalts containing normative andesine. This includes most of these analyses, except for three of more altered rocks (802963, 802960, 802962). However, the term as revived and redefined (Macdonald, 1960; Macdonald and Katsura, 1964) also implied K_2O/Na_2O 0·5. Coombs and Wilkinson (1969, p. 489) term relatively potassic alkali-basalts with Thornton-Tuttle differentiation indices ($\Sigma Q + or + ab + ne + lc$) <65, such as these, as trachyandesites (andesine or oligoclase normative) and trachybasalts (labradorite normative). However, such classifications based on normative feldspar are now not recommended.

COMPARISON WITH TASMANIAN TERTIARY BASALTS

The chief sources of chemical analyses of the alkali olivine basalts are Edwards (1941, 1950), Spry (1962), Joplin (1963), Sutherland (1969a, 1969b, 1972, 1976, 1977, 1984, 1985), Sutherland and Kershaw (1971), Gee (1971), Frey *et al* (1978), Brown and McClenaghan (1982) and Everard (1984). Only the more recent of the above include trace element data. Unlike the Triassic basalts, the Tertiary basalts also include tholeiites.

In general, the Triassic basalts lie within, although near the limit of, the compositional field of the Tasmanian Tertiary alkali olivine basalts (fig. A4–A6), and have no unequivocally distinctive chemical features, at least with respect to major elements.

When K_2O is plotted against Na_2O (fig. A4), the Triassic basalts appear to plot outside the main Tertiary trend, largely because of Na_2O

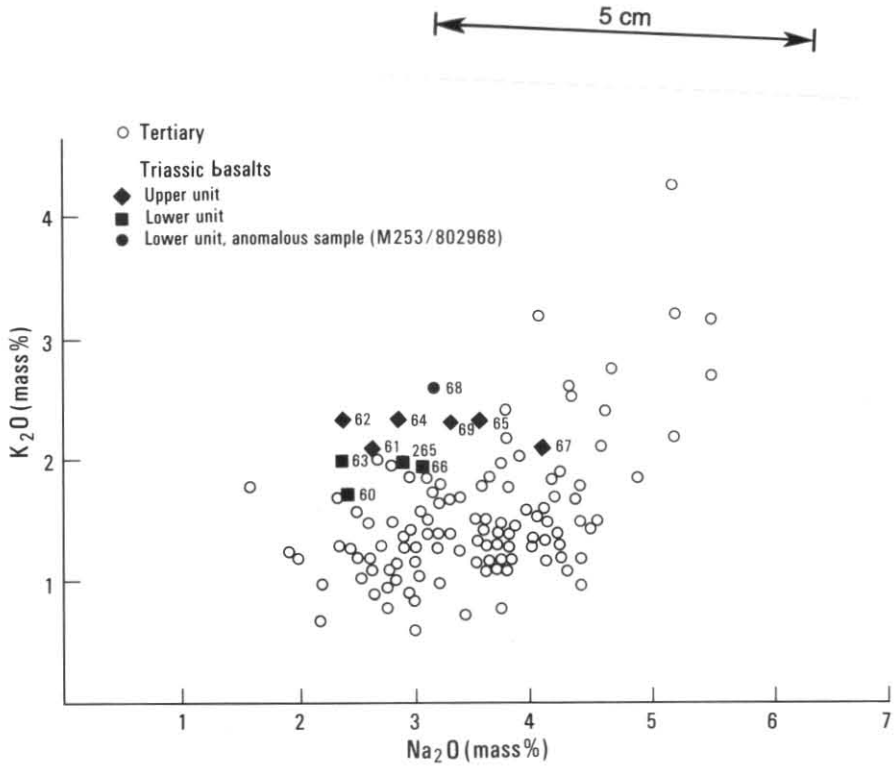

Figure A4. *Alkali content in Triassic basalts and Tasmanian Tertiary alkali basalts.*

depletion by alteration (fig. A1). The least altered samples (analyses 802966, 802967) have fairly high total alkalis ($Na_2O + K_2O$); Tertiary basalts with similar values are usually more undersaturated. The K_2O content (generally >2 mass%) is also higher than most Tertiary basalts. The relatively high total alkali content is accompanied by high Al_2O_3 (fig. A5), reflecting the abundance of feldspar, and does not indicate peralkaline affinities, as in the Tertiary basalts of Lower Sandy Bay and Droughty Point (Sutherland, 1976).

A plot of Al_2O_3/CaO against Mg number (fig. A6) emphasises the relatively differentiated nature of the Triassic basalts. Primary melts of mantle peridotite are thought to have Mg numbers of 68–72 in equilibrium with mantle olivine of Fo_{88-90} and Al_2O_3/CaO ratios near 1·2, close to that of chondrites, or somewhat higher if clinopyroxene is a residual phase (Frey *et al.* 1978, p. 468–473). Except for the very differentiated sample M253/802968, high Al_2O_3/CaO and low Mg numbers similar to the Triassic basalt are also found in some Tertiary basalts.

Total iron and MnO values are unremarkable. The TiO_2 content of the upper unit falls within range exhibited by Tertiary basalts, but only a few very under-saturated nephelinites are as titaniferous as the lower unit (*e.g.* from Scottsdale, Frey *et al.*, 1978; from Shannon Tier, Joplin 1963, p. 252). P_2O_5 is rather high, particularly in the upper unit and M253 (802968) but again is comparable to Tertiary values.

Analyses of the least altered samples of the lower and upper basalt units are recalculated to 100% major elements for comparison with four particularly similar Tertiary basalts (table A7). These are all representatives of the relatively alkaline Southern Hobart Group and its correlates (Sutherland, 1976).

When compared to the available trace element data from Tertiary basalts, the Triassic basalts appear to be more depleted in Ni and Cr, particularly in the lower unit, and to have higher but very variable Ba contents.

On the Ti–Zr–Y diagram (fig. A7) of Pearce and Cann (1973), the Triassic basalts plot in or near the 'correct' within-plate-basalt field, like the Tasmanian Tertiary basalts but in contrast to the anomalous Jurassic tholeiitic dolerite.

CHEMICAL VARIATION WITHIN UPPER UNIT

Gravitational settling of olivine

The Mg number, 100 Mg/Mg + Fe*, is the most useful measure of differentiation, decreasing as Mg-rich mafic minerals fractionate. The six upper unit analyses were statistically analysed for any correlation between major or trace element abundance and Mg number (fig. A8 graphically illustrates the data for TiO_2). Correlation coefficients (table A8) were calculated (*e.g.* Young, 1962, pp. 130-132, 164) for each element. Two elements, MgO (as might be expected) and Ni show definite positive

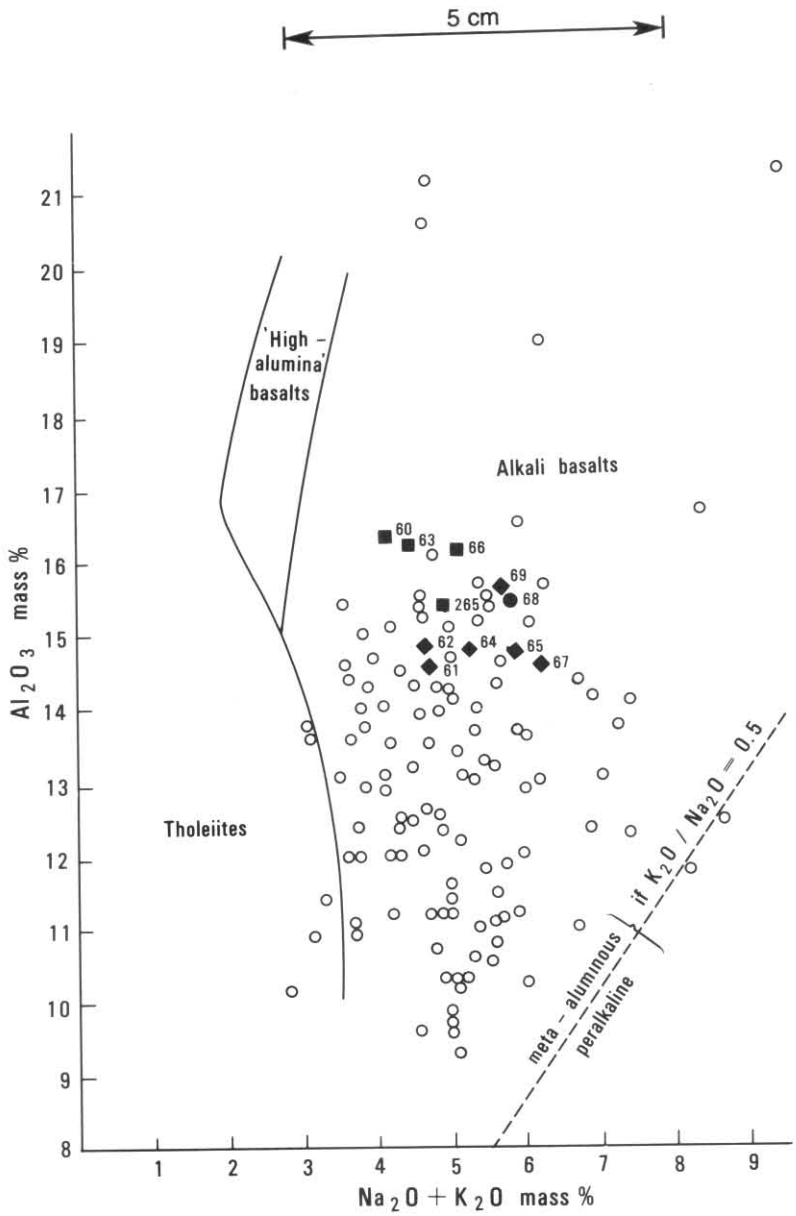

Figure A5. *Al_2O_3 versus total alkalis. Comparison of Triassic basalts and Tasmanian Tertiary alkali basalts. Basalt field boundaries after Kuno (1960). Symbols as for Figure A4.*

correlation with the Mg number, whilst many others, mostly relatively incompatible elements (TiO_2, Al_2O_3, K_2O, P_2O_5, Zr Nb, Ba and Pb) definitely decrease. These trends are consistent with fractionation of the abundant Mg-rich olivine phenocrysts. Possible positive trends for CaO and Cr suggest that this may have been accompanied by some fractionation of clinopyroxene (titanaugite).

The probable mechanism is *in situ* gravitational settling of olivine phenocrysts and possibly titanaugite granules within the hot flow or intrusion, immediately following eruption or emplacement and before cooling caused a prohibitive increase in viscosity. Rough Stoke's Law calculations indicate that this is a feasible mechanism. Settling of olivine in basaltic flows and pillows has been reported previously (Fuller, 1939; Mathews *et al.*, 1964). A less likely explanation is that the olivine phenocrysts settled in a subvolcanic magma chamber, producing lavas varying in phenocryst content, either during a single eruption or in successive eruptions. However, there is no field evidence that either basalt unit comprises more than one flow (C. R. Calver, pers. comm.).

Due to insufficient data and probably the much lower abundance of olivine phenocrysts, similar trends cannot be identified in the lower basalt unit with any certainty.

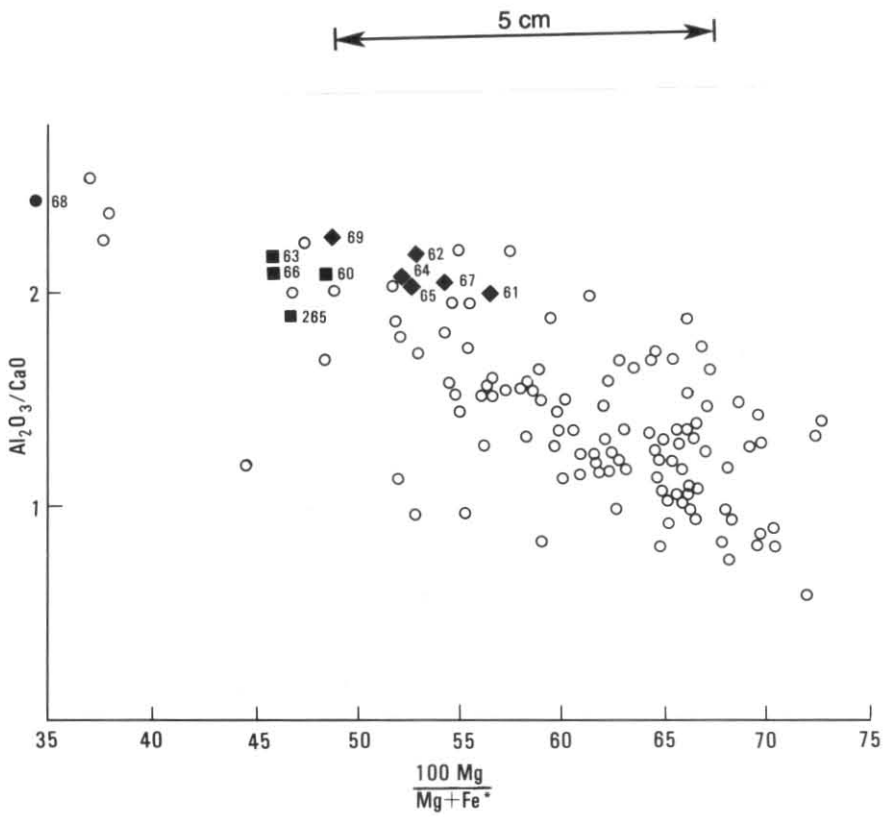

Figure A6. *Al_2O_3/CaO versus Mg number. Comparison of Triassic basalts and Tasmanian Tertiary alkali basalts. Symbols as for Figure A4.*

Table A7
COMPARISON OF TRIASSIC BASALT WITH SIMILAR TERTIARY BASALTS (MAJOR ELEMENTS NORMALISED TO 100 MASS%)

	Triassic Basalt St Marys Quadrangle		Tertiary basalt Sorell Quadrangle		Hobart Quadrangle	
Field no.	M240	M250	SC34	D22	15	15A
SiO_2	47·34	49·14	48·63	49·44	49·04	49·43
TiO_2	3·82	2·48	2·58	1·60	2·37	2·42
Al_2O_3	16·95	15·12	15·08	17·07	15·18	16·15
Σ FeO	12·37	11·27	12·74	10·19	12·79	12·09
MnO	0·18	0·16	0·15	0·16	0·19	0·18
MgO	5·22	6·60	6·05	6·84	5·57	5·43
CaO	8·02	7·39	7·51	7·73	7·54	7·18
Na_2O	3·24	4·25	4·33	4·63	4·23	4·50
K_2O	2·08	2·20	1·95	1·49	1·65	1·75
P_2O_5	0·78	1·39	0·97	0·85	1·45	0·87
Total	100·00	100·00	99·99	100·00	100·01	100·00
100 Mg/Mg + Fe*	46·0	54·3	49·0	57·7	46·8	47·6
Al_2O_3/CaO	2·11	2·05	2·01	2·21	2·01	2·25
K_2O/Na_2O	0·64	0·52	0·45	0·32	0·39	0·39

SC34—alkali olivine basalt, Wattle Hill (Everard, 1984).
D22—alkali olivine basalt, East Bay, Dunalley (Everard, 1984).
15—'mugearitic hawaiite', Southern Outlet Road, Kingston (Sutherland, 1976).
15A—'mugearitic hawaiite', Whitewater Creek, Kingston (Sutherland, 1976.).

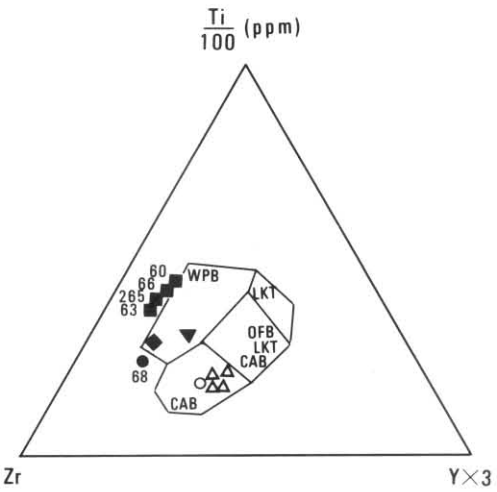

Tertiary
- ▼ Basalt, Barnes Road

Jurassic
- ○ Chilled dolerite, Fingal Tier
- △ Dolerite, Fingal Tier

Triassic
- ◆ Upper basalt unit
- ■ Lower basalt unit
- ● Lower basalt unit, anomalous sample (M253/802968)

WPB within plate basalt
CAB calc-alkali basalt
OFB ocean floor basalt
LKT low potash tholeiite
} see Ti-Zr-Sr diagram

Figure A7. *Basic lavas and intrusive rocks from St Marys Quadrangle. Ti–Zr–Y discrimination diagram for tectonic setting, after Pearce and Cann (1973). Note that Jurassic dolerites do not plot 'correctly' as within-plate basalts.*

Introduction of barium

The behaviour of Ba is puzzling. Its abundance is strongly correlated with Mg number in both upper and lower units, but, especially when compared with other incompatible elements such as Zr and Nb, which also tend to remain in the melt, its range is too large to have been produced by olivine fractionation. Probably it was introduced later, particularly into the upper parts of each unit, by some deuteric or diagenetic metasomatic process.

Anomalous barium is known from Triassic rocks elsewhere in the quadrangle. A thin vein of barium-bearing heulandite within carbonaceous mudstone was reported from Fingal Tier (DDH 55/164.22 m, EP912870) by Green (1980), who considered it to have formed from groundwater solutions following the breakdown of vitric tuff components in the Triassic sediments.

Alteration

The residuals, produced by the above procedure of plotting each element against Mg number, were plotted against loss-on-ignition (H_2O + CO_2) presumed to indicate the degree of alteration. Figure A9) graphically illustrates the data for TiO_2. Calculated correlation coefficients (table A8) show that, as well as Na_2O (fig. A1), SiO_2, Cr, V, Co and possibly Ni are depleted by alteration. On the other hand, the 'immobile' elements TiO_2, P_2O_5, Ga and Zr, thought to be unaffected by weathering (*e.g.* Pearce and Cann, 1973; Floyd and Winchester, 1975) are actually more abundant in altered rocks. As selective introduction of these elements is highly unlikely, this probably indicates a net mass loss, probably of a few per cent, during the alteration of these rocks. Removal of particularly Na_2O and SiO_2 is only partially offset by an increase in H_2O and CO_2 during alteration.

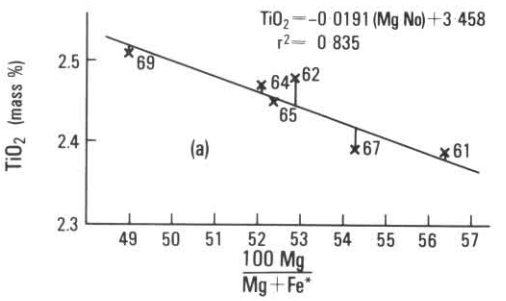

Figure A8. *TiO_2 versus Mg number, upper unit of Triassic basalts, showing increase in TiO_2 with differentiation.*

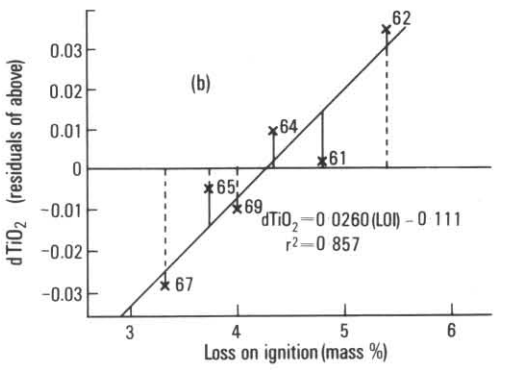

Figure A9. *Residuals from Figure A8 plot versus loss on ignition, showing apparent increase in TiO_2 content with differentiation. A similar procedure was used for other elements (see text).*

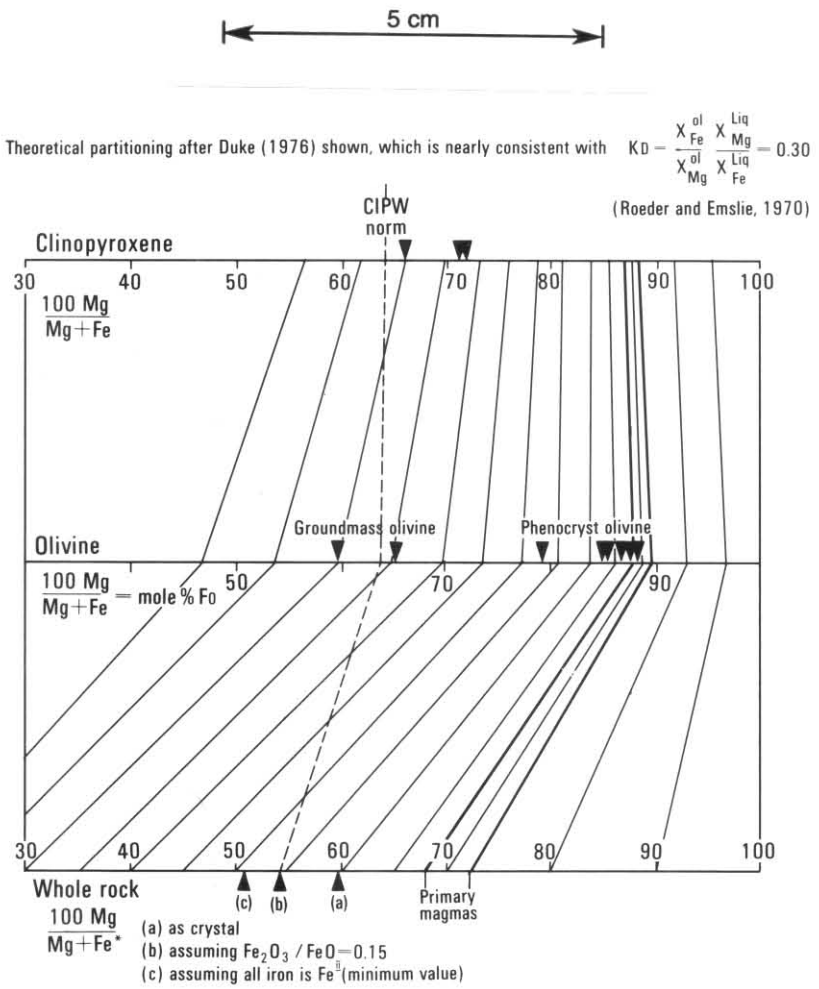

Figure A10. *Partitioning of Fe and Mg between olivine, clinopyroxene and whole rock. Sample M250 (upper unit of Triassic basalts).*

MINERAL CHEMISTRY

Electron probe microanalyses of mineral grains from six selected and polished thin sections of relatively fresh basalt were obtained at the University of Tasmania. Results, together with calculated cation formulae are presented in Tables A9a to 9h. All tabulated analyses were obtained on the 'spot' made (in which a volume of surface diameter of 0·5 μm and a beam penetration of 3–5 μm is analysed), and are recalculated to 100%.

OLIVINE (tables A9a, b; fig. A10)

Fresh phenocryst olivine is present in only four, possibly five, thin sections, mostly from the upper unit, and fresh groundmass olivine is still scarcer.

The analyses from the freshest sample, M250, shows that phenocryst olivine is much more magnesian (Fo_{79-88}) than groundmass olivine (Fo_{60-65}).

As detected optically, the olivine phenocrysts are often zoned. The more iron-rich rim composition is roughly in equilibrium with the bulk rock composition (fig. A10), whilst the more magnesian cores are close to being in equilibrium with a primary magma (*i.e.* a partial melt of mantle peridotite, unmodified by crystal fractionation) with an Mg number of 68–72 (Frey *et al.*, 1978, pp. 468–469).

Nickel was detected (2500, 3000 ppm) in the two most magnesian of the analysed phenocrysts. The strong partitioning of Ni into olivine, correlating with Mg content is well documented (*e.g.* Vogt, 1923; Simkin and Smith, 1970; Sato, 1977), but the crystal-liquid distribution coefficient depends on both temperature (data summarised by Brown, 1982, p.352) and pressure (Mysen and Kushiro, 1979) and therefore equilibrium is difficult to prove or disprove by this criterion. As the whole rock contains only 114 ppm Ni (table A3, sample M250, analysis 802967) it is likely that most nickel in the upper basalt unit is present in the olivine phenocrysts.

Table A8
STATISTICAL ANALYSIS OF CHEMICAL VARIATION IN UPPER BASALT UNIT

	(1) Linear least-squares correlation with 100 Mg/Mg+Fe* (r_M)	(2) Correlation of residuals of (1) with loss-on-ignition (r_L)
SiO_2	−0·450	*−0·859*
TiO_2	*−0·914*	*+0·926*
Al_2O_3	*−0·875*	+0·313
FeO	−0·532	−0·308
MnO	+0·609	+0·346
MgO	*+0·993*	−0·247
CaO	+0·725	−0·611
Na_2O	−0·136	*−0·954*
K_2O	*−0·767*	+0·511
P_2O_5	*−0·830*	*+0·871*
Sc	−0·190	−0·241
V	+0·401	*−0·914*
Cr	+0·704	*−0·948*
Co	+0·473	*−0·762*
Ni	*+0·861*	−0·682
Cu	+0·009	−0·060
Zn	−0·525	−0·196
Ga	+0·368	*−0·788*
Rb	−0·674	+0·072
Sr	−0·244	+0·361
Y	−0·725	−0·012
Zr	*−0·873*	*+0·936*
Nb	*−0·873*	−0·091
Ba	*−0·891*	−0·348
Pb	*−0·992*	−0·303

Confidence levels for $n = 6$ (*i.e.* probability distribution is not independent):
90% (*i.e.* P 0·10) if $|r|$ 0·729.
95% (*i.e.* P 0·05) if $|r|$ 0·811.
Correlation coefficients (r) indicating 90% confidence are italicised.
See text and Figure A9 for further explanation.

CaO and MnO, although only minor constituents, are significantly higher in iron-rich groundmass olivine than in phenocryst olivine. In a survey of minor element content in natural terrestrial olivine, Simkin and Smith (1970) found a similar strong correlation between Mn and Fe, but noted that Ca content depends instead on the crystallisation environment: olivines from hypabyssal or volcanic rocks usually contain more than 0·10 mass% Ca (0·14 mass% CaO), whilst those from plutonic rocks usually contain less. They suggested that at lower pressures more Ca is able to enter olivine, a conclusion supported by the experimental studies of Finnerty and Boyd (1978). This suggests that the olivine phenocrysts, which have plutonic CaO contents, crystallised at considerable depth, not merely in relatively shallow sub-volcanic magma chambers.

The olivine phenocrysts common in the upper basalt unit are probably xenocrysts that originally equilibrated at depth with a more primitive magma, their more iron-rich rims representing reaction with the more evolved host magma. By contrast, the anhedral iron-rich groundmass olivine crystallised at a relatively late stage from the remaining interstitial melt, after emplacement or extrusion of the basalt.

PLAGIOCLASE MEGACRYSTS (table A9e, fig. A11)

Electron probe microanalyses show that these are labradorites (An_{54-64}) and are thus similar to the groundmass plagioclase as discussed below. In thin section, the megacrysts are typically embayed and homogeneous, only three of about thirty examined showing definite but weak zoning. However, the analyses show that several are reversely zoned near their rims, which may contain about 5 mol% more *An*.

Clearly the plagioclase megacrysts, like the olivine phenocrysts, are an intra-telluric phase from depth and, in contrast to the groundmass plagioclase, were present in the magma before final ascent. The most obvious explanation is that they are xenocrysts — fragments of perhaps granitic basement, detached from the walls of a magma chamber or conduit, and partly resorbed because of thermal and/or compositional disequilibrium with the magma. However, this possibility is discounted because of their compositional similarity to the groundmass plagioclase and the absence of any composite glomerocrysts or xenoliths in the basalts. There is little doubt that the plagioclase megacrysts are cognate and probably represent the low pressure liquidus phase, reflecting the aluminous composition of the magma and the high normative feldspar content (tables A3, A4; Cox *et al.*, 1979, p. 115, 132).

Resorbtion of plagioclase may occur during the final stages of equilibrium crystallisation in the system Ab-An-Or (e.g. Deer *et. al.*, 1963, p. 72–73) but this is rejected as an explanation for the embayment of the plagioclase megacrysts, because the finer groundmass plagioclase shows no sign of resorbtion. Since the liquidus of dry or partially water-saturated magma increases with pressure, rapid decompression at more or less constant temperature during magma ascent is the likely cause of embayment. Possibly local disequilibrium resulting from resorbtion is the cause of the reverse zoning near the megacryst rims.

GROUNDMASS FELDSPAR (tables A9c, d; fig. A11)

Groundmass plagioclase is mostly sodic labradorite (An_{49-62}) in both upper and lower basalt units. One analysis (M211/2C) is a potassic andesine.

The alkali feldspar analyses indicate sanidine ($Or_{>37}$, monoclinic), consistent with the apparently uniaxial interference figure obtained in one thin section (M214). However, some

Table A9
ELECTRON PROBE MICROANALYSES OF TRIASSIC BASALTS

	(a) Phenocryst olivine											(b) Groundmass olivine	
	M250 (upper unit)						M155 (upper unit)					M250 (upper unit)	
	1	2	3	5A	7A(core)	7B(rim)	1A	1B	1C	2A	2B	5B	6E
SiO_2	40·01	40·24	40·36	39·84	39·74	38·40	40·32	39·96	39·81	38·63	40·28	36·05	35·36
Σ FeO	12·10	12·28	11·53	14·00	14·38	19·45	13·91	13·92	14·67	20·04	12·93	30·54	34·41
MnO	-	-	-	-	-	0·26	-	-	-	-	-	0·37	0·67
NiO	0·32	-	0·38	-	-	-	-	-	-	-	-	-	-
MgO	47·44	47·48	47·72	46·02	45·76	41·71	45·77	46·13	45·53	41·32	46·78	32·80	29·26
CaO	0·13	-	-	0·14	0·12	0·19	-	-	-	-	-	0·24	0·31
Total	100·00	100·00	99·99	100·00	100·00	100·01	100·00	100·01	100·01	99·99	99·99	100·00	100·01
Si	0·993	0·997	0·998	0·995	0·994	0·987	1·005	0·997	0·997	0·993	1·000	0·980	0·982
Fe^{II}	0·251	0·254	0·238	0·293	0·301	0·418	0·290	0·290	0·307	0·431	0·268	0·695	0·799
Mn	-	-	-	-	-	0·006	-	-	-	-	-	0·008	0·016
Ni	0·006	-	0·008	-	-	-	-	-	-	-	-	-	-
Mg	1·754	1·753	1·758	1·713	1·707	1·598	1·700	1·716	1·700	1·583	1·731	1·330	1·212
Ca	0·003	-	-	0·004	0·003	0·005	-	-	-	-	-	0·007	0·009
Ion total	3·007	3·004	3·002	3·005	3·005	3·014	2·995	3·003	3·004	3·007	2·999	3·020	3·018
100 Mg/ Mg + Fe^{II}*	87·5	87·3	88·1	85·4	85·0	79·0	85·4	85·5	84·7	78·6	86·6	65·4	59·8

* Ni included with Mg; Mn included with Fe.
Cations calculated on the basis of oxygen number (O) = 4, all Fe as Fe^{II}.

Table A9 (continued)

	(c) Groundmass plagioclase									
	M250 (upper unit)			M155 (upper unit)				M211 (lower unit)		
	4B	6F	7D	1A	1B	1L	1B	1C	2B	2C	3C
SiO_2	55·03	55·70	54·82	55·86	54·46	55·02	54·31	53·47	54·76	60·47	56·65
TiO_2	-	-	-	-	-	0.20	-	-	-	-	0.31
Al_2O_3	28·48	27·06	28·59	27·58	28·72	28·10	28·48	29·47	24·69	23·64	26·34
Σ FeO	0·58	1·36	0·59	0·70	0·69	0·64	0·67	0·60	4·65	1·46	1·03
MgO	-	0·47	-	-	-	-	-	-	1·65	0·54	-
CaO	11·09	9·59	10·92	10·27	11·38	10·69	11·35	12·16	9·48	5·35	9·95
Na_2O	4·50	5·21	4·71	4·89	4·33	4·36	4·66	3·99	4·21	6·56	4·76
K_2O	0·32	0·53	0·36	0·70	0·42	0·99	0·54	0·31	0·56	1·98	0·96
Cl	-	0·07	-	-	-	-	-	-	-	-	-
Total	100·00	99·99	99·99	100·00	100·00	100·00	100·01	100·00	100·00	100·00	100·00
Si	2·489	2·547	2·482	2·529	2·471	2·500	2·469	2·429	2·612	2·747	2·579
Al	1·518	1·459	1·526	1·472	1·535	1·505	1·526	1·577	1·387	1·266	1·413
Ca	0·537	0·470	0·530	0·498	0·553	0·520	0·553	0·592	0·484	0·260	0·485
Na	0·394	0·462	0·414	0·429	0·381	0·384	0·410	0·352	0·389	0·578	0·420
K	0·019	0·031	0·021	0·041	0·024	0·057	0·031	0·018	0·034	0·115	0·056
Si + Al	4·007	4·006	4·008	4·001	4·006	4·005	3·995	4·006	3·999	4·013	3·992
Ca + Na + K	0·950	0·963	0·965	0·968	0·958	0·961	0·994	0·962	0·907	0·953	0·961
An	56·5	48·8	54·9	51·4	57·8	54·1	55·6	61·6	53·4	27·3	50·5
Ab	41·4	48·0	42·9	44·3	39·7	39·9	41·3	36·6	42·9	60·6	43·7
Or	2·0	3·2	2·2	4·2	2·5	6·0	3·1	1·9	3·7	12·1	5·8

Cations calculated on the basis of oxygen number (O) = 8.
Fe, Mg, Ti, Cl assumed to be impurities.

Table A9 (continued)

	(d) Alkali feldspar				(e) Plagioclase megacrysts (from lower unit)							
	M250 (upper unit)			M232 (lower unit)	M232						M139	
	4D	5C	7E	1K	2A (core)	2B (rim)	3A (core)	3B (rim)	4A (core)	4B (rim)	1A	1B
SiO_2	64·93	65·89	66·45	63·16	54·25	53·05	54·92	53·97	55·70	54·10	54·19	53·93
TiO_2	0·28	0·38	-	-	-	-	-	-	-	-	-	-
Al_2O_3	19·41	19·61	19·66	19·22	28·96	29·61	28·82	29·22	28·16	29·12	29·04	28·99
Σ FeO	-	0·37	-	3·09	0·30	0·38	-	0·53	-	0·38	-	-
MgO	-	-	-	1·43	-	-	-	-	-	-	-	-
CaO	0·69	0·79	0·59	0·68	11·78	12·85	11·10	11·74	10·80	11·72	12·40	12·38
Na_2O	2·17	5·73	5·44	4·08	4·17	3·66	4·56	4·03	4·71	4·15	3·86	4·14
K_2O	12·53	7·22	7·85	8·35	0·54	0·45	0·59	0·52	0·62	0·53	0·52	0·57
Total	100·01	99·99	99·99	100·01	100·00	100·00	99·99	100·01	99·99	100·00	100·01	100·01
Si	2·968	2·970	2·977	2·967	2·456	2·411	2·476	2·447	2·507	2·451	2·449	2·441
Al	1·046	1·042	1·038	1·064	1·546	1·586	1·531	1·562	1·494	1·555	1·546	1·546
Fe	-	-	-	-	excl	excl	-	excl	-	excl	-	-
Ca	0·034	0·038	0·029	0·034	0·571	0·626	0·536	0·570	0·521	0·569	0·600	0·600
Na	0·192	0·501	0·472	0·371	0·366	0·323	0·398	0·354	0·411	0·364	0·338	0·363
K	0·730	0·415	0·449	0·501	0·031	0·026	0·034	0·030	0·036	0·031	0·030	0·033
Si + Al	4·014	4·012	4·015	4·031	4·002	3·997	4·007	4·009	4·001	4·006	3·995	3·987
Ca + Na + K	0·956	0·954	0·950	0·906	0·968	0·975	0·968	0·954	0·968	0·964	0·968	0·996
An	3·5	4·0	3·0	3·8	59·0	64·2	55·4	59·8	53·8	59·0	62·0	60·2
Ab	20·1	52·5	49·8	41·0	37·8	33·1	41·1	37·1	42·5	37·8	34·9	36·5
Or	76·4	43·5	47·2	55·2	3·2	2·7	3·5	3·1	3·7	3·2	3·1	3·3

Cations calculated on the basis of oxygen number (O) = 8.
Fe, Mg and Ti assumed to be impurities.

Table A9 (continued)

(f) Titanaugite

	M250 (upper unit)			M151 (lower unit)			M211 (lower unit)				M232 (lower unit)			
	4A	5D	6B	1B	1C	2A	2B	1E	1F	2A	3D	1D	1H	1J
SiO_2	49·26	51·08	48·90	47·73	50·46	46·42	48·58	47·36	46·77	46·39	46·86	45·32	45·14	46·63
TiO_2	2·77	1·49	2·50	3·25	1·82	3·59	2·95	2·81	3·41	3·56	3·29	4·40	4·83	3·76
Al_2O_3	2·73	1·86	3·49	4·48	3·34	6·65	3·87	5·07	5·37	5·40	5·36	6·31	5·51	5·24
Σ FeO	10·96	9·51	9·56	10·36	9·65	10·95	10·33	10·84	9·47	9·50	10·01	10·50	10·38	10·00
MnO	-	0·24	-	-	-	-	-	-	-	-	-	-	-	-
MgO	11·63	13·90	13·26	12·50	12·98	11·49	12·50	12·71	12·34	12·40	12·21	10·75	11·09	11·89
CaO	21·75	21·58	21·80	21·67	21·11	20·18	21·79	20·84	21·87	22·32	21·76	22·28	22·36	21·96
Na_2O	0·90	0·33	0·50	-	0·61	0·74	-	0·37	0·60	0·43	0·51	0·43	0·68	0·52
P_2O_5	-	-	-	-	-	-	-	-	0·17	-	-	-	-	-
Total	100·00	99·99	100·01	99·99	99·97	100·02	100·02	100·00	100·00	100·00	100·00	99·99	99·99	100·00
Si	1·857	1·909	1·829	1·802	1·887	1·747	1·834	1·779	1·759	1·740	1·759	1·717	1·707	1·755
Al	0·121	0·082	0·154	0·198	0·113	0·253	0·166	0·221	0·238	0·239	0·237	0·282	0·246	0·233
Fe^{III}	0·022	0·009	0·017	-	-	-	-	-	0·003	0·021	0·004	0·001	0·047	0·012
Al	-	-	-	0·001	0·034	0·042	0·006	0·003	-	-	-	-	-	-
Ti	0·078	0·042	0·070	0·092	0·051	0·102	0·084	0·079	0·097	0·100	0·093	0·126	0·138	0·106
Fe^{III}	0·051	0·031	0·068	0·013	0·021	0·062	-	0·086	0·091	0·090	0·091	0·064	0·068	0·070
Fe^{II}	0·273	0·257	0·214	0·314	0·281	0·283	0·326	0·254	0·204	0·187	0·219	0·267	0·213	0·233
Mn	-	0·008	-	-	-	-	-	-	-	-	-	-	-	-
Mg	0·654	0·774	0·739	0·704	0·723	0·644	0·703	0·712	0·692	0·694	0·683	0·607	0·625	0·667
Ca	0·878	0·864	0·873	0·876	0·846	0·813	0·881	0·839	0·872	0·897	0·875	0·904	0·906	0·886
Na	0·066	0·024	0·036	-	0·044	0·054	-	0·027	0·044	0·032	0·037	0·032	0·050	0·038
100 Mg/ Mg+ Fe	65·4	71·7	71·2	68·3	70·5	65·1	68·3	67·7	69·9	70·0	68·5	64·6	65·6	67·9
Charge excess	-	-	-	-	-	-	0·008	-	-	-	-	-	-	-

Cations calculated on basis of cation number (Z) = 4, and iron distributed to Fe^{II} and Fe^{III} so that the oxygen number (O) = 6, where possible.
Analysis 211/1F: stoichiometric apatite subtracted before cations calculated.

Table A9 (continued)

(g) Ulvospinel (titanomagnetite series)

	M232 (lower unit)	M250 (upper unit)			M211 (lower unit)	
	4C	6C	8A	8B	1A	1E
SiO_2	-	1·21	0·18	0·30	-	0·50
TiO_2	27·94	29·26	28·47	27·45	30·75	28·76
Al_2O_3	1·19	1·47	1·74	1·54	1·62	2·20
Cr_2O_3	0·28	0·22	-	0·40	-	-
Σ FeO	68·85	65·33	67·65	68·53	63·12	66·15
MnO	1·73	1·61	1·74	1·78	1·83	1·59
MgO	-	0·46	-	-	2·67	0·47
CaO	-	0·43	0·21	-	-	-
Na_2O	-	-	-	-	-	0·34
Total	99·99	99·99	99·99	100·00	99·99	100·01
Ti	0·772	0·825	0·788	0·759	0·832	0·795
Al	0·052	0·062	0·076	0·067	0·069	0·095
Cr	0·008	0·006	-	0·012	-	-
Fe^{III}	0·397	0·282	0·348	0·403	0·267	0·314
Fe^{II}	1·718	1·763	1·734	1·704	1·633	1·720
Mn	0·054	0·051	0·054	0·055	0·056	0·050
Mg	-	0·010	-	-	0·143	0·026
Arbitrary components (mol %) — after Anderson, 1968.						
$(Mg,Mn)Cr_2O_4$	0·4	0·3	-	0·6	-	-
$MgAl_2O_4$	-	0·7	-	-	3·4	2·6
Mg_2TiO_4	-	-	-	-	5·4	-
$MnAl_2O_4$	2·6	2·4	3·8	3·3	-	2·1
Mn_2TiO_4	1·2	1·3	0·8	1·6	2·8	1·4
Fe_2TiO_4	76·0	81·2	78·0	74·3	75·0	78·1
Fe_3O_4	19·8	14·1	17·4	20·2	13·4	15·8
$Fe_3O_4/Fe_3O_4 + Fe_2TiO_4$	20·7	14·8	18·2	21·4	15·1	16·9
$R^{II}R^{III}O_4$	22·8	17·5	21·2	24·1	16·8	20·5

Cations calculated on the basis of cation number (Z) = 3, and oxygen number (O) = 4.
Si, Ca and Na assumed to be impurities.
M250/6C: Titanaugite of composition M250/6B subtracted before cations calculated.

Table A9 (continued)

(h) Ilmenite (all from lower unit)

	M250 (upper unit)		M211 (lower unit)	M232 (lower unit)
	1A	3A	3B	1F	1G
SiO_2	-	-	0·41	1·25	4·59
TiO_2	51·28	51·56	51·20	49·60	46·25
Al_2O_3	0·57	0·23	0·38	0·68	1·54
Σ FeO	43·38	44·22	44·17	45·32	43·28
MnO	0·54	0·55	0·60	0·65	0·69
MgO	4·23	3·43	3·10	2·50	2·38
CaO	-	-	0·15	-	0·46
K_2O	-	-	-	-	0·82
Total	100·00	99·99	100·01	100·00	100·01
Ti	0·938	0·950	0·953	0·929	0·924
Al	0·016	0·007	0·010	0·020	0·017
Fe^{III}	0·109	0·093	0·084	0·121	0·136
Fe^{II}	0·773	0·814	0·829	0·823	0·823
Mn	0·011	0·011	0·013	0·014	0·015
Mg	0·153	0·125	0·111	0·093	0·085
Arbitrary components (mol %) — after Anderson, 1968.					
$FeTiO_3$	77·3	81·4	82·9	82·3	82·3
$MgTiO_3$	15·3	12·5	11·1	9·3	8·5
$MnTiO_3$	1·1	1·1	1·3	1·4	1·6
Fe_2O_3	5·5	4·7	4·2	6·0	6·8
Al_2O_3	0·8	0·3	0·5	1·0	0·8
$Fe_2O_3/Fe_2O_3 + FeTiO_3$	7·1	5·7	5·1	7·4	8·3
$R^{III}{}_2O_3$	6·3	5·0	4·7	7·0	7·6

Cations calculated on the basis of cation number (Z) = 2, and oxygen number (O) = 3.
M211/3B: Titanaugite of composition of M211/3D subtracted, and the remaining Si excluded from cation calculation.
M232/1F: Si excluded from cation calculation.
M232/1G: Stoichiometric potash feldspar and titanaugite of composition M232/1F subtracted before cations calculated.

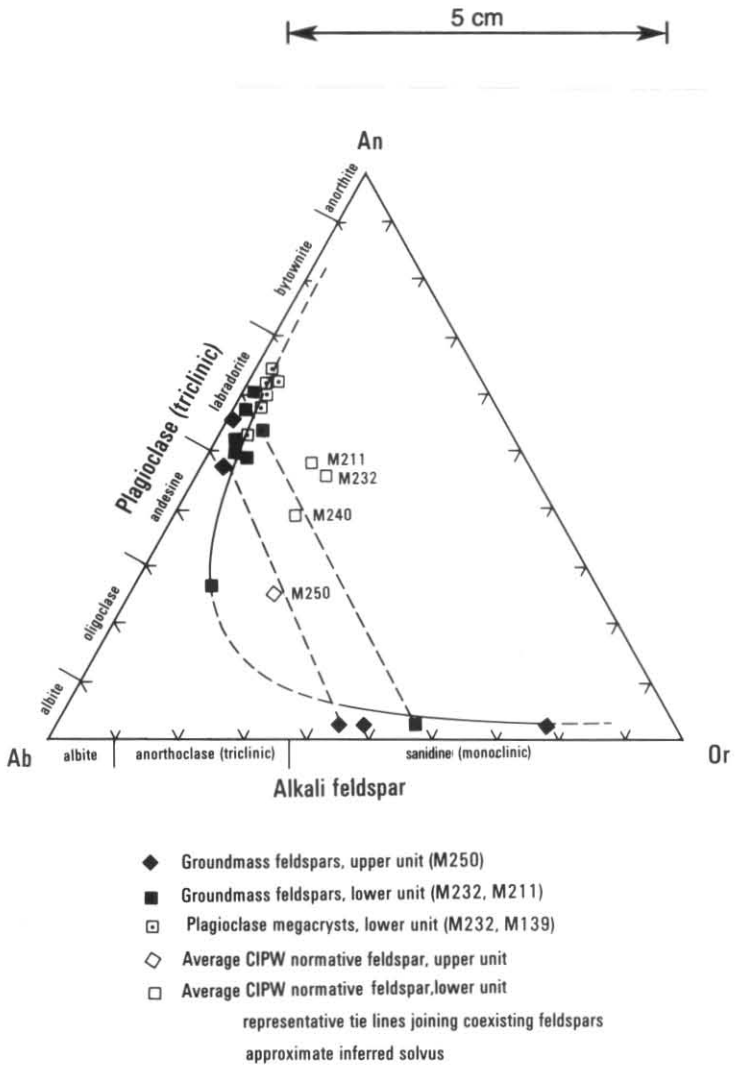

Figure A11. *Comparison of feldspars in Triassic basalt (see Table A9c–e).*

unmixing of sodic and potassic components to form sanidine cryptoperthite is possible, and together with alteration, could account for the cloudiness of much interstitial feldspar. Some of this interstitial material may also contain nepheline (table A5).

Both plagioclase and alkali feldspar plot along the inferred solvus in the system Ab-An-Or (fig. A11), becoming progressively more sodic with *in situ* fractional crystallisation (e.g. Deer *et al.*, 1963).

The significance of minor elements reported in some analyses of groundmass feldspar (tables A9c, d) is difficult to evaluate, due to the possibility of contamination by tiny inclusions or adjacent mineral grains. Mg and Ti are almost certainly due to impurities such as chlorite and iron-titanium oxides, since values of these elements are well above normal upper limits in feldspar (Smith, 1974*b*, pp. 62–63, 106–108) and most such analyses also contain anomalously high Fe.

However, six otherwise 'clean' analyses of groundmass plagioclase show low but consistent Fe contents (average $0{\cdot}64 \pm 0{\cdot}02$ mass% as FeO) typical of calcic plagioclase in volcanic rocks (Smith, 1974*b* pp. 108-112). Because of doubt as to its valence and site occupancy, and the possibility of sub-solidus exsolution of iron oxides, iron is not included in the calculated structural formulae.

TITANAUGITE (table A9f, fig. A12)

A distinctive petrographic feature of these rocks is the abundance of pinkish titanaugite in the groundmass. Fourteen microanalyses were obtained from both upper and lower units. The method used to distribute iron to Fe^{II} and Fe^{III}

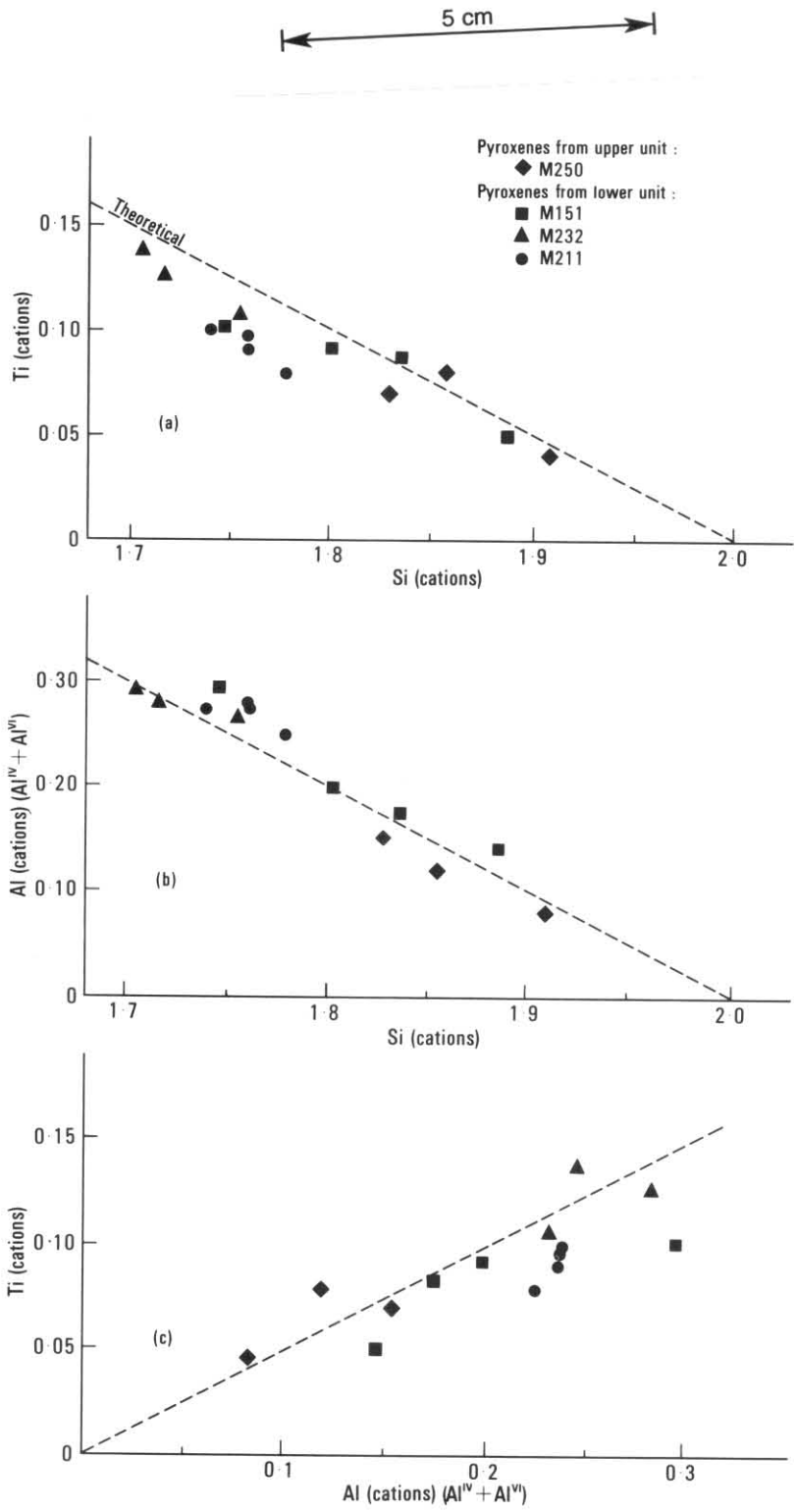

Figure A12. *Correlation between cation contents in electron probe microanalyses of titanaugite from Triassic basalts (tables A9f, A10). Lines show trend expected from theoretical coupled substitution Mg—Ti, 2Al—2Si, i.e. solid solution* $CaMgSi_2O_6$–$CaTiAl_2O_6$. *(see text).*

when calculating cation numbers, although widely accepted, is very sensitive to analytical error, and results for these cations should be treated with caution.

The most interesting feature of the titanaugite chemistry is the presence of the 'non-quadrilateral' cations Ti, residing in the octahedral sites, and Al, almost entirely in the Si-deficient tetrahedral sites. A strong inverse correlation exists between Ti and Al on the one hand, and Si and Mg on the other (table A10), representing the coupled substitution Mg^{2+} (0·67Å) = Ti^{4+} (0·68Å), $2Si^{4+}$ = $2Al^{3+}$. This could be alternatively be regarded as the presence of up to 14 mol% solid solution of the hypothetical clinopyroxene component $CaTiAl_2O_6$ (fig. A16). Titanaugites from the lower basalt unit are generally more deeply coloured and richer in Ti and Al, reflecting the higher TiO_2 content of the whole rock (table A3) which appears to the major cause of chemical variation in these pyroxenes.

Na is a minor constituent and varies erratically, whilst Mn is detectable only in the least titaniferous analysis.

In general, these are fairly typical titaniferous calcic pyroxenes (Robinson, 1980, p. 420–429).

In sample M250 (upper unit), titanaugite is in equilibrium with groundmass olivine (fig. A10), according to the Fe/Mg olivine-clinopyroxene data of Duke (1976). However both minerals, together with iron-titanium oxides, probably crystallised from a melt more iron-rich than suggested by the whole rock composition, because of the abundance of phenocrysts of Mg-rich olivine. It is noteworthy that titanaugites from the lower basalt unit, which contains very few olivine phenocrysts, have similar 100 Mg/Mg + Σ Fe ratios, despite the lower Mg number of the whole rock.

Table A10
STATISTICALLY SIGNIFICANT CORRELATIONS BETWEEN CATIONS (table A9f) IN TITANAUGITE

	r	r^2	P
Si:Al	-0·936	0·876	0·001
Si:Ti	-0·931	0·867	0·001
Ti:Mg	-0·869	0·755	0·001
Ti:Al	+0·826	0·681	0·001
Si:Mg	+0·744	0·554	0·01
Al:Mg	-0·711	0·506	0·01
ΣFe:Mg	-0·614	0·378	0·02

P = probability that distribution is independent (*i.e.* cations not correlated).
Correlation coefficients and probabilities calculated after Young (1962, p. 126–132, 164)

IRON-TITANIUM OXIDES (tables A9g–h, fig. A13)

Electron microprobe analyses show that, on the basis of Fe:Ti ratios, two separate opaque phases are present in the Triassic basalts. Since this method determines only total iron, they cannot be unequivocally assigned to the magnetite-ulvospinel, hematite-ilmenite or pseudobrookite series by this method alone (fig. A13).

Examination of three polished thin sections (M211, M232, M250) in reflected light shows that almost all opaque ninerals are dull grey with moderately low reflectivity, but some are isotropic and other distinctly anisotropic. The isotropic grains are more or less equant and are almost certainly ulvospinel, whilst the anisotropic grains, range from elongate to equant and are ilmenite. Although several types of exsolution phenomena involving these minerals are known, as well as the oxidation of ulvospinel-magnetite solid solution to ilmenite-hematite solid solution, in these rocks all opaque grains appear to be homogeneous, and probably both ulvospinel and ilmenite are unexsolved primary phases.

Traces of a brighter pinkish anisotropic sulphide (?pyrrhotite) are present in sample M211 and M232; the latter also contains traces of yellowish ?pyrite.

Electron microprobe analyses are assigned to the appropriate series and recalculated (table A9g, h) accordingly. Both minerals are low in Fe^{III} and plot near the Fe^{II}-Ti rich end member of each series (fig. A13). The higher content of Al and Cr in the ulvospinel phase is typical for coexisting iron titanium oxides (*e.g.* Haggerty, 1976, p. 142–158, 258–260) and is consistent with the much more extensive solid solutions involving these elements in spinels in rhombohedral phases. The high Mg content in ilmenite is also typical of basic igneous rocks. In these TiO_2-rich rocks, groundmass ilmenite probably crystallised relatively early, before or with titanaugite and groundmass olivine, from a liquid therefore not already depleted in MgO.

Mn is higher in ulvospinel than in ilmenite. The significance of this, which is in contrast to the usual situation (Haggerty, p. 158), is not clear.

Because of the abundance and freshness of coexisting ulvospinel and ilmenite these rocks are ideal for iron-titanium oxide geothermometry (Buddington and Lindsley, 1964). However, more detailed electron probe work is desirable. An additional problem is the presence of minor Mg, Mn and Al in the minerals, the effect on equilibrium of which is not fully known. Speidel (1970) showed that MgO tended to cause oxygen fugacities to be overestimated, and the method of calculating end members of Anderson (1968), adopted here, minimises this error.

Preliminary estimates, based on approximate compositions of $Mt_{20}Usp_{80}$ and Hm_5Ilm_{95} (tables A9g, h) indicate a minimum temperature of about 1140° and minimum log f_{O_2} of -9·5 for equilibrium of groundmass iron-titanium oxides (fig. A14). These estimates, like most from basic

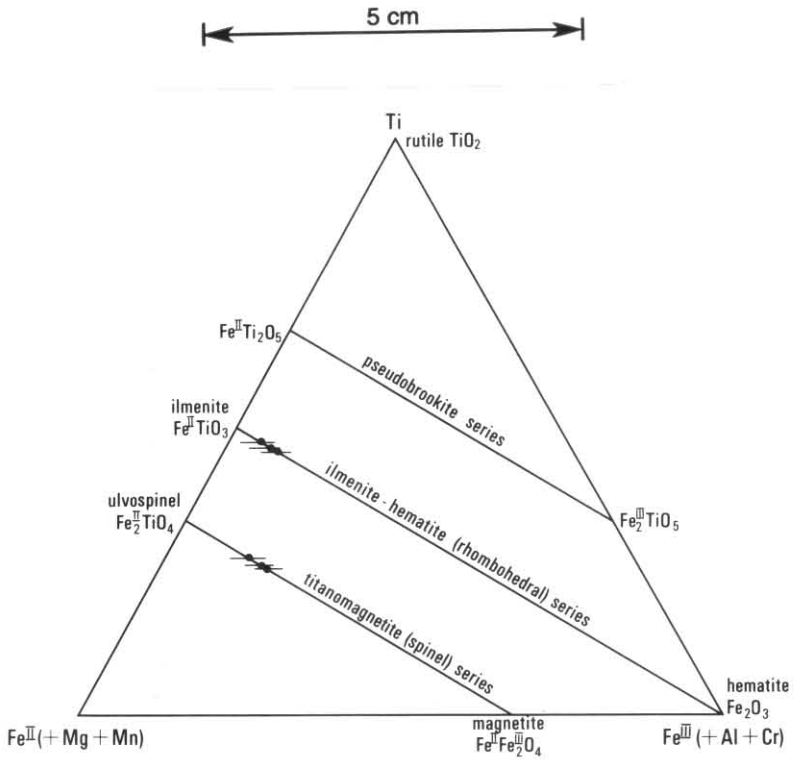

Figure A13. *Composition of Fe–Ti oxides in Triassic basalts. Electron probe microanlyses (tables A9g, A9h) plotted as horizontal isopleths of constant* $Fe^{I} + Fe^{III}$ *(+ Mg + Mn + Al + Cr):Ti. Isopleths shown only near intersection with assigned solid solution series.*

extrusives (Haggerty, 1976, p. 163, p. 189–196), lie close to the quartz-fayalite-magnetite buffer, but are toward the upper limit of T and f_{O_2} displayed by this data. This probably reflects the high TiO_2 content of these rocks and the consequent relatively early crystallisation of ulvospinel and ilmenite.

PETROGENESIS

ORIGIN OF PARENTAL MAGMA

It is generally thought that primary alkali olivine type magma is generated at greater depths and/or by lower amounts of partial melting of mantle than tholeiitic magma (*e.g.* Carmichael *et al.*, 1974, p. 487). In a study of various Tertiary basalts from Tasmania and Victoria, Frey *et al*, (1978) showed that the alkali olivine basalts could have been produced by 11–15% partial melting of a source of composition similar to the pyrolite model of the mantle (Ringwood, 1966), leaving a residue containing garnet as well as clinopyroxene, orthopyroxene and olivine.

A primary alkali-olivine type magma, parental to these basalts, was probably generated by a similar process. Their relatively high Zr:Y ratio of 10–15 (table A4) is consistent with a residue containing garnet, into which Y, like the heavy rare earths, is strongly partitioned (*e.g.* Pearce and Norry, 1979). This is consistent with a relatively small degree of partial melting (since garnet is the least refractory phase), at depths and pressures of greater than about 55 km and 17 kb respectively, corresponding to the garnet peridotite zone of the mantle (*e.g.* Yoder, 1976, p. 28).

At face value, the K_2O contents (2·08%, 2·20%, table A7) imply about 6% partial melting, when compared to the model pyrolite composition (0·13% K_2O; Ringwood, 1966). However, because of the highly differentiated nature of these rocks, this should be regarded as a minimum estimate. If the lower unit basalt has undergone 30% crystal fractionation, as estimated below, the amount of partial melting required, assuming that K_2O is always partitioned into the melt, is about 9%. In addition, the rather high K_2O content of these rocks, compared to similar Tasmanian Tertiary basalts (fig. A4, table A7) suggests that they may have been derived from a more potassic, relatively phlogopite-rich source, therefore requiring a greater amount of partial melting. This is supported by the uniformly rather high K:Zr ratio (table A4) which should reflect that of the source, as both elements are incompatible with respect to early crystallising minerals.

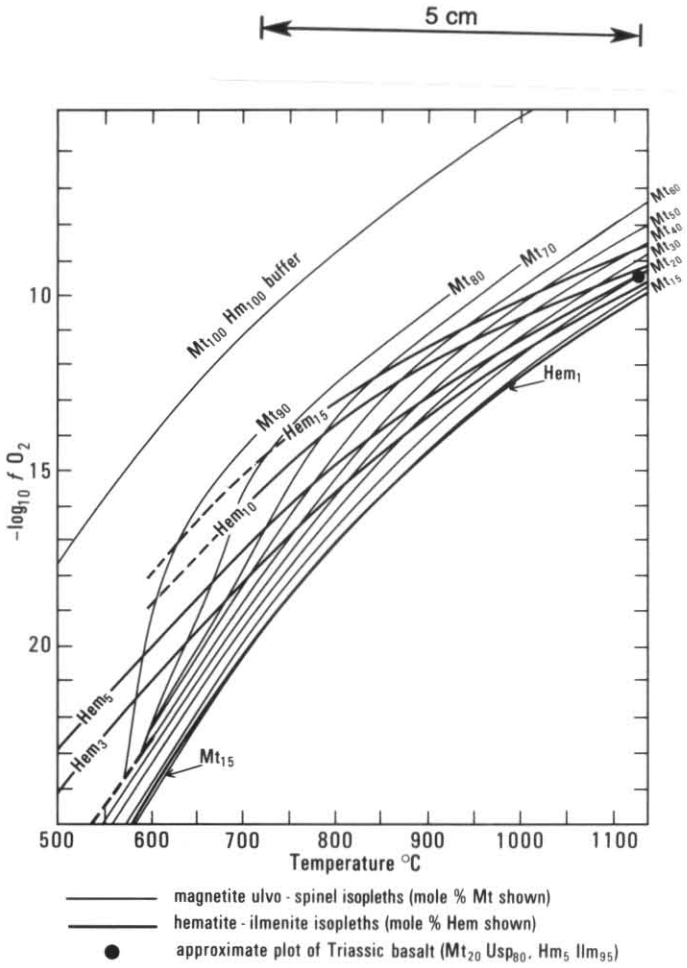

Figure A14. *Equilibrium temperatures and oxygen fugacities from coexisting iron-titanium oxides in Triassic basalts. As the oxides may be slightly more Hm-rich and Mt-poor, these are minimum estimates and the true values may lie to the right of the diagram. Modified after Buddington and Lindsley (1964). Projection onto fO_2–T plane of conjugate surfaces in fO_2–T–X space. Projection is parallel to two composition axes, magnetite-ulvöspinel$_{ss}$ and the coexisting hematite-ilmenite$_{ss}$, so that intersecting contours are the projection of tie lines connecting conjugate pairs.*

INITIAL DIFFERENTIATION: FRACTIONATION AT MODERATE PRESSURES

As discussed previously, these basalts are clearly evolved relative to any possible parental magma. The simplest model, crystal fractionation of olivine, would reduce the Mg number and Ni content from the expected primitive values of 68–72 and 320 ppm respectively (Frey *et al.*, 1978, pp 468–471) towards the observed values. On this basis, the less magnesian lower unit is the more differentiated. However, many other features cannot be reconciled with this model. The lower unit basalts are slightly higher in total FeO, but fractionation of equilibrium olivine (approximately $Fo_{74\text{-}80}$, 23·8–18·9 mass% FeO) should reduce it (Roeder and Emslie, 1970). Likewise, the lower SiO_2 in the lower unit (tables A3, A7, fig. A2) contradicts the expected trend. The Al_2O_3:CaO ratio, which is unaffected by olivine fractionation, is much higher than that of primary magmas (*e.g.* Frey *et al.*, 1978, p. 468–473), suggesting that a Ca-rich phase, probably clinopyroxene, also fractionated.

Green and Ringwood (1967) investigated the crystallisation sequence of magma of alkali olivine basalt composition at a range of pressures. At moderate pressures of (5)–9–(11) kb, clinopyroxene is the second phase, after olivine, to appear below the liquidus. In contrast to the situation at low pressures, plagioclase crystallisation is suppressed until near the solidus. Under these conditions, corresponding to depths of (15)–30–(35) km, fractionation of olivine and clinopyroxene will generate derivative magmas with high Al_2O_3 and low MgO contents, whilst not markedly affecting SiO_2 (Green and Ringwood, 1967, p. 142–148). Such a mechanism is envisaged to have produced these basalts, particularly the more aluminous lower unit, from a parental primary alkali-olivine type magma.

Table A11
GENERATION OF ALUMINOUS MAGMA (LOWER BASALT UNIT) FRACTIONATION AT MODERATE PRESSURES

	M240	Cpx	Ol	M240*	69–1036	2128
SiO_2	47·34	50·37	40·01	47·48	48·09	46·31
TiO_2	3·82	-	-	2·69	2·14	2·52
Al_2O_3	16·95	8·97	-	13·94	13·94	12·41
Σ FeO + MnO	12·55	6·32	14·35	11·30	11·12	11·99
MgO	5·22	19·79	45·63	11·41	11·41	11·74
CaO	8·02	14·55	-	8·88	8·37	8·58
Na_2O	3·24	-	-	2·29	3·24	3·55
K_2O	2·08	-	-	1·47	1·18	2·01
P_2O_5	0·78	-	-	0·55	0·51	0·90
Total	100·00	100·00	99·99	100·01	100·00	100·01
100Mg/Mg + Fe*	46·0	(85·0)	(85·0)	67·4	67·8	66·8

M240: Analysis 802966, major elements normalised to 100%.
Cpx: Estimated average composition of fractionated clinopyroxene (see text).
Ol: Estimated average composition of fractionated olivine (Fo_{85}).
M240*: Estimate of composition of primary magma parental to M240: M240 + 31·4% Cpx + 10·4% Ol, sufficient to make Al_2O_3 and MgO contents equal to that of 69–1036.
69–1036: Alkali olivine basalt (primary magma), Mt Frazer, Victoria (Frey *et al.*, 1978, p. 468–469).
2128: Basanite (primary magma), Mt Porndon, Victoria (*ibid.*).

Mixing calculations (table A11) show that addition of about 42% crystal extract, consisting of sub-calcic clinopyroxene ($En_{53}Fs_{9\cdot5}Wo_{28}Co_{9\cdot5}$) and olivine ($Fo_{85}$) in approximately the ratio 3:1, to the least altered lower basalt unit analysis (M240/802966) can produce a composition very similar in major elements to some alkali-olivine basalts identified by Frey *et al.* (1978) as unfractionated primary magmas — this is equivalent to the loss of about 30% crystals from the initial primary magma. Clinopyroxene was assumed to have CaO and Al_2O_3 contents similar to analysis 4 of Green and Ringwood (1967, p. 136) and Mg/Mg + Fe similar to the coprecipitating olivine. This model is also consistent, at least qualitatively, with the strong depletion, especially in the lower basalt unit, of Ni and Cr relative to less fractionated magmas, since Cr is strongly partitioned into clinopyroxene, and Ni into olivine and also clinopyroxene (*e.g.* Cox *et al.*, 1978, p. 334).

DIFFERENTIATION OF LOWER AND UPPER BASALT UNITS: LOW PRESSURE FRACTIONATION

Important geochemical differences between the lower and upper units are:

(1) MgO, Ni and especially Cr are much more depleted in the lowerunit.

(2) TiO_2, total Fe, V, Co and Sc are markedly lower in the upper unit. These elements are mostly moderately compatible in many mafic minerals (olivine, amphiboles, spinel), but are more strongly partitioned into Fe-Ti oxides (*e.g.* Frey *et al.* 1978, p. 512; Walker, 1984, p. 321; Frondel, 1969).

(3) CaO, Al_2O_3 and Sr are somewhat lower in the upper unit, consistent with plagioclase fractionation.

(4) Rb, Y, Zr, Nb, Pb, P_2O_5, K_2O and possibly Na_2O (fig. A1) are slightly lower in the lower unit. These so called incompatible elements will not substitute into the crystal lattice of early-formed minerals, but are partitioned into the melt, finally crystallising in later minerals such as alkali feldspar, apatite and zircon. If both basalt units are derived from a common parent, this suggests that the upper unit has lost a greater amount of material by crystal fractionation.

(5) SiO_2 is slightly lower in the lower unit (comparison is best made after normalising analyses to 100% anhydrous, Table A7, Figure A2). Fractionation of Fe-Ti oxides and, to a lesser extent, olivine will tend to increase SiO_2; fractionation of plagioclase and pyroxene will only slightly decrease it in basaltic compositions.

(6) Ba and, to a large extent, Na_2O are controlled by secondary processes, including alteration and possible metasomatism, as discussed previously.

(7) MnO, Cu, Zn and Ga differ little between units. Most of these elements probably substitute mainly for FeO, but apparently are not strongly partitioned into iron-titanium oxides or any other possibly fractionated phase.

The high Al_2O_3 and TiO_2 content of these rocks, the presence of plagioclase megacrysts in the lower unit, and the high equilibrium temperatures of coexisting ulvospinel and ilmenite (fig. A14) suggest that plagioclase and iron-titanium oxides were the low pressure liquidus or near-liquidus phases. Co-fractionation of these phases from

Table A12
GENERATION OF UPPER BASALT UNIT BY CRYSTAL FRACTIONATION FROM MAGMA OF LOWER BASALT UNIT COMPOSITION

	M250	Pl	Usp	Ilm	M250*	M240
SiO_2	49·14	53·05	-	-	46·94	47·34
TiO_2	2·48	-	29·50	51·42	3·82	3·82
Al_2O_3	15·12	30·01	1·60	0·40	16·95	16·95
Σ FeO + MnO	11·43	-	68·40	44·35	12·55	12·55
MgO	6·60	-	0·50	3·83	5·10	5·22
CaO	7·39	12·38	-	-	7·84	8·02
Na_2O	4·25	4·56	-	-	4·05	3·24
K_2O	2·20	-	-	-	1·68	2·08
P_2O_5	1·39	-	-	-	1·06	0·78
Total	100·00	100·00	100·00	100·00	99·99	100·00
100Mg/Mg + Fe*	54·3	-	-	-	45·4	46·0

M250: Analysis 802967 (upper unit), major elements normalised to 100%.
Pl: Estimated average composition of fractionated plagioclase (An_{60}).
Usp: Estimated average composition of fractionated ulvospinel (from electron microprobe data.
Ilm: Estimated average composition of fractionated ilmenite (from electron microprobe data.
M250*: Estimate of composition of M250 before low-pressure fractionation: M250 + 23·2% Pl + 6·6% Usp + 1·1% Ilm. Proportions chosen to make TiO_2, Al_2O_3 and ΣFeO contents equal to that of M240 (see text).
M240: Analysis 802966 (lower unit), major elements normalised to 100%.

the lower unit to produce the upper unit as a differentiate, can account for most of the above differences. In mixing calculations (table A12), plagioclase was assumed to be compositionally similar to the more calcic of the megacryst cores (about An_{60}) and ulvospinel and ilmenite were assumed to be similar to the groundmass grains (table A9e, g–h). Simultaneous mass balance equations were written for differences in TiO_2, Al_2O_3 and total FeO between the least altered analyses of the lower and upper unit basalts, normalised to 100% major elements. The solutions show that fractionation of about 24 mass% crystal extract, consisting of about 18% plagioclase, 5% ulvospinel and 1% ilmenite, from the lower unit basalt (M240/802966) is required. When the entire composition is calculated, the remaining oxide components fit well: all change towards the observed values in the upper unit (M250/802967) at nearly the right magnitude (except for alkalis). Sharp differences between the two basalt units in the ratios Rb:Sr and Ti:Zr (table A4) are also consistent with this model.

SEGREGATION OF PLAGIOCLASE MEGACRYSTS

Consideration of the relative densities of magmas of lower and upper unit composition, and of plagioclase, suggest a mechanism for the process.

Major element analyses of the least altered samples, M240/802966 and M250/802967, were converted to oxide mole fractions and the revised density calculation method of Bottinga *et al.* (1982) was used.

As no molar volume data are available for P_2O_5, values ($\bar{V}^0_1$ = 53·5 cm³/mol, $\bar{\alpha}^0_1$ = 0·1 × $10^5 deg^{-1}$ at 1400°C) analogous to those of SiO_2 were assumed; this barely affects the results.

The effect on density of adding 0·4 mass% H_2O, a moderate amount of a basaltic magma (*e.g.* Carmichael *et al.*, 1974, p. 321–322) at 0.1 kb and 4 kb was estimated using an equation for partial molar volume of H_2O (Burnham *et al.*, 1969), as originally outlined by Bottinga and Weill (1970).

Plagioclase densities were calculated for the compositions $An_{60}Ab_{37}Or_3$ and $An_{55}Ab_{42}Or_3$, between which most of the analyses of megacrysts lie. Data from a previously heat-treated plagioclase of composition $An_{55}Ab_{42\cdot6}Or_{2\cdot4}$ (Grundy and Brown, 1972, tabulated by Smith, 1974*a*, p. 333) was used to infer a molar volume at 950°C of 101·7 cm³/mol and a nearly temperature-independent coefficient of volume expansion of 1·21 × $10^{-5} deg^{-1}$, assumed to extend to the liquidus. Possible errors introduced by these assumptions are unlikely to alter the conclusions discussed below.

The results (fig. A15) show that at near liquidus temperatures of approximately 1250°C plagioclase is appreciably denser than magma of upper unit composition, but the density contrast with the magma of lower unit composition is small or even negative. Addition of a small amount of water will lower the magma densities, but as their liquidus temperatures will also be lowered a similar situation would exist.

As magma of the lower unit composition slowly cooled below its liquidus in a shallow crustal magma chamber, plagioclase megacrysts would crystallise, but because of the small or negative density contrast, remain fairly buoyant, becoming readily entrained in the magma. On ascent, they would tend to resorb, as previously discussed. However, as the magma remaining in the chamber cooled and more plagioclase crystallised, a significant amount of iron-titanium

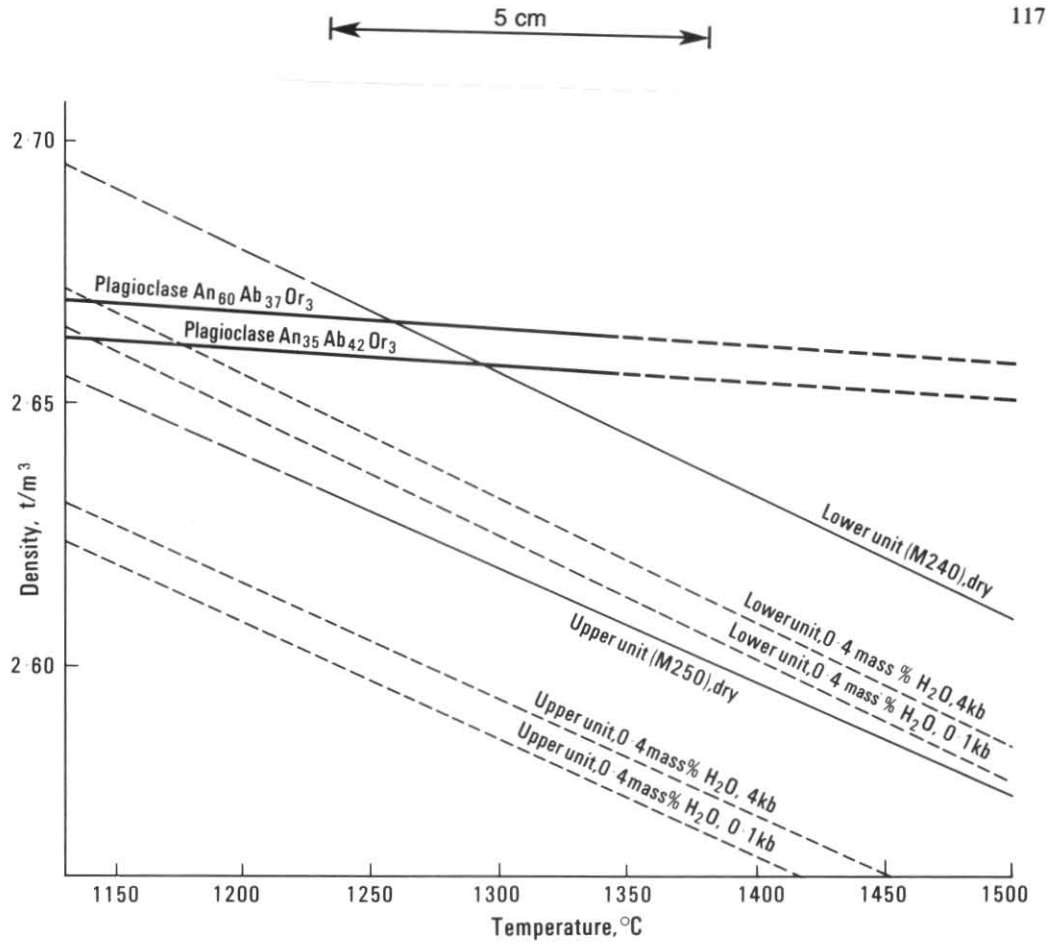

Figure A15. *Comparison of calculated densities of plagioclase megacrysts and calculated magmatic densities of Triassic basalts, as a function of temperature, H_2O content and pressure. See text for explanation and discussion.*

oxides would also crystallise and quickly settle. This would reduce the iron content and thus the density of the remaining liquid, and the plagioclase megacrysts would also settle. Thus the magma would approach the composition of the upper basalt unit.

The density contrast between olivine (Fo_{85}) and the upper unit magma is about 0·6 g/cm³, much larger than that of plagioclase (probably not more than 0·04 g/cm³) and thus olivine crystals of similar size would settle on order of magnitude faster. Therefore the olivine phenocrysts (xenocrysts) particularly abundant in the upper basalt unit could not have been present at the time of plagioclase fractionation, but must have been introduced later.

This hypothesis explains the differences between lower and upper units in major element chemistry, phenocryst assemblages, age and, at least qualitatively, most trace elements. However, the major problem is the abundance of Ni and particularly Cr, both of which partition at least to some extent into iron-titanium oxides (*e.g.* Walker, 1984) and therefore should be even more depleted in the upper unit. The exact significance of sample M253/802968, apparently an extreme segregation of the lower unit, is also not clear.

Attempts have been made to extend the above fractionation model by also allowing for fractionation of olivine, clinopyroxene and orthopyroxene and formulating additional equations for balancing SiO_2, MgO and CaO to produce six equations in six unknowns. However the solutions suggest small amounts of fractionation of pyroxenes, often in contradictory directions inconsistent with trace element data. Fractionation of other mafic phases into which Ni and Cr are partitioned, such as amphibole or spinel, could be considered. However, these possibilities are difficult to model because of the large range in possible composition of these materials and the lack of petrographic evidence or experimental data for their stability or composition.

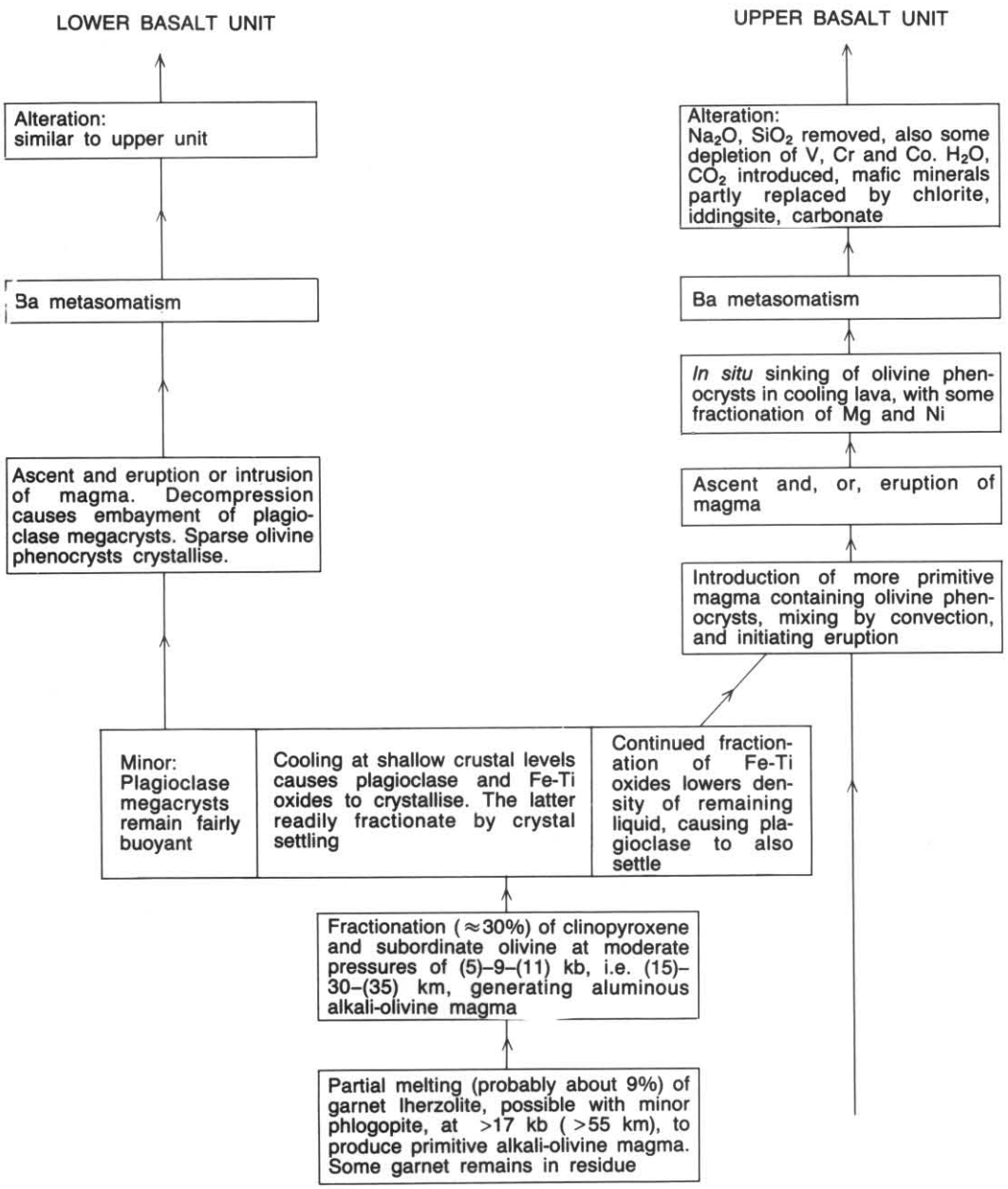

Figure A16. *Summary of processes involved in the petrogenesis of the Triassic basalts.*

POSSIBLE MAGMA MIXING (UPPER BASALT UNIT)

Probably the lower and upper basalt units, although obviously related, are not directly derived from one another or from a common parental magma by crystal fractionation alone. One possibility is that, after fractionation of plagioclase and iron-titanium oxides, a more primitive magma much richer in Ni and Cr but less contrasted in major-and other trace elements was injected into the magma chamber and mixed with its contents to produce magma of upper basalt unit composition. The Mg-rich xenocrysts of olivine were probably introduced as phenocrysts within the more primitive magma and account for the higher Ni content of the upper unit, whilst at the time Cr probably was contained in the melt, and crystallised later in groundmass ulvospinel (table A9g) and possibly titanaugite.

Mixing of magmas is increasingly being recognised as an important process in the evolution of volcanic rocks. In a recent review article, Sparks (1983) comments: 'A surprisingly simple picture has emerged from these studies which, in hindsight, appears all too obvious. Most volcanoes are underlain by complex plumbing systems which allow magma from the mantle to ascend to the surface. Magma often gets caught in traps (magma chambers) on the way to the surface where cooling and crystallisation cause differentiation. At intervals, varying from a few years to tens of thousands of years, the system is recharged by new magma rising from depth. As recharge occurs the fluid pressure in the plumbing system and magma chambers increases until the volcanic edifice fails and an eruption begins. In many cases recharge also causes mixing between magmas of different composition in the system by both natural and forced convection. It is thus hardly surprising that so many studies show that magma mixing occurs shortly before or during eruptions. Most eruptions occur because the plumbing system is activated by ascent of new magma'.

This model, summarised in Figure A16, combines both crystal fractionation and magma mixing, and is too arbitrary for a worthwhile attempt to be made to formulate it in completely quantitative manner, at least on the basis of the present data. However, it is considered to be the most plausible explanation for the petrographic and geochemical features of the Triassic basalts. Further work, possibly including rare-earth analyses, could test it and provide further constraints.

REGIONAL SIGNIFICANCE

It is noteworthy that the emplacement of the Triassic basalts coincided with the commencement of deposition of the Upper Parmeener Super-Group in this area. The volcanism may be related to a regional tectonic event, such as tilting or down-faulting, which resulted in a return to depositional conditions. As discussed elsewhere, acid to intermediate volcaniclastic material is abundant in sandstones higher in the sequence. Much of this material is reworked, but rare tuffs are present, and rhyolitic pebbles containing sanidine phenocrysts suggests the possibility of coeval coherent lavas (Bacon, 1979; Bacon and Everard, 1981). The differences in age and composition would appear to preclude a direct relationship between the basalts at Webber Falls and the younger more acidic volcanics, but further work is needed to assess whether a distinctive province of alkaline volcanism can be defined in the Tasmanian Triassic.

REFERENCES

ANDERSON, A. T. 1968. The oxygen fugacity of alkaline basalt and related magmas, Tristan da Cunha. *Am. J. Sci.* 266:704–727.

BACON, C. A. 1979. *Regional geology of the Apsley River area.* B.Sc. thesis [Part A], University of Tasmania : Hobart.

BACON, C. A.; EVERARD, J. L. 1981. Pyroclastics in the Upper Parmeener Super-group, near Bicheno, eastern Tasmania. *Pap. Proc. R. Soc. Tasm.* 115:29–36.

BOTTINGA, Y.; WEILL, D. 1970. Densities of liquid silicate systems calculated from partial molar volumes of oxide components. *Am. J. Sci.* 269:169–182.

BOTTINGA, Y.; WEILL, D.; RICHET, P. 1982. Density calculations for silicate liquids. I. Revised method for aluminosilicate compositions. *Geochim. cosmochim. Acta.* 46:909–919.

BROOKS, C. K. 1976. The Fe_2O_3/FeO ratio of basalt analyses: an appeal for a standard procedure. *Bull. geol. Soc. Denmark* 25:117–120.

BROWN, A. V.; MCCLENAGHAN, M. P. 1982. Tertiary basaltic rocks, *in* MCCLENAGHAN *et al.*, Geology of the Ringarooma–Boobyalla area. *Bull. geol. Surv Tasm.* 61:92–114.

BROWN, G. E. 1982. Olivines and silicate spinels, *in* RIBBE, P. H. (ed.), Orthosilicates. *Rev. Mineral., Mineral. Soc. Am.* 5:275–381. [2 ed.]

BUDDINGTON, A. F.; LINDSLEY, D. H. 1964. Iron-titanium oxide minerals and synthetic equivalents. *J. Petrology* 5:310–357.

BURNHAM, C. W.; HOLLOWAY, J. R.; DAVIS, N. F. 1969. Thermodynamic properties of water to 1000° and 10 000° bars. *Spec. Pap. geol. Soc. Am.* 132:1–96.

CARMICHAEL, I. S. E.; TURNER, F. J.; VERHOOGEN, J. 1974. *Igneous petrology.* McGraw Hill : New York.

COOMBS, D. S.; WILKINSON, J. F. G. 1969. Lineages and fractionation trends in undersaturated volcanic rocks from the East Otago volcanic province (New Zealand) and related rocks. *J. Petrology* 10:440–501.

COX, K. G.; BELL, J. D.; PANKHURST, R. J. 1979. *The interpretation of igneous rocks.* Allen and Unwin : London.

DEER, W. A.; HOWIE, R. A.; ZUSSMAN, J. 1963. *Rock-forming minerals minerals. Vol. 4. Framework silicates.* Longmans : London.

DUKE, J. M. 1976. Distribution of the period four transition elements among olivine, calcic clinopyroxene and mafic silicate liquid: experimental results. *J. Petrology* 17:499–521.

EDWARDS, A. B. 1941. The crinanite laccolith of Circular Head. *Proc. R. Soc. Vict.* 53:403–415.

EDWARDS, A. B. 1950. The petrology of the Cainozoic rocks of Tasmania. *Proc. R. Soc. Vict.* 62:97–120.

EVERARD, J. L. 1984. Petrology of Tertiary basalt, altered dolerite and tuff samples, *in* GULLINE, A. B. Geological atlas 1:50 000 series. Sheet 83(8412N). Sorell. *Explan. Rep. geol. Surv. Tasm.*

FINNERTY, A. A.; BOYD, F. R. 1978. Pressure dependent solubility of calcium in forsterite coexisting with diopside and enstatite. *Yb. Carnegie Inst. Wash.* 77:713–717.

FLOYD, P. A.; WINCHESTER, J. A. 1975. Magma type and tectonic setting discrimination using immobile elements. *Earth planet. Sci. Lett.* 27:211–218.

FORSYTH, S. M. 1980. Preliminary palynological report on Upper Parmeener Super-Group rocks interbedded with basalt at Webber Falls. *Unpubl. Rep. Dep. Mines Tasm.*

FREY, F. A.; GREEN, D. H.; ROY, S. D. 1978. Integrated models of basalt petrogenesis: a study of quartz tholeiites to olivine melilitites from south eastern Australia utilizing geochemical and experimental petrological data. *J. Petrology* 19:463–513.

FRONDEL, C. 1969. Scandium, *in* WEDEPOHL, K. H. (ed.) *Handbook of geochemistry. Vol. II/2. Elements Si(14) to V(23).* Springer-Verlag : Berlin.

FULLER, R. E. 1939. Gravitative accumulation of olivine during the advance of basaltic flows. *J. Geol.* 47:303–313.

GEE, R. D. 1971. Geological atlas 1 mile series. Sheet 22(8016S). Table Cape. *Explan. Rep. geol. Surv. Tasm.*:35-39.

GREEN, D. C. 1980. Barium-bearing heulandite from DDH 55, Fingal. *Unpubl. Rep. Dep. Mines Tasm.* 1980/27.

GREEN, D. H.; RINGWOOD, A. E. 1967. The genesis of basaltic magmas. *Contrib. Mineral. Petrology* 15:103–190.

GRUNDY, H. D.; BROWN, W. L. 1974. A high-temperature X-ray study of low and high plagioclase feldspars, *in* MACKENZIE, W. S.; ZUSSMAN, J. *The feldspars*:162–173. Manchester University Press.

HAGGERTY, S. E. 1976. Opaque mineral oxides in terrestrial igneous rocks, *in* RUMBLE, D. (ed.). Chapter 8. Oxide minerals. *Short Course Notes, Mineral. Soc. Am.* 3.

HALE, G. E. 1962. Triassic system, *in* SPRY, A. H.; BANKS, M. R. (ed.). The geology of Tasmania. *J. geol. Soc. Aust.* 9(2):217–231.

JOPLIN, G. A. 1963. Chemical analyses of Australian rocks. Part I: Igneous and metamorphic. *Bull. Bur. Geol. Geophys. Aust.* 65.

KUNO, H. 1960. High-alumina basalt. *J. Petrology* 1:121–145.

LE MAITRE, R. W. 1979. A new generalized petrological mixing model. *Contrib. Mineral. Petrology* 71:133–137.

MACDONALD, G. A. 1960. Dissimilarity of continental and oceanic rock types. *J. Petrology* 1:172–177.

MACDONALD, G. A.; KATSURA, T. 1964. Chemical composition of Hawaiian lavas. *J. Petrology* 5:82–133.

MCNEIL, R. D. 1965. The geology of the Mt Elephant, Picanniny Point area, Tasmania. *Pap. Proc. R. Soc. Tasm.* 99:27–49.

MANSON, V. 1967. Geochemistry of basaltic rocks: major elements, *in: The Poldervaart treatise on rocks of basaltic composition.* 1:215–269. Wiley : New York.

MATHEWS, W. H.; THORARINSSON, S.; CHURCH, N. B. 1964. Gravitative settling of olivine in pillows of an Icelandic basalt. *Am. J. Sci.* 262:1036–1040.

MYSEN, B. O.; KUSHIRO, I. 1979. Pressure dependence of nickel partitioning between forsterite and aluminous silicate melts. *Earth planet. Sci. Lett.* 42:383–388.

PEARCE, J. A.; CANN, J. R. 1973. Tectonic setting of basic volcanic rocks determined using trace element analyses. *Earth planet. Sci. Lett.* 19:290–300.

PEARCE, J. A.; NORRY, M. J. 1979. Petrogenetic implications of Ti, Zr, Y and Nb variations in volcanic rocks. *Contrib. Mineral. Petrology* 69:33–47.

RINGWOOD, A. E. 1966. The chemical composition and origin of the earth, *in* HURLEY, P. M. (ed.). *Advances in earth science.* MIT Press : Cambridge, Mass.

ROBINSON, P. 1980. The composition space of terrestrial pyroxenes — internal and external limits, *in* PREWITT, C. T. (ed.). *Pyroxenes. Reviews in mineralogy* 7(9):419–494.

SATO, H. 1977. Nickel content of basaltic magmas: identification of primary magmas and a measure of the degree of olivine fractionation. *Lithos* 10:113–120.

SIMKIN, T.; SMITH, J. V. 1970. Minor element distribution in olivine. *J. Geol.* 78:304–325.

SMITH, J. V. 1974*a*. *Feldspar minerals. I. Crystal structure and physical properties.* Springer-Verlag : Berlin.

SMITH, J. V. 1974*b*. *Feldspar minerals. II. Chemical and textural properties.* Springer-Verlag : Berlin.

SPARKS, R. S. J. 1983. Mixed-up magmas. *Nature, Lond.* 306: 315–316.

SPEIDEL, D. H. 1970. Effect of magnesium on the iron-titanium oxides. *Am. J. Sci.* 268:341–353.

SPRY, A. H. 1962. Igneous activity, *in* SPRY, A. H.; BANKS, M. R. (ed.). The geology of Tasmania. *J. geol. Soc. Aust.* 9(2):255–284.

STRECKEISEN, A. 1967. Classification and nomenclature of igneous rocks. *Neues Jb. Mineral., Abh.* 107:144–240.

STRECKEISEN, A. L. 1978. Classification and nomenclature of volcanic rocks, lamprophyres, carbonatites and melilitic rocks. *Neues Jb. Miner., Abh.* 134:1–14.

SUTHERLAND, F. L. 1969*b*. A review of the Tasmanian Cainozoic Province. *Spec. Publ. geol. Soc. Aust.* 2:133–144.

SUTHERLAND, F. L. 1976. Cainozoic volcanic rocks, *in Leaman, D. E.* Geological atlas 1:50 000 series. Sheet 82(8312S). Hobart. *Explan. Rep. geol. Surv. Tasm.*:35–56.

SUTHERLAND, F. L. 1977. Cainozoic volcanic rocks, *in Leaman, D. E.* Geological atlas 1:50 000 series. Sheet 75(8312N). Brighton. *Explan. Rep. geol. Surv. Tasm.*:25–37.

SUTHERLAND, F. L. 1984. Cainozoic basalts, *in* FORSYTH, S. M. Geological atlas 1:50 000 series. Sheet 68(8313S). Oatlands. *Explan. Rep. Dep. Mines Tasm.*:103–120.

SUTHERLAND, F. L. 1985. Cainozoic volcanic rocks, *in* FARMER, N. Geological atlas 1:50 000 series. Sheet 94(8311N). Kingborough. *Explan. Rep. geol. Surv. Tasm.*:73–83.

SUTHERLAND, F. L.; KERSHAW, R. C. 1971. The Cainozoic geology of Flinders Island, Bass Strait. *Pap. Proc. R. Soc. Tasm.* THREADER, V. M. 1968. An interim report on the geology and coal resources of the northeast coalfields of Tasmania. *Unpubl. Rep. Dep. Mines Tasm.*

VOGT, J. H. L. 1923. Nickel in igneous rocks. *Econ. Geol.* 18:307–353.

WALKER, J. A. 1984. Volcanic rocks from the Nejapa and Granada cinder cone alignments, Nicaragua, Central America. *J. Petrology* 25:299–342.

WALKER, K. R. 1957. The geology of the St Helens–Scamander area, Tasmania. *Pap. Proc. R. Soc. Tasm.* 91:23–39.

WINCHESTER, J. A.; FLOYD, P. A. 1976. Geochemical magma type discrimination: application to altered and metamorphosed basic igneous rocks. *Earth planet. Sci. Lett.* 28:459–469.

YODER, H. S. 1976. *Generation of basaltic magma.* National Academy of Sciences : Washington.

YOUNG, H. D. 1962. *Statistical treatment of experimental data.* McGraw-Hill : New York.

APPENDIX B

Petrology of the Jurassic dolerite

CONTENTS

LIST OF FIGURES

LIST OF TABLES

APPENDIX B

Petrology of the Jurassic dolerite

J. L. Everard

INTRODUCTION

Six samples of various types of dolerite (table B1) were chosen for further study including major and trace element analyses (table B3) and electron probe microanalyses of constituent minerals (table B2). Petrographic descriptions are incorporated in an earlier section. Three other chemical analyses of dolerite from the St Marys quadrangle are listed in Table B3, but thin sections of these rocks are not available.

In addition, four analyses, all from drill core near the lower chilled margin of the sheet on Fingal Tier (table B5), are available. These are clearly of altered samples, with high H_2O, CO_2 and/or Fe_2O_3, and are excluded from further consideration. However, when compared with fresh chilled margin material (analyses 783469, 831455) many trace elements appear to have behaved in an immobile manner.

The geochemistry and differentiation of Tasmanian Jurassic dolerite has been investigated previously (Edwards, 1942; McDougall, 1962, 1964; McDougall and Lovering, 1963). However, subsequent advances in analytical methods, particularly the advent of the electron microprobe, greatly facilitate this type of investigation. In addition, an improved understanding of the properties and behaviour of magmas, together with faster computational methods, offer the prospect of a more detailed and quantitative treatment. This represents only a preliminary investigation in this direction.

MINERAL CHEMISTRY

PLAGIOCLASE

The most striking feature of the plagioclase analyses (table B2a) is the very large compositional range, even within a single specimen, reflecting the normal zoning clearly apparent in thin section. The most extreme range is found in plagioclase crystals from the mafic cumulate (DDH68/361·95) which have cores as calcic as bytownite (An_{87}) and rims as sodic as andesine (An_{41}). However, even in the glassy differentiated dolerites, (M363 and M364), plagioclase varies in composition by more than 20 mole% An. The data are generally consistent with previous optical determinations of zoned plagioclase in dolerite from the Red Hill dyke (McDougall, 1962), Great Lake (McDougall, 1964) and elsewhere (Edwards, 1942).

The very fine-grained groundmass plagioclase of the chilled margin (DDH/451·96) is labradorite (An_{62-70}), closely matching the composition of the normative plagioclase (An_{65}, table B4). Two bytownite analyses (An_{81}, An_{85}), although not from coarser crystals, may represent incipient microphenocrysts that had nucleated before the

Table B1
LOCALITIES OF ANALYSED DOLERITE SPECIMENS

Field no. or DDH no./ depth (m)	Analysis no.	Grid ref. [EP]	Collar R.L. (m)	Sample R.L. (m)	Base of sheet R.L. (m)	Sample height above base (m)	Description
DDH 6/129·5	783469	86198858	739·8	610·3	610·3	0·1	lower chilled margin
DDH71/182.....	831456	92918605	653·9	471·9	419·6	52·3	fine-grained late dyke
DDH68/451·96	831455	92068791	779·1	327·1	326·5	0·6	near lower chilled margin
DDH68/361·95	831454			417·2		90·7	coarse grained (mafic) dolerite
DDH68/214·8	831453			564·3		237·8	medium-grained (normal) dolerite
DDH68/58·7	831452			720		393·9	medium-grained (normal) dolerite
M364.....	831450	964872	705	705	227	478	glassy porphyritic dolerite
M363.....	831449	964872	705	705	227	478	glassy porphyritic dolerite
DDH24/385·9	783039	89318776	830·8	445	445	0	lower chilled margin, altered
DDH25/193·8	783040	88098854	784·1	590	590	0	lower chilled margin, altered
DDH26/240·8	783041	85608667	733·8	493	493	0	lower chilled margin, altered
DDH31/302·3	783042	89558874	828·9	486	486	0	lower chilled margin, altered

Drill hole survey data from Threader and Bacon (1983), surface outcrop data from C. R. Calver (pers. comm.).
All holes more-or-less vertical.

dolerite magma was emplaced and quenched. McDougall (1962) reported microlites of An_{65} and microphenocrysts of An_{85} from a similar chilled dolerite.

Zoning completely masks any correlation of plagioclase composition with height in the sheet or degree of differentiation. As the normative plagioclase (table B4) becomes only slightly more sodic with differentiation, little correlation is expected. Elsewhere in Tasmania (McDougall, 1962, 1964; Edwards, 1942) there is a slight tendency for plagioclase to become increasingly more sodic with differentiation, but cores of bytownite and calcic labradorite persist until granophyre is developed.

The K_2O content (*i.e. Or* component) increases linearly with Na_2O (*Ab* component) and nearly all analyses lie very close to the join $Ab_{95}Or_5$–An_{100}.

All analyses show low but consistent iron contents (average 0·65 as mass% FeO). This probably represents substitution in the crystal structure, but the site and valence is unknown, as is the extent of any subsolidus exsolution (*e.g.* Smith, 1974*b*. p. 108–112).

Calculation of cation numbers shows apparent cation deficiency in both the tetrahedral sites (Si + Al) and the interstitial sites (Ca + Na + K). This is common in plagioclase and cannot be

Table B2
ELECTRON PROBE MICROANALYSES OF JURASSIC DOLERITE FROM FINGAL TIER

(a) PLAGIOCLASE

	DDH68/451·96						DDH68/361·95				
	1A	1C	3C	5C	6B	6E	2B	4A	7E	7F	7G
SiO_2	53·23	53·99	49·10	48·51	51·72	53·60	53·51	56·02	59·63	52·72	47·68
Al_2O_3	29·08	28·21	31·68	32·43	29·96	28·86	29·00	27·25	24·95	29·86	33·17
Σ FeO	0·83	0·94	0·55	0·51	0·74	0·77	0·53	0·67	0·80	0·53	0·37
MgO	-	-	-	0·22	0·20	-	-	-	0·37	-	-
CaO	13·11	12·49	16·53	16·60	13·95	12·60	12·84	10·44	7·76	13·30	17·39
Na_2O	3·46	3·90	1·99	1·58	3·16	3·81	3·83	5·21	5·76	3·36	1·38
K_2O	0·29	0·36	0·15	0·15	0·26	0·36	0·29	0·41	0·74	0·23	-
Total	100·00	100·00*	100·00	100·00	99·99	100·00	100·00	100·00	100·01	100·00	99·99
Si	2·427	2·465	2·258	2·233	2·370	2·441	2·433	2·536	2·684	2·396	2·192
Al	1·563	1·518	1·717	1·759	1·618	1·549	1·554	1·454	1·324	1·600	1·798
Ca	0·641	0·611	0·815	0·819	0·685	0·615	0·626	0·506	0·374	0·648	0·857
Na	0·305	0·345	0·178	0·141	0·278	0·336	0·337	0·457	0·502	0·296	0·123
K	0·017	0·021	0·009	0·009	0·015	0·021	0·017	0·024	0·043	0·014	-
Si + Al	3·990	3·983	3·975	3·992	3·988	3·990	3·987	3·990	4·008	3·996	3·990
Ca + Na + K	0·963	0·977	1·002	0·969	0·978	0·972	0·980	0·987	0·919	0·958	0·980
Or	1·8	2·2	0·9	0·9	1·6	2·1	1·7	2·4	4·6	1·4	-
Ab	31·7	35·3	17·8	14·6	28·6	34·6	34·4	46·3	54·7	30·9	12·6
An	66·5	62·5	81·4	84·5	69·8	63·3	63·9	51·3	40·7	67·7	87·4

* includes 0·11% Cl.
Cations calculated on the basis of oxygen number (O) = 8. FeO, MgO, Cl assumed to be due to impurities.

Table B2 (continued)

(a) PLAGIOCLASE

	DDH68/214·8			DDH68/58·7					
	2C	4B	5B	5B	3A	3B	3E	4B	4C
SiO_2	47·57	47·91	47·39	51·28	48·66	50·01	48·15	50·13	53·40
Al_2O_3	32·92	32·93	32·96	30·74	32·50	31·59	32·24	31·33	29·19
Σ FeO	0·87	0·70	0·70	0·65	0·54	0·55	1·45	0·52	0·76
MgO	-	-	0·19	-	-	-	-	-	-
CaO	17·01	16·81	17·23	14·06	16·57	15·43	16·29	15·43	12·79
Na_2O	1·50	1·53	1·38	3·04	1·74	2·30	1·74	2·41	3·58
K_2O	0·14	0·13	0·14	0·23	-	0·12	0·13	0·18	0·26
Total	100·01	100·01	99·99	100·00	100·01	100·00	100·00	100·00	99·98
Si	2·199	2·207	2·192	2·343	2·234	2·290	2·233	2·297	2·431
Al	1·793	1·789	1·797	1·656	1·759	1·705	1·762	1·692	1·566
Ca	0·843	0·830	0·854	0·688	0·815	0·757	0·809	0·757	0·624
Na	0·134	0·137	0·124	0·269	0·155	0·205	0·157	0·214	0·316
K	0·008	0·007	0·008	0·014	-	0·007	0·008	0·010	0·015
Si + Al	3·992	3·996	3·989	3·999	3·993	3·995	3·995	3·989	3·997
Ca + Na + K	0·985	0·974	0·986	0·971	0·970	0·969	0·974	0·981	0·955
Or	0·9	0·7	0·8	1·4	-	0·7	0·8	1·1	1·6
Ab	13·6	14·0	12·6	27·7	16·0	21·2	16·1	21·8	33·1
An	85·6	85·2	86·6	70·9	84·0	78·1	83·1	77·1	65·3

5 cm

explained by any assumption as to the role of Fe. It probably represents either an excess Si content in the mineral as a vacancy-coupled substitution for Al, or sub-microscopic inclusions of silica.

PYROXENE

In the dolerite at Fingal Tier, as elsewhere in Tasmania, there are three types of pyroxene — orthopyroxene, pigeonite and augite. Electron microprobe analyses (table B2b–d) are plotted on to the pyroxene quadrilateral (Ca:Mg:total Fe, atomic ratios) in Figure B1.

Near the chilled margin the dolerite contains scattered micro-phenocrysts of orthopyroxene (Ofs_{15}) and rather less abundant micro-phenocrysts of magnesian augite. These microphenocrysts were probably present in the magma at the time of intrusion, indicating that it was at a temperature just below its liquidus. The very fine-grained groundmass pyroxene in the chilled dolerite is difficult to determine optically. X-ray diffraction suggests that it is entirely monoclinic, and electron microprobe analyses (table B2b) show that it is dominantly augite of composition $En_{53}Fs_{10}Wo_{37}$. However, analyses 6C and 6D are considerably less calcic, and probably represent augite finely intergrown with pigeonite of composition of about $En_{65}Fs_{26}Wo_9$. However, another possibility is that they represent homogeneous, probably metastable clinopyroxene produced by quenching of the magma.

Away from the chilled margins, the dominant pyroxenes of the dolerites are augite and pigeonite in roughly equal proportions; in thin section they can be distinguished only by the lower $2V$ of the latter. Orthopyroxene is restricted to the lower part of the sheet, probably because of rapid gravitational settling of the original microphenocrysts and any crystals formed in the early stages of cooling. Compositionally it is restricted to En 70 mole% (*i.e.* Mg >1·4 in the structural formulae). More iron-rich pyroxene crystallises as a slightly more calcic pigeonite (fig. B1). In a thin section of the medium-grained, pyroxene-rich dolerite (DDH68/361·95), orthopyroxene is frequently mantled by pigeonite, and sometimes by augite, indicating that these minerals crystallised at least mostly, if not wholly, later. McDougall (1961*b*) noted that, in the Red Hill Dyke, orthopyroxene occurs both as a primary phase and as a secondary inversion product of early-formed magnesian pigeonite. Although this latter process cannot be said to be definitely absent at Fingal Tier, there is no textural evidence, such as the presence of augite lamellae, in these samples. Exsolution lamellae, like those reported by McDougall (1961*b*, p. 680–681) and Edwards (1942, p. 584, 587), are here also rare in augite and pigeonite, particularly in the upper part of the sheet, suggesting perhaps a more rapid rate of cooling.

Both clinopyroxenes tend to become more iron-rich with increasing height in the sheet, reflecting a trend common to many tholeiitic intrusions

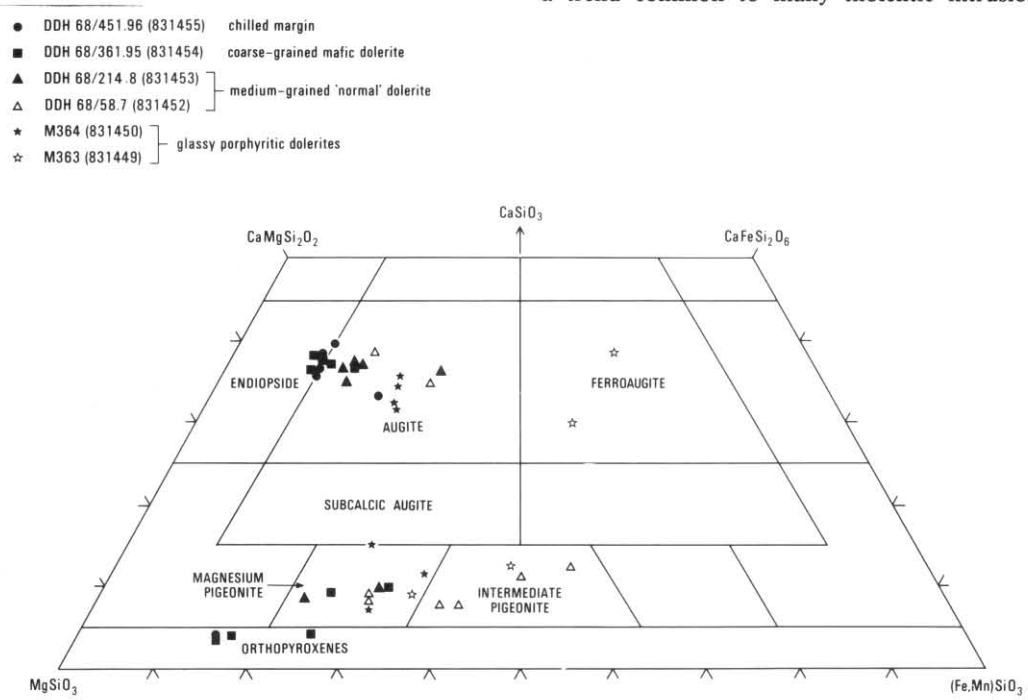

Figure B1. *Electron probe microanalyses of pyroxenes from Jurassic dolerite, Fingal Tier, plotted on the pyroxene quadrilateral (Ca:Mg:total Fe+Mn, atomic ratios).*

(fig. B1). This is most marked in the case of pigeonite, but at Fingal Tier the 'two-pyroxene field boundary', beyond which it is replaced by fayalitic olivine, was not attained; pigeonite occurs even in the most differentiated sample (M363). In the early and middle stages of differentiation, iron-enrichment in augite is less marked and ferroaugite is restricted to crystal rims and needles surrounded by black glass in sample M363.

In thin section both pigeonite and augite often show zoning, although it is much less extreme than in plagioclase. Electron probe microanalyses of a pigeonite from sample DDH68/58·7 show reverse zoning, with a rim more magnesian than the core. As discussed later, this could be produced by crystals sinking through a compositionally layered, cooling sill.

Table B2 (continued)

	(a) PLAGIOCLASE							
	M364					M363		
	1A	1B	4A	4B	6B	3A	3B	3C
SiO_2	53·08	52·09	53·29	53·31	55·23	49·43	53·47	50·22
Al_2O_3	29·46	29·96	29·26	29·27	28·00	31·89	29·17	31·38
Σ FeO	0·59	0·73	0·59	0·60	0·54	0·55	0·68	0·50
MgO	-	-	-	-	-	-	-	-
CaO	13·38	13·84	13·04	13·03	11·54	15·93	12·88	15·26
Na_2O	3·33	3·16	3·54	3·55	4·31	2·06	3·59	1·96
K_2O	0·17	0·21	0·27	0·24	0·38	0·14	0·21	0·68
Total	100·01	99·99	99·99	100·00	100·00	100·00	100·00	100·00
Si	2·414	2·392	2·424	2·424	2·500	2·268	2·432	2·301
Al	1·579	1·951	1·569	1·569	1·494	1·724	1·563	1·694
Ca	0·652	0·681	0·635	0·635	0·560	0·783	0·627	0·749
Na	0·293	0·282	0·313	0·313	0·378	0·183	0·316	0·175
K	0·010	0·012	0·016	0·014	0·022	0·008	0·012	0·040
Si + Al	3·993	3·983	3·993	3·993	3·994	3·992	3·995	3·995
Ca + Na + K	0·995	0·975	0·964	0·962	0·960	0·974	0·955	0·964
Or	1·1	1·3	1·6	1·5	2·3	0·8	1·3	4·1
Ab	30·7	28·9	32·4	32·5	39·4	18·8	33·1	18·1
An	68·2	69·8	65·9	66·0	58·3	80·3	65·6	77·8

M364/6B—large (1·5 mm) broadly oblong euhedron surrounded by black glass.
M363/3A, 3C—cores of zoned subhedral crystals; 3B - rim.

Table B2 (continued)

	(a) AUGITE DDH68/451·96							
	1B	1E	3A	3B	6A	6C	6D	6F
SiO_2	53·75	52·80	53·56	53·75	53·64	53·92	53·54	53·23
TiO_2	-	-	-	-	-	-	-	-
Al_2O_3	1·71	1·96	1·35	1·79	1·63	0·92	1·11	1·93
Cr_2O_3	-	-	0·25	0·28	0·38	-	-	0·41
Σ FeO	6·34	11·13	5·98	6·29	6·12	9·97	14·18	6·32
MnO	-	-	-	-	-	-	-	-
MgO	17·89	17·00	18·66	18·89	19·32	20·93	22·74	19·51
CaO	19·51	16·00	18·75	18·29	18·91	14·26	8·44	18·60
Na_2O	0·69	0·45	1·19	0·70	-	-	-	-
K_2O	0·11	-	-	-	-	-	-	-
Cl	-	0·65	-	-	-	-	-	-
SO_3	-	-	0·25	-	-	-	-	-
Total	100·00	99·99	99·99	99·99	100·00	100·00	100·01	100·00
Si	1·995	1·927	1·938	1·947	1·950	1·964	1·953	1·933
Al	0·073	0·057	0·058	0·076	0·076	0·040	0·047	0·083
Cr	-	-	0·007	0·008	0·011	-	-	0·012
Ti	-	-	-	-	-	-	-	-
Fe^{III}	0·066	0·123	0·143	0·072	0·019	0·032	0·046	0·038
Fe^{II}	0·127	0·234	0·038	0·119	0·167	0·271	0·387	0·154
Mn	-	-	-	-	-	-	-	-
Mg	0·970	0·970	1·006	1·019	1·047	1·136	1·237	1·056
Ca	0·760	0·656	0·727	0·710	0·737	0·556	0·330	0·724
Na	0·049	0·033	0·083	0·049	-	-	-	-
100 Mg/Mg + Fe + Mn	83·4	73·1	84·8	84·3	84·9	78·9	74·1	84·6

Cations calculated on the basis of cation total (Z) = 4, oxygen number (O) = 6.
DDH68/451.96/1B, 1E, 3A, 3B—microphenocrysts, 3A and 3B from some grain. SO_3 and Cl assumed to be impurities, K_2O removed as $KAlSi_3O_8$. Na_2O probably spurious, possibly feldspar or fingerprint contamination.
DDH68/451.96/6—fine pyroxene from mesostasis. 6C and 6D probably intergrown with pigeonite (see text).

Pigeonite and augite are frequently intergrown, and augite sometimes mantles pigeonite, although the reverse was not observed. Thus the two minerals crystallised at about the same time, with augite perhaps tending to form a little later.

Twinning is common in both augite and pigeonite.

The Al_2O_3 content of augite (average 1·46%) is consistently higher than in pigeonite (average 0·83%), and in both minerals remains roughly constant with differentiation. However, MnO and TiO_2 appear to be correlated with FeO and are detectable in pyroxene, particularly pigeonite which generally contains more iron than augite, from the more differentiated samples higher in the sheet. On the other hand, Cr_2O_3 is detectable

Table B2 (continued)

	(b) AUGITE									
	DDH68/361·95						DDH68/214·8			
	2E	5	7A	7B	7C	1	2A	2B	2D	4A
SiO_2	53·49	53·53	53·88	53·93	53·41	53·93	53·42	53·75	51·68	53·31
TiO_2	-	-	-	-	-	-	-	-	0·34	-
Al_2O_3	1·68	1·33	1·49	1·51	1·76	1·37	1·41	1·30	1·28	1·31
Cr_2O_3	-	-	0·37	0·31	0·35	-	-	-	-	-
Σ FeO	6·99	8·56	6·01	5·93	6·40	7·86	8·64	8·73	14·55	9·06
MnO	-	-	-	-	-	-	-	-	-	-
MgO	19·05	18·05	19·58	19·23	19·24	18·35	17·83	18·50	14·39	17·61
CaO	18·79	18·53	18·67	19·08	18·85	18·49	18·70	17·73	17·76	18·71
Na_2O	-	-	-	-	-	-	-	-	-	-
Other	-	-	-	-	-	-	-	-	-	-
Total	100·00	100·00	100·00	99·99	100·01	100·00	100·00	100·01	100·00	100·00
Si	1·948	1·964	1·957	1·961	1·943	1·974	1·962	1·970	1·949	1·961
Al	0·072	0·057	0·064	0·064	0·075	0·059	0·061	0·056	0·057	0·057
Cr	-	-	0·011	0·009	0·010	-	-	-	-	-
Ti	-	-	-	-	-	-	-	-	0·010	-
Fe^{III}	0·032	0·015	0·012	0·005	0·030	-	0·016	0·004	0·026	0·021
Fe^{II}	0·181	0·248	0·170	0·175	0·165	0·241	0·250	0·263	0·432	0·258
Mn	-	-	-	-	-	-	-	-	-	-
Mg	1·034	0·987	1·060	1·042	1·043	1·001	0·976	1·011	0·808	0·966
Ca	0·733	0·728	0·727	0·743	0·734	0·725	0·736	0·696	0·718	0·738
Na	-	-	-	-	-	-	-	-	-	-
100 Mg/Mg + Fe + Mn	82·9	79·0	85·3	85·2	84·3	80·6	78·6	79·1	63·8	77·6

DDH68/361.95/5 encloses orthopyroxene crystal (4A), boundary irregular.

Table B2 (continued)

	(b) AUGITE							
	DDH68/58·7		M364				M363	
	1	2C	3B	3D	3E	4D	4	6B
SiO_2	53·24	52·02	52·59	52·94	52·66	52·75	48·08	49·64
TiO_2	-	0·28	0·18	-	-	0·18	1·09	0·49
Al_2O_3	1·37	1·31	1·27	1·16	1·08	1·12	2·34	1·20
Cr_2O_3	-	-	-	-	-	-	-	-
Σ FeO	9·59	14·02	12·18	12·43	12·66	13·09	23·93	24·01
MnO	-	0·28	-	-	0·24	-	0·27	0·43
MgO	16·69	14·96	16·16	16·46	17·14	17·02	6·75	10·17
CaO	19·10	17·00	17·62	17·01	16·21	15·85	17·55	14·06
Na_2O	-	-	-	-	-	-	-	-
K_2O	-	0·12	-	-	-	-	-	-
Total	99·99	99·99	100·00	100·00	99·99	100·01	100·01	100·00
Si	1·968	1·952	1·959	1·970	1·957	1·968	1·909	1·945
Al	0·060	0·052	0·056	0·051	0·047	0·049	0·109	0·055
Cr	-	-	-	-	-	-	-	-
Ti	-	0·008	0·005	-	-	0·005	0·032	0·014
Fe^{III}	0·004	0·027	0·016	0·008	0·039	0·015	0·008	0·026
Fe^{II}	0·292	0·417	0·364	0·379	0·354	0·392	0·786	0·761
Mn	-	0·009	-	-	0·008	-	0·009	0·014
Mg	0·919	0·845	0·897	0·913	0·949	0·944	0·399	0·594
Ca	0·756	0·690	0·703	0·678	0·645	0·632	0·747	0·590
Na	-	-	-	-	-	-	-	-
100 Mg/Mg + Fe + Mn	75·6	65·1	70·3	70·2	70·3	69·9	33·2	42·6

M364/4D—partially mantles pigeonite (4C). Both pyroxenes go to optical extinction together.
M363/4—parallel needles (*c.* 30 μm x 1 mm) in black glass.
M363/6B—rim irregularly mantling pigeonite (6A) and surrounded by black glass.

only in early magnesian orthopyroxene and augite from the lower part of the sheet. As discussed below, it is strongly partitioned into pyroxene and becomes rapidly depleted in the liquid phase during differentiation.

The general characteristics and chemistry of pyroxene from the dolerite sill at Fingal Tier closely parallel, in nearly all respects, those reported from dolerite of Red Hill Dyke (McDougall, 1961*b*), the Great Lake sill (McDougall, 1964) and from elsewhere in Tasmania (Edwards, 1942). This illustrates the geographic uniformity of the Tasmanian dolerite and the quality of this early work, performed by classical analytical methods.

OTHER MINERALS

Alkali feldspar and quartz are present in the mesostasis of all holocrystalline samples. A single electron microanalysis (table B2e) from chilled dolerite near the lower margin of the sill (DDH68/451·96) suggests an alkali feldspar composition of about $Or_{76}Ab_{21}An_3$. X-ray diffraction shows that quartz steadily increases in abundance with mafic index ($FeO + Fe_2O_3/MgO + FeO + Fe_2O_3$) from cumulate dolerites (DDH68/451·96) through the chilled margin to the differentiated dolerite (DDH68/58·7) but is absent in glassy dolerite (M364 and M363) which does not have a well-crystallised mesostasis.

Table B2 (continued)

	(c) PIGEONITE									
	DDH68/361·9		DDH68/214·8				DDH68/58·7			
	1B	2C	3	5A	2A	2B	3C (rim)	3D (core)	4A	5C
SiO_2	53·76	52·49	54·77	52·72	51·91	53·29	53·23	50·59	49·77	52·16
TiO_2	-	0·26	-	-	0·18	-	-	0·28	0·36	-
Al_2O_3	0·76	0·99	0·68	1·68	0·72	0·69	0·77	0·87	0·85	0·62
Σ FeO	15·97	19·28	14·62	18·67	24·26	18·77	18·43	26·96	29·44	23·14
MnO	0·26	0·28	-	0·32	0·38	0·28	0·28	0·54	0·56	0·48
MgO	24·51	21·75	25·48	21·76	18·73	22·65	22·39	15·32	13·17	19·69
CaO	4·74	4·96	4·45	4·85	3·83	4·32	4·89	5·43	5·85	3·92
Total	100·00	100·01	100·00	100·00	100·01	100·00	99·99	99·99	100·00	100·01
Si	1·958	1·945	1·982	1·949	1·968	1·966	1·964	1·955	1·951	1·965
Al	0·033	0·043	0·029	0·073	0·032	0·030	0·033	0·040	0·039	0·028
Ti	-	0·007	-	-	0·005	-	-	0·008	0·011	-
Fe^{III}	0·052	0·052	0·007	0·030	0·022	0·038	0·038	0·033	0·037	0·043
Fe^{II}	0·435	0·545	0·435	0·548	0·747	0·541	0·531	0·839	0·928	0·686
Mn	0·008	0·009	-	0·010	0·012	0·009	0·009	0·018	0·019	0·015
Mg	1·330	1·202	1·374	1·199	1·058	1·245	1·232	0·883	0·770	1·105
Ca	0·185	0·197	0·173	0·192	0·155	0·171	0·193	0·225	0·246	0·158
100 Mg/Mg + Fe + Mn	72·9	66·5	75·6	67·1	57·5	67·9	68·1	49·8	43·9	59·8

Cations calculated on the basis of cation total (Z) = 4 and oxygen number (O) = 6
DDH68/361·95/1B encloses orthopyroxene crystal (1A).

Table B2 (continued)

	(c) PIGEONITE					
	M364				M363	
	2	3A	3C	4C	1	6A
SiO_2	53·32	53·38	53·34	52·11	52·69	50·87
TiO_2	-	-	-	0·18	-	0·25
Al_2O_3	0·88	0·63	0·73	0·79	0·74	0·80
Σ FeO	16·98	19·13	18·42	21·21	21·25	25·92
MnO	-	0·35	0·36	0·29	0·30	0·46
MgO	21·36	22·95	22·40	19·62	20·46	15·64
CaO	7·47	3·57	4·74	5·80	4·55	6·06
Total	100·01	100·01	99·99	100·00	99·99	100·00
Si	1·968	1·969	1·969	1·955	1·970	1·959
Al	0·038	0·027	0·032	0·035	0·033	0·036
Ti	-	-	-	0·005	-	0·007
Fe^{III}	0·026	0·035	0·031	0·045	0·027	0·031
Fe^{II}	0·498	0·555	0·537	0·621	0·638	0·804
Mn	-	0·011	0·011	0·009	0·010	0·015
Mg	1·175	1·262	1·232	1·097	1·140	0·898
Ca	0·295	0·141	0·187	0·233	0·182	0·250
100Mg/Mg + Fe + Mn	69·2	67·7	68·0	61·9	62·8	51·4

Notes: M364/4C: partly mantled by augite (4D). Both pyroxenes go to optical extinction together.
M363/6A: zoned, and irregularly mantled by augite (6B), which is in turn surrounded by black glass.

Table B2 (continued)

	(e) MESOSTASIS AND GLASS					
	DDH68/ 451·96	DDH68/361·95		M364		M363
	1D	2D	4C	5	6	2
SiO_2	82·33	56·49	60·47	68·74	67·84	66·89
TiO_2	-	0·50	-	0·87	0·79	1·07
Al_2O_3	9·01	14·95	16·68	11·88	12·33	12·23
Σ FeO	0·48	10·24	6·13	8·85	8·48	9·10
MnO	-	-	-	-	-	-
MgO	-	6·68	4·24	0·23	0·34	0·48
CaO	0·32	0·58	0·50	3·76	3·64	4·22
Na_2O	1·17	2·92	2·99	3·19	3·10	3·47
K_2O	6·48	7·31	8·75	1·83	2·76	1·53
P_2O_5	-	-	-	0·32	0·33	0·33
SO_3	0·22	0·33	0·24	0·21	0·25	0·59
Cl	-	-	-	0·11	0·14	0·10
Total	100·01	100·00	100·00	99·99	100·00	100·01
Original total	95·29	86·37	96·93	94·49	95·81	75·90

DDH68/451·96/1D: alkali feldspar rich domain of mesostasis. Approximately 51% quartz, 49% alkali feldspar ($Or_{76}Ab_{21}An_3$).
DDH68/361·95/2D,4C: minor interstitial brown alteration, possibly devitrified glass.
M364/5,6: abundant black glass
M363: abundant black glass

Table B3
CHEMICAL ANALYSES OF JURASSIC DOLERITE, ST MARYS QUADRANGLE
(mass%)

Field or hole no.	DDH6	DDH68	DDH68	DDH71	DH68	DDH68	M364	M363	
Depth (m)	129	361·95	451·96	182·0	214·8	58·7			
Analysis no.	6	783469	831454	831455	831456	831453	831452	831450	831449
SiO_2	52·50	52·4	53·21	53·45	52·75	53·71	54·38	54·64	54·81
TiO_2	0·60	0·65	0·45	0·63	0·62	0·65	0·68	0·73	0·78
Al_2O_3	14·30	15·0	13·43	14·56	14·79	15·41	15·51	15·39	15·91
Fe_2O_3	0·15	2·9	1·63	3·04	1·86	2·22	2·93	1·42	1·58
FeO	8·63	6·5	6·74	6·50	7·62	6·97	6·66	8·68	8·39
MnO	0·11	0·21	0·16	0·16	0·16	0·16	0·16	0·17	0·16
MgO	7·15	6·7	8·86	5·77	5·70	4·97	4·12	3·48	3·11
CaO	10·55	11·0	11·08	10·18	11·01	10·82	10·46	10·01	10·12
Na_2O	1·82	1··	1·39	1·57	1·57	1·86	1·73	1·81	1·93
K_2O	1·15	0·81	0·56	0·87	0·80	0·89	0·98	0·77	0·66
P_2O_5	0·02	0·14	0·07	0·10	0·09	0·10	0·11	0·10	0·12
H_2O^+	1·46	0·84	1·15	1·33	0·94	1·19	1·19	1·94	1·84
H_2O^-	1·25	0·56	0·45	1·07	1·04	0·43	0·96	0·85	0·87
CO_2	-	0·30	0·05	0·26	0·11	0·11	0·09	0·03	0·06
SO_3	nd	0·08	0·09	0·10	0·08	0·09	0·10	0·12	0·12
Traces as oxides	nd	0·16	0·17	0·16	0·15	0·14	0·14	0·14	0·16
Total	99·69	100·0	99·49	99·75	99·29	99·72	100·20	100·28	100·62
Trace elements (ppm)									
Li	nd	6	nd	nd	nd	nd	nd	nd	nd
Sc	nd	32	37	36	43	39	39	40	36
V	nd	278	200	220	220	200	210	210	210
Cr	nd	130	380	130	140	65	32	19	63
Co	nd	42	44	39	37	38	40	33	33
Ni	nd	104	135	75	79	66	50	39	37
Cu	nd	94	44	72	73	74	78	98	99
Zn	nd	nd	65	87	88	81	85	95	127
Ga	nd	nd	11	15	15	15	18	17	17
Rb	nd	23	25	35	33	38	41	41	49
Sr	nd	119	105	145	130	115	125	135	145
Y	nd	22	15	22	21	21	25	26	26
Zr	nd	108	56	91	92	94	105	115	125
Nb	nd	6	3	3	3	3	3	4	3
Ba	nd	278	130	230	165	210	200	250	270
Pb	nd	nd	4	8	7	8	14	15	40

Analysis 6 from chilled base, eastern end of Mt Nicholas Range (Edwards, 1942), remaining analyses from Fingal Tier, previously unpublished.

Table B4
CIPW NORMS OF JURASSIC DOLERITE

Analysis no.	6	783469	831454	831455	831456	831453	831452	831450	831449
Q	4·10	5·31	6·53	9·42	7·89	8·30	10·78	12·48	12·68
or	7·00	4·90	3·40	5·32	4·89	5·39	5·94	4·70	4·01
ab	15·86	14·69	12·04	13·72	13·69	16·10	14·99	15·74	16·72
an	28·28	31·56	29·45	31·14	31·91	31·79	32·44	32·48	33·61
di	20·85	19·13	21·45	16·91	19·71	18·67	16·74	15·14	14·45
hy	20·95	20·90	24·32	20·05	18·53	16·38	15·59	15·71	14·67
mt	1·73	1·79	1·61	1·83	1·83	1·76	1·82	1·96	1·93
il	1·17	1·27	0·87	1·24	1·22	1·27	1·32	1·43	1·52
ap	0·05	0·34	0·17	0·25	0·22	0·25	0·27	0·25	0·29
Z,cm,py	-	0·11	0·16	0·12	0·11	0·10	0·10	0·12	0·13
Total	99·99	100·00	100·00	100·00	100·00	100·01	99·99	100·01	100·01
mol% An,plag.	62·69	66·94	69·73	68·11	68·70	65·04	67·08	66·03	65·43
(100Mg/Mg+Fe)px	65·30	62·84	71·08	59·08	58·57	56·23	50·72	44·83	42·64
Calculated assuming $Fe_2O_3/FeO = 0·15$; Sr and Ba distributed to an, Rb to or, Ni with Mg, Mn with Fe.									
CHEMICAL PARAMETERS									
Mafic index	55·1	58·4	48·6	62·3	62·5	64·9	69·9	74·4	76·6
Felsic index	22·0	18·6	15·0	19·3	17·3	20·3	20·6	20·5	20·4
$100Mg/Mg+Fe^{II}$ (a)	59·6	64·8	70·1	61·3	57·1	56·0	52·4	41·7	39·8
(b)	62·3	59·8	68·6	55·8	55·4	52·9	47·3	41·4	39·1
(c)	59·3	56·7	65·8	52·7	52·2	49·7	44·1	38·4	36·1
Al_2O_3/CaO	1·36	1·36	1·21	1·43	1·34	1·42	1·48	1·54	1·57
K_2O/Na_2O	0·63	0·48	0·40	0·55	0·51	0·48	0·57	0·43	0·34
K/Rb	-	292	156	206	201	194	198	156	112
K/Zr	-	62·3	83·0	79·4	72·2	78·6	77·5	55·6	43·8
Rb/Sr	-	0·193	0·238	0·241	0·254	0·330	0·328	0·304	0·338
Ti/Zr	-	36·1	48·2	41·5	40·4	41·5	38·8	46·1	37·4
Zr/Y	-	4·91	3·73	4·14	4·38	4·48	4·20	4·42	4·81
Zr/P_2O_5	-	0·077	0·080	0·091	0·102	0·094	0·095	0·115	0·104

Mafic index = 100 $(Fe_2O_3/FeO+Fe_2O_3+MgO)$. Felsic index = 100 $(Na_2O+K_2O/Na_2O+K_2O+CaO)$.
(a) as analysed; (b) assuming $Fe_2O_3/FeO = 0·15$; (c) all iron calculated as Fe^{II}.
100 $Mg/Mg+Fe^{II}$ calculated as atomic proportions, all other ratios on a mass basis.

Opaque minerals are scarce and fine grained, but gradually increase in abundance and grain size with differentiation; their mineralogy has not been investigated in this study. Other accessory minerals, including apatite and zircon, are rare.

CHILLED MARGINS

GENERAL ASPECTS

Chilled dolerite from within a few centimetres of the contact of a sill or dyke usually represents the initial composition of the magma, provided that it was homogeneous at the time of intrusion, since rapid cooling would probably cause solidification before crystal settling or other mechanisms of *in situ* differentiation could take place. Chilled dolerite from Fingal Tier and the Nicholas Range (Edwards, 1942) is very similar in composition to chilled dolerite from localities elsewhere in Tasmania apart from slight oxidation, probably a result of weathering, reflected in the Fe_2O_3/FeO ratio (tables B2, B5). Trace elements are also very similar to those of the only available, substantially complete other analysis, previously unpublished, from Margate (P. L. F. Collins, 1978 *pers. comm.*).

COMPARISON WITH ANTARCTIC FERRAR DOLERITES

Since Australian and Antarctica were part of a single continent from before the Cambrian until the Eocene, with Tasmania juxtaposed against North Victoria Land (*e.g.* Griffiths, 1971; Solomon and Griffiths, 1972; Laird, Cooper and Jago, 1977), the Tasmanian Jurassic dolerite and the comparable Jurassic Ferrar dolerite of Antarctica (Compston *et al.*, 1968) can be considered as a single province. The Ferrar dolerite crops out semi-continuously in a belt 4700 km long and 25 km wide across Antarctica (Gunn, 1962, 1966) and has a volume of at least 100 000 km³ (Kyle, 1980), together with the related Dufek intrusion of 300 000 km³ (Ford *et al.*, 1977), compared to an estimate of 12 000 km³ for the Tasmanian dolerite (Veevers, 1976).

Three types of Ferrar dolerite have been distinguished (Gunn, 1966). The Youngest, hypersthene tholeiite, usually occurs as flat-lying sheets in the folded Precambrian to mid-Cambrian of the Ross System. They are composed of pigeonite dolerite, but with a central, very mafic zone of hypersthene gabbro ('norite zone') which was probably intruded slightly later as a genetically related, hypersthene-rich mush. The second type, pigeonite tholeiite, is more voluminous and occurs as sheets or sills at or above the early Palaeozoic Kukri peneplain, the unconformity between the basement and the flat overlying sediments of the Beacon Group. The pigeonite tholeiite sills show relatively little

Table B5
OTHER ANALYSES OF CHILLED DOLERITE

Hole no.	24	25	26	31	NF87
Analysis no.	783039	783040	783041	783042	783468
SiO_2	45·9	50·8	38·1	44·2	53·8
TiO_2	0·64	0·72	0·68	0·71	0·62
Al_2O_3	15·9	15·9	15·6	15·8	14·4
Fe_2O_3	2·6	4·6	3·1	5·0	0·85
FeO	7·6	4·3	6·1	4·0	8·2
MnO	0·35	0·17	0·27	0·32	0·17
MgO	6·0	5·6	5·2	5·7	7·2
CaO	7·9	7·7	13·9	11·9	10·9
Na_2O	2·2	1·7	2·1	1·7	1·8
K_2O	0·69	0·79	0·69	0·77	0·69
P_2O_5	0·07	0·08	0·08	0·08	0·08
H_2O^+	7·0	4·1	4·4	5·4	1·5
H_2O^-	1·8	2·5	1·6	2·5	0·23
CO_2	1·3	0·43	8·1	1·5	0·22
SO_3	nd	nd	nd	nd	0·07
Traces as oxides	0·17	0·16	0·17	0·17	0·16
Total	100·1	99·6	100·1	99·8	100·9
Li	29	10	25	11	10
Sc	39	39	35	34	35
V	278	271	272	273	252
Cr	139	131	137	131	171
Co	28	44	40	48	37
Ni	79	90	75	82	99
Cu	92	103	85	114	99
Zn	nd	nd	nd	nd	nd
Ga	nd	nd	nd	nd	nd
Rb	28	24	20	22	31
Sr	122	165	172	172	101
Y	21	21	32	23	22
Zr	109	108	102	102	108
Nb	5	5	9	5	6
Ba	343	255	310	300	209
Pb	nd	nd	nd	nd	nd

Analyses 783039–783042 from lower contacts, Fingal Tier; very altered.
Analysis 783468 from upper contact, Margate, Kingborough Quadrangle [EN 212363], per P. L. F. Collins.

internal variation, and each was probably intruded as a single homogeneous magma. The third type, olivine tholeiite, is the most mafic and the least abundant.

Based on the major and trace element chemistry of the chilled margins (particularly SiO_2, MgO, Na_2O, K_2O, Cr and Ni), the Tasmanian dolerite is very similar to the hypersthene tholeiite of Antarctica, and differs from both the pigeonite and olivine tholeiites (table B6). However, in Tasmania evidence for multiple intrusion or magma inhomogeneity is lacking, (except for a minor degree, represented by late stage dykes) and no central mafic zones of hypersthene gabbro ('norite zones'), like those found in Antarctica, are known. As discussed below, fractional crystallisation can account for essentially all the observed chemical variation in Tasmanian dolerite.

In Antarctica, lavas and pyroclastic rocks related to the Ferrar dolerite occur locally (Gunn, 1962), but none are known associated with the Tasmanian dolerite. However, any extruded in Tasmania would have been highly susceptible to erosion.

Sutherland (1966) commented that dolerite sills were more extensive and sill horizons more numerous in Antarctica, and attributed the more frequently transgressive dolerite structures in Tasmania to a more uneven, faulted and folded basement.

As Jurassic dolerite does not occur on the Australian mainland or on the Bass Strait Islands, the Tasmanian dolerite should be considered as a small fragment from the extreme tip of the Antarctic Ferrar dolerite province.

PETROGENESIS

The Tasmanian Jurassic dolerite is a quartz normative tholeiite (table B4). Characteristically tholeiitic features of its chemistry are relatively low total alkali content, the presence of both calcium-rich and calcium-poor pyroxene in both norms and modes, and the Zr/P_2O_5 and Nb/Y ratios (fig. A3). However, on the TiZrY diagram of Pearce and Cann (1973) they plot anomalously, outside the 'within-plate-basalt' field (fig. A7). This is a feature shared by many continental tholeiites, including the Antarctic Ferrar dolerites (Holm, 1982) and may be an important, petrogenetically significant characteristic related to its tectonic setting.

Heier *et al.* (1965) showed that Tasmanian Jurassic dolerite has anomalously high Th/K, U/K and initial $^{87}Sr/^{86}Sr$ ratios, and anomalously low K/Rb, more characteristic of acidic crustal rocks such as granite, than basalt derived from the upper mantle. Compston *et al.* (1968) showed that these features extended to the Antarctic Ferrar dolerite, but not to the Mesozoic tholeiites of South Africa and South America.

Th, U and Rb are all incompatible, or large-ion lithophile (LIL) elements which are not readily incorporated into early-crystallising minerals such as olivine or pyroxene. The present data shows that, whilst Li may also be anomalous, other incompatible or LIL elements such as Sr, Zr and Nb have abundances typical of many tholeiitic basaltic rocks.

The petrogenesis of the Tasmanian and Antarctic dolerite is a fundamental problem in petrology and is reviewed only briefly here. Despite the paucity of previously published trace element data (McDougall and Lovering, 1963; Heier *et al*, 1965; Compston *et al.*, 1968; Tiller, 1959) the present data does little to clarify the problem.

Heier *et al.* (1965) suggested that the crustal chemical features of the dolerite reflected an unusual composition of the mantle beneath Tasmania; if they are the result of crustal contamination, it was thought more likely to have occurred by selective diffusion of certain

Table B6
GEOCHEMICAL COMPARISON OF CHILLED MARGINS, TASMANIAN AND ANTARCTIC DOLERITES

	Tasmanian dolerites					Antarctic (Ferrar) dolerites			
	783469	783468	M200	M172	Average	26902	4012	(2)	4174
SiO_2	....	....	....	....	53·85	51·13	54·17	54·60	56·93
TiO_2	....	....	....	....	0·65	0·45	0·65	0·66	1·01
Al_2O_3	15·47	....	....	....	....	15·73	14·94	15·36	14·24
FeO	....	....	....	....	9·14	8·85	9·37	9·38	10·54
MnO	....	....	....	....	0·16	0·17	0·19	0·15	0·19
MgO	....	....	....	....	6·84	10·75	7·31	6·42	4·54
CaO	....	....	....	....	1·17	11·03	10·81	11·19	8·70
Na_2O	....	....	....	....	0·69	1·44	1·61	1·63	2·32
K_2O	....	....	....	....	0·93	0·38	0·76	0·53	1·29
P_2O_5	....	....	....	....	0·10	0·08	0·20	0·08	0·22
Total	....	....	....	....	100·00	100·01	100·01	100·00	99·98
Sc	32	35	nd	nd	....	30	38	nd	41
V	278	252	nd	nd	....	126	175	207	210
Cr	130	171	145	158	....	352	142	126	59
Co	42	37	47	47....		62	60	nd	62
Ni	104	99	95	92	....	249	85	68	53
Cu	94	99	80	75	....	69	118	85	123
Zn	[80]	nd	nd	nd	....	65	99	75	104
Rb	23	31	nd	33	....	12	30	21	50
Sr	119	101	nd	130	....	100	126	132	138
Y	22	22	nd	nd	....	nd	nd	25	nd
Zr	108	108	nd	nd	....	53	83	66	157
Ba	278	209	nd	nd	....	157	232	nd	376
Th	nd	nd	3·2	3·3	....	nd	4·2	2	5·6
U	nd	nd	0·83	0·84	....	1·20	1·70	nd	nd

783469: Fingal Tier (see Table B3). Zn interpolated from Figure B3g.
783468: Margate (see Table B5).
M200, M172: Longley; Red Hill Dyke (McDougall, 1962).
Average: average of 17 analyses of chilled margins (Edwards, 1942; McDougall, 1962, 1964; Spry, 1958*b*, this study).
26903: lower contact of olivine tholeiite, Painted Cliff Sill (Gunn, 1966).
4012: upper aphyric contact, hypersthene tholeiite, Lake Vanda sill (Gunn, 1966).
(2): average of 4 analyses from lower contact of hypersthene tholeiite sills, Warren Range, South Victoria Land (Kyle, 1980).
4174: lower contact of pigeonite tholeiite, New Mountain Sill (Gunn, 1962).

elements into the magma, rather than bulk assimilation of continental crust. Compston *et al.* (1968) considered the possibility of contamination by assimilation of 10–30% of average continental crust, or possibly a smaller proportion of more granitic material. Faure *et al.* (1974) favoured assimilation to account for major element and $^{87}Sr/^{86}Sr$ variations in the Jurassic Kirkpatrick Basalt, an extrusive phase related to the Ferrar dolerite, and attempted to estimate the composition of the contaminant.

Kyle (1980) showed that crystal fractionation could account for chemical differences between various phases of the Ferrar dolerite with the olivine tholeiites being the most primitive. He argued against wholesale crustal assimilation, principally on grounds of the regional uniformity of their initial $^{87}Sr/^{86}Sr$ ratios, the concordance of $^{87}Sr/^{86}Sr$ with Rb/Sr, the absence of any granitic xenoliths and the large amounts of superheat required to assimilate material. He considered that selective contamination was a possibility, but that diffusion was too slow to be a viable mechanism, and that a fluid phase enriched in ^{87}Sr and incompatible elements would be necessary as a transport medium. The most likely explanation for the anomalous crustal features of the dolerites, according to Kyle, is that they are derived from a sub-continental mantle that has been enriched in incompatible elements by metasomatism from the underlying asthenosphere or mesosphere, either as a steady state process or as a shorter event. Possibly this is related to the evolution of the continental crust itself. Anomalous but variable $^{87}Sr/^{86}Sr$, Th and U values were reported in some Tasmanian Tertiary basalts by Compston *et al.* (1968), but more data on both the Jurassic dolerite and other Tasmanian basaltic rocks might be useful in evaluating this hypothesis.

DIFFERENTIATION

MAJOR ELEMENTS

The differentiation trend shown by major elements in the dolerite at Fingal Tier closely parallels that elsewhere in Tasmania (Edwards, 1942; McDougall, 1962, 1964; Joplin, 1963) and likewise is due to the gravitational fractionation of crystals from an initially homogeneous magma, its composition represented by the

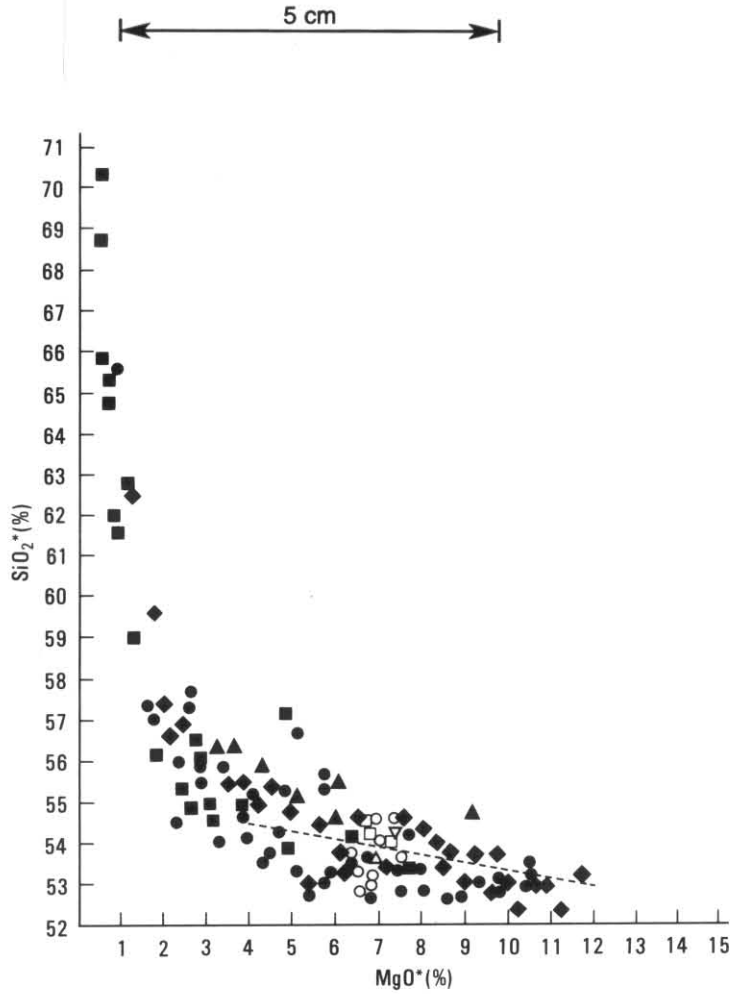
5 cm
SiO_2^*(%)
MgO*(%)

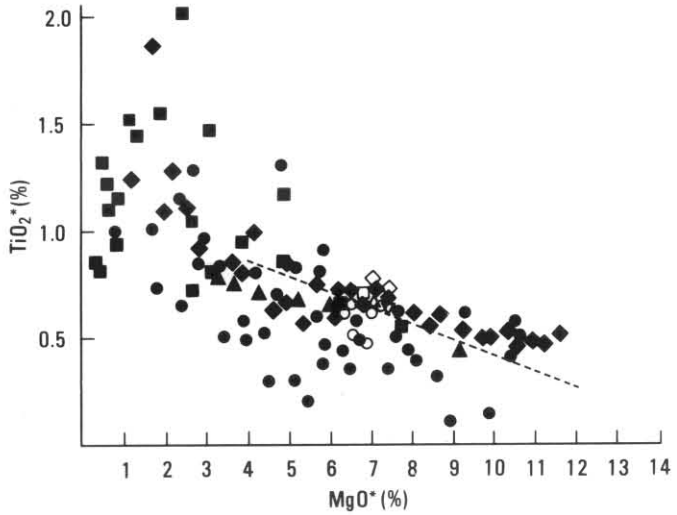
TiO_2^*(%)
MgO*(%)

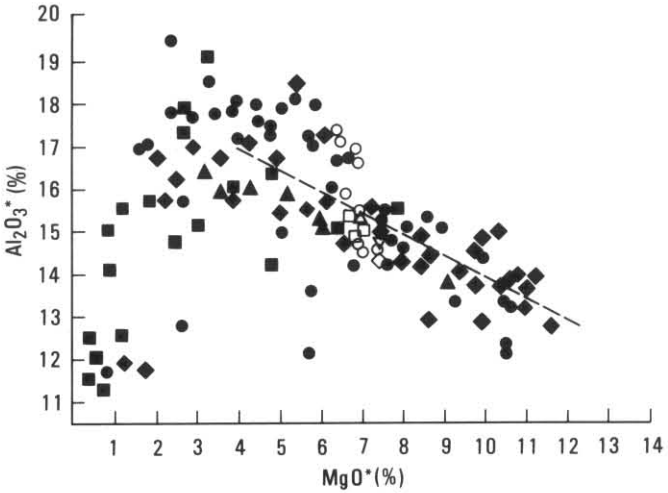
$Al_2O_3^*$(%)
MgO*(%)

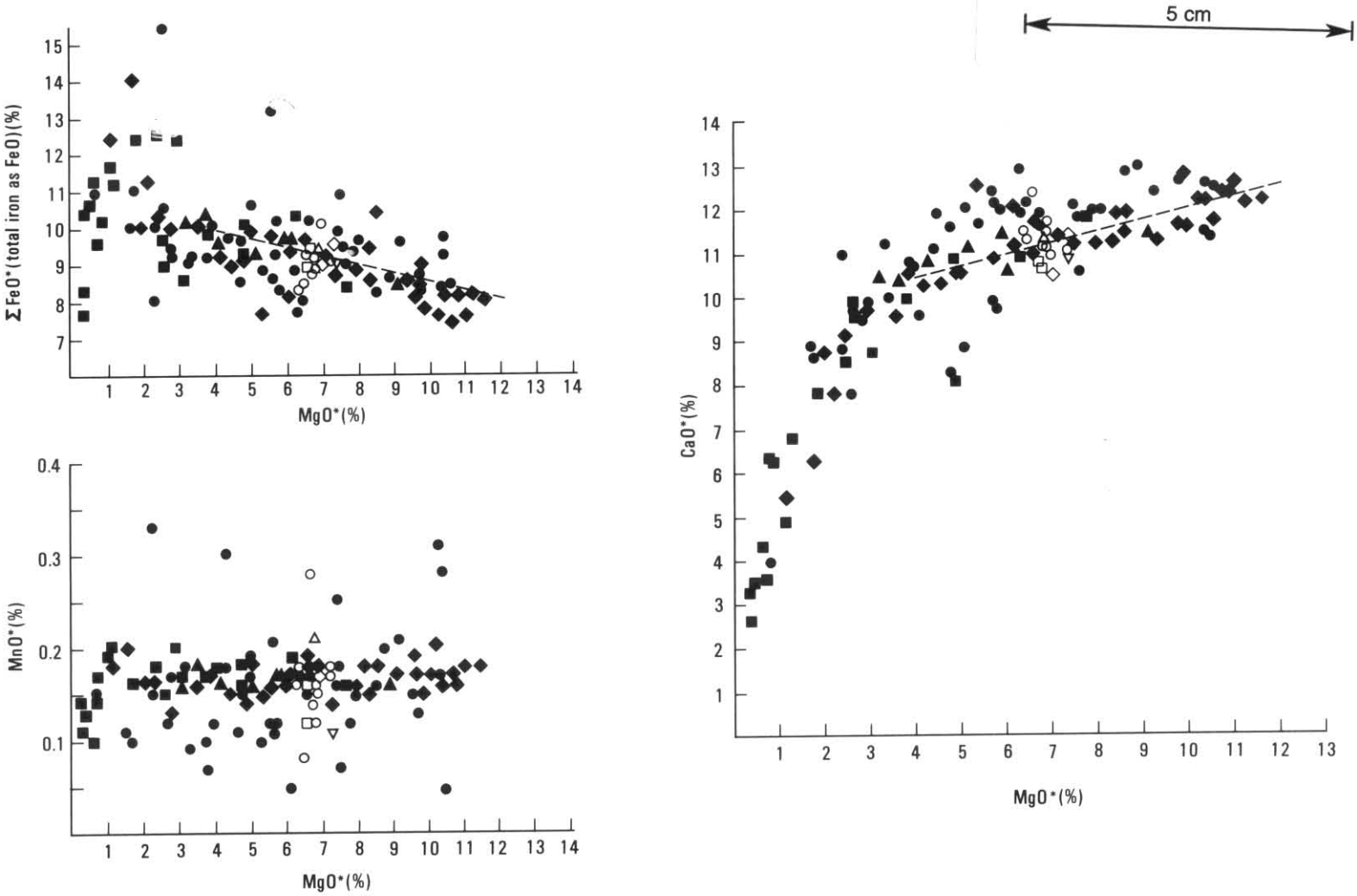

Figure B2. *Differentiation of dolerite at Fingal Tier and elsewhere in Tasmania. Major elements, normalised to 100 mass% anhydrous. Variation diagrams plotted using MgO* as the abscissa. Continuation and legend on p.136.*

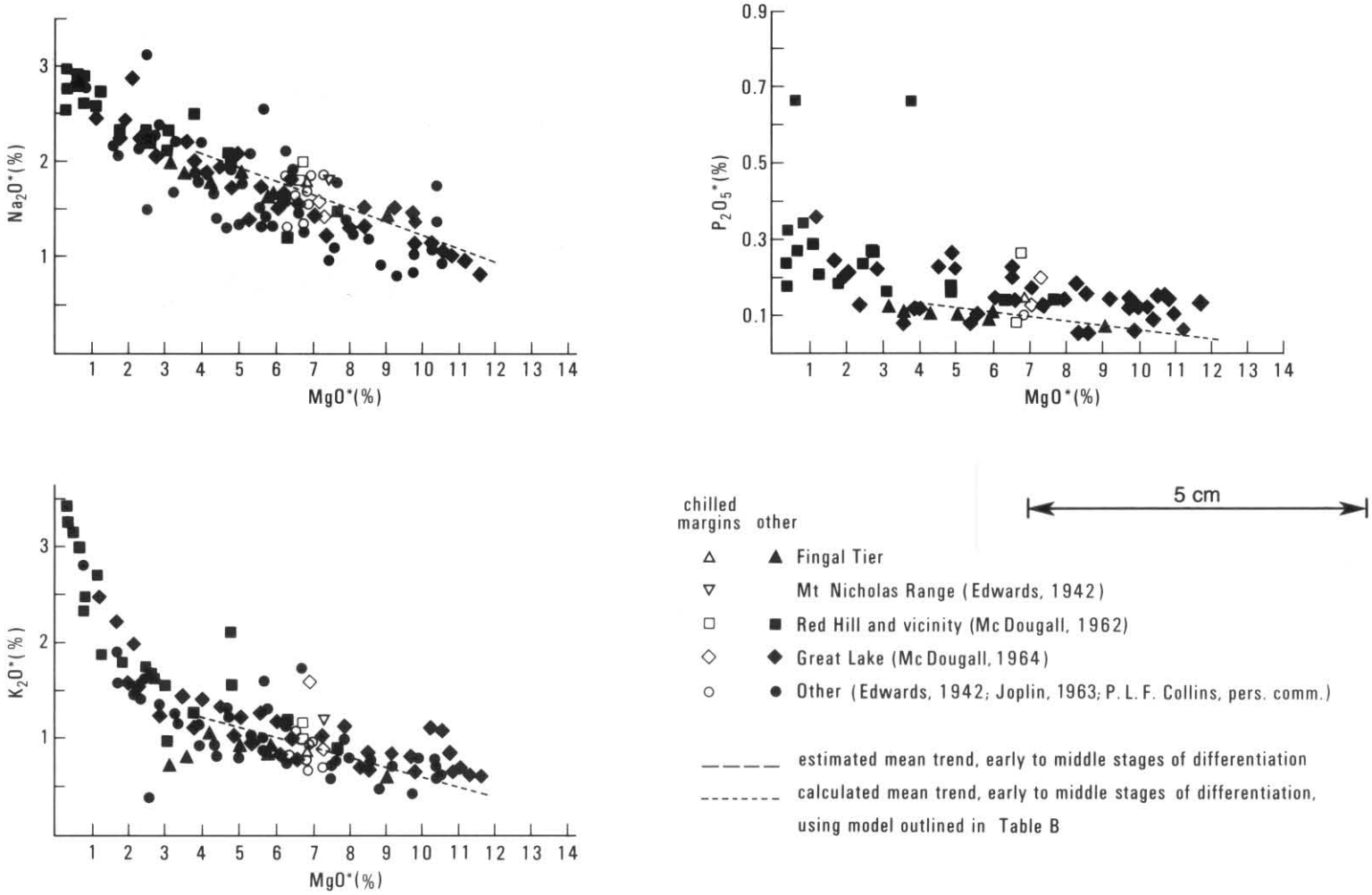

Figure B2. *Differentiation of dolerite at Fingal Tier and elsewhere in Tasmania. Major elements.* *(Continued from p. 135).*

chilled margins (analysis 783469, tables B3, B5). The lower zone, medium-grained dolerite (*e.g.* analysis 831454, table B3) is a crystal-enriched cumulate, more mafic and denser than the chilled margin. The remaining analyses are of differentiated dolerites, which have suffered varying degrees of crystal loss.

Variation diagrams for major elements (fig. B2) are plotted using MgO, which shows the greatest and most even change during differentiation, as the abscissa. Before plotting, all analyses were recalculated to 100% major elements (SiO_2, TiO_2, Al_2O_3, total iron as FeO, MnO, CaO, Na_2O, K_2O, P_2O_5). For comparative purposes, all previously published analyses of fresh Tasmanian Jurassic dolerite are also plotted. McDougall (1962, 1964) used the mafic index, (FeO + Fe_2O_3) x 100/FeO + Fe_2O_3 + MgO) and the felsic index (Na_2O + K_2O) x 100/Na_2O + K_2O + CaO) to plot variation diagrams. However, the more direct method adopted here illustrates the trends equally well, and is easier to interpret, because addition or subtraction of material of constant composition from any initial bulk composition will produce cumulates or differentiates which plot along straight lines in all diagrams.

The analyses from Fingal Tier generally plot amongst those from elsewhere in each diagram. Small inconsistencies shown by SiO_2 are attributed to secondary silicification, as manifested by the presence of chalcedony amygdales. Lower K_2O in the surface outcrops of porphyritic glassy dolerite is probably due to slight weathering. The trend of the early and middle stages of differentiation, represented at Fingal Tier and increasing with height in the sheet, is of falling MgO and CaO and increasing SiO_2, TiO_2, Al_2O_3, Na_2O, K_2O and P_2O_5. Total FeO increases only slightly and MnO remains roughly constant.

Although there is considerable scatter, probably partly due to slight alteration and analytical error, all major elements show at first a nearly linear trend in both cumulates and earlier-formed differentiates (roughly MgO* >4%), suggesting that the composition and relative proportions of the fractionating minerals were more-or-less constant in the early stages of differentiation. The composition of the fractionated material was estimated, by assuming that it consisted of plagioclase (An_{85}, with 0·65 mass % FeO, comparable to the most calcic cores analysed by electron microprobe) and pyroxene (stoichiometric solid solution of *en, fs* and *wo,* except for an estimated average 1·1% Al_2O_3). The average Tasmanian chilled dolerite (table B6) was used as the initial composition. Trends for Al_2O_3, FeO + MnO, MgO and CaO were estimated visually using the variation diagrams, and used to derive simultaneous equations.

The results (table B7) suggest that the fractionated crystals comprised roughly co-equal proportions of augite (38·2%), pigeonite and orthopyroxene (31·3%) and plagioclase (30·5%).

The calculated trends for the other elements, SiO_2, TiO_2, Na_2O, K_2O and P_2O_5 are generally consistent with the analytical data (fig. B2), within the observed scatter. The observed trend for TiO_2, particularly in the Mg-rich cumulates, is slightly flatter and may be due to slight fractionation of small but dense iron-titanium oxide crystals, probably ilmenite.

Using this model, the amount of crystals gained or lost in a dolerite sample, as a weight proportion of the final rock, can be estimated from its MgO content as

f = (mass% MgO - 6·84)/8·69— provided MgO >4%

On this basis, the most mafic, Mg-rich analysed sample from Fingal Tier (analysis 831455, 9·09% MgO*) is estimated to comprise 26% fractionated crystals, the remaining 74% to have directly crystallised *in situ*. Although it lies just beyond the linear section of the variation diagrams, the most differentiated glassy porphyritic dolerite (analysis M363/831499, 3·19% MgO*) has probably lost at least 42% fractionated crystals (30% of the initial magma).

Attempts have been made to refine this model, both by allowing for additional components (*e.g.*

Table B7
MODEL FOR EARLY AND MIDDLE STAGES OF DOLERITE DIFFERENTIATION BY FRACTIONATION OF PLAGIOCLASE AND PYROXENE

	Chilled	Plag	Px	Crystals	Cumulate
SiO_2	53·85	46·51	54·51	52·07	52·87
TiO_2	0·65	-	-	-	0·29
Al_2O_3	15·47	33·96	1·10	11·13	13·07
Σ FeO + MnO	9·30	0·65	10·24	7·31	8·20
MgO	6·84	-	22·36	15·53	11·65
CaO	11·17	17·16	11·79	13·43	12·42
Na_2O	1·69	1·59	-	0·49	1·02
K_2O	0·93	0·13	-	0·04	0·44
P_2O_5	0·10	-	-	-	0·04
Total	100·00	100·00	100·00	100·00	100·00

Chilled: average chilled margin of Tasmanian Jurassic dolerite (Table B5).
Plag: assumed composition of fractionated plagioclase: An_{85}, 0.65% iron as FeO, on join $Ab_{95}Or_5$–An.
Px: calculated average composition of fractionated pyroxene (1·10% Al_2O_3 assumed): $En_{60\cdot4}Fs_{15\cdot5}Wo_{22\cdot9}C_{1\cdot2}$. Corresponds to approximately 55% augite, 45% pigeonite and orthopyroxene.
Crystals: calculated average composition of fractionated crystals: 30·5% plagioclase, 69·5% pyroxene (approximately 38·2% augite, 31·3% pigeonite and orthopyroxene).
Cumulate: composition of lower zone dolerite comparable to the most mafic analysed dolerite (Great Lake): Al_2O_3, FeO + MnO, MgO, CaO average estimates, SiO_2, TiO_2, Na_2O, K_2O, P_2O_5 calculated assuming 44·7% chilled margin composition + 55·3% average fractionated crystals.

ab and *an*, and by adopting a more sophisticated mathematical approach, such as least-squares mixing model of Le Maitre (1979). However, a major problem is that only small differences (of the order of 0·1%) in estimates of the initial (chilled) or final whole-rock compositions produce quite large differences in the solutions, particularly with regard to the total amount of crystal fractionation. Thus estimates of the amount of fractionation calculated using the above equation should not be regarded as particularly accurate. However, all models suggest that the fractionated crystals comprise roughly co-equal proportions of calcic plagioclase, Mg-rich augite, and Mg-rich pigeonite and/or orthopyroxene.

As discussed later, both pyroxene and calcic plagioclase crystals were denser than the liquid at all stages of differentiation, and readily sank to form a pile of crystals on the floor of the intrusion, with an interstitial intercumulus liquid. In the early stages of cooling and crystallisation, this intercumulus liquid was close in composition to the initial magma. The zoning of pyroxene and particularly plagioclase, and the presence of the late stage minerals quartz and alkali feldspar throughout the intrusion, suggest that the intercumulus liquid crystallised more-or-less *in situ*, with only limited diffusional or convectional interchange with the overlying magma. This process, implicit in the above fractionation model (table B7) implies that the lower zone coarse-grained dolerite (represented by analysis 831454) is essentially an orthocumulate (*e.g.* Cox *et al.*, 1979, p. 290). The intercumulus liquid crystallised both as an overgrowth around settled pyroxene and plagioclase crystals, to form zoned rims, and as newly nucleated crystals, to form a mesostasis of quartz and feldspar.

At temperatures just below the equilibrium temperature, the lower entropy of fusion of plagioclase, relative to pyroxene, causes it to grow more slowly and nucleate more readily (*e.g.* Carmichael *et al.*, 1974, p. 147–168). Thus postcumulus crystallisation provides an explanation for the frequent ophitic intergrowth of large pyroxene partly or completely enclosing smaller plagioclase laths; there is no evidence that these minerals settled as composite glomerocrysts or aggregates as advocated by McDougall (1962, 1964). The higher nucleation rate of plagioclase is also consistent with its presence as small crystals within the mesostasis.

The most mafic dolerite known in Tasmania, from near the base of the Great Lake sheet (McDougall, 1964) contains an estimated 55% content of settled crystals, and probably represents a limit to the extent of crystal enrichment in cumulates, imposed by packing considerations. At Fingal Tier, cooling was probably more rapid because of the smaller thickness of the sheet (up to about 460 m, compared to about 600 m at Great Lake) and the lower zone dolerite is less mafic, possibly because faster crystallisation of the intercumulus liquid limited the extent of the settling process.

As cooling and crystallisation proceeded, the remaining liquid differentiated, becoming in particular poorer in CaO and MgO. Crystals continued to sink and accumulate on the rising floor of the intrusion, the intercumulus liquid crystallising to form solid dolerite. Eventually the process became one of net crystal loss relative to the initial composition of the magma, but the process remained qualitatively similar.

The most differentiated rocks at Fingal Tier are porphyritic, glassy dolerites which are only locally developed toward the top of the sheet, and crop out on the eroded surface (samples M364/831450 and M363/831449). Granophyre, the more extreme differentiate known from Red Hill, Great Lake and locally elsewhere in Tasmania (McDougall, 1962, 1964) is not known from Fingal Tier. However, the composition of the glass (table B2e) is very similar to some of the whole rock analyses of granophyre reported by McDougall (1962), and the incipient texture suggested by microlites and crystallites within the glass is strongly reminiscent of textures of granophyres, which often contain very elongate crystals of pyroxene and plagioclase. Had the large pyroxene and plagioclase phenocrysts present in these rocks fractionated and the glass fully crystallised, they would have become true granophyres.

Elsewhere in Tasmania, glass in dolerite occurs only sporadically in chilled margins where cooling was very rapid. However, the strongly differentiated nature of this dolerite suggests quenching occurred well after emplacement and was not caused by cooling along. As discussed later, sudden loss of volatiles from the liquid is an alternative explanation. A similar mechanism was invoked by McDougall (1964, p. 130) to explain the texture of some granophyres. In any case, the presence of glass suggests that porphyritic glassy dolerite formed very close to the original, now eroded upper contact of the sheet.

The variation diagrams (fig. B2) show non-linear trends in the later stages of differentiation, typified by the Red Hill dyke, indicating a progressively changing mineralogy of the settling crystals. SiO_2 and K_2O rise more rapidly and CaO falls more rapidly. Al_2O_3 reaches a maximum and then falls, as do total FeO and TiO_2, but with more pronounced peaks.

This is consistent with an increasing proportion of plagioclase in the settling crystals. For the Al_2O_3 content in granophyre to decrease from about 17%, the settling crystals must comprise more than 50% plagioclase (An_{85}, 34% Al_2O_3); if the plagioclase is becoming less calcic at this stage, as is likely, the proportion must be still higher. As well as becoming relatively less abundant, the settling pyroxene crystals must,

as suggested by the electron microprobe data, become more iron-rich. The K_2O-MgO diagram (fig. B2h suggests that crystals settling from granophyre contain overall only 3–5% MgO. The sudden maxima and rapid falling away shown by total FeO and TiO_2 suggests the onset of significant ilmenite fractionation, resulting in the net gain of these elements by settling of ilmenite to the floor, in dolerite otherwise strongly fractionated by crystal depletion.

Because of the greater complexities, involving probably fractionation of plagioclase, pyroxene, fayalite and ilmenite, and the lack of new chemical data, no attempt has been made to quantitatively model the differentiation process in granophyre. The changing mineralogy is largely the effect, as well as the cause, of the change in liquid composition. Because of the likelihood that some rocks have suffered a net gain of some minerals as well as a net loss of others, the whole rock chemical analyses probably do not represent the exact liquid line-of-descent.

TRACE ELEMENTS

Only a limited amount of trace element data from Tasmanian dolerite has been published previously. Tiller (1959) analysed V, Co, Ni, Cu, Zn, Ga, Zr and Mo in the Mt Wellington sill by emission spectroscopy. McDougall and Lovering (1963) used a similar method to analyse for Cr, Co, Ni, and Cu in the Red Hill dyke, and Heier *et al.*, (1965) used X-ray spectrometry to analyse for Rb, Sr, Th and U in samples from the Red Hill area and the Great Lake sheet.

Trace element data from Fingal Tier (table B3) is plotted against MgO* (mass% MgO after normalisation to 100% major elements, as before) in Figures B3. Where available, previous data is also plotted. As with the major elements, trace elements show well-behaved differentiation trends at Fingal Tier, similar to those from elsewhere in Tasmania. For some elements (V, Cu, Zr, Nb, Ba) the chilled margin data lie off the main trend, and processes such as local contamination by the country rock and alteration by deuteric processes or meteoric water must be considered. As discussed previously the rather erratic data for Ba are consistent with mobile behaviour, perhaps on a regional scale, since emplacement.

In general, the behaviour of trace elements, at least in the early and middle stages of differentiation, is consistent with fractionation of plagioclase and pyroxene, together with known approximate trace element distribution coefficients for these minerals. Rayleigh crystal fractionation, in which the minerals are effectively removed from the system as soon as they crystallise, provides the most appropriate model (*e.g.* Cox *et al.*, 1979, p. 345-346). If F is the proportion of liquid remaining after fractional crystallisation of a magma in which a trace element initially had a concentration C_0, its concentration in the differentiated liquid is given by:

$$C_L = C_0 F^{D-1}$$

where D, the distribution coefficient, is the ratio at any one time of the concentration of the element in the material crystallising at the moment and the melt. If, as in this case, several minerals are crystallising simultaneously, the bulk distribution coefficient is calculated from the weight proportions (W_i) of each mineral and its particular distribution (or partition) coefficient (K_{Di}):

$$D = \Sigma W_i K_{Di}$$

In cumulates, the trends are reversed, but the trace element concentrations depend on the amount of crystal settling and the concentration in the settled crystals.

At Fingal Tier, the relative amount of depletion or enrichment of the various trace elements, in the early and middle stages of dolerite differentiation represented there, suggests that qualitatively the order of bulk distribution coefficients is:

$$D_{Cr} > D_{Ni} > D_{Co} > 1 \approx D_V, D_{Sc} > D_{Sr} > D_{Cu} \quad D_Y > D_{Zn} > D_{Rb} > D_{Zr} > D_{Cu}$$

However, because of scatter in the data and the difficulty in accurately estimating F, a measure of the amount of crystal fractionation, it is not worthwhile to attempt to calculate D for most elements. Distribution coefficients are,to some extent, a function of physicochemical variables, particularly temperature, whilst changes in the mineralogy of the fractionating crystals, especially in later stages of differentiation, may also cause variations in the bulk distribution coefficients.

Cr (fig. B3c), shows the most dramatic depletion with differentiation, implying a bulk distribution coefficient of about 7. Electron microprobe data (table B1), the analysed mineral separates of McDougall and Lovering (1963) and published estimates of partition coefficients all suggest that this is due to strong partitioning into pyroxene, particularly augite. McDougall and Lovering (1963) also reported high Cr in iron oxide minerals, but these are probably not abundant enough in normal dolerite to be important in this regard. Analysis M363/831449 contains anomalously high Cr, the reason for which is not clear.

Partition coefficients for pyroxene decrease from Cr through Ni and Co to Sc and V (*e.g.* Bougault and Hekinian, 1974; Frey *et al.*, 1978). As none of these elements substitute into the plagioclase lattice to any appreciable extent, their depletion with differentiation is progressively weaker, Sc and V showing little variation. Co

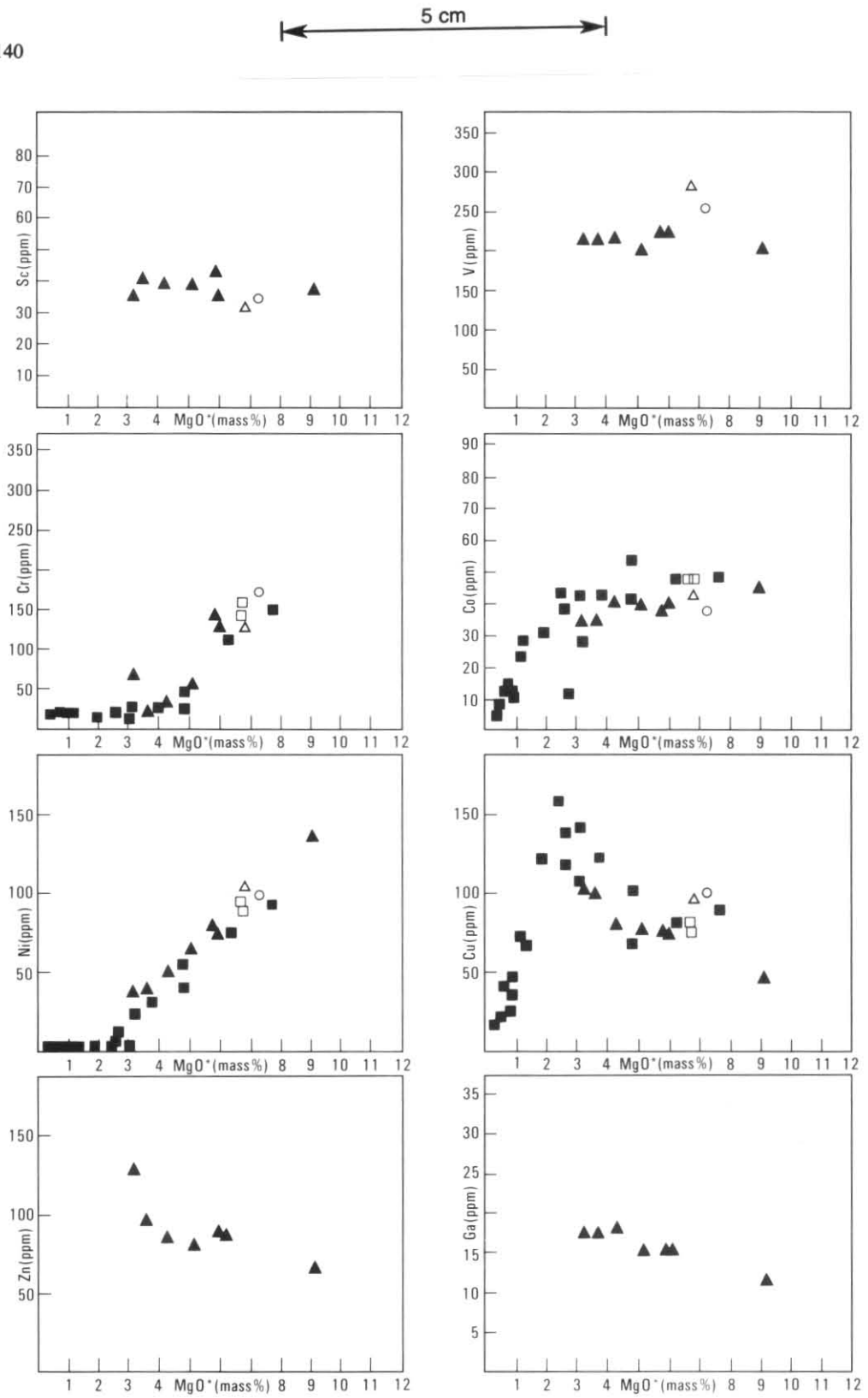

Figure B3. *Differentiation of dolerite at Fingal Tier and elsewhere in Tasmania. Trace elements, variation diagrams plotted using MgO* as the abscissa. Symbols as for Figure B2.*

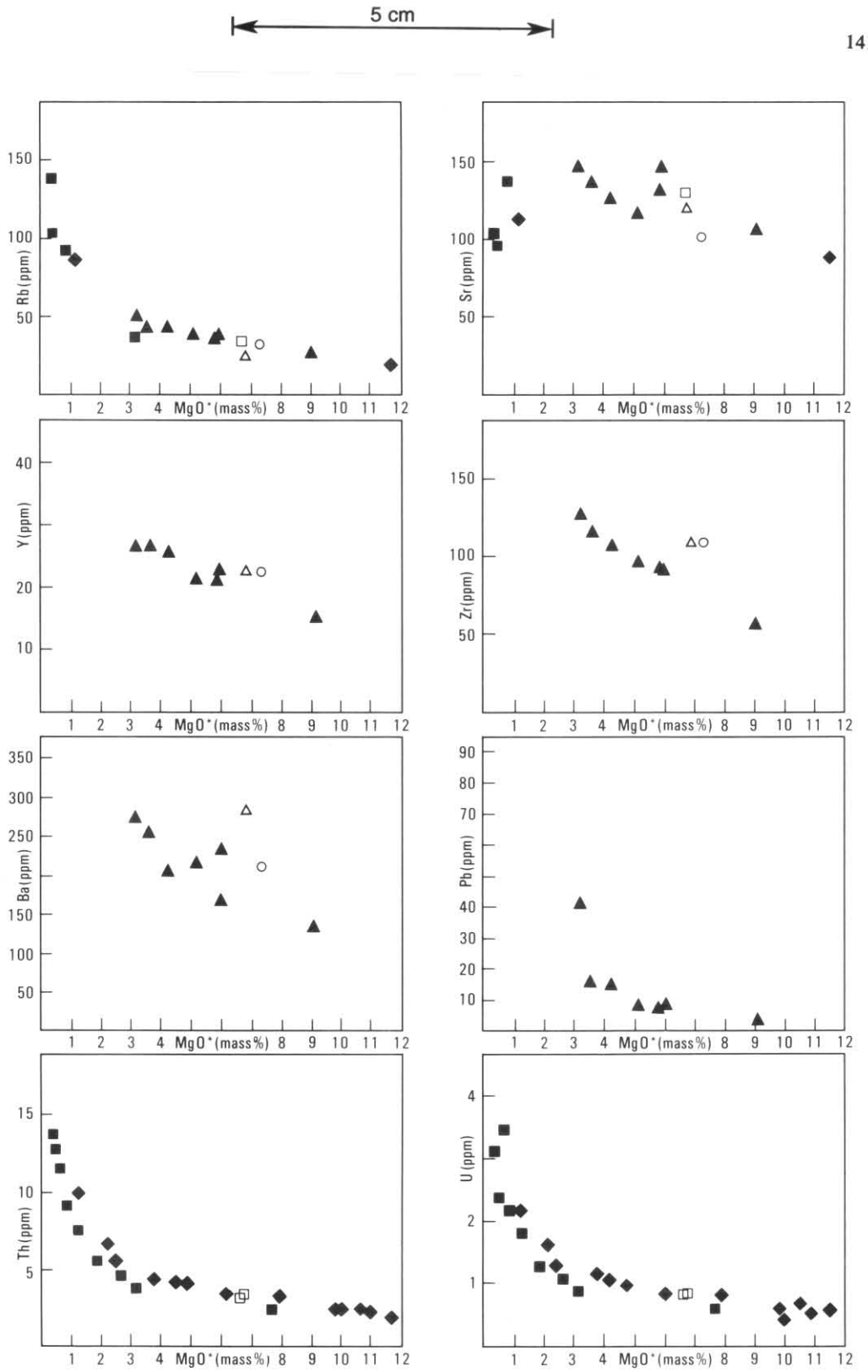
5 cm
Rb (ppm)
Sr (ppm)
Y (ppm)
Zr (ppm)
Ba (ppm)
Pb (ppm)
Th (ppm)
U (ppm)
MgO* (mass%)

5 cm

is depleted more rapidly in the Red Hill granophyre, probably due to the onset of significant iron-titanium oxide fractionation. Data for Sc and V from granophyres is not available, but would probably show a similar trend.

The remaining elements increase in abundance with differentiation, as they are progressively concentrated in the remaining liquid. Sr is partitioned into plagioclase ($K \sim 2$, *e.g.* Cox *et al.*, 1979, p. 334; Bougault and Hekinian, 1974) but this is more than compensated for by its incompatibility in pyroxene. Ga also to some extent enters plagioclase (Goodman, 1972), and Y and Zn to some extent enter pyroxene (*e.g.* Pearce and Norry, 1979; Bougault and Hekinian, 1974).

Rb, Zr and Cu are probably almost completely incompatible in both plagioclase and pyroxene. McDougall and Lovering (1963) attributed the later depletion of Cu in granophyres at Red Hill to the crystallisation of small amounts of chalcopyrite.

Cu and Zr are more abundant in the chilled margin than in either cumulates or early differentiates. Because they are highly incompatible they may tend to be excluded from the crystals even during postcumulus crystallisation, and gradually diffuse upward back to the liquid magma as a concentration gradient develops between it and the intercumulus liquid.

Data for Nb, Ba and Pb are rather erratic, due to their low abundance and the effects of alteration, but these elements also show a general tendency to increase. However, the best examples of progressive enrichment with increasing differentiation are provided by the data for K_2O (fig. B3h) and Th and U (Heier *et al.*, 1965; fig. B3o–p).

The enrichment of incompatible elements in differentiates and their depletion in cumulates can be used to derive independent estimates of the amount of crystal fractionation, but this is complicated by the possibility of partial compatibility on the one hand, and diffusion between the intercumulus liquid and the overlying magma or the other. For example, data for Cu and Zr suggest that sample M363 has lost 37 mass% crystals by fractionation, relative to the original undifferentiated magma, and that sample DDH68/361·95 contains 27 mass% cumulate crystals. The estimate for M363 is significantly higher than the value (30%) estimated from its MgO content.

The contents of K_2O, Th and U in the most extreme granophyres analysed at Red Hill (McDougall, 1962; Heier *et al.*, 1965) are about four times the chilled margin values, suggesting that this rock is derived from about four times its mass of original undifferentiated magma, by 75% crystal fractionation. This estimate is considerably less than that implied by McDougall (1962, p. 307).

PHYSICAL CONSIDERATIONS

TEMPERATURE

At the time of emplacement the dolerite magma was just below its liquidus, containing a few microphenocrysts of orthopyroxene (Ofs_{15}) and augite. However, orthopyroxene was replaced, as the stable low-Ca-pyroxene, by pigeonite at a relatively early stage of differentiation. The electron probe microanalyses (table B2) suggests that this occurred at an orthopyroxene and pigeonite composition of about Fe/Fe+Mg = 0·25.

Although pigeonite is the stable high temperature phase, the temperature of its inversion to orthopyroxene decreases with increasing Fe/Fe+Mg (fig. B4). Thus pigeonite is stable at later stage than orthopyroxene in the evolution of the dolerite magma, because the effect of iron-enrichment is more important than cooling.

Currently available experimental data (fig. B4) suggest that the inversion temperature at Fe/Fe+Mg = 0·25 is about 1180°C, and that orthopyroxene (Fe/Fe+Mg = 0·15) is stable below about 1230°C. The temperature of the dolerite magma at the time of emplacement must have been between these limits; a value of 1200°C is adopted here.

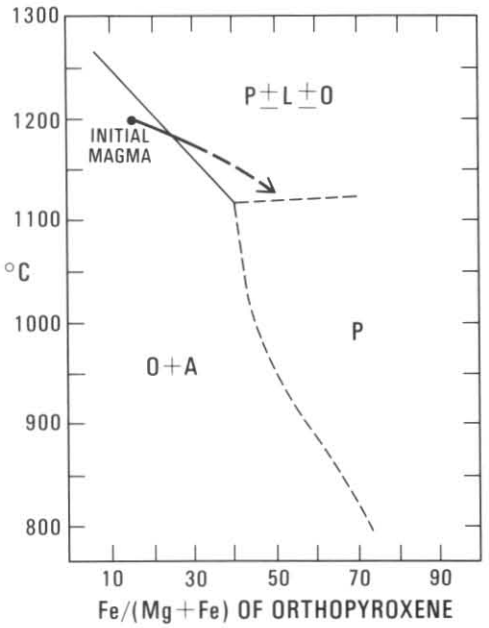

Figure B4. *Temperature versus orthopyroxene composition, showing approximate trend during early to middle stages of dolerite differentiation, and constraints on magmatic temperature provided by the pigeonite-orthopyroxene inversion. Phase relations from Huebner (1980, p. 249).*

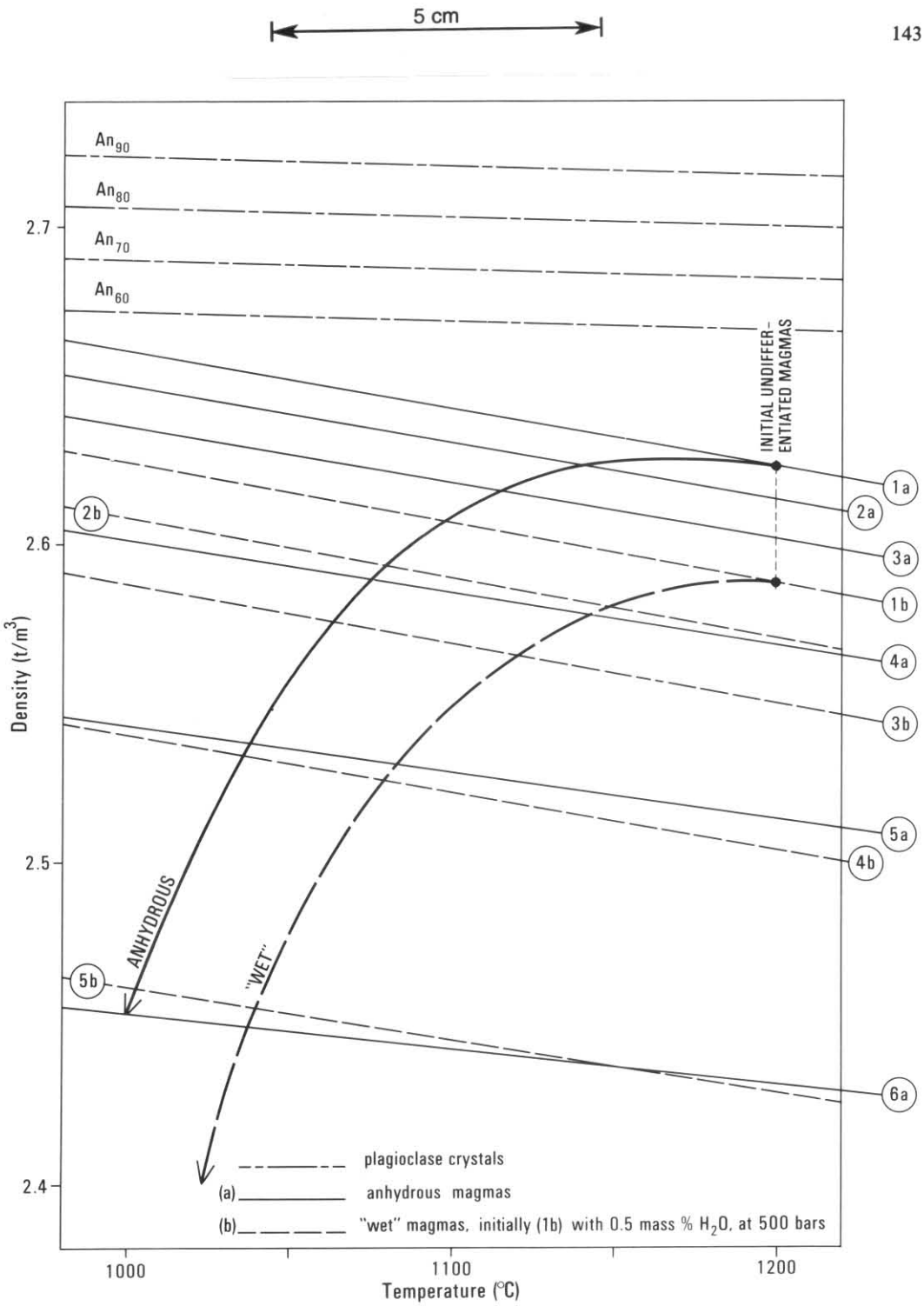

Figure B5. *Calculated density of plagioclase crystals, undifferentiated dolerite magma and various hypothetical, progressively more differentiated, liquids (table B7), assuming (a) anhydrous magma, and (b) initially 0·5 mass% H_2O. Schematic temperature–density paths of liquid during differentiation of an intrusion are also shown. See text for discussion).*

McDougall (1961*a*, 1962) used a similar argument to estimate the initial temperature. His lower estimate of 1100-1140° is due to the use of older experimental data.

No attempt has been made here to estimate solidus temperatures or the magmatic temperatures of differentiated dolerite magma.

PRESSURE AND DEPTH OF EMPLACEMENT

This is difficult to estimate with any confidence. The country rocks overlying the dolerite on Fingal Tier have been completely removed by erosion, but the form of the body and field evidence suggests that it is highly unlikely that the main body of dolerite magma reached the surface.

The younger strata intruded at Fingal Tier, as discussed in an earlier section (C. R. Calver), are near the Karnian-Norian boundary, with a probable absolute age of about 215 Ma. Stratigraphically higher rocks occur in the Triassic sequence in the Douglas River area, immediately to the south.

Schmidt and McDougall (1977) found no systematic age differences amongst a series of K-Ar age determinations of Tasmanian dolerite and gave a best overall estimate of $170{\cdot}5 \pm 8$ Ma. This should be adjusted to $174{\cdot}5 \pm 8$ Ma for new decay constants.

Assuming an age difference of 40 Ma between the dolerite and its country rock at Fingal Tier, and extrapolating an average sedimentation rate of 20 m/Ma for the Upper Parmeener Super-Group (C. R. Calver, pers. comm.) to the time of dolerite emplacement results in a crude estimate of 800 m for the thickness of the roof rocks at Fingal Tier.

Sutherland (1977) estimated former depths of burial as exceeding 1600 to 2200 m, from the occurrence of secondary prehnite and laumontite in dolerite at several localities in Tasmania.

Field evidence, such as associated brittle fracturing, suggests that the country rocks were consolidated at the time of emplacement of the dolerite (C. R. Calver, pers. comm.). Adopting an estimate of 2350 kg/m^3 for the density of the Triassic country rocks (Leaman and Richardson, 1981, p. 17) results in estimates of lithostatic pressure at the top of the intrusion of 180 bars (800 m roof thickness) to >510 bars (>2200 m roof thickness).

The relatively passive nature of emplacement of the dolerite and the general absence of features such as the explosive disruption of the country rocks, may be partly attributable to a low volatile content of the magma, and the consequence absence of vesiculation and expansion on decompression. However, there is also little evidence for disruption of the country rocks by phreatic explosions, although they were probably saturated with water at the time of dolerite emplacement. If the confining pressure exceeded that of the critical point of H_2O, 221 bars, the increase in volume of the fluid phase with increasing temperature is always gradual. This explanation implies a minimum thickness of the overlying roof racks of about 960 m, provided as is likely, the pressure was lithostatic. If the pores in the roof rocks were continuous to the surface, resulting in a hydrostatic pressure regime, this minimum is increased to 2260 m.

MAGMATIC DENSITY

Densities of the liquid portion of the dolerite magma, as a function of composition and temperature, were calculated by the method of Bottinga *et al.* (1982). Initially the magma was assumed to be of the average Tasmanian chilled dolerite composition (table B6), the effect of the few per cent microphenocrysts being neglected. There is little direct evidence as to the H_2O content of the initial magma, although the general absence of hydrous minerals in the rock and the relatively limited thermal effects around dolerite intrusions suggest that it was low. The initial density was calculated for both an anhydrous magma and one with a H_2O content of 0·5 mass%.

At the likely initial temperature of about 1200°, the density of undifferentiated magma is estimated as 2·624 t/m^3 (anhydrous) to 2·588 (0·5% H_2O). The average density of cold dolerite rock at Fingal Tier is about 2·91 (C. R. Calver, this work), and similar values have been reported from elsewhere in Tasmania (*e.g.* Jaeger, 1964). Therefore the loss of volume on solidification was 9·8–11%, implying substantial subsidence of the roof rocks. However, the structural effects of this contraction are likely to be much smaller than those of emplacement, which involved a dilation an order of magnitude greater.

Estimates for differentiated liquids are more difficult to make, because analyses of actual rocks show considerable scatter, and do not necessarily represent the exact liquid line-of-descent. However, an approximation (table B8) was made using Figure B2. Fortunately, the density is not critically dependent on the exact composition. The densities were again calculated for both 'dry' and 'wet' magmas, the latter containing initially 0·5 mass% H_2O which, with increasing crystal fractionation, becomes more concentrated if the liquid phase. It was assumed to increase in proportion to K_2O (table B8), the most incompatible of the major elements in the major cumulus phases, pyroxene and plagioclase.

The results (fig. B5) show that the magmatic density falls with differentiation, particularly in the later stages when SiO_2 increases rapidly. As expected, densities increase slightly with cooling at constant composition.

The actual change in the density of the liquid during crystallisation is difficult to estimate

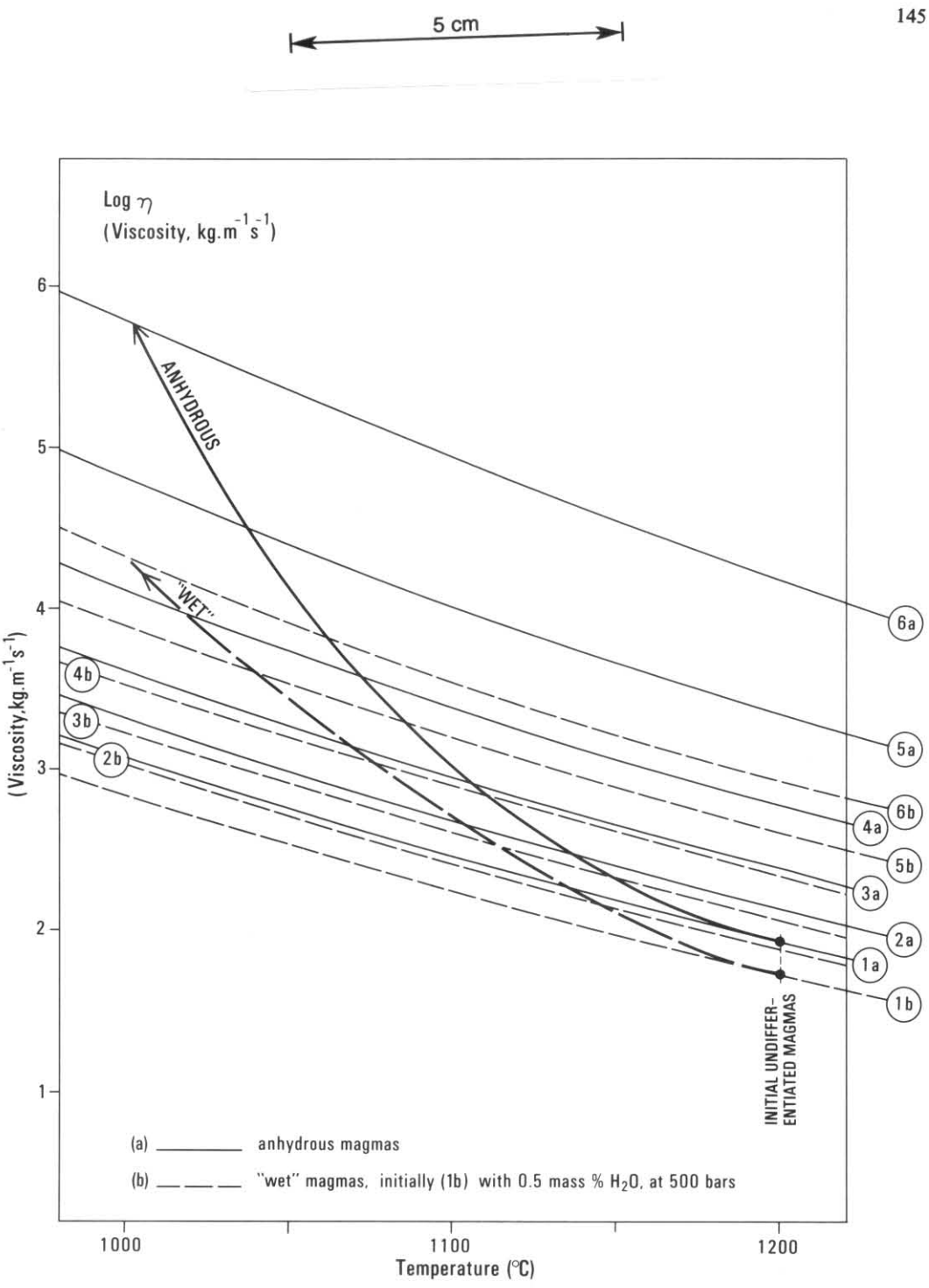

Figure B6. *Calculated viscosity of undifferentiated doleritic magma and various hypothetical, progressively more differentiated, liquids (table B8), assuming (a) anhydrous magma, and (b) initially 0·5 mass% H_2O. Schematic temperature–viscosity paths of liquid during differentiation of an intrusion are also shown. See text for discussion.*

Table B8
IDEALISED, APPROXIMATE LIQUID LINE-OF-DESCENT, USED TO CALCULATE MAGMATIC DENSITIES AND VISCOSITIES

	(1) initial	(2)	(3)	(4)	(5)	(6)
SiO_2	53·85	54·26	54·92	57·64	62·19	68·72
TiO_2	0·65	0·79	0·94	1·00	0·98	0·85
Al_2O_3	15·47	16·30	17·00	16·30	14·50	12·51
FeO	9·14	9·60	10·10	10·30	10·20	8·27
MnO	0·16	0·16	0·16	0·16	0·16	0·11
MgO	6·84	5·00	3·20	2·00	1·00	0·33
CaO	11·17	10·70	10·00	8·20	5·50	2·56
Na_2O	1·69	1·95	2·18	2·45	2·70	2·97
K_2O	0·93	1·12	1·35	1·75	2·50	3·44
P_2O_5	0·10	0·12	0·15	0·20	0·27	0·24
Total	100·00	100·00	100·00	100·00	100·00	100·00
$Fe^{III}/Fe^{II}+Fe^{III}$	0·05	0·07	0·10	0·14	0·22	0·32
H_2O	0·50	0·60	0·73	0·94	1·34	1·85

precisely, because of the lack of constraints on the temperature of differentiated liquids. However, it is likely that, at first, cooling was rapid and the density increased slightly, before crystals grew large enough to fractionate. As differentiation increased, its effect dominated and the density fell rapidly. This is particularly so for the 'wet' model, in which increasing H_2O progressively depresses the density relative to an anhydrous magma.

Schematic density-temperature paths are shown (fig. B5) for both 'dry' and 'wet' magmas. Although only approximate, they are used in the subsequent discussion to illustrate general trends.

The high-temperature density of plagioclase (An_{60}–An_{90}) was calculated by a method described in an earlier section (petrogenesis of Triassic basalt). The results (fig. B5) show that plagioclase, of compositions appropriate to dolerite, is likely to be significantly denser than the liquid at all stages of differentiation, and there is no possibility of upward flotation of plagioclase. Pyroxene is much denser (3·2 t/m³) than the liquid. Thus, although the remaining liquid became less dense with crystallisation, the total volume of the intrusion decreased, as noted above.

SOLIDIFICATION TIME

Jaeger (1957) calculated the time for complete solidification of a dolerite sheet as 0·014 D^2 years, where D is the thickness of the sheet in metres. Although it may be necessary to re-assess the assumptions and parameters used by Jaeger, this suggests that the Fingal Tier sheet, with a thickness of up to about 460 m, took about 3000 years to solidify. If convection was important as a mechanism of heat transfer, as is likely, the time would be reduced. Nevertheless, crystal settling is unlikely to have been important if velocities were much less than 0·1 m/year

VISCOSITY

Viscosity of the liquid is an important parameter, affecting the rate of crystal settling and the fluid dynamics of the intrusion. Viscosities were calculated, as a function of composition (table B8) and temperature, for both 'dry' and 'wet' magmas, by the method of Shaw (1972).

The results (fig. B6) show that viscosity increases rapidly with both cooling and differentiation. The schematic temperature-viscosity paths shown correspond to those of Figure B6. The presence of H_2O decreases viscosity, particularly in the later stages of differentiation, when that of anhydrous magma is up to 30 times that of the 'wet' model.

This is relevant to the origin of the glassy porphyritic dolerite (M363, M364) found on Fingal Tier, and of granophyre elsewhere in Tasmania. If the roof rocks of the Fingal Tier sheet fractured at this stage of differentiation, possibly due to subsidence caused by the contraction of the dolerite on crystallisation, the H_2O concentrated in the residual liquid would have exsolved due to sudden decompression. Because of the resultant greatly increased viscosity of the liquid, crystal settling would have ceased — the crystals being suddenly 'frozen' in place. Since the liquidus temperature of anhydrous magmas is higher than their hydrous equivalents, the liquid may have thus become supercooled and rapidly congealed as glass.

SETTLING VELOCITIES

The settling velocity of a crystal is that at which gravitational and viscous forces are equal. For more-or-less spherical crystal, the latter is given by Stokes' Law, so that:

$$4/3\,\pi r^3 \Delta\rho = 6\pi\eta r v$$

$$\text{or} \quad v = 2gr^2\Delta\rho/9\eta$$

where v is the settling velocity, g gravity, r the mean radius of the crystal, $\Delta\rho$ the density contrast between crystal and liquid and η the viscosity.

Settling velocities calculated by this equation from Figures B5 and B6 are shown in Figure B7. Because of the lack of constraints on the model, these should be regarded as only order-of-magnitude estimates. Because plagioclase crystals are usually far from spherical or equant, orientation effects will be important; these will probably decrease the settling velocity.

Despite the assumptions involved, Figure B7 shows that highly fractionated liquids (<1%MgO) similar in composition to granophyre or the glass of porphyritic dolerite at Fingal

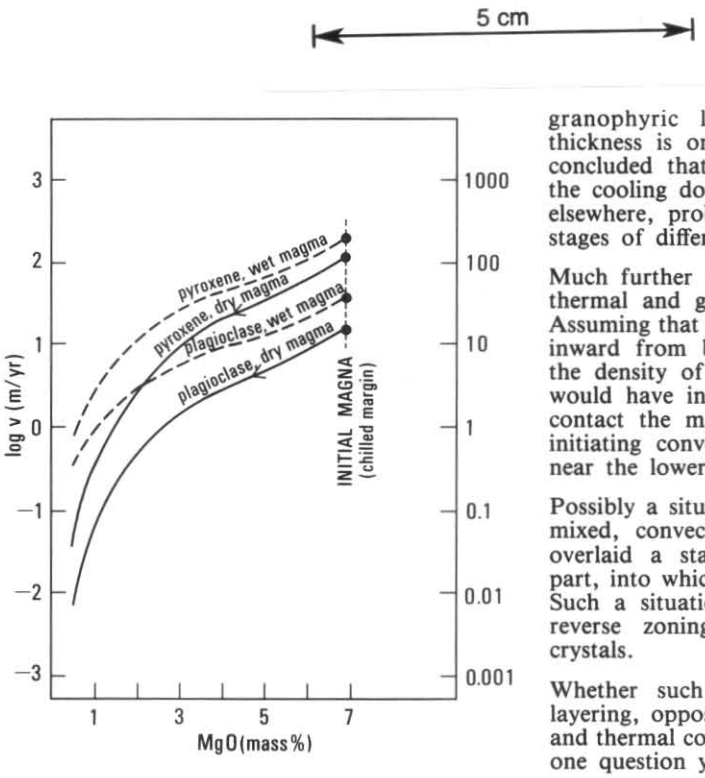

Figure B7. *Calculated Stokes Law settling velocities of one millimetre diameter crystals of pyroxene and plagioclase, as a function of composition of magmatic liquid, in a differentiating dolerite intrusion. Density and viscosity assumed to vary as shown in Figures D5 and D6. Data are approximate only.*

Tier, are unlikely to have developed by fractionation of an anhydrous magma, due to the high viscosity and consequent low crystal settling velocities. For granophyre to have formed, the crystallising dolerite intrusion must have remained a closed system with respect to H_2O, in spite of any roof subsidence.

The necessity of H_2O for its formation may explain why granophyre is frequently localised in or near structural highs in the roof of dolerite intrusions (*e.g.* McDougall, 1964), where less dense fluids tended to concentrate. Because of the depression of the liquidus, magma would have crystallised last in these places.

CONVECTION

The likelihood of convection occurring in dolerite intrusions was assessed using the Rayleigh criterion, for the case of a viscous fluid bounded by a horizontal upper and lower surface (*e.g.* Bartlett, 1969; Cox *et al.*, 1979, p. 316).

Preliminary calculations, using physical parameters calculated above or derived from the literature (*e.g.* Murase and McBirney, 1973) indicate that convection is likely in undifferentiated magma at 1200°C if the sheet is more than about 1 m thick; even for a granophyric liquid at 1000°C the critical thickness is only about 5 m. Thus is can be concluded that convection occurred during of the cooling dolerite magma at Fingal Tier and elsewhere, probably almost until the very last stages of differentiation.

Much further work is required to evaluate the thermal and geochemical implications of this. Assuming that the sheet cooled, at least initially, inward from both lower and upper contacts, the density of the magma near both contacts would have increased at first. Near the upper contact the magma would tend to sink, thus initiating convection, but the density gradient near the lower contact would be more stable.

Possibly a situation developed in which a well-mixed, convecting upper part of the magma overlaid a stagnant, less differentiated lower part, into which fractionating crystals dropped. Such a situation could explain the occasional reverse zoning observed in some pyroxene crystals.

Whether such compositional and/or thermal layering, opposed by the processes of diffusion and thermal conductivity, could be stable is only one question yet to be answered.

REFERENCES

BARTLETT, R. W. 1969. Magma convection, temperature distribution, and differentiation. *Am. J. Sci.* 267:1067–1082.

BOTTINGA, Y.; WEILL, D. 1970. Densities of liquid silicate systems calculated from partial molar volumes of oxide components. *Am. J. Sci.* 269:169–182.

BOTTINGA, Y.; WEILL, D.; RICHET, P. 1982. Density calculations for silicate liquids. I. Revised method for aluminosilicate compositions. *Geochim. cosmochim. Acta.* 46:909–919.

BOUGAULT, H.; HEKINIAN, R. 1974. Rift valley in the Atlantic Ocean near 36°50′N: Petrology and geochemistry of basaltic rocks. *Earth planet. Sci. Lett.* 24:249–261. BROOKS, C. K. 1976. The Fe_2O_3/FeO ratio of basalt analyses: an appeal for a standard procedure. *Bull. geol. Soc. Denmark* 25:117–120.

CARMICHAEL, I. S. E.; TURNER, F. J.; VERHOOGEN, J. 1974. *Igneous petrology.* McGraw Hill : New York.

COMPSTON, W.; MCDOUGALL, I.; HEIER, K. S. 1968. Geochemical comparison of the Mesozoic basaltic rocks of Antarctica, South Africa, South America and Tasmania. *Geochim. cosmochim. Acta* 32:129–149.

COX, K. G.; BELL, J. D.; PANKHURST, R. J. 1979. *The interpretation of igneous rocks.* Allen and Unwin : London.

EDWARDS, A. B. 1942. Differentiation of the dolerites of Tasmania. *J. Geol.* 50:451–480, 579–610.

FAURE, G.; BOWMAN, J. R.; ELLIOT, D. H.; JONES, L. M. 1974. Strontium isotope composition and petrogenesis of the Kirkpatrick Basalt, Queen Alexandra Range, Antarctica. *Contrib. Mineral. Petrology* 48:153–169.

FORD, A. B.; CARLSON, C.; CZAMENSKE, G. K.; NELSON, W.H.; NUTT, C. J. 1977. Geological studies of the Dufek intrusion, Pensacola Mountains, 1976–1977. *Antarct. J.* 12:90–92.

FREY, F. A.; GREEN, D. H.; ROY, S. D. 1978. Integrated models of basalt petrogenesis: a study of quartz tholeiites to olivine melilitites from south eastern Australia utilizing geochemical and experimental petrological data. *J. Petrology* 19:463–513.

GOODMAN, R. J. 1972. The distribution of Ga and Rb in coexisting groundmass and phenocryst phases of some basic volcanic rocks. *Geochim. cosmochim. Acta* 36:303–317.

GRIFFITHS, J. R. 1971. Reconstruction of the south-west Pacific margin of Gondwanaland. *Nature, Lond.* 234:203–207.

GUNN, B. M. 1962. Differentiation in Ferrar dolerites, Antarctica. *N. Z. J. Geol. Geophys.* 5:820–863.

GUNN, B. M. 1966. Modal and element variation in Antarctic tholeiites. *Geochim. cosmochim. Acta* 30:881–920.

HEIER, K. S.; COMPSTON, W.; MCDOUGALL, I. 1965. Thorium and uranium concentrations, and the isotopic composition of strontium in the differentiated Tasmanian dolerites. *Geochim. comsochim. Acta* 29:643–659.

HOLM, P. E. 1982. Non-recognition of continental tholeiites using the Ti-Y-Zr diagram. *Contrib. Mineral. Petrology* 79:308–310.

HUEBNER, J. S. 1980. Pyroxene phase equilibria at low pressure, *in* PREWITT, C. T. (ed.). *Pyroxenes.* Reviews in mineralogy 7(9):419–494. Mineralogical Society of America : Washington.

JAEGER, J. C. 1957. The temperature in the neighborhood of a cooling intrusive sheet. *Am. J. Sci.* 255:306–318.

JAEGER, J. C. 1964. The value of measurements of density in the study of dolerites. *J. geol. Soc. Aust.* 11:133–140.

JOPLIN, G. A. 1963. Chemical analyses of Australian rocks. Part I: Igneous and metamorphic. *Bull. Bur. Geol. Geophys. Aust.* 65.

KYLE, P. R. 1980. Development of heterogeneities in the subcontinental mantle: evidence from the Ferrar Group, Antarctica. *Contrib. Mineral. Petrology* 73:89–104.

LAIRD, M. G.; COOPER, R. A.; JAGO, V. B. 1977. New data on the Lower Palaeozoic sequence of northern Victoria Land, Antarctica, and its significance for Australian–Antarctic relations in the Palaeozoic. *Nature, Lond.* 265:107–110.

LE MAITRE, R. W. 1979. A new generalized petrological mixing model. *Contrib. Mineral. Petrology* 71:133–137.

LEAMAN, D. E.; RICHARDSON, R. G. 1981. Gravity survey of the East Coast coalfields. *Bull. geol. Surv. Tasm.* 60.

MCDOUGALL, I. 1961*b*. Optical and chemical studies of pyroxenes in a differentiated Tasmanian dolerite. *Am. Mineral.* 44:661–687.

MCDOUGALL, I. 1962. Differentiation of the Tasmanian dolerites: Red Hill dolerite-granophyre association. *Bull. geol. Soc. Am.* 73:279–316.

MCDOUGALL, I. 1964. Differentiation of the Great Lake dolerite sheet, Tasmania. *J. geol. Soc. Aust.* 11:107–132.

MCDOUGALL, I.; LOVERING, J. F. 1963. Fractionation of chromium, nickel, cobalt and copper in a differentiated dolerite-granophyre sequence at Red Hill, Tasmania. *J. geol. Soc. Aust.* 10:325–338.

MURASE, T.; MCBIRNEY, A. R. 1973. Properties of some common igneous rocks and their melts at high temperatures. *Bull. geol. Soc. Am.* 84:3563–3592.

PEARCE, J. A.; CANN, J. R. 1973. Tectonic setting of basic volcanic rocks determined using trace element analyses. *Earth planet. Sci. Lett.* 19:290–300.

PEARCE, J. A.; NORRY, M. J. 1979. Petrogenetic implications of Ti, Zr, Y and Nb variations in volcanic rocks. *Contrib. Mineral. Petrology* 69:33–47.

ROEDER, P. L.; EMSLIE, R. F. 1970. Olivine-liquid equilibrium. *Contrib. mineral. Petrology* 29:275–289.

SCHMIDT, P. W.; MCDOUGALL, I. 1977. Palaeomagnetic and potassium-argon dating studies of the Tasmanian dolerites. *J. geol. Soc.Aust.* 24:321–328.

SHAW, H. R. 1972. Viscosities of magmatic silicate liquids: an empirical method of prediction. *Am. J. Sci.* 272:870–893.

SMITH, J. V. 1974*a*. *Feldspar minerals. I. Crystal structure and physical properties.* Springer-Verlag : Berlin.

SMITH, J. V. 1974*b*. *Feldspar minerals. II. Chemical and textural properties.* Springer-Verlag : Berlin.

SOLOMON, M.; GRIFFITHS, J. R. 1972. Tectonic evolution of the Tasman orogenic zone, eastern Australia. *Nature (Phys. Sci.)* 237:3–6.

SPRY, A. H. 1958. The Precambrian rocks of Tasmania, Part III, Mersey–Forth area. *Pap. Proc. R. Soc. Tasm.* 92:117–137.

SUTHERLAND, F. L. 1966. Considerations on the emplacement of the Jurassic dolerites of Tasmania. *Pap. Proc. R. Soc. Tasm.* 100:133–145.

SUTHERLAND, F. L. 1977. Zeolite minerals in the Jurassic dolerites of Tasmania: their possible use as indicators of burial depth. *J. geol. Soc. Aust.* 24:171–178.

THREADER, V. M.; BACON, C. A. 1983. The Department of Mines coal exploration programme, Fingal Tier. *Unpubl. Rep. Dep. Mines Tasm.* 1983/46.

TILLER, K. G. 1959. The distribution of trace elements during differentiation of the Mt Wellington dolerite sill. *Pap. Proc. R. Soc. Tasm.* 93:153–158.

VEEVERS, J. J. 1976. Early Phanerozoic events on and alongside the Australian-Antarctic Platform. *J. geol. Soc. Aust.* 23:183–206.

APPENDIX C

Petrology of the Tertiary basalt

CONTENTS

LIST OF PLATES

LIST OF TABLES

5 cm

APPENDIX C

Petrology of the Tertiary basalt

J. L. Everard

INTRODUCTION

The only occurrence of Tertiary basalt, in the extreme north-west of the quadrangle, was mapped by P. W. Baillie. Field relations are discussed in an earlier section. A sample of fresh float, field number M366, was collected from near Barnes Road [EQ848044] by C. R. Calver, and a chemical analysis (831451) obtained from the Department of Mines laboratories, Launceston (table C1).

PETROGRAPHY

The hand specimen is a massive, medium-grained rock containing equant pale greenish ferromagnesian crystals (≤1 m) in a grey groundmass.

In thin section (plate C1) the rock is seen to consist of plagioclase (about 35%), augite and olivine (about 25%) and black to sometimes brown glass (about 40%) interstitial to, or sometimes surrounding, the crystals (*i.e.* a dominantly intersertal to hyalophitic texture). However, almost holocrystalline domains of intergranular to rarely ophitic texture are also present. There is no flow lamination or oriented fabric.

Table C1
ANALYSIS AND CIPW NORM OF BARNES ROAD BASALT (M366/831451)

Major elements	*mass%*
SiO_2	52·53
TiO_2	1·54
Al_2O_3	14·27
Fe_2O_3	2·19
FeO	9·69
MnO	0·19
MgO	5·99
CaO	9·08
Na_2O	2·71
K_2O	0·50
P_2O_5	0·19
H_2O^+	0·68
H_2O^-	0·32
CO_2	0·43
SO_3	0·06
Traces as oxides	0·19
Total	100·56

Trace elements	*ppm*
Sc	23
V	145
Cr	290
Co	48
Ni	210
Cu	52
Zn	125
Ga	20
Rb	21
Sr	230
Y	22
Zr	145
Nb	12
Ba	110
Pb	4

Chemical parameters	
$100Mg/Mg+Fe^{II}$	52·4[1] 51·0[2] 47·8[3]
Al_2O_3/CaO	1·57
K_2O/Na_2O	0·18
K/Rb	198·0
K/Zr	28·6
Rb/Sr	0·091
Ti/Zr	63·7
Nb/Y	0·55
Zr/Y	6·6
Zr/P_2O_5	0·175

[1] As analysed.
[2] Assuming $Fe_2O_3/FeO = 0·15$.
[3] All iron as FeO.

CIPW Norm	*%*
Q	4·01
or	2·99
ab	23·17
an	25·58
di	15·58
hy	22·88
mt	2·25
il	2·95
ap	0·46
cm, z, py	0·13
Total	100·00
Fe/Fe+Mg (pyroxene)	0·44
mol% *an* (plagioclase)	51·0

Calculated assuming $Fe_2O_3/FeO = 0·15$ (Brooks, 1976). Recalculated to 100 mass% anhydrous.

Plate C1. *Sample M366, Tertiary tholeiitic basalt, Barnes Road, Showing an embayed olivine phenocryst (centre left), plagioclase laths, olivine and augite granules and black glass. Texture grades from hyalophitic (upper left) to intersertal or almost intergranular in less glass-rich areas (left). Crossed nicols. Field of view 4·3 × 2·9 mm.*

Table C2
ELECTRON PROBE MICROANALYSES OF TERTIARY THOLEIITIC BASALT, BARNES ROAD

	Olivine				Plagioclase			Augite	Glass
SiO_2	38·21	37·86	37·59	37·94	55·31	55·48	53·12	52·34	57·90
TiO_2	-	-	-	-	-	-	-	1·75	1·99
Al_2O_3	-	-	-	-	28·05	27·45	29·42	6·59	12·10
FeO	21·38	23·94	22·02	21·45	0·48	0·72	0·44	12·72	10·37
MgO	40·23	38·06	40·21	40·40	-	0·22	0·16	8·66	3·88
CaO	0·18	0·14	0·18	0·21	11·72	11·50	12·96	16·15	9·92
Na_2O	-	-	-	-	4·30	4·39	3·75	1·17	2·84
K_2O	-	-	-	-	0·14	0·24	0·15	0·34	0·81
P_2O_5	-	-	-	-	-	-	-	0·28	0·19
Total	100·00	100·00	100·00	100·00	100·00	100·00	100·00	100·00	100·00

Number of cations calculated on the basis of oxygen number:

	(O) = 4				(O) = 8			(O) = 6
Si	0·990	0·992	0·978	0·984	2·500	2·519	2·416	1·977
Ti	-	-	-	-	-	-	-	0·066
Al	-	-	-	-	1·494	1·469	1·577	-
Fe	0·463	0·525	0·479	0·465	excl.	excl.	excl.	0·537
Mg	1·553	1·487	1·560	1·561	-	excl.	excl.	0·651
Ca	0·005	0·004	0·005	0·006	0·567	0·559	0·632	0·725
Na	-	-	-	-	0·377	0·387	0·331	-
K	-	-	-	-	0·008	0·014	0·009	-
Cation total	3·011	3·008	3·022	3·016	4·946	4·948	4·965	3·956
Fe/Fe + Mg	0·230	0·261	0·235	0·230	-	-	-	0·452
an	-	-	-	-	59·6	58·3	65·0	-
ab	-	-	-	-	39·6	40·3	34·1	-
or	-	-	-	-	0·9	1·4	0·9	

MnO, Cr_2O_3, SO_3 sought but not detected.
Fe and Mg assumed to be impurities in plagioclase.
Augite calculated after subtracting inferred apatite and feldspar impurities; composition approximate only.
Glass composition is average of four similar analyses.

Plagioclase occurs typically as narrow, multiply twinned laths (200–700 μm × 30–100 μm) or, less commonly, as more equant, often zoned subhedra. The moderately large extinction angles and positive optic sign are consistent with probe analyses (labradorite, table C2).

Olivine crystals (40 μm–1·5 mm) are generally polygonal subhedra, sometimes ophitically enclosing plagioclase laths. They are often embayed by black glass, and a few are very corroded anhedra. The mineral is optically negative, in agreement with probe analyses (about Fo_{76}, table C2). Despite the relative lack of grain size contrast, the low CaO content suggests that the olivine at least partly represents phenocrysts that crystallised at plutonic depths (Brown, 1982, p. 292–295; Simkin and Smith, 1970).

Augite occurs as small equant subhedra, lying in the interstices between plagioclase laths or sometimes clumped in glomerocrysts. It is difficult to distinguish from the more abundant olivine, except by its positive optic sign and commonly smaller grain size. A probe analysis is given (table C2).

The black glass contains microlites and crystallites of incipient skeletal plagioclase, granular augite and scaly (<5 μm) opaque blebs. Minor patches of clearer greenish brown glass and irregular patches of off-white carbonate, probably calcite, are also present.

An analysis of the glass (table C2) shows that is richer in K_2O and SiO_2 than the bulk rock (table C1) and therefore contains the potential alkali feldspar and quartz indicated in the CIPW norm.

Evidently cooling was too rapid to allow these minerals to nucleate. Normative *hy* is largely represented by partly resorbed olivine, which is common in saturated Tasmanian Tertiary basalts (*e.g.* Edwards, 1950).

The above estimate of the mode, together with the probe analysis of minerals and glass (table C2) are roughly consistent with the analysed bulk rock composition (table C1).

The rock is petrographically similar to the 'basalts with black glass' described by Edwards (1950) and, in particular, the mineralogy, texture and glass content is similar to Edward's

Bridgewater Type. This variety is widespread in Tasmania and is texturally intermediate between the more glassy Ouse Type and the almost holocrystalline Midlands Type.

GEOCHEMISTRY

Chemically, the Barnes Road basalt is a quartz tholeiite. The presence of normative *Q* and *hy* (table C1) and the low total alkali content (fig. A2) are characteristic, as are certain trace elements (fig. A2).

About twenty other analyses are available of Tasmanian Tertiary tholeiites (Edwards, 1950; Everard, 1984; Frey *et al.*, 1978; Spry, 1958; Sutherland, 1969*b*, 1972, 1976; Sutherland and Corbett, 1967; Sutherland and Hale, 1970). The Barnes Road basalt falls compositionally well within the range shown by most major elements, and is particularly similar to other quartz-normative tholeiites. However, SiO_2 is high, and MgO and Mg/Mg + Fe* are rather low. The Barnes Road basalt is therefore more differentiated than most. According to the total alkali-silica chemical classification of Le Maitre (1984) (fig. A2) it is a basaltic andesite.

Trace element values are also generally very similar to other tholeiites for which data are available (Everard, 1984; Frey *et al.*, 1978).

PETROGENESIS

This is considered by the same method used by Frey *et al.* (1978) for similar, though less evolved, Tasmanian and Victorian tholeiites.

The simplest way of deriving the Barnes Road basalt from a primitive olivine-normative tholeiite, with 100 Mg/Mg + Fe* of about 70, is equilibrium fractionation of about 22 mass% olivine (*i.e.* addition of about 28 mass% olivine to the actual rock is required to produce a possible parental primitive magma). This is almost twice the estimates for the tholeiites studied by Frey *et al.*, and emphasises the relatively differentiated nature of the Barnes Road basalt.

However, the relatively high Al_2O_3/CaO ratio and only moderate Ni depletion suggests that subordinate fractionation of clinopyroxene occurred. Minor plagioclase fractionation is possible, and is consistent with the relatively low Sr content, although $CaO:Na_2O$ is not particularly low. These possibilities are far too arbitrary to model quantitatively, but would tend to further increase estimates of the amount of crystal fractionation.

Differentiation of tholeiites by low pressure fractionation of olivine, clinopyroxene and plagioclase is commonplace and is well documented, both in case studies (*e.g.* Wright, 1971) and experimentally (*e.g.* Green and Ringwood, 1967, p. 139-142).

The relatively low K_2O content of the Barnes Road basalt suggests either a potassium-poor source or a large amount of partial melting. The latter is consistent with the values of other incompatible elements, such as P_2O_5 and Zr, which are not appreciably higher than in other, less fractionated, tholeiites. After allowing for a minimum of 22% crystal fractionation, and assuming a mantle source of pyrolite composition (0·13% K_2O; Ringwood, 1966), a minimum of 33% partial melting would be required to produce the parental magma. This must be regarded as a crude estimate because of the assumptions involved, uncertainty as to the source composition and the possibility of mantle heterogeneities.

REFERENCES

BROOKS, C. K. 1976. The Fe_2O_3/FeO ratio of basalt analyses: an appeal for a standard procedure. *Bull. geol. Soc. Denmark* 25:117–120.

BROWN, G. E. 1982. Olivines and silicate spinels, *in* RIBBE, P. H. (ed.), Orthosilicates. *Rev. Mineral., Mineral. Soc. Am.* 5:275–381. [2 ed.]

EDWARDS, A. B. 1950. The petrology of the Cainozoic rocks of Tasmania. *Proc. R. Soc. Vict.* 62:97–120.

EVERARD, J. L. 1984. Petrology of Tertiary basalt, altered dolerite and tuff samples, *in* GULLINE, A. B. Geological atlas 1:50 000 series. Sheet 83(8412N). Sorell. *Explan. Rep. geol. Surv. Tasm.*

FREY, F. A.; GREEN, D. H.; ROY, S. D. 1978. Integrated models of basalt petrogenesis: a study of quartz tholeiites to olivine melilitites from south eastern Australia utilizing geochemical and experimental petrological data. *J. Petrology* 19:463–513.

GREEN, D. H.; RINGWOOD, A. E. 1967. The genesis of basaltic magmas. *Contrib. Mineral. Petrology* 15:103–190.

LE MAITRE, R. W. 1984. A proposal by the IUGS Subcommission on the Systematics of Igneous Rocks for a chemical classification of volcanic rocks based on the total alkali silica (TAS) diagram. *Aust. J. earth Sci.* 31:343–255.

RINGWOOD, A. E. 1966. The chemical composition and origin of the earth, *in* HURLEY, P. M. (ed.). *Advances in earth science.* MIT Press : Cambridge, Mass.

SIMKIN, T.; SMITH, J. V. 1970. Minor element distribution in olivine. *J. Geol.* 78:304–325.

SPRY, A. H. 1958. The Precambrian rocks of Tasmania, Part III, Mersey–Forth area. *Pap. Proc. R. Soc. Tasm.* 92:117–137.

SUTHERLAND, F. L. 1969*b*. A review of the Tasmanian Cainozoic Province. *Spec. Publ. geol. Soc. Aust.* 2:133–144.

SUTHERLAND, F. L.; CORBETT, K. D. 1967. The Tertiary volcanic rocks of far north-western Tasmania. *Pap. Proc. R. Soc. Tasm.* 101:71–90.

SUTHERLAND, F. L.; HALE, G. E. A. 1970. Cainozoic volcanism in and around Great Lake, central Tasmania. *Pap. Proc. R. Soc. Tasm.* 104:17–32.

WRIGHT, T. L. 1971. Chemistry of Kilauea and Mauna Loa lava in space and time. *Prof. Pap. U. S. geol. Surv.* 735.

APPENDIX D

Economic geology

CONTENTS

LIST OF TABLES

APPENDIX D

Economic geology

COAL

C. A. Bacon

INTRODUCTION

The St Marys Quadrangle contains the bulk of Tasmania's reserves of black coal, contained within the Triassic Upper Parmeener Super-Group.

The Quadrangle includes the Mt Nicholas, Fingal, Dalmayne and Seymour coalfields. Coal has been mined in each of these areas. The earliest mining activity in the Quadrangle was at Seymour, where operations commenced in 1861. Today two colleries operate in the Quadrangle, the Duncan Colliery near Fingal and the Blackwood Colliery near Cornwall. Both are owned by the Cornwall Coal Company N. L. and produce some 450 000 t (run of mine) coal annually for domestic consumption in local steam-raising industries.

MINING HISTORY

Mt Nicholas Coalfield. Milligan (1849) visited various outcrops of coal in the Mt Nicholas area. Prospecting activity continued in the area until the opening of the Conara-St Marys railway link made transport of the coal to markets possible, and mining commenced in earnest. The Mt Nicholas coal was tested by the Launceston gas works in 1861, in various steamships in 1862 (Falconer and Robertson, 1862) and on the railways in 1883 (Grant 1883, Thureau 1883*b*).

Cornwall Colliery (1886–1964). Developmental work at the Cornwall Colliery started in 1885. The mine was opened in 1886, and was worked continuously by the Cornwall Coal Company until 1964. Three seams were worked in all, these being the Blue (M1), Hittit (M3) and Fenton (L1) seams. The most extensive workings were on the Hittit seam.

Most of the coal was extracted using the bord and pillar method of mining. During the first few years of mining, coal was extracted from the Blue seam using a longwall method of mining.

Total production from this mine was 4 053 104 t.

Mt Nicholas Colliery (1888–1958). Developmental work was commenced by the Mt Nicholas Company Pty Ltd in 1885, with the mine opening in 1888. Until 1925 most of the coal extraction was made using the longwall or step longwall method of mining. This method was replaced in 1925 with the more suitable bord and pillar system.

The mine was bought by the Cornwall Coal Company in 1937. After a brief closure, production resumed in 1941. The mine was finally closed in 1958, leaving workings on a total of five seams. These are Rileys (U8), the Six Foot (M1), the Four Foot (M2); the Four Foot Nine Inches (M3) and the Eight Foot (L1). A total of 1 748 609 t of coal was extracted during mining operations.

Jubilee Colliery (1920–1960). Small scale production was commenced in 1897 by the Jubilee Company, but operations ceased in 1902. Mining commenced in 1920 when the Jubilee Coal Mining Company began operations. Coal was transported from the pit top to bins via a 3·6 km long aerial ropeway. The mine closed in 1960.

Cardiff Colliery (1901–1914). The Coronation Coal Syndicate started prospecting activities in 1901 which led to the opening of the Cardiff Colliery. The mine was worked on a minor scale until 1914. Open cut activities at the seam outcrop were pursued on a weekend basis in 1966.

Blackwood Colliery (1980–present day). This colliery was opened on the Blue Upper seam by the Cornwall Coal Company in 1980. Production for 1983–1984 was 157 235 t.

Fingal Coalfield

Outcrops of coal near Fingal were visited by Milligan (1849), Selwyn (1855) and Gould (1861). The colonial government financed the driving of an adit in 1864 into one of these outcrops. (HAJ95 1867, p. 7) and the coal was tested on two steamships, (Falconer and Robertson, 1862). Small scale mining was recommenced in 1883 (Thureau 1883*a*) and the coal tested by the railways (Thureau 1883*b*). In this area three mines, the Fingal, Duncan and Tasmanian Collieries all worked the Duncan seam and were all located within a few hundred metres of each other on the eastern bank of the Cat and Kitten Creek.

Fingal Colliery (1920–1965). In 1920 the Fingal Coal Prospecting Syndicate was formed and a number of prospecting adits were driven into outcrops of coal near Fingal. Production from these activities was very small. The two adits driven in on an outcrop of coal near Cat and Kitten Creek were named the Cat and Kitten tunnels respectively. Some 18 000 t of coal were produced from these adits during the period from 1920 to 1940. In 1942 the leases held by the Syndicate were transferred to J. E. Yates, who formed the Fingal Coal Company Pty Ltd. One of the Syndicate's adits (the Cat Tunnel) was renamed the Fingal Tunnel and became part of workings known as the Fingal Colliery. These workings were forced to close in 1965 due to a loss of markets.

Duncan Colliery (1945–present day). The Duncan Colliery was opened in 1945 by the Cornwall Coal Company, N.L., adjacent to the Fingal Colliery. The mine was partly mechanized in 1955 with the introduction of an arc-wall coal cutter and two shuttle cars. Some hand mining continued until 1961 when the mine was completely mechanized. A coal washing plant was installed in 1959 to wash coal from this colliery and the Company's Cornwall mine near St Marys. The leases covering the Fingal Colliery workings were acquired in 1965, and in 1970 the old Fingal (Cat) tunnel was completely retimbered for use as a means of access to virgin coal beyond previous workings. A second means of egress was provided in 1982 in the south-western part of the mine area. The Duncan Colliery produced 296 053 t of coal in 1983–1984.

*Tasmanian Colliery (1954–*1957; 1962–*1963).* In 1954 two adits were dug a few metres to the south west of the Kitten tunnel. These new workings were adjacent to the Fingal Colliery workings. The ground was badly faulted and the workings were abandoned after the coal was found to have been intruded by dolerite 220 m from the entrance (Blake, 1960). The mine was reopened by the Fingal Coal Company from 1962–1963.

Barbers (Valley) Colliery (1955–1964). Two kilometres north of the Duncan, Fingal and Tasmanian Collieries are two small sets of workings known as Barbers or the Valley Colliery. The seam worked in this area appears to be a lower split of the Duncan seam. Coal was extracted from the first set of workings, Barbers (Valley No. 1) Colliery, from 1955–1962 and from the second set of workings from 1963–1964. Coal was cut mechanically and drawn to the surface in horse-drawn skips.

Dalmayne Coalfield

Outcrops of coal in the Dalmayne coalfield were inspected by Gould (1861). Reward claims for coal were issued in 1887 in the area and held until 1892. Only prospecting activity was pursued on these leases, as described by Twelvetrees (1902). Mining in this coalfield began in 1914 when the Dalmayne Collieries Company was floated. Coal was transported from the pit top to a jetty at Piccaninny Point by an aerial ropeway haulage system. A shortage of boats suitable for coal transport in 1917 and severe storm damage to the jetty in 1918 caused the venture to collapse. The mine was reopened in 1939 and continued under a number of different ownerships until 1953. Mining was done from adits using the bord and pillar system of extraction.

Seymour Coalfield

Mining commenced at Seymour in 1861 under the direction of A. H. Swift The workings, which consisted of two shafts and one drive 50 m in length, were inspected by Charles Gould, in response to Swift's request for financial assistance from the colonial government (CSD 4/6/40 11 December 1861). Funds for the construction of a tramway and jetty were provided by the colonial government in 1862. The Seymour Coal Mining Company was formed by Swift in 1863. Mining continued at Seymour until 1880. In 1868, Swift formed the Australian Coal and Kerosene Company to use the 50–60 per month of 'slack' coal from the mine. One batch of 2700 litres of oil was retorted from the coal and sent to Melbourne to be refined (Tasmanian Times, 18 June 1868). One of the original shafts was circular and lined with bricks.

Leases covering 10 000 acres (4 000 ha) for coal, fireclay, limestone, ironstone and shale were granted to the East Coast Harbour and Coal Mining Company for a period of sixty years in 1888 (The East Coast Harbour and Coal Mining Company Act, 24 October 1888). The company was registered on 10 October 1891, Edward Gaunt being mine manager at the time. This venture was short-lived. The Morning Star Company held leases over parts of the Seymour coalfield in 1897 but no work was done.

In 1923 a new company, the Seymour Coal Mines Limited cleaned out and retimbered one of the old shafts. Bins and a jetty 400 m long were constructed. A dip tunnel was driven in 1928 to connect with old underground workings to the west of the circular shaft for ventilation purposes. Storms partially demolished the jetty in 1931, and mining activity was suspended. The workings were dewatered and reopened in 1959. The mine finally closed in 1965.

Recent Exploration

Since prospecting activity in the Quadrangle began in the 1840s exploration for coal has been continuous. Last century holes were drilled by the government in the Fingal Valley (2 holes) and at Seymour (4 holes). A number of holes have been drilled in the Mt Nicholas area by colliery management, the Department of Mines and exploration companies. Coal mining leases are held on Mt Nicholas by the Cornwall Coal Company and the Shell Company of Australia Ltd, and part of the Mt Nicholas coalfield is covered by E.L. 50/82, held by the Cornwall Coal Company.

Scout drilling in the Fingal coalfield was commenced in 1959 by the Department of Mines, to delineate the extension of the Duncan seam south of the area of mine workings. The exploration was accelerated in 1972 with the aim of defining possible reserves of coal for power generation. The results of this phase of exploration from 1972–1982 are given in Threader and Bacon (1983).

A detailed gravity survey over the central eastern highlands (Leaman and Richardson, 1981)

defined dolerite feeders, dolerite cap variations and specified definite exploration target zones.

Exploration in the Dalmayne coalfield has consisted of drilling by the Department of Mines around the Dalmayne colliery between 1949–1952 and more recent exploration by the IMI-Shell Company of Australia joint venture partnership. The coalfield is covered by E.L. 5/61 held jointly by these two companies.

At Seymour, four holes were drilled by the government in 1888 and another four by the Department of Mines in 1944–1945. The coalfield is covered by a mining lease held by the Cornwall Coal Company N.L.

Boreholes with data publicly available as at mid-1984 are indicated on the geological map. Two holes drilled in 1888 in the Fingal Valley on the Harefield and Killymoon properties are denoted HA and KI, respectively. Near Seymour, SE1a was drilled in 1888, and SE1b and SE2 were drilled in 1944–1945. On the Nicholas Range, Cornwall 1 and 2 (CO1, CO2) and Jubilee 1 (JU) were drilled in the 1950s. Eighty-five holes were drilled by the Department of Mines between 1959 and 1983 (mostly in the latter part of this period), seven near Mt Nicholas and the rest on the western Fingal Tier. these are indicated on the map with unprefixed numbers. Some earlier holes drilled by the Department near Dalmayne are denoted DA4, DA6 and DA8. Nine holes drilled by the H.E.C. on Fingal Tier are denoted C1–C9. The holes drilled by the Shell-I.M.I. consortium in the eastern Fingal Tier–Dalmayne area in the late 1970s are indicated GY1–GY18.

Coal geology

Mt Nicholas. There are three intervals in the Upper Parmeener Super-Group on Mt Nicholas in which coal seams are found. These are known informally as the upper, middle and lower groups of seams. The upper group of seams are of poor quality coal interbedded with claystone and mudstone. As many as eight seams occur in this interval, although most are better described as richly carbonaceous mudstone rather than coal. Only one of these seams (U8) or Rileys has been worked, being mined for a short time at the Mt Nicholas Colliery.

The middle group of seams comprises three main seams from which all the major coal extraction on Mt Nicholas has taken place. The Blue and Hittit seams worked at the Cornwall Colliery belong in this interval, as do the 6ft, 4ft and 4ft 9in seams worked at the Mt Nicholas Colliery. The Blue Upper (M1) seam currently worked at the Blackwood Colliery is the topmost seam in this interval.

The lower interval usually contains four seams. The topmost two seams (L1, L2) often coalesce to form one seam. The L1 seam and in parts the combined L1, L2 seams have been worked at the Cornwall Colliery (as the Fenton seam) and at the Mt Nicholas Colliery (as the 8ft seam). The two lower seams have never been worked.

Fingal. There are eight major coal seams in the Upper Parmeener Super-Group on Fingal Tier; these have been labelled seams A-H by the Department of Mines. Some, notably the A and B seams, are better described as carbonaceous intervals, as they consist of plies of coal less than 0·5 m thick interbedded with carbonaceous mudstone and claystone over intervals of 5–10 m. All the seams are characterised by a high inherent ash content, and have only a small (10%) component of bright coal. The coal is of medium rank, with a high ash and low sulphur content, and is suitable for steam raising purposes.

No satisfactory marker horizons have been recognised in the fluvial sequence on Fingal Tier. In order to obtain a reliable correlation of coal seams it has been necessary to drill to the top of the glaciomarine sequence of the Lower Parmeener Super-Group (formerly referred to as 'Permian' sediments). This basement dips gently to the east and forms a known horizon from which correlation of coal seams may be more confidently undertaken. Drill holes must commonly be 500–600 m deep in order to reach this horizon.

Over parts of the coalfield a one metre to three metre thick conglomerate horizon has proved to be a reasonable marker where present. The conglomerate band (informally called the Dalmayne Conglomerate) is composed of well rounded pebbles and cobbles of green and white quartzite, acid pyroclastic rocks, and slate, elongate to spherical in shape, and set in a matrix of coarse-grained lithic sandstone. The conglomerate band is, however, high in the sequence, and often absent due to intrusion by the dolerite at a lower horizon.

A number of tuff intersections have been recorded in the eastern part of the coalfield. The tuff is an acid, air-fall vitric tuff, occurring in layers up to one metre thick. However, the patchy areal distribution of the tuffs severely limits their viability as marker beds.

The two seams which are of greatest economic interest on Fingal Tier are the Duncan (seam F) and the East Fingal (seam G). The Duncan seam is currently mined at the Duncan Colliery and is the only seam to have been extensively worked. Typically the seam consists of 2–3 m of dull coal with minor clay and mudstone partings. The raw ash content is approximately 30% and the specific energy 22–24 MJ/kg.

The East Fingal seam is about 30 m stratigraphically below the Duncan seam, and is commonly split. The upper and lower splits (Gu and Gl) of the East Fingal seam are commonly 1–2 m in thickness, with the intraseam

Table D1

PROXIMATE ANALYSES OF COAL FROM THE MT NICHOLAS, FINGAL, DALMAYNE AND SEYMOUR COLLIERIES

	1	2	3	4	5	6	7	8
Moisture (%)	5·0	4·4	5·3	6·7	2·9	4·1	3·3	1·54
Ash (%).....	23·3	35·45	41·4	16·8	23·4	19·4	20·25	17·50
Volatile matter (%).....	28·6	21·10	25·0	31·1	26·7	31·2	24·15	25·00
Fixed carbon (%)	48·2	43·45	33·6	52·1	47·0	45·3	52·57	55·97
Total sulphur (%)	0·30	0·33	0·30	0·46	0·28	0·41	0·43	0·81
Specific energy (MJ/Kg)..	26·3	19·87	17·94	25·56	23·1	25·1	25·6	27·5

1. Duncan seam, DOM DDH 2 Fingal Tier, top 1·70 m of seam. (Departmental records)

2. Duncan seam, Duncan Colliery, channel sample including bands, 1983. (Knott and Warbrooke, 1983).

3. Blue Upper Seam, Blackwood Colliery, channel sample, 1981, including bands. (Bacon, 1984*a*).

4. Blue Upper Seam, Blackwood Colliery channel sample, 1981, excluding bands. (12·7 mm x F1.60) (Bacon, 1984*a*).

5. Hittit seam, Cornwall Colliery, basal 1·70 m of working section, (Threader, 1968).

6. Six Foot Seam, Mt Nicholas Colliery; sample from Main Heading, 1947 (Bacon, 1983*b*).

7. Dalmayne Colliery, channel sample of lower 1·4 m of seam, 1943. (Bacon and Calver, 1984*a*).

8. Seymour colliery, channel sample of main seam worked, 1930 exclusive of dirt bands. (Bacon and Calver, 1984*b*).

sediments being 0–10 m in thickness. The upper split is less well developed west of the Mitchell Fault. The coal quality is similar to that of the Duncan seam.

Dalmayne. The Dalmayne coalfield is an easterly extension of the Fingal coalfield. Most of the coaly intervals in the Fingal coalfield can be traced into the Dalmayne coalfield. The Dalmayne Conglomerate is widespread. The seam mined at the Dalmayne colliery is located in the upper part of the stratigraphic sequence and probably correlates with the DOM Fingal Tier B seam interval. The seam is described as being composed of 1·8 m (6ft) of 'top coal' overlying a mudstone band 1·0 m thick, which in turn overlies 1·4 m (4ft 6in) of 'bottom coal' which constituted the working section of the seam. Several seams of economic interest exists in the Dalmayne coalfield. Figures 9 and 10 shows the relationship between the seams in the Dalmayne and Fingal coalfields.

Seymour. Four thin seams (S1–S4) exist over most of the coalfield area. Stratigraphically these seams are located towards the bottom of the lithic sandstone sequence. Coal has been mined from two seams, the S1 and S3 seams, although most of the extraction has been made from the S3 seam, which ranges in thickness from 1·14 m to 1·68 m.

For more detailed information on the coalfields of the St Marys Quadrangle, see Bacon (1983*a*, 1983*b*), and Bacon and Calver (1984*a*, 1984*b*).

Coal quality. The quality of coal from the four coalfields is quite similar. The coal is medium rank, bituminous steaming coal. Typical proximate analyses are listed in Table D1.

The *in situ* ash content of whole seam samples ranges from 15–45%, typically being around 25–30%. Selective mining procedures have enabled the historic hand mining operations to produce a coal with an ash content of around 20%. With mechanical mining methods the whole seam is mined, but the ash content is reduced by beneficiation in a coal washery to consumer requirements.

The saleable product coal has an ash content of around 20%, and a specific energy value of 24–26 MJ/Kg. The sulphur content is very low, usually less than 0·5%, and is found in the form of organic sulphur.

Coal reserves. The majority of the State's reserves of black coal are contained within the Quadrangle area. In a portion of the Mt Nicholas coalfield, the Shell Company of Australia Ltd have, after three years of exploration defined a measured *in situ* reserve of 44 million tonnes of black coal. In the Dalmayne–Douglas River areas the same company have delineated an indicated *in situ* reserve of 190 million tonnes of black coal in one seam. In the Fingal coalfield measured and indicated reserves of coal total 250 million tonnes in a total of four seams, although only a small part of this *in situ* coal is accessible using current mining methods. The potential exists for additional reserves to be defined within the quadrangle.

INDUSTRIAL MINERALS

V. M. Threader

Limestone (Pc) crops out abundantly in the Silkstone area and to a lesser extent around Dublin Town and Mt Elephant. Fifty-eight

Table D2

ROAD-MAKING MATERIALS IN THE ST MARYS QUADRANGLE

No.	Grid Ref.	Owner	Locality	Rock type	Remarks
1	FP051863	DMR	Chain of Lagoons	Granite	
2	FP027999	DMR	St Marys Pass	Granite	
3	EQ850040	Forestry Commn	Beauty Flat	Quartz gravel	
4	EQ914010	Forestry Commn	Mt Nicholas	Dolerite talus	disused
5	EQ946036	Forestry Commn	Haslemere Rd, Dublin Town	Basal Permian quartz sandstone	
6	EQ918044	Forestry Commn	Haslemere Rd, N of Huntsmans Ck	Mathinna Beds slate and sandstone	
7	EQ937040	Forestry Commn	Haslemere Rd, Dublin Town	Basal Permian quartz sandstone	disused
8	FP072881	Forestry Commn	Chain of Lagoons	Granite	
9	FQ035033	Mr Wardlaw	Tasman H'Way N of Falmouth T/O	Mathinna Beds slate and sandstone	
10	FP071973	Mr Aulich	Four Mile Creek	Granite	
11	FP021994	DMR	Tasman H'way, St Marys Pass	Granite	
12	FP012990	DMR	Tasman H'way, St Marys Pass	Granite	
13	FP064848	Mr Wardlaw	Chain of Lagoons	Granite	
14	FP009921	DMR	Gray	Permian quartz sandstone	
15	EP997957	Fingal Council	St Marys	Mathinna Beds hornfels	
16	EP985966	DMR	St Marys	Mathinna Beds hornfels	

metres of limestone were intersected in borehole no. 9 in the Fingal Range but the average $CaCO_3$ content was only 41%. In the uppermost 10–12 m, the content rose to 75%.

Interest was briefly shown in the 1920s when a new cement factory site was being sought following the closure of the Maria Island cement venture. Keid (1920) and Nye (1926) examined Silkstone and Dalmayne respectively. The attraction was the proximity of coal and limestone deposits, but the poor quality of the limestone discouraged any further work on the venture.

The limestone would be satisfactory either for lime burning or could be sold as crushed limestone for agricultural purposes. It is doubtful if a local industry would be economic while superior lime and crushed limestone from Railton, Mole Creek and Flowery Gully are readily available.

ROAD-MAKING MATERIAL

Tertiary quartz gravel (Ts) occurs in the north-west of the Quadrangle and consists of well-rounded quartz and quartzite pebbles derived from Mathinna Beds. This material has been used extensively by the Forestry Commission on plantation roads. It is completely non-plastic and requires the addition of a binder when used in pavement construction.

Quartz gritstone at the base of the freshwater quartz sandstone (Ps) sometimes forms gravel deposits on the exhumed pre-Permian surface. The deposits are similar to the Tertiary quartz gravel but are usually much thinner and are soon worked out.

Dolerite talus (Qptd) is abundant on Fingal Tier and the Nicholas Range. It consists of angular fragments in a clay matrix and is used extensively for logging roads but is too plastic for pavement construction.

Mathinna Beds slate and sandstone (SDs) has been used on Forestry Commission roads and by the Department of Main Roads for pavement construction. For the latter use, material from close to granite contacts is preferred as it is more durable.

Granitic rocks (Dpr and Daec) yield coarse sand and fine gravel and is the main source of surface-course material in the area.

Reserves of dolerite talus, Mathinna Beds and granitic rocks are almost unlimited and it should not be difficult to locate new pit or quarry sites by studying the rock distribution on the geological map.

REFERENCES

BACON, C. A. 1983*a*. The Fingal coalfield. *Unpubl. Rep. Dep. Mines Tasm.* 1983/34.

BACON, C. A. 1983*b*. The Mt Nicholas coalfield. *Unpubl. Rep. Dep. Mines Tasm.* 1983/41.

BACON, C. A. 1984*a*. Analysis of coal from the Blue Seam, Blackwood Colliery, Mt Nicholas. *Unpubl. Rep. Dep. Mines Tasm.* 1984/41.

BACON, C. A. 1984*b*. Petrographic analysis of the Duncan Seam, Duncan Colliery, Fingal. *Unpubl. Rep. Dep. Mines Tasm.* 1984/66.

BACON, C. A.; CALVER, C. R. 1984*a*. The Dalmayne coalfield. *Unpubl. Rep. Dep. Mines Tasm.* 1984/10.

BACON, C. A.; CALVER, C. R. 1984*b*. The Seymour coalfield. *Unpubl. Rep. Dep. Mines Tasm.* 1984/12.

FALCONER, W. R.; ROBERTSON, J. 1864. Experiments with Tasmanian coal on board the steamship 'Tasmania'; Experiments with coal at the Launceston gas works. *House of Assembly Pap. Tasm.* 1864(61).

GOULD, C. 1861. Examination of the coal fields existing in the Break o' Day valley, and upon a portion of the East Coast. *House of Assembly Pap. Tasm.* 1861(9).

GRANT, C. H. 1883. Trial of Mount Nicholas coal: report from Manager of Tasmanian Main Line Railway. *House of Assembly Pap. Tasm.* 1883(110).

KEID, H. G. W. 1920. Report on the proposal to establish cement works on the Silkstone properties. *Unpubl. Rep. Dep. Mines* 1920–1922:155–159.

KNOTT, A. C.; WARBROOKE, P. 1983. Determination of trace elements in coal and coal products. Part 5. *NERDDP Project Grant* 80/0220.

LEAMAN, D. E.; RICHARDSON, R. G. 1981. Gravity survey of the East Coast coalfields. *Bull. geol. Surv. Tasm.* 60.

MILLIGAN, J. 1849. Reports on the coal basins of Van Diemens Land. Fingal and East Coast. *Proc. R. Soc. V.D.L.* 1:1–81.

NYE, P. B. 1926*a*. Geological report on cement materials at Dalmayne and Mt Peter. *Unpubl. Rep. Dep. Mines Tasm.* 1926:146–151.

NYE, P. B. 1926*b*. Second report on cement materials at Dalmayne and Saltwater Lagoon. *Unpubl. Rep. Dep. Mines Tasm.* 1926:128–132.

SELWYN, A. R. C. 1855. Report on the geological relations of some of the coal seams of Van Diemen's Land, their probable extent and relative economic value. *Pap. Proc. R. Soc. V.D.L.* 3:116–141.

THREADER, V. M. 1968. An interim report on the geology and coal resources of the northeast coalfields of Tasmania. *Unpubl. Rep. Dep. Mines Tasm.*

THREADER, V. M.; BACON, C. A. 1983. The Department of Mines coal exploration programme, Fingal Tier. *Unpubl. Rep. Dep. Mines Tasm.* 1983/46.

THUREAU, G. 1883*a*. Report on Fingal and Mount Nicholas coal districts. *House of Assembly Pap. Tasm.* 1883(90).

THUREAU, G. 1883*b*. Fingal coal: reports on the tests of Fingal coal on the Launceston and Western and Main Line Railways. *House of Assembly Pap. Tasm.* 1883(131).

TWELVETREES, W. H. 1902. Report on coal seams at Thornedale, near Thompson's Marshes, and the Jubilee Colliery, near St Marys. *Rep. Secr. Mines Tasm.* 1901–1902:124–1313.